TAMPEREEN TEKNILLINEN YLIOPISTO
TAMPERE UNIVERSITY OF TECHNOLOGY

Joonas Puukko

Issues on Dynamic Modeling and Design of Grid-Connected Three-Phase VSIs in Photovoltaic Applications

Julkaisu 1084 • Publication 1084

Tampere 2012

Tampereen teknillinen yliopisto. Julkaisu 1084
Tampere University of Technology. Publication 1084

Joonas Puukko

Issues on Dynamic Modeling and Design of Grid-Connected Three-Phase VSIs in Photovoltaic Applications

Thesis for the degree of Doctor of Science in Technology to be presented with due permission for public examination and criticism in Sähkötalo Building, Auditorium S4, at Tampere University of Technology, on the 2nd of November 2012, at 12 noon.

Tampereen teknillinen yliopisto - Tampere University of Technology
Tampere 2012

ISBN 978-952-15-2930-6 (printed)
ISBN 978-952-15-2956-6 (PDF)
ISSN 1459-2045

ABSTRACT

Power electronics (PE) plays an important role in grid integration of photovoltaic (PV) power systems. According to present knowledge, the PV modules are said to be the most reliable component and PE is said to possess most of the reliability problems in the power processing chain. Solving the reliability issues is of high priority since these phenomena will naturally increase because the annual growth rate of distributed generation is constantly growing. Practical time-domain testing and simulations are of great value in designing PE converters but they do not necessarily give comprehensive information according to which the observed problems can be solved. Therefore, the key for solving these problems lies in frequency-domain modeling of PV power systems.

This thesis analyzes the dynamic properties of grid-connected voltage source inverters (VSI) and shows that the inverter dynamics are determined not only by the power stage but also by the application where it is to be used. In power production, under grid-parallel mode, a VSI controls its input voltage and has to be analyzed as a current-fed topology having corresponding dynamic properties. Important information e.g. about the control dynamics is lost if the same power-stage is analyzed as a voltage-fed topology.

In addition, a general method to model the dynamic effect of source/load non-idealities in grid-connected current-fed and voltage-fed inverters regardless of the topology is presented. The source/load non-idealities can include either the internal impedance of the source/load subsystem and/or the dynamic effect of a passive input/output filter.

It is also demonstrated that a grid-connected input-voltage-controlled VSI incorporates an operating-point-dependent pole in the input-voltage-control loop caused by the cascaded input-voltage-output-current control scheme. The location of the pole on the complex plane can be given explicitly according to the input capacitance, operating point voltage and current, and the dynamic resistance of the PV generator. The pole shifts between the left and right halves of the complex plane according to the PVG operating point. Naturally, the pole causes control-system-design constraints when it is located on the right half of the complex plane (RHP). Furthermore, the RHP pole frequency is inversely proportional to the input capacitance, which implies that minimizing the input capacitance can lead to an unstable input voltage loop because the control loop has to be designed so that the loop crossover frequency is higher than the RHP pole frequency.

Therefore, a design rule between the input-capacitor sizing and input-voltage-control design is proposed. Typically, the input capacitor design is based on energy-based design criteria, e.g. input-voltage ripple or transient behavior. The energy-based criteria are important, although subjective, and do not necessarily guarantee the inverter stability. Therefore, in addition to the energy-based criteria, the control-based rule proposed in this thesis has to always be considered because it can be used to determine the inverter stability, which results in more reliable and robust PV inverter design.

PREFACE

This work was carried out at the Department of Electrical Energy Engineering at Tampere University of Technology (TUT) during the years 2010 – 2012. The research was funded by TUT and ABB Oy. Financial supports in the form of personal grants from the Finnish Foundation for Economic and Technology Sciences – KAUTE, Ulla Tuominen Foundation, Walter Ahlström Foundation, and Foundation for Technology Promotion (Tekniikan edistämissäätiö) are greatly appreciated.

I want to express my gratitude to Professor Teuvo Suntio for supervising my thesis and providing mentoring throughout my academic career as a researcher. The inspiring conversations and guidance were the main contributors to my fast graduation. My colleagues, M.Sc. Lari Nousiainen, M.Sc. Tuomas Messo, M.Sc. Anssi Mäki, M.Sc. Juha Huusari, M.Sc. Diego Torres Lobera, Dr.Tech. Jari Leppäaho, and the rest of the personnel in the Department of Electrical Energy Engineering provided a productive and inspiring working environment. Lic.Tech. Panu Lauttamus was a fair opponent in the gym as well as in the skiing tracks and shared my enthusiasm for listening to live music. I am thankful to Professors Hortensia Amaris and Hans-Peter Nee for examining my thesis and their constructive comments that improved the quality of my manuscript. I would also like to thank Merja Teimonen for providing valuable assistance regarding practical everyday matters. Pentti Kivinen and Pekka Nousiainen, in turn, deserve a special distinction for their craftsmanship in building experimental devices.

Finally, I want to thank my parents Sanna-Kaisa and Antti, my sister Susanna, my brother Aleksi, my spouse Minna, and her parents Raili and Pertti for all the support, encouragement and patience during my studies. Our Whippets also helped brighten up the days if the skies were gray.

Vantaa, September 2012

Joonas Puukko

SYMBOLS AND ABBREVIATIONS

ABBREVIATIONS

A	Ampere
AC, ac	Alternative current
AD	Analog-to-digital (conversion)
CC	Constant current
CCR	Constant current region (of a photovoltaic generator)
CF	Current-fed (i.e. supplied by a current source)
CV	Constant voltage
CVR	Constant voltage region (of a photovoltaic generator)
DA	Digital-to-analog (conversion)
DC, dc	Direct current
dB	Decibel
dBA	Decibel-ampere
dBS	Decibel-siemens
dBV	Decibel-volt
dBΩ	Decibel-ohm
DSP	Digital signal processor, processing
EMI	Electromagnetic interference
ESR	Equivalent series resistance
G	G-parameter model (i.e. voltage-to-voltage)
H	H-parameter model (i.e. current-to-current)
Hz	Hertz
IGBT	Insulated gate bipolar transistor
IU	Current-voltage (curve of a photovoltaic generator)
L1, L2, L3	Utility grid phases
LHP	Left half of the complex plane
m	Meter
MPP	Maximum power point
MPPT	Maximum power point tracking
N	Neutral (line), negative dc-bus
OC	Open circuit
P	Positive dc-bus
PE	Power electronics
PLL	Phase locked loop
p.u.	Per unit value
PV	Photovoltaic
PVG	Photovoltaic generator

PWM	Pulse width modulation
RHP	Right half of the complex plane
SC	Short circuit
SSA	State space averaging
V	Volt
VF	Voltage-fed (i.e. supplied by a voltage source)
VSI	Voltage source inverter
W	Watt
Y	Y-parameter model (i.e. voltage-to-current)
Z	Z-parameter model (i.e. current-to-voltage)

GREEK CHARACTERS

Δ	Characteristic equation of a transfer function (determinant), small perturbation
θ_{ref}	Voltage reference angle
φ	Angle
ω_{grid}	Grid frequency (rad/s)
ω_{loop}	Control loop crossover frequency (rad/s)
ω_{RHP}	RHP (pole/zero) frequency (rad/s)
ω_{s}	Grid frequency (rad/s)
ω_{z}	Transfer function zero frequency (rad/s)
Ω	Ohm

LATIN CHARACTERS

A	Diode ideality factor
$\mathbf{A}$	State coefficient matrix A
$\mathbf{B}$	State coefficient matrix B
C	Capacitance
C	Capacitor
$\mathbf{C}$	State coefficient matrix C
c_{pv}	Internal capacitance of a photovoltaic generator
d	Differential operator in Leibniz's notation for differentiation
d	Duty ratio
$\boldsymbol{d}$	Duty ratio space vector in stationary reference frame
$\hat{d}$	Perturbed duty ratio
D	Steady-state value of the duty ratio
$\mathbf{D}$	State coefficient matrix D
$\boldsymbol{f}$	General function in time domain
$f_{\text{-3dB}}$	Cut-off frequency of PV impedance magnitude curve (Hz)
f_{loop}	Control loop crossover frequency (Hz)

$\mathbf{G}$	Transfer function matrix
G_{a}	Modulator gain
G_{cc}	(Output) current controller transfer function
G_{ci}	Control-to-input transfer function
$\mathbf{G}_{\mathrm{ci}}$	Control-to-input transfer function matrix
G_{co}	Control-to-output transfer function
$\mathbf{G}_{\mathrm{co}}$	Control-to-output transfer function matrix
G_{cr}	Cross-coupling admittance
G_{io}	Forward (input-to-output) transfer function
$\mathbf{G}_{\mathrm{io}}$	Forward (input-to-output) transfer function matrix
$G_{\mathrm{se\text{-}v}}$	(Input) voltage sensing gain
G_{vc}	(Input) voltage controller transfer function
i_{ac}	Grid current
i_{C}	Capacitor current
i_{cpv}	Current through the capacitance c_{pv}
i_{d}	Diode current
i_{in}	Input current
$\hat{i}_{\mathrm{in}}$	Perturbed input current
$i_{\mathrm{inj.}}$	Injection current
i_{inv}	Inverter source (input) current
i_{L}	Inductor current
$\hat{i}_{\mathrm{L}}$	Perturbed inductor current
$\boldsymbol{i}_{\mathrm{L}}$	Inductor current space vector in stationary reference frame
i_{o}	Output current, diode saturation current
$\hat{i}_{\mathrm{o}}$	Perturbed output current
i_{P}	(Positive) dc-bus current
i_{ph}	Photocurrent, i.e. current generated via photovoltaic effect
i_{pv}	Terminal (output) current of a photovoltaic generator
i_{rsh}	Current through the resistance r_{sh}
I_{in}	Average input current
I_{L}	Average load or inductor current
I_{o}	Average output current
$\mathbf{I}$	Identity matrix
j	Complex variable
k	Boltzmann constant
k_{grid}	Coefficient regarding the input voltage control loop bandwidth
k_{i}	Safety coefficient regarding the short-circuit current of a PVG
k_{RHP}	Safety coefficient regarding RHP pole in the input voltage loop
L	Inductance
L	Inductor

L_{in}	Loop gain for input-voltage control loop
L_{out}	Loop gain for output-current control loop
N_{S}	Number of series-connected cells in a photovoltaic generator
p_{pv}	Power of a photovoltaic generator
q	Elementary charge
r_{C}	Equivalent series resistance of a capacitor
r_{d}	Diode resistance (non-linear)
r_{eq}	Equivalent resistance in a current path
r_{L}	Equivalent series resistance of an inductor
r_{pv}	Internal (dynamic) resistance of a photovoltaic generator
r_{s}	Internal series resistance of a photovoltaic generator
r_{sh}	Internal shunt resistance of a photovoltaic generator
r_{sw}	Switch on-state resistance
R_{eq}	Equivalent (output) current sensing resistor
R_{load}	Load resistance
R_{pv}	Static resistance of a photovoltaic generator
s	Laplace variable
T	Temperature
T_{oi}	Reverse (output-to-input) transfer function
$\mathbf{T}_{\text{oi}}$	Reverse (output-to-input) transfer function matrix
$\boldsymbol{u}(t)$	Input variable vector in time domain
$\hat{\boldsymbol{u}}(t)$	Perturbed input variable vector in time domain
u_{ac}	Grid voltage
u_{d}	Diode voltage
u_{in}	Input voltage
$\hat{u}_{\text{in}}$	Perturbed input voltage
u_{inv}	Inverter source (input) voltage
u_{C}	Capacitor voltage
u_{ch}	Frequency response analyzer input channel voltage
$u_{\text{inj.}}$	Injection voltage
u_{L}	Inductor voltage
$\boldsymbol{u}_{\text{L}}$	Inductor voltage space-vector in stationary reference frame
$\hat{u}_{\text{o}}$	Perturbed output voltage
$\boldsymbol{u}_{\text{o}}$	Output (grid) voltage space-vector in stationary reference frame
u_{pv}	Terminal (output) voltage of a photovoltaic generator
u_{ref}	Reference voltage
$u_{\text{trig.}}$	Trigger signal
U_{C}	Average capacitor voltage
U_{in}	Average input voltage
U_{o}	Average output voltage

$\boldsymbol{U}(s)$	Input variable vector in Laplace domain
$\boldsymbol{x}(t)$	State variable vector in time domain
$x_{\mathrm{z}}(t)$	Zero sequence component
$\hat{\boldsymbol{x}}(t)$	Perturbed state variable vector in time domain
$\boldsymbol{X}(s)$	State variable vector in Laplace domain
$\boldsymbol{y}(t)$	Output variable vector in time domain
$\hat{\boldsymbol{y}}(t)$	Perturbed output variable vector in time domain
$\boldsymbol{Y}(s)$	Output variable vector in Laplace domain
Y_{in}	Input admittance
Y_{o}	Output admittance
$\mathbf{Y}_{\mathrm{o}}$	Output admittance matrix
$Z_{\mathrm{elg.}}$	Elgar impedance
Z_{in}	Input impedance
$\mathbf{Z}_{\mathrm{in}}$	Input impedance matrix
Z_{o}	Output impedance

SUBSCRIPTS

-3dB	Refers to a minus three decibel point
α	Real component of stationary reference frame space vector
β	Imaginary component of stationary reference frame space vector
$-\infty$	Ideal transfer function
a,b,c	Utility grid phases
A,B,C	Utility grid phases
d, -d	Real component of synchronous reference frame space vector
dq, -dq	Between d and q-channels (cross-coupling)
grid	Utility grid
inj	Injection
L	Load, load-affected
loop	Control loop
max	Maximum
min	Minimum
n	Neutral point
N	Negative dc-rail
oc	Open-circuit
P	Positive dc-rail
q, -q	Imaginary component of synchronous reference frame space vector
qd, -qd	Between q and d-channels (cross-coupling)
RHP	Right half of the complex plane
rms	Root mean square value
S	Source, source-affected

SUPERSCRIPTS

$*$	Complex conjugate
-1	Matrix inverse
G	G-parameter model (i.e. voltage-to-voltage)
H	H-parameter model (i.e. current-to-current)
in	Input
iod	d-channel current
ioq	q-channel current
L	Load-affected
pv	Photovoltaic generator
r	Reduced-order transfer function
s	Synchronous reference frame
S	Source-affected
T	Transpose
out	Output current control loop is closed
out-in	Output current and input voltage control loops are closed
Y	Y-parameter model (i.e. voltage-to-current)
Z	Z-parameter model (i.e. current-to-voltage)

CONTENTS

1 INTRODUCTION

This chapter guides the reader through the backgrounds of grid-connected renewable power generation to the dynamic modeling of power electronic converters that are needed to interface renewables into the utility grid. A concise literature review about the previous work in this field will be given and several ambiguities will be pointed out. The structure, objectives and main scientific contributions of this thesis will be introduced.

1.1 Renewable Power Generation

Fossil fuels are the main energy source of the worldwide economy at the moment. In 2010, 87 % of total energy consumed was generated using fossil fuels, 6 % came from nuclear plants and the remaining 7 % from renewables such as solar, wind, hydro, geothermal, biofuels, tides and waves (Bose, 2010). Unfortunately, burning of fossil fuels has been shown to cause environmental pollution and global warming. Furthermore, there are limited supplies of fossil fuels and nuclear resources on our planet. Combined with the increasing need for energy and the rising prices of fossil fuels, cheaper and cleaner energy resources, the renewables, have lately become noteworthy alternatives for the traditional energy resources. (Bose, 2010; Liserre et al., 2010)

The substantial growth of utilizing renewables can be explained by their abundance on our planet and that once implemented they generate little or no emissions concerning the observed environmental issues (Bull, 2001). To date, hydro remains the most utilized renewable resource in the world (Wiese et al., 2009, 2010). However, wind and solar have shown constantly growing annual growth rates of which the latter is the fastest growing of the renewables at the moment with over 40 % of annual increase in the installed capacity during the last decade (Barroso et al., 2010; Kroposki et al., 2009).

Solar energy seems to be one of the most promising alternatives to fossil fuels. Kroposki et al. (2009) estimate that the Earth receives more energy from the Sun as electromagnetic radiation in an hour than the whole mankind consumes in a year. Abbott (2010), on the other hand, considers that utilizing 1 % of global sunlight with a conversion efficiency of 1 % would be enough to cover our energy needs and that "a 99 % solar future" is the only option in the long run. However, Abbott judges that the world's energy needs cannot be satisfied with just one type of energy source because they are unevenly distributed in our planet. This implies that the energy portfolio in the future

will be a mixture of existing technologies with an increasing portion of different renewables. Bull (2001); Valkealahti (2011) estimate that renewables have started to impact the global energy generation already from the beginning of 21st century and will have major impacts by the year 2050.

Major challenges regarding large scale utilization of renewables, especially solar power systems, are the intermittent nature of the source (Hart et al., 2012) and the relatively high cost per energy yield (Liserre et al., 2010). Hart et al. consider that generation planning and load balancing/regulation will become important issues in the future due to possible power fluctuations caused by the renewables. Taggart et al. (2012) argue in turn that averaging effects caused by a mixture of different renewables over a large geographic area will partly cancel out these problems. The cost of renewables has been decreasing steadily and according to Bull (2001), renewables could already be cheaper than fossil fuels if "the true hidden costs of fossil fuels – environmental costs, health costs, and energy security costs – were considered." Bull continues that, unfortunately, an acceptable way to include these expenses to the cost of energy have not yet been found.

1.2 Grid Integration of Photovoltaic Power Systems

Efficient grid integration of renewables requires the use of power electronics (PE) (Omura, 2010). PE devices contain circuitry that convert electrical energy from one form to a more desirable and usable form, provide protective functions for both the source and the utility grid that allow safe connection to the electric power system, and also metering and control functionality (Kroposki et al., 2010). PE devices process electrical power with semiconductors that are operated in switching mode yielding converters that may reach efficiencies of over 99 % (Rabkowski et al., 2012).

Besides converter topology selection and component sizing, the aforementioned control functionality of grid-connected PE devices is a key aspect in ensuring high quality power flow to the utility grid. Naturally, a high-bandwidth grid current control is a must in grid-connected applications so that undistorted sinusoidal currents can be injected into the grid. In addition to the grid-side control, photovoltaic (PV) power systems require some kind of a source-side control so that maximum power can be supplied to the utility grid.

The necessity of source-side control can be understood by considering the PV generator (PVG) current-voltage and power-voltage characteristics illustrated in Fig. 1.1: The produced electrical power p_{pv} reaches its maximum only at a single point along the current-voltage (IU) curve which is known as the maximum power point (MPP). Maximal power transfer can be achieved either by controlling the PVG voltage or current to the value dictated by the MPP, which is known as MPP tracking (MPPT). Various MPPT

methods can be found e.g. in Esram and Chapman (2007); Jain and Agarwal (2007).

According to Xiao et al. (2007, 2011), the PVG voltage is taken as the control variable in most applications because:

- voltage measurement is more accurate, cheaper and has a higher resolution than current measurement
- a voltage-oriented MPPT is the best way to avoid controller saturation that could happen under PV current control in fast-changing irradiance conditions because the PVG current is linearly proportional to the solar irradiance

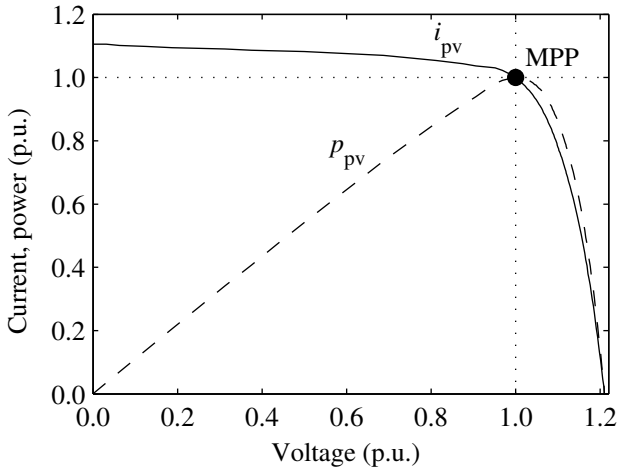

Fig. 1.1: Electrical characteristics of a photovoltaic generator.

1.2.1 Module Integrated, String, Multi String and Central Inverter Concepts

Fig. 1.2 presents one possible classification of different PV power systems. They are categorized by the type of connection of PV modules on the dc-side and are named from left to right as: module integrated, string, multi string and central inverter concepts (Araújo et al., 2010; Kjaer et al., 2005).

According to Araújo et al. (2010); Kjaer et al. (2005), the central inverter concept is the oldest one of the introduced concepts. PV modules are connected in series to form strings with high enough voltages required by the grid connection and further connected in parallel to increase the system power. String diodes can be used as protective devices to prevent reverse currents e.g. in case of a ground fault in one of the strings. A single inverter, which in the early days was a line-commutated three-phase thyristor bridge,

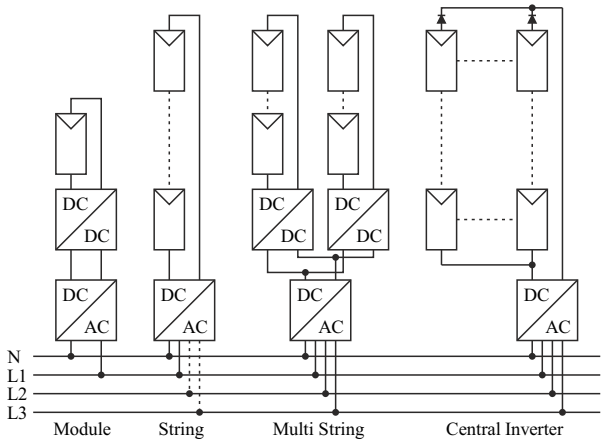

Fig. 1.2: Different photovoltaic generator configurations.

resulted in poor power quality because of large amounts of generated current harmonics. Nowadays, the thyristors have been replaced by modern switching devices such as insulated gate bipolar transistors (IGBTs) resulting in better harmonic performance because of faster switching speeds and frequencies. According to Araújo et al. (2010); Kjaer et al. (2005), drawbacks with this approach include:

- the considerable length of high-voltage dc cabling
- possible power losses due to centralized MPPT
- mismatch losses between PV modules
- additional losses in the string diodes
- a nonflexible design when the system upgrade to higher power levels is considered

The string concept, in turn, is a reduced version of the central inverter concept, where only one (or few) PV string(s) is (are) connected to the inverter. Grid connection can be single or three-phase, of which the former was preferred due to available single-phase full-bridge topologies that have lower voltage requirements in the dc-side compared to three-phase half-bridge topologies. However, three-phase topologies in the power range of 5–30 kW have have gained in popularity during the last few years. The number of series-connected PV modules is typically between 15–30, which yields open circuit voltages as high as 1000 volts. It is also possible to connect fewer modules in series or to expand the MPP voltage range if a two-stage interfacing scheme is applied (consider the multi-string concept with only one dc-dc converter) or a step-up line-frequency transformer is used.

The multi string concept is a development of the string concept: Each string is interfaced with its own dc-dc converter to a common dc-bus and further into the grid with a three-phase inverter. Each string is independently controlled with its own dc-dc converter, also known as a MPP-tracking converter, which may be beneficial e.g. in case of partial shading conditions (Mäki and Valkealahti, 2012). The dc-dc stage can also regulate its input to practically pure direct voltage, i.e. provides power decoupling, which can increase the energy yield compared to the single-stage single-phase inverters where the input power fluctuates at twice the grid frequency (Wu et al., 2011). String and multi-string interfacing schemes have better MPPT performance and fewer mismatch losses compared to the central inverter concept because of lower number of modules in dc-side and because each dc-dc converter has its own MPPT.

The module integrated concept is considered to be the future alternative composing of a single-phase grid connection and typically an isolated voltage-boosting dc-dc converter. Power levels are in the order of 100–200 watts. The main advantage of this concept is the individual MPPT for each module, which reduces the mismatch losses significantly compared to the other schemes. This concept is also highly modular and is considered to be a "plug-and-play-type" power plant, when the increase of system power level is considered. According to Araújo et al. (2010); Kjaer et al. (2005), the main challenges of this concept are:

- to design a converter that can efficiently step the PVG voltage up (and current down) to enable the grid connection
- highly reliable converters have to be designed because the number of converters in the system is high
- the cost of the overall plant can become higher compared to the other schemes

1.2.2 Single and Two-Stage Conversion Schemes

Another possibility in categorizing the interfacing schemes would be the number of power processing stages connected in series. The interfacing converter can be composed of one or two stages. The former is known as single and the latter as two-stage conversion scheme (Carrasco et al., 2006). Figs. 1.3 and 1.4 illustrate the aforementioned interfacing schemes as well as their highly simplified control structures.

Considering Figs. 1.3 and 1.4, it is obvious that the dc-ac inverter is responsible for both the grid current control and the MPPT function in the single-stage scheme. In the two-stage scheme, the dc-dc converter regulates its input voltage (thus performs the MPPT function) and the dc-ac inverter controls the grid currents. Goh et al. (2009); Konstantopoulos and Alexandridis (2011); Kroposki et al. (2010); Kwon et al. (2006);

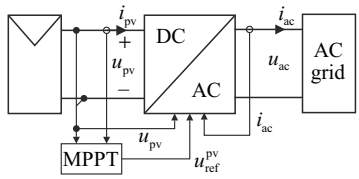

Fig. 1.3: Single-stage grid interface.

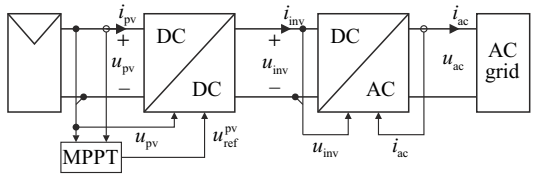

Fig. 1.4: Two-stage grid interface.

Tirumala et al. (2002); Vighetti et al. (2012) indicate that the dc-dc converter would control the dc-link voltage in the two-stage conversion scheme. However, it has been proven by Leppäaho et al. (2010); Nousiainen et al. (2012); Puukko, Nousiainen, Mäki, Messo, Huusari and Suntio (2012) that the dc-dc converter cannot regulate the dc-link voltage if maximum power is to be supplied to the power grid. Therefore, the dc-ac inverter has to control its input voltage also in the two-stage conversion scheme as correctly stated in Teodorescu and Blaabjerg (2004); Trujillo et al. (2012). Hence, the dc-ac inverter incorporates a cascaded input-voltage output-current control structure in both of the conversion schemes. This obvious notion is of utmost importance when the small-signal (i.e. dynamic) modeling of three-phase inverters is discussed later in this thesis.

1.3 Photovoltaic Generator as an Input Source for Power Electronic Converters

Electrical characteristics of a PV cell can be represented by a single-diode model, which consists of a photocurrent source with a parallel connected diode and parasitic elements as illustrated in Fig. 1.5 (Liu and Dougal, 2002; Villalva et al., 2009a), where i_{pv} and u_{pv} are the PV cell terminal current and voltage, i_{ph} is the photocurrent, i_{cpv} the current through the capacitance c_{pv} and i_{rsh} the current through the shunt resistance r_{sh}. The series and shunt resistances r_{s} and r_{sh} represent various non-idealities in a real PV cell such as the ohmic losses in the conductors and the diffusion current through the pn-junction. The relation between diode current i_{d} and voltage u_{d} can be modeled with an exponential equation, yielding a non-linear resistance r_{d} that can be used instead of the diode-symbol in Fig. 1.5 (Chenvidhya et al., 2005; Liu and Dougal, 2002). The one-diode model can also be used to model the operation of a PV module (i.e. a series connection

of PV cells) or a PVG (i.e. a series and/or parallel connection of PV modules), by scaling model parameters as presented in Villalva et al. (2009a). The terminal current i_{pv} can be given e.g. by

$$i_{\mathrm{pv}} = i_{\mathrm{ph}} - i_{\mathrm{o}} \left[exp\left(\frac{u_{\mathrm{pv}} + r_{\mathrm{s}} i_{\mathrm{pv}}}{N_{\mathrm{S}} A k T / q} \right) - 1 \right] - \frac{u_{\mathrm{pv}} + r_{\mathrm{s}} i_{\mathrm{pv}}}{r_{\mathrm{sh}}}, \tag{1.1}$$

where i_{o} is the diode saturation current, N_{S} the number of cells connected in series, A the diode ideality factor, k the Boltzmann coefficient and q the elementary charge.

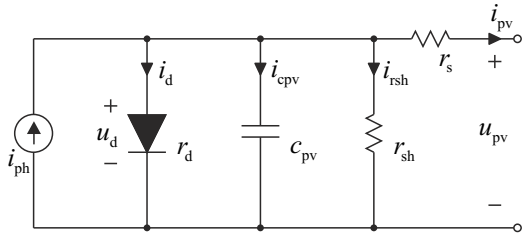

Fig. 1.5: Single-diode model of a photovoltaic cell.

Measured static (current-voltage and power-voltage-curves) and dynamic (r_{pv} and c_{pv}) characteristics of a commercial 36-cell PV module are shown in Fig. 1.6 as per unit (p.u.) values. Considering Figs. 1.5 and 1.6, it is obvious that a PVG is a highly non-linear current source having both limited output voltage and power. More detailed information about the electrical properties of the PVG presented in Fig. 1.6 can be found in (Mäki et al., 2010; Nousiainen et al., 2012; Puukko, Nousiainen, Mäki, Messo, Huusari and Suntio, 2012) and Chapter 4 in this thesis.

The dynamic resistance r_{pv} in Fig. 1.6, also known as small-signal or incremental resistance, represents the low-frequency value of the PVG impedance being the most significant variable that will have an effect on converter dynamics as will be discussed in more detail later in Section 4.2.

Some articles consider the r_{pv} to be a negative resistance (Bae et al., 2008; Lee et al., 2008; Venturini et al., 2008; Xiao et al., 2007) and others positive (Figueres et al., 2007; Mäki et al., 2010; Thongpron et al., 2006). The sign of r_{pv} is important to be defined correctly because of its fundamental effect on the dynamic behavior of the converter supplied by the PVG. Improper treatment of r_{pv} can e.g. lead to false conclusions on the stability of the interface between the PVG and the converter, which naturally can affect the system design.

If the direction of positive current flow is defined out of the PVG as usually done (Fig. 1.5), that, in turn, produces the IU-curve as in Fig. 1.6, r_{pv} can be defined according

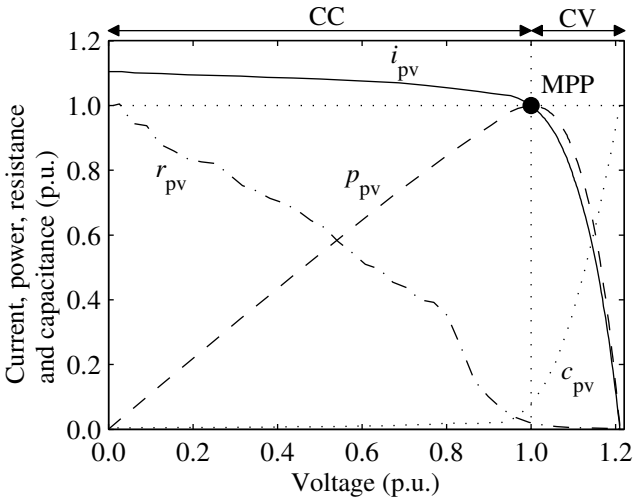

Fig. 1.6: Measured electrical characteristics of a photovoltaic generator.

to Kirchhoff's and Ohm's laws by

$$r_{\mathrm{pv}} = -\frac{\mathrm{d}u_{\mathrm{pv}}}{\mathrm{d}i_{\mathrm{pv}}} \approx -\frac{\Delta u_{\mathrm{pv}}}{\Delta i_{\mathrm{pv}}}, \tag{1.2}$$

which is positive since $\mathrm{d}u_{\mathrm{pv}}/\mathrm{d}i_{\mathrm{pv}} \approx \Delta u_{\mathrm{pv}}/\Delta i_{\mathrm{pv}}$ in Fig. 1.6 is negative.

1.4 Motivation of the Thesis

Power electronics plays an important role in grid integration of PV power systems. It has been discussed e.g. by Guerrero et al. (2010); Kroposki et al. (2009); Liserre et al. (2010); Petrone et al. (2008) that the PV modules are the most reliable components and that the power electronics possess most of the reliability problems in the power processing chain.

According to Kotsopoulos et al. (2001); Krein and Balog (2009); Rodriguez and Amaratunga (2008), the major reliability issue in PV inverters is said to be the type and size of the input capacitor that is needed to filter the pulsating current drawn by a VSI-type PV inverter. Electrolytic capacitors are preferred because they have high capacitance to volume ratios and are relatively cheap. However, the lifetime of electrolytic capacitors in elevated temperatures is known to be limited, which could be one source of the aforementioned reliability problems. Minimizing the input capacitance would enable e.g. the use of film capacitors that do not have similar life limiting properties but can, on the other hand, introduce e.g. sub-harmonic oscillation problems or instability (Fratta et al., 2002; Puukko, Nousiainen and Suntio, 2011).

Correct selection of the input capacitor can improve the reliability of the PV inverter

itself, but a robust component design is not the only aspect that needs to be taken into account when designing grid-connected power systems. Grid-connected inverters can interact with each other or with the power grid and have actually been observed to increase harmonic distortion and reduce damping in the grid caused by negative output impedance -behavior (Chen and Sun, 2011; Enslin, 2005; Enslin and Heskes, 2004; Heskes et al., 2010; Liserre et al., 2004; Sun, 2008, 2009; Visscher and Heskes, 2005). Reduction of damping in the grid can be avoided if the origin of negative output impedance can be found and corrective actions are taken (Nousiainen et al., 2011b; Puukko, Messo, Nousiainen, Huusari and Suntio, 2011). Harmonic distortion caused by the inverters can be diminished, in turn, if the output impedance of the inverter can be made as high as possible (Céspedes and Sun, 2009; Enslin and Heskes, 2004; Prodanović and Green, 2003; Wang et al., 2011).

Solving the aforementioned issues is of high priority since these phenomena will naturally increase because the penetration level of distributed generation is constantly growing. Practical time-domain testing and simulations are of great value in designing PE converters but they do not necessarily give comprehensive information according to which the observed problems can be solved. Therefore, the key for solving these problems lies in proper frequency-domain modeling of PV power systems.

1.4.1 Frequency-Domain Modeling of Power Electronic Converters

Small-Signal Modeling of Dc-Dc Converters

The dynamic behavior of dc-dc converters can be modeled up to half the switching frequency in the frequency-domain using the well known state-space averaging (SSA) techniques developed by Middlebrook in the 70's. The resulting small-signal model is in a key role in deterministic control design and analysis of different impedance interactions within the system. (Middlebrook, 1988; Middlebrook and Ćuk, 1976, 1977)

The SSA-model itself has to be constructed so that the model describes only the internal dynamics of the converter. This means that the effect of source/load as well as possible input/output filters are removed. With this approach the dynamic model of the converter is general and the effects of source/load non-idealities or input/output filters can later be included in the model depending on the application.

Formulation of the small-signal model begins by averaging the converter behavior over a single switching cycle. The average-valued equations for the time derivatives of state variables $\boldsymbol{x}(t)$ (inductor currents and capacitor voltages in the circuit) and the controllable output variables $\boldsymbol{y}(t)$ are expressed as functions of state $\boldsymbol{x}(t)$ and uncontrollable input variables $\boldsymbol{u}(t)$ as presented in (1.3), where the angle brackets denote average values and

bold-italic fonts denote vectors.

$$\begin{aligned} \frac{\mathrm{d}\langle \boldsymbol{x}(t)\rangle}{\mathrm{d}t} &= \boldsymbol{f}_1\big(\langle \boldsymbol{x}(t)\rangle, \langle \boldsymbol{u}(t)\rangle\big) \\ \langle \boldsymbol{y}(t)\rangle &= \boldsymbol{f}_2\big(\langle \boldsymbol{x}(t)\rangle, \langle \boldsymbol{u}(t)\rangle\big) \end{aligned} \tag{1.3}$$

The average-valued equations in (1.3) are next used to compute the steady-state operating point of the converter by letting the time-derivatives be zero and replacing the lower-case average values with their corresponding upper-case steady-state values.

In order to define the transfer functions between the system inputs and outputs, the averaged state-space in (1.3) has to be linearized at the predefined operating point as presented in (1.4), where the hat over the state, input, and output variable vectors denotes a small perturbation around the operating point. The linearization is mandatory since the average model is non-linear due to the switching action.

$$\begin{aligned} \frac{\mathrm{d}\hat{\boldsymbol{x}}(t)}{\mathrm{d}t} &= \mathbf{A}\,\hat{\boldsymbol{x}}(t) + \mathbf{B}\,\hat{\boldsymbol{u}}(t) \\ \hat{\boldsymbol{y}}(t) &= \mathbf{C}\hat{\boldsymbol{x}}(t) + \mathbf{D}\,\hat{\boldsymbol{u}}(t) \end{aligned} \tag{1.4}$$

The linearized time-domain state-space representation in (1.4) can be transformed into the Laplace domain as presented in (1.5) from which the transfer functions can be solved by using basic matrix algebra as given by (1.6), which describes the relationship between the input and state variables, and (1.7), which describes the relationship between input and output variables.

$$\begin{aligned} s\boldsymbol{X}(s) &= \mathbf{A}\,\boldsymbol{X}(s) + \mathbf{B}\,\boldsymbol{U}(s) \\ \boldsymbol{Y}(s) &= \mathbf{C}\,\boldsymbol{X}(s) + \mathbf{D}\,\boldsymbol{U}(s) \end{aligned} \tag{1.5}$$

$$\boldsymbol{X}(s) = (s\mathbf{I} - \mathbf{A})^{-1}\,\mathbf{B}\,\boldsymbol{U}(s) \tag{1.6}$$

$$\boldsymbol{Y}(s) = \Big[\mathbf{C}\,(s\mathbf{I} - \mathbf{A})^{-1}\,\mathbf{B} + \mathbf{D}\Big]\;\boldsymbol{U}(s) = \mathbf{G}\,\boldsymbol{U}(s) \tag{1.7}$$

According to Suntio (2009); Tse (1998), there exist four types of converters depending on the definition of the system inputs and outputs: voltage-to-voltage, voltage-to-current, current-to-current or current-to-voltage converter. A common feature to all these different converters is the existence of duality in the source and load side interfaces: a current source is loaded by a voltage-type load and a voltage source by a current sink.

Eq. (1.7) can be presented for voltage-to-voltage converters (an input-current- and/or output-voltage-controlled converter) as a G-parameter model in matrix form as in (1.8)

and as a linear model as in Fig. 1.7.

$$\begin{bmatrix} \hat{i}_{\mathrm{in}} \\ \hat{u}_{\mathrm{o}} \end{bmatrix} = \begin{bmatrix} Y_{\mathrm{in}}^{\mathrm{G}} & T_{\mathrm{oi}}^{\mathrm{G}} & G_{\mathrm{ci}}^{\mathrm{G}} \\ G_{\mathrm{io}}^{\mathrm{G}} & -Z_{\mathrm{o}}^{\mathrm{G}} & G_{\mathrm{co}}^{\mathrm{G}} \end{bmatrix} \begin{bmatrix} \hat{u}_{\mathrm{in}} \\ \hat{i}_{\mathrm{o}} \\ \hat{d} \end{bmatrix} \tag{1.8}$$

Eq. (1.7) can be presented for voltage-to-current converters (an input-current- and/or output-current-controlled converter) as a Y-parameter model in matrix form as in (1.9) and as a linear model as in Fig. 1.8.

$$\begin{bmatrix} \hat{i}_{\mathrm{in}} \\ \hat{i}_{\mathrm{o}} \end{bmatrix} = \begin{bmatrix} Y_{\mathrm{in}}^{\mathrm{Y}} & T_{\mathrm{oi}}^{\mathrm{Y}} & G_{\mathrm{ci}}^{\mathrm{Y}} \\ G_{\mathrm{io}}^{\mathrm{Y}} & -Y_{\mathrm{o}}^{\mathrm{Y}} & G_{\mathrm{co}}^{\mathrm{Y}} \end{bmatrix} \begin{bmatrix} \hat{u}_{\mathrm{in}} \\ \hat{u}_{\mathrm{o}} \\ \hat{d} \end{bmatrix} \tag{1.9}$$

Eq. (1.7) can be presented for current-to-current converters (an input-voltage- and/or output-current-controlled converter) as an H-parameter model in matrix form as in (1.10) and as a linear model as in Fig. 1.9.

$$\begin{bmatrix} \hat{u}_{\mathrm{in}} \\ \hat{i}_{\mathrm{o}} \end{bmatrix} = \begin{bmatrix} Z_{\mathrm{in}}^{\mathrm{H}} & T_{\mathrm{oi}}^{\mathrm{H}} & G_{\mathrm{ci}}^{\mathrm{H}} \\ G_{\mathrm{io}}^{\mathrm{H}} & -Y_{\mathrm{o}}^{\mathrm{H}} & G_{\mathrm{co}}^{\mathrm{H}} \end{bmatrix} \begin{bmatrix} \hat{i}_{\mathrm{in}} \\ \hat{u}_{\mathrm{o}} \\ \hat{d} \end{bmatrix} \tag{1.10}$$

Eq. (1.7) can be presented for current-to-voltage converters (an input-voltage- and/or output-voltage-controlled converter) as a Z-parameter model in matrix form as in (1.11) and as a linear model as in Fig. 1.10.

$$\begin{bmatrix} \hat{u}_{\mathrm{in}} \\ \hat{u}_{\mathrm{o}} \end{bmatrix} = \begin{bmatrix} Z_{\mathrm{in}}^{\mathrm{Z}} & T_{\mathrm{oi}}^{\mathrm{Z}} & G_{\mathrm{ci}}^{\mathrm{Z}} \\ G_{\mathrm{io}}^{\mathrm{Z}} & -Z_{\mathrm{o}}^{\mathrm{Z}} & G_{\mathrm{co}}^{\mathrm{Z}} \end{bmatrix} \begin{bmatrix} \hat{i}_{\mathrm{in}} \\ \hat{i}_{\mathrm{o}} \\ \hat{d} \end{bmatrix} \tag{1.11}$$

The same power-stage can be analyzed as any one of these four different alternatives each having unique dynamic properties compared to the others. Therefore, the definition of input and output variables, which is the first step in performing SSA, should be considered carefully because it is the main factor in determining the dynamic behavior of the converter.

Small-Signal Modeling of Three-Phase Converters

Ngo (1986) suggests that it is natural to expect a common analysis technique to exist for all PE converters regardless of whether they are dc-dc, dc-ac or ac-dc, single or three-phase converters. The SSA-method requires that the non-linear average-valued model is

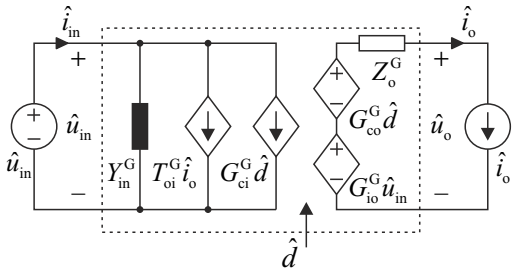

Fig. 1.7: Linear G-parameter model of a voltage-to-voltage converter.

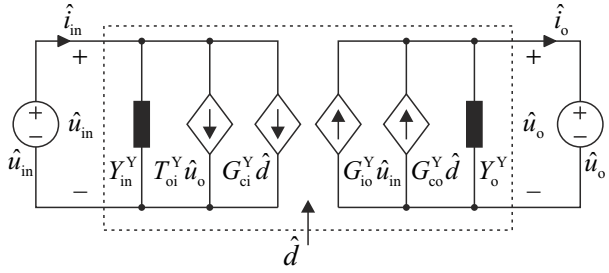

Fig. 1.8: Linear Y-parameter model of a voltage-to-current converter.

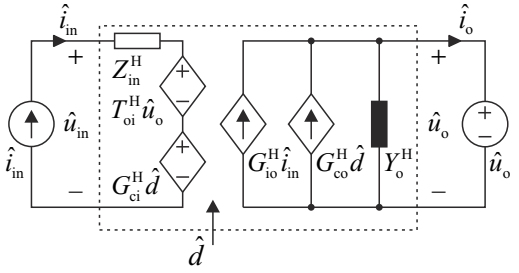

Fig. 1.9: Linear H-parameter model of a current-to-current converter.

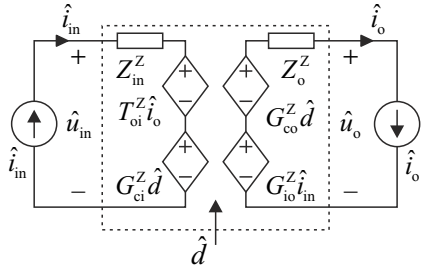

Fig. 1.10: Linear Z-parameter model of a current-to-voltage converter.

linearized at the steady-state operating point. However, for dc-ac and ac-dc converters such a point does not exist since the grid-variables are constantly varying sinusoidal quantities. This implies that the SSA-method cannot be implemented as such for the analysis of these converters.

Fortunately, sinusoidal three-phase variables can be expressed in the synchronous reference frame, i.e. in a coordinate system that rotates at the grid frequency, as two complex-valued time-invariant variables and a real-valued zero-sequence component by using the transformation formulated by Park (1929), which is later referred to as Park's or dq-transformation in this thesis.

The major difference between the analysis of dc-dc and three-phase dc-ac or ac-dc converters is that after the three-phase average-valued equations have been computed, they have to be transformed into the synchronous reference frame so that the operating point can be solved at which the linearization is later performed. Otherwise the analysis follows similar guidelines in both cases.

Despite the frequency-domain analysis of dc-dc converters being well established in the literature, there are three major unambiguities in analyzing grid-connected three-phase converters yielding in small-signal models that may not predict the correct dynamics of the system.

Firstly, a dc-ac converter used in grid-parallel mode of operation can be assumed to be loaded by a passive circuit (resistive-inductive or resistive) as e.g. in Alepuz et al. (1999, 2005); Bordonau et al. (1997); Hiti et al. (1994); Yazdani and Dash (2009). This assumption will result in heavily damped frequency responses, which can hide important information on the converter dynamics as discussed in Puukko, Nousiainen and Suntio (2012) and Section 3.2.

Secondly, the definition of system inputs and outputs can be inconsistent compared to the proposed application. Basic control and circuit theories dictate that a converter connected to a stiff voltage-type load (i.e. the grid for dc-ac inverters) has to be analyzed so that the grid voltage is a system input, which makes the grid current a system output, i.e. as either an H-parameter model as in Fig. 1.9 or a Y-parameter model as in Fig. 1.8. Furthermore, if the input voltage of the converter is to be controlled (i.e. it is also a system output), the converter has to be analyzed so that it is supplied by a current-type input source (input current is a system input). This means that an input-voltage-controlled grid-connected converter, as usually is the case in PV applications, has to be analyzed as the H-parameter model. Examples about inconsistencies in defining the correct input and output variables can be found e.g. from Alepuz et al. (2003); Castilla et al. (2008); Liu et al. (2011); Sahan et al. (2008).

Thirdly, an explicit way of formulating the effect of source/load non-idealities in three-phase inverters has not been presented in the literature even though it is known

that the source properties can change the dynamic behavior of the converter profoundly as emphasized by Suntio et al. (2011).

1.4.2 Modeling of Photovoltaic Power Systems

In general, the static current-voltage characteristics, the different operating regions (constant current and voltage), the previously discussed single-diode model and the internal current source structure of a PVG as well as the cascaded input-voltage-output-current control scheme of a PV interfacing converter are well known among the practicing engineers. The input-voltage control of the interfacing converter necessitates its analysis as a current-fed (CF) topology as previously discussed and the non-linear terminal characteristics of a PVG cause the converter dynamics to change according to different PVG operating points (Nousiainen et al., 2011a; Puukko, Messo and Suntio, 2011; Puukko and Suntio, 2012a).

Despite all this information, a PVG can be considered as a voltage-type input source sometimes as such or connected in series with a static resistor as can be seen in Cao et al. (2011); Chen and Smedley (2008); Mirafzal et al. (2011); Photong et al. (2010); Schonardie and Martins (2007, 2008); Sun et al. (2011); Tse et al. (2004); Villalva et al. (2010, 2009b); Zhao et al. (2012). The validity of this kind of research can be questionable since wrong definition of the input and output variables as well as not treating the PVG as an operating-point-dependent source hides important information about the converter dynamics as will be shown in Chapter 4.

Few articles consider the PVG correctly as a current source, but Figueres et al. (2009) fail to notice certain important dynamic properties of a PV inverter although the information is clearly visible in the article, and Alepuz et al. (2006); Yazdani et al. (2011) consider only time-domain waveforms. Femia et al. (2008), in turn, have included the operating-point-dependent dynamics correctly, but unfortunately the article covers only dc-dc converters.

1.5 Structure of the Thesis

Frequency-domain modeling of grid-connected three-phase VSI-type inverters is covered in detail in Chapter 2. An explicit method to include the effects of source/load non-idealities and cascaded input-output-control system are formulated and the main differences between a VSI-type inverter supplied by either a voltage or a current source are discussed.

A method to verify the proposed VSI small-signal model is presented in Chapter 3. The problematics in measuring three-phase inverter transfer functions are discussed, which include processing of virtual quantities (i.e. voltages and currents in the synchronous reference frame) that do not exist in real life. Also the significance of using an

active load instead of a passive one is analyzed.

Chapter 4 analyses the effect that a PVG will have on the inverter control dynamics. Theoretical analyses are proven by experimental frequency response measurements. A control-system-based design criteria that can be used to compute the minimum input capacitance that is required to guarantee the stability of a VSI-type inverter in all PVG operating points is also proposed.

Final conclusions are drawn and the future research topics are discussed in Chapter 5.

1.6 Objectives and the Main Scientific Contributions

Firstly, this thesis analyzes the dynamic properties of grid-connected VSI-type inverters and shows that the VSI dynamics are determined by the application where it is to be used, not just by the power stage. In power production applications under grid-parallel mode of operation, a VSI controls its input voltage and has to be analyzed as a CF topology having corresponding specific dynamic properties. Important information about the control dynamics (i.e. how the control system should be designed) or the output impedance of the VSI (i.e. what kind of grid interactions the VSI could cause) is lost if the same power stage is analyzed as a VF topology.

Secondly, this thesis presents an explicit method to model the dynamic effect of source/load non-idealities in all grid-connected CF and VF inverters regardless of the topology. The source non-idealities can include either the internal impedance of the source subsystem and/or the dynamic effect of a passive input filter. The load non-idealities, in turn, can include either the internal impedance of the load subsystem and/or the dynamic effect of a passive output filter.

Thirdly, the aforementioned issues are verified when the dynamic properties of a grid-connected three-phase VSI-type inverter are analyzed in PV applications in theory as well as in practice. The results show that a PVG is a challenging input source when inverter design is considered. This is due to the fact that the dynamic properties of the inverter change according to the operating point along the PVG IU-curve. Changes are caused by the non-linear source impedance of a PVG. Therefore, the source-effect of a PVG should always be taken into account when a PV inverter is designed.

Fourthly, this thesis demonstrates that a grid-connected input-voltage-controlled inverter in PV applications incorporates an operating-point-dependent pole in the input-voltage-control loop caused by the cascaded input-voltage-output-current control scheme. The location of the pole on the complex plane can be given explicitly according to the input capacitance, input (i.e. PV) voltage and current, and the dynamic resistance of the PVG. The pole shifts between the left and right halves of the complex plane according to the operating point along the PVG IU-curve. Naturally, the pole causes control-system-design constraints when it is located on the right half of the complex plane (RHP).

Furthermore, the RHP pole frequency is inversely proportional to the input capacitance, which implies that minimizing the input capacitance can lead to unstable input voltage loop because the control loop has to be designed so that the loop crossover frequency is higher than the RHP pole frequency.

Therefore, a design rule between the input-capacitor sizing and input-voltage-control design is proposed. Typically, the input capacitor design is based on energy-based design criteria, e.g. input-voltage ripple or transient behavior. The energy-based criteria are important, although subjective, and do not necessarily guarantee the inverter stability. Therefore, in addition to the energy-based criteria, the rule proposed in this thesis has to be always considered because it determines the inverter stability, which results in more reliable and robust PV inverter design.

The practical verification of the theoretical findings by means of frequency-response measurements from the three-phase inverter prototype requires also special attention since the small-signal model of a three-phase converter uses virtual quantities (currents and voltages in the synchronous reference frame) that do not exist in real life.

The main scientific contributions of this thesis can be summarized as:

- An explicit formulation that the input source (voltage/current source) determines the dynamics of a three-phase converter has been presented and verified
- An explicit method to include the effects of source and load non-idealities in three-phase converter dynamics have been formulated
- Dynamic effects of a photovoltaic generator in grid-connected VSI-type inverters have been analyzed
- A control-system-design-based input-capacitor-design constraint for a three-phase VSI-type inverter has been proposed

1.6.1 Related Publications

The following publications relate to the topic of this thesis.

[P1] Puukko, J., Messo, T., and Suntio, T. (2011). "Effect of photovoltaic generator on a typical VSI-based three-phase grid-connected photovoltaic inverter dynamics," in *IET Renew. Power Gener. Conf., RPG*, pp. 1–6.

[P2] Puukko, J., Messo, T., Nousiainen, L., Huusari, J., and Suntio, T. (2011). "Negative output impedance in three-phase grid-connected renewable energy source inverters based on reduced-order model," in *IET Renew. Power Gener. Conf., RPG*, pp. 1–6.

[P3] Puukko, J., Nousiainen, L., and Suntio, T. (2011). "Effect of minimizing input capacitance in VSI-based renewable energy source converters," in *IEEE Int. Telecommun. Energy Conf., INTELEC*, pp. 1–9.

[P4] Puukko, J., Nousiainen, L., and Suntio, T. (2012). "Three-phase photovoltaic inverter small-signal modelling and model verification," in *IET Power Electron. Machines Drives Conf., PEMD*, pp. 1–6.

[P5] Puukko, J., Nousiainen, L., Mäki, A., Messo, T., Huusari, J., and Suntio, T. (2012). "Photovoltaic generator as an input source for power electronic converters," in *Int. Power Electron. Motion Control Conf. Expo., EPE-PEMC*, pp. 1–9.

[P6] Puukko, J., and Suntio, T. (2012). "Modelling the effect of a non-ideal load in three-phase converter dynamics," *IET Electron. Lett.*, Vol. 48, No. 7, pp. 402–404.

[P7] Puukko, J., and Suntio, T. (2012). "Dynamic properties of a VSI-based three-phase inverter in photovoltaic application," *IET Renew. Power Gener.*, accepted for publication.

[P8] Nousiainen, L., Puukko, J., Mäki, A., Messo, T., Huusari, J., Jokipii, J., Viinamäki, J., Torres Lobera, D., Valkealahti, S., and Suntio, T. (2012). "Photovoltaic generator as an input source for power electronic converters," *IEEE Trans. Power Electron*, DOI: 10.1109/TPEL.2012.2209899.

[P9] Nousiainen, L., Puukko, J., and Suntio, T. (2011). "Appearance of a RHP-zero in VSI-based photovoltaic converter control dynamics," in *IEEE Int. Telecommun. Energy Conf., INTELEC*, pp. 1–8.

[P10] Nousiainen, L., Puukko, J., and Suntio, T. (2011). "Simple VSI-based single-phase inverter: dynamical effect of photovoltaic generator and multiplier-based grid synchronization," in *IET Renew. Power Gener. Conf., RPG*, pp. 1–6.

[P11] Messo, T., Puukko, J., and Suntio, T. (2012). "Dynamic effect of MPP-tracking converter on the dynamics of VSI-based inverter in PV applications," in *IET Power Electron. Machines Drives Conf., PEMD*, pp. 1–6.

Publications [P1]–[P8] are written and the theoretical analysis/experimental measurements are performed by the author of this thesis. In [P1], M.Sc. Messo helped with the dynamic modeling of the three-phase inverter. In [P2], M.Sc. Messo helped with the experimental measurements and writing of the article, M.Sc. Nousiainen with the experimental measurements and the DSP implementation of the prototype control system, and M.Sc. Huusari with the prototype power stage and layout design. In [P3] and [P9], the theory and idea behind the article was formulated together with M.Sc.

Nousiainen. The theoretical analysis and writing of [P3] was done by the author of this thesis and [P9] by M.Sc Nousiainen. In [P4], M.Sc. Nousiainen helped with designing the frequency response measurement setup, the prototype power-stage, layout design, DSP coding, as well as the experimental measurements. In [P5], M.Sc. Nousiainen performed the analysis regarding single-phase inverter interfacing and helped with the experimental measurements, M.Sc Mäki helped with the experimental measurements and writing of the article, M.Sc. Messo performed the analysis regarding the dc-dc converter interfacing and helped with the experimental measurements, and M.Sc. Huusari helped with the experimental measurements. In [P8], the author of this thesis performed the analysis regarding three-phase inverter interfacing and experimental measurements and wrote the article together with M.Sc. Nousiainen. The other authors helped with the measurements and proofreading of the article. In [P10], the author of this thesis helped with the experimental measurements and theoretical analyses although M.Sc. Nousiainen was the main contributor. In [P11], the author of this thesis helped writing the article and theoretical analyses although M.Sc Messo was the main contributor. Professor Teuvo Suntio, the supervisor of this thesis, gave valuable and inspiring comments regarding these publications.

2 FREQUENCY-DOMAIN MODELING OF THREE-PHASE VSI-TYPE INVERTERS

The first part of this chapter presents the dynamic profiles of grid-connected voltage (VF) and current-fed (CF) VSI-type inverters when supplied and loaded by ideal sources and loads, i.e. their un-terminated models. The difference between the analyzed converters is the type of the input source, one is supplied by a voltage source and the other by a current source. It will be shown that although the power stages resemble each other the inverters have unique dynamic properties.

This chapter also presents an explicit way of computing the effect of source and load non-idealities for both the VF and CF-VSIs. The presented method is general, i.e. it is not power-stage-dependent and can be used to model the effects of source/load non-idealities in all grid-connected VF and CF inverters. The last section of this chapter concentrates on analyzing the differences between the dynamics of VF and CF-VSIs.

2.1 Grid-Connected Voltage-Fed VSI

Fig. 2.1 presents a grid-connected VF-VSI. The power stage consists of the switch matrix and the output inductors. It is well known that in order to supply undistorted currents to the utility grid, the presented topology requires the input voltage to be greater in magnitude than twice or $\sqrt{3}$ times the peak value of the grid phase voltages with an adequate margin depending on the modulating method. This implies that the VF-VSI has buck-type characteristics (since the voltage level steps down between the source and load terminals) as will be shown in Section 2.6.

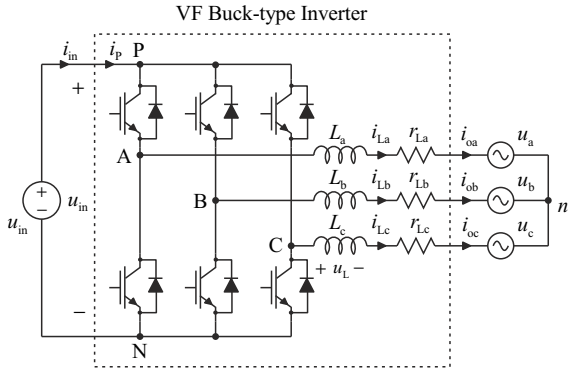

Fig. 2.1: Grid-connected three-phase voltage-fed VSI-type inverter.

In case of the VF-VSI in Fig. 2.1, the system inputs are the input and grid phase voltages (u_{in} and $u_{(\mathrm{a,b,c})\mathrm{n}}$). Thus, the outputs are the input and grid phase currents (i_{in} and $i_{\mathrm{o(a,b,c)}}$).

2.1.1 Average Model

SSA modeling begins by computing the average-valued equations for the time derivatives of the state variables $\boldsymbol{x}(t)$ and the controllable output variables $\boldsymbol{y}(t)$ as functions of state $\boldsymbol{x}(t)$ and uncontrollable input variables $\boldsymbol{u}(t)$ as discussed in Chapter 1. Average values for the inductor voltages can be given according to the notations of Fig. 2.1

$$\langle u_{\mathrm{La}}\rangle = \langle u_{\mathrm{AN}}\rangle - r_{\mathrm{La}}\langle i_{\mathrm{La}}\rangle - \langle u_{\mathrm{an}}\rangle - \langle u_{\mathrm{nN}}\rangle, \tag{2.1}$$

$$\langle u_{\mathrm{Lb}}\rangle = \langle u_{\mathrm{BN}}\rangle - r_{\mathrm{Lb}}\langle i_{\mathrm{Lb}}\rangle - \langle u_{\mathrm{bn}}\rangle - \langle u_{\mathrm{nN}}\rangle, \tag{2.2}$$

$$\langle u_{\mathrm{Lc}}\rangle = \langle u_{\mathrm{CN}}\rangle - r_{\mathrm{Lc}}\langle i_{\mathrm{Lc}}\rangle - \langle u_{\mathrm{cn}}\rangle - \langle u_{\mathrm{nN}}\rangle, \tag{2.3}$$

where the angle brackets denote average values. Using (2.1)–(2.3), $r_{\mathrm{L}} = r_{\mathrm{L(a,b,c)}}$, $r_{\mathrm{eq}} = r_{\mathrm{sw}} + r_{\mathrm{L}}$ and averaging the inverter phase-leg behavior over a single switching cycle yields the average-valued model of a VF-VSI as presented in (2.4)–(2.10), where $d_{\mathrm{A,B,C}}$ is the

duty ratio of the upper switch in the corresponding phase-leg, r_{eq} is the equivalent series resistance including the switch on-state resistance r_{sw} and the inductor ESR r_{L}.

$$\langle u_{\mathrm{La}}\rangle = d_{\mathrm{A}}\langle u_{\mathrm{in}}\rangle - r_{\mathrm{eq}}\langle i_{\mathrm{La}}\rangle - \langle u_{\mathrm{an}}\rangle - \langle u_{\mathrm{nN}}\rangle \tag{2.4}$$

$$\langle u_{\mathrm{Lb}}\rangle = d_{\mathrm{B}}\langle u_{\mathrm{in}}\rangle - r_{\mathrm{eq}}\langle i_{\mathrm{Lb}}\rangle - \langle u_{\mathrm{bn}}\rangle - \langle u_{\mathrm{nN}}\rangle \tag{2.5}$$

$$\langle u_{\mathrm{Lc}}\rangle = d_{\mathrm{C}}\langle u_{\mathrm{in}}\rangle - r_{\mathrm{eq}}\langle i_{\mathrm{Lc}}\rangle - \langle u_{\mathrm{cn}}\rangle - \langle u_{\mathrm{nN}}\rangle \tag{2.6}$$

$$\langle i_{\mathrm{in}}\rangle = d_{\mathrm{A}}\langle i_{\mathrm{La}}\rangle + d_{\mathrm{B}}\langle i_{\mathrm{Lb}}\rangle + d_{\mathrm{C}}\langle i_{\mathrm{Lc}}\rangle \tag{2.7}$$

$$\langle i_{\mathrm{oa}}\rangle = \langle i_{\mathrm{La}}\rangle \tag{2.8}$$

$$\langle i_{\mathrm{ob}}\rangle = \langle i_{\mathrm{Lb}}\rangle \tag{2.9}$$

$$\langle i_{\mathrm{oc}}\rangle = \langle i_{\mathrm{Lc}}\rangle \tag{2.10}$$

According to space-vector theory, a three-phase variable $x_{\mathrm{a,b,c}}(t)$ can be expressed as a single complex valued variable $\boldsymbol{x}(t)$ and a real valued zero sequence component $x_{\mathrm{z}}(t)$ at the stationary reference frame as presented in (2.11) and (2.12). The zero sequence component is zero under symmetrical and balanced grid conditions as will be assumed in this thesis. The real and imaginary parts of the stationary-reference-frame space-vector are known as alpha (x_α) and beta (x_β) components.

$$\begin{aligned}\boldsymbol{x}(t) &= \frac{2}{3}\Big(x_{\mathrm{a}}(t)\mathrm{e}^{\mathrm{j}0} + x_{\mathrm{b}}(t)\mathrm{e}^{\mathrm{j}2\pi/3} + x_{\mathrm{c}}(t)\mathrm{e}^{\mathrm{j}4\pi/3}\Big)\\ &= |\boldsymbol{x}(t)|\,\mathrm{e}^{\mathrm{j}\varphi} = x_\alpha(t) + \mathrm{j}x_\beta(t)\end{aligned} \tag{2.11}$$

$$x_{\mathrm{z}}(t) = \frac{1}{3}\Big(x_{\mathrm{a}}(t) + x_{\mathrm{b}}(t) + x_{\mathrm{c}}(t)\Big) \tag{2.12}$$

The coefficient 2/3 in (2.11) scales the magnitude of the space vector to equal the peak value of the phase variables in a symmetrical and balanced three-phase system. This is known as the non-power or amplitude invariant form of the space vector representation. Another possibility would be to use the non-amplitude or power invariant version of Park's transformation where a coefficient of $\sqrt{2/3}$ would be used instead of the 2/3.

Multiplying (2.4) with $\frac{2}{3}\mathrm{e}^{\mathrm{j}0}$, (2.5) with $\frac{2}{3}\mathrm{e}^{\mathrm{j}2\pi/3}$, (2.6) with $\frac{2}{3}\mathrm{e}^{\mathrm{j}4\pi/3}$, summing the equations, and using (2.11) yields

$$\begin{aligned}\langle \boldsymbol{u}_{\mathrm{L}}\rangle &= -r_{\mathrm{eq}}\langle \boldsymbol{i}_{\mathrm{L}}\rangle + \boldsymbol{d}\langle u_{\mathrm{in}}\rangle - \langle \boldsymbol{u}_{\mathrm{o}}\rangle - \frac{2}{3}\overbrace{\Big(\mathrm{e}^{\mathrm{j}0} + \mathrm{e}^{\mathrm{j}2\pi/3} + \mathrm{e}^{\mathrm{j}4\pi/3}\Big)}^{=0}\langle u_{\mathrm{nN}}\rangle\\ &= -r_{\mathrm{eq}}\langle \boldsymbol{i}_{\mathrm{L}}\rangle + \boldsymbol{d}\langle u_{\mathrm{in}}\rangle - \langle \boldsymbol{u}_{\mathrm{o}}\rangle,\end{aligned} \tag{2.13}$$

where $\boldsymbol{u}_{\mathrm{L}}$ is the inductor voltage, $\boldsymbol{d}$ the duty ratio, $\boldsymbol{i}_{\mathrm{L}}$ the inductor current, and $\boldsymbol{u}_{\mathrm{o}}$ the grid voltage space-vector.

The time derivative of the inductor current (i.e. the time derivative of the state variable) can be computed using (2.13), $L = L_{\mathrm{a,b,c}}$, and the inductor current-voltage equation yielding

$$\frac{\mathrm{d}\langle \boldsymbol{i}_{\mathrm{L}} \rangle}{\mathrm{d}t} = \frac{1}{L}\Big[- r_{\mathrm{eq}} \langle \boldsymbol{i}_{\mathrm{L}} \rangle + \boldsymbol{d} \langle u_{\mathrm{in}} \rangle - \langle \boldsymbol{u}_{\mathrm{o}} \rangle \Big]. \tag{2.14}$$

The stationary-reference-frame space-vector $\boldsymbol{x}(t)$ can be transformed into the rotating or synchronous reference frame using

$$\boldsymbol{x}^{\mathrm{s}}(t) = \boldsymbol{x}(t)\mathrm{e}^{-\mathrm{j}\omega_{\mathrm{s}} t} = x_{\mathrm{d}} + \mathrm{j}x_{\mathrm{q}}, \tag{2.15}$$

where the superscript 's' denotes the synchronous reference frame and ω_{s} is the grid frequency in rad/s. The real and imaginary parts of the synchronous-reference-frame space-vector $\boldsymbol{x}^{\mathrm{s}}(t)$ are known as direct (x_{d}) and quadrature (x_{q}) components. Transforming (2.14) into the synchronous reference frame using (2.15) yields

$$\frac{\mathrm{d}\langle \boldsymbol{i}^{\mathrm{s}}_{\mathrm{L}} \rangle}{\mathrm{d}t} = \frac{1}{L}\Big[- (r_{\mathrm{eq}} + \mathrm{j}\omega_{\mathrm{s}} L) \langle \boldsymbol{i}^{\mathrm{s}}_{\mathrm{L}} \rangle + \boldsymbol{d}^{\mathrm{s}} \langle u_{\mathrm{in}} \rangle - \langle \boldsymbol{u}^{\mathrm{s}}_{\mathrm{o}} \rangle \Big]. \tag{2.16}$$

The direct and quadrature components of (2.16) can be given by

$$\frac{\mathrm{d}\langle i_{\mathrm{Ld}} \rangle}{\mathrm{d}t} = \frac{1}{L}\Big[- r_{\mathrm{eq}} \langle i_{\mathrm{Ld}} \rangle + \omega_{\mathrm{s}} L \langle i_{\mathrm{Lq}} \rangle + d_{\mathrm{d}} \langle u_{\mathrm{in}} \rangle - \langle u_{\mathrm{od}} \rangle \Big], \tag{2.17}$$

$$\frac{\mathrm{d}\langle i_{\mathrm{Lq}} \rangle}{\mathrm{d}t} = \frac{1}{L}\Big[- \omega_{\mathrm{s}} L \langle i_{\mathrm{Ld}} \rangle - r_{\mathrm{eq}} \langle i_{\mathrm{Lq}} \rangle + d_{\mathrm{q}} \langle u_{\mathrm{in}} \rangle - \langle u_{\mathrm{oq}} \rangle \Big]. \tag{2.18}$$

The input current i_{in} in (2.7) can be expressed with the space-vector theory as $d_{\mathrm{A}}\langle i_{\mathrm{La}} \rangle + d_{\mathrm{B}}\langle i_{\mathrm{Lb}} \rangle + d_{\mathrm{C}}\langle i_{\mathrm{Lc}} \rangle = \frac{3}{2}\mathrm{Re}\left\{ \boldsymbol{d}^{\mathrm{s}} \langle \boldsymbol{i}^{\mathrm{s}}_{\mathrm{L}} \rangle^{*} \right\}$ by

$$\langle i_{\mathrm{in}} \rangle = \frac{3}{2}\Big[d_{\mathrm{d}} \langle i_{\mathrm{Ld}} \rangle + d_{\mathrm{q}} \langle i_{\mathrm{Lq}} \rangle \Big]. \tag{2.19}$$

The three-phase output currents $i_{\mathrm{o(a,b,c)}}$ can be expressed with the space-vector theory by

$$\langle i_{\mathrm{od}} \rangle = \langle i_{\mathrm{Ld}} \rangle, \tag{2.20}$$

$$\langle i_{\mathrm{oq}} \rangle = \langle i_{\mathrm{Lq}} \rangle. \tag{2.21}$$

Eqs. (2.17)–(2.21) are known as the synchronous-reference-frame average-valued or large-signal model of a VF-VSI.

2.1.2 Operating Point

The steady-state operating point (duty ratios, inductor currents) of the VF-VSI will be computed as functions of input voltage, input current and output voltages. Computing the operating point as proposed can be justified by considering grid-connected PV power systems: the grid voltage and PVG specifications (i.e. open-circuit/MPP voltages and short-circuit/MPP currents) are naturally known *a priori* since they are important design parameters.

The operating point can be obtained from the average-valued equations in (2.17)–(2.21) by letting the time derivatives be zero and replacing the lower case average values with their corresponding upper case steady-state values as

$$-r_{\mathrm{eq}}I_{\mathrm{Ld}} + \omega_{\mathrm{s}}LI_{\mathrm{Lq}} + D_{\mathrm{d}}U_{\mathrm{in}} - U_{\mathrm{od}} = 0, \tag{2.22}$$

$$-\omega_{\mathrm{s}}LI_{\mathrm{Ld}} - r_{\mathrm{eq}}I_{\mathrm{Lq}} + D_{\mathrm{q}}U_{\mathrm{in}} - U_{\mathrm{oq}} = 0, \tag{2.23}$$

$$I_{\mathrm{in}} = \frac{3}{2}\Big[D_{\mathrm{d}}I_{\mathrm{Ld}} + D_{\mathrm{q}}I_{\mathrm{Lq}}\Big], \tag{2.24}$$

$$I_{\mathrm{od}} = I_{\mathrm{Ld}}, \tag{2.25}$$

$$I_{\mathrm{oq}} = I_{\mathrm{Lq}}, \tag{2.26}$$

The steady-state operating point for a case when

$$I_{\mathrm{Lq}} = 0, \tag{2.27}$$

$$U_{\mathrm{oq}} = 0, \tag{2.28}$$

i.e. when only real power is transferred, can be calculated as follows: The steady-state value for the d-channel inductor current I_{Ld} can be obtained from (2.24) by substituting (2.27) as

$$I_{\mathrm{Ld}} = \frac{2}{3}\frac{I_{\mathrm{in}}}{D_{\mathrm{d}}}. \tag{2.29}$$

Eqs. (2.27) and (2.29) can be substituted in (2.22) to obtain a second order polynomial for the d-channel duty ratio D_{d} as

$$U_{\mathrm{in}}D_{\mathrm{d}}^2 - U_{\mathrm{od}}D_{\mathrm{d}} - \frac{2}{3}r_{\mathrm{eq}}I_{\mathrm{in}} = 0, \tag{2.30}$$

which can be solved by

$$D_{\mathrm{d}} = \frac{U_{\mathrm{od}} + \sqrt{U_{\mathrm{od}}^2 + \frac{8}{3}r_{\mathrm{eq}}U_{\mathrm{in}}I_{\mathrm{in}}}}{2U_{\mathrm{in}}}. \tag{2.31}$$

Eq. (2.31) can be used to express the operating point value of I_{Ld} in (2.29) as functions of the aforementioned input parameters as

$$I_{\mathrm{Ld}} = \frac{4}{3}\frac{U_{\mathrm{in}}I_{\mathrm{in}}}{U_{\mathrm{od}} + \sqrt{U_{\mathrm{od}}^2 + \frac{8}{3}r_{\mathrm{eq}}U_{\mathrm{in}}I_{\mathrm{in}}}}. \tag{2.32}$$

The q-channel duty ratio D_{q} can be solved by substituting (2.27), (2.28) and (2.32) in (2.23) as

$$D_{\mathrm{q}} = \frac{2\omega_{\mathrm{s}}LI_{\mathrm{in}}}{3U_{\mathrm{in}}D_{\mathrm{d}}} = \frac{4}{3}\frac{\omega_{\mathrm{s}}LI_{\mathrm{in}}}{U_{\mathrm{od}} + \sqrt{U_{\mathrm{od}}^2 + \frac{8}{3}r_{\mathrm{eq}}U_{\mathrm{in}}I_{\mathrm{in}}}}. \tag{2.33}$$

Eqs. (2.27), (2.28), (2.31)–(2.33) and $U_{\mathrm{in}}, I_{\mathrm{in}}, U_{\mathrm{od}}$ define the operating point of a VF-VSI.

2.1.3 Linearized Model

The average-valued model is non-linear and has to be linearized at the predefined operating point as discussed in Chapter 1. Linearization can be performed by developing partial derivatives for the state (i_{Ld} and i_{Lq}), input (u_{in}, u_{od}, u_{oq}, d_{d} and d_{q}) and output variables (i_{in}, i_{od} and i_{oq}) in (2.17)–(2.21) as

$$\frac{\mathrm{d}\hat{i}_{\mathrm{Ld}}}{\mathrm{d}t} = \frac{1}{L}\Big[-r_{\mathrm{eq}}\hat{i}_{\mathrm{Ld}} + \omega_{\mathrm{s}}L\hat{i}_{\mathrm{Lq}} + D_{\mathrm{d}}\hat{u}_{\mathrm{in}} - \hat{u}_{\mathrm{od}} + U_{\mathrm{in}}\hat{d}_{\mathrm{d}}\Big], \tag{2.34}$$

$$\frac{\mathrm{d}\hat{i}_{\mathrm{Lq}}}{\mathrm{d}t} = \frac{1}{L}\Big[-\omega_{\mathrm{s}}L\hat{i}_{\mathrm{Ld}} - r_{\mathrm{eq}}\hat{i}_{\mathrm{Lq}} + D_{\mathrm{q}}\hat{u}_{\mathrm{in}} - \hat{u}_{\mathrm{oq}} + U_{\mathrm{in}}\hat{d}_{\mathrm{q}}\Big], \tag{2.35}$$

$$\hat{i}_{\mathrm{in}} = \frac{3}{2}\Big[D_{\mathrm{d}}\hat{i}_{\mathrm{Ld}} + D_{\mathrm{q}}\hat{i}_{\mathrm{Lq}} + I_{\mathrm{Ld}}\hat{d}_{\mathrm{d}} + I_{\mathrm{Lq}}\hat{d}_{\mathrm{q}}\Big], \tag{2.36}$$

which can be simplified using (2.27) and (2.29) as

$$\hat{i}_{\mathrm{in}} = \frac{3}{2}\Big[D_{\mathrm{d}}\hat{i}_{\mathrm{Ld}} + D_{\mathrm{q}}\hat{i}_{\mathrm{Lq}} + \frac{2}{3}\frac{I_{\mathrm{in}}}{D_{\mathrm{d}}}\hat{d}_{\mathrm{d}}\Big], \tag{2.37}$$

$$\hat{i}_{\mathrm{od}} = \hat{i}_{\mathrm{Ld}}, \tag{2.38}$$

$$\hat{i}_{\mathrm{oq}} = \hat{i}_{\mathrm{Lq}}. \tag{2.39}$$

Eqs. (2.34)–(2.39) can be expressed in matrix form according to (1.4) as

$$\begin{aligned}\frac{\mathrm{d}\hat{\boldsymbol{x}}(t)}{\mathrm{d}t} &= \mathbf{A}\hat{\boldsymbol{x}}(t) + \mathbf{B}\hat{\boldsymbol{u}}(t),\\ \hat{\boldsymbol{y}}(t) &= \mathbf{C}\hat{\boldsymbol{x}}(t) + \mathbf{D}\hat{\boldsymbol{u}}(t),\end{aligned} \tag{2.40}$$

where the state, input and output variable vectors are defined as

$$\hat{\boldsymbol{x}} = \begin{bmatrix} \hat{i}_{\mathrm{Ld}} & \hat{i}_{\mathrm{Lq}} \end{bmatrix}^{\mathrm{T}}, \ \hat{\boldsymbol{u}} = \begin{bmatrix} \hat{u}_{\mathrm{in}} & \hat{u}_{\mathrm{od}} & \hat{u}_{\mathrm{oq}} & \hat{d}_{\mathrm{d}} & \hat{d}_{\mathrm{q}} \end{bmatrix}^{\mathrm{T}}, \ \hat{\boldsymbol{y}} = \begin{bmatrix} \hat{i}_{\mathrm{in}} & \hat{i}_{\mathrm{od}} & \hat{i}_{\mathrm{oq}} \end{bmatrix}^{\mathrm{T}}, \tag{2.41}$$

and the state matrices $\mathbf{A}$, $\mathbf{B}$, $\mathbf{C}$ and $\mathbf{D}$ are defined as

$$\begin{aligned} \mathbf{A} &= \begin{bmatrix} -\frac{r_{\mathrm{eq}}}{L} & \omega_{\mathrm{s}} \\ -\omega_{\mathrm{s}} & -\frac{r_{\mathrm{eq}}}{L} \end{bmatrix}, \quad \mathbf{B} = \begin{bmatrix} \frac{D_{\mathrm{d}}}{L} & -\frac{1}{L} & 0 & \frac{U_{\mathrm{in}}}{L} & 0 \\ \frac{D_{\mathrm{q}}}{L} & 0 & -\frac{1}{L} & 0 & \frac{U_{\mathrm{in}}}{L} \end{bmatrix}, \\ \mathbf{C} &= \begin{bmatrix} \frac{3}{2}D_{\mathrm{d}} & \frac{3}{2}D_{\mathrm{q}} \\ 1 & 0 \\ 0 & 1 \end{bmatrix}, \quad \mathbf{D} = \begin{bmatrix} 0 & 0 & 0 & \frac{I_{\mathrm{in}}}{D_{\mathrm{d}}} & 0 \\ 0 & 0 & 0 & 0 & 0 \\ 0 & 0 & 0 & 0 & 0 \end{bmatrix}. \end{aligned} \tag{2.42}$$

According to (1.7), Eqs. (2.40)–(2.42) can be used to solve the transfer functions between the input and output variables as

$$\boldsymbol{Y}(s) = \left[\mathbf{C} \left(s\mathbf{I} - \mathbf{A} \right)^{-1} \mathbf{B} + \mathbf{D} \right] \boldsymbol{U}(s) = \mathbf{G}_{\mathrm{Y}} \boldsymbol{U}(s), \tag{2.43}$$

where the transfer function matrix $\mathbf{G}_{\mathrm{Y}}$ is known as the modified Y-parameter representation of a VF-VSI and is presented in (2.44). The top row describes the input dynamics and the two bottom rows the d-channel and q-channel output dynamics of the inverter. The term 'modified' is used since the output current flows out of the converter and has to be taken into account in the transfer function matrix by multiplying the output admittances $Y_{\mathrm{o\text{-}d}}$ and $Y_{\mathrm{o\text{-}q}}$ by '-1'.

$$\begin{bmatrix} \hat{i}_{\mathrm{in}} \\ \hat{i}_{\mathrm{od}} \\ \hat{i}_{\mathrm{oq}} \end{bmatrix} = \begin{bmatrix} Y^{\mathrm{Y}}_{\mathrm{in}} & T^{\mathrm{Y}}_{\mathrm{oi\text{-}d}} & T^{\mathrm{Y}}_{\mathrm{oi\text{-}q}} & G^{\mathrm{Y}}_{\mathrm{ci\text{-}d}} & G^{\mathrm{Y}}_{\mathrm{ci\text{-}q}} \\ G^{\mathrm{Y}}_{\mathrm{io\text{-}d}} & -Y^{\mathrm{Y}}_{\mathrm{o\text{-}d}} & G^{\mathrm{Y}}_{\mathrm{cr\text{-}qd}} & G^{\mathrm{Y}}_{\mathrm{co\text{-}d}} & G^{\mathrm{Y}}_{\mathrm{co\text{-}qd}} \\ G^{\mathrm{Y}}_{\mathrm{io\text{-}q}} & G^{\mathrm{Y}}_{\mathrm{cr\text{-}dq}} & -Y^{\mathrm{Y}}_{\mathrm{o\text{-}q}} & G^{\mathrm{Y}}_{\mathrm{co\text{-}dq}} & G^{\mathrm{Y}}_{\mathrm{co\text{-}q}} \end{bmatrix} \begin{bmatrix} \hat{u}_{\mathrm{in}} \\ \hat{u}_{\mathrm{od}} \\ \hat{u}_{\mathrm{oq}} \\ \hat{d}_{\mathrm{d}} \\ \hat{d}_{\mathrm{q}} \end{bmatrix} \tag{2.44}$$

The input dynamics as presented in (2.45) can be described as follows: the transfer function between the input voltage and the input current is known as the input admittance Y_{in}. The transfer function between the output voltages and the input current is known as the reverse or output-to-input transfer function or transmittance T_{oi}. The transfer function between the control variable and the input current is known as the control-to-input-current transfer function G_{ci}.

$$\hat{i}_{\mathrm{in}} = Y^{\mathrm{Y}}_{\mathrm{in}} \hat{u}_{\mathrm{in}} + T^{\mathrm{Y}}_{\mathrm{oi\text{-}d}} \hat{u}_{\mathrm{od}} + T^{\mathrm{Y}}_{\mathrm{oi\text{-}q}} \hat{u}_{\mathrm{oq}} + G^{\mathrm{Y}}_{\mathrm{ci\text{-}d}} \hat{d}_{\mathrm{d}} + G^{\mathrm{Y}}_{\mathrm{ci\text{-}q}} \hat{d}_{\mathrm{q}} \tag{2.45}$$

The output dynamics as presented in (2.46) and (2.47) can be described as follows: the transfer function between the input voltage and the output current is known as the forward or input-to-output transfer function or audio susceptibility G_{io}. The transfer function between the channel voltage and the same channel current is known as the output admittance Y_{o}. The transfer function between the channel voltage and the other channel current is known as the cross-coupling transfer function G_{cr}. The transfer function between the control variable and the output current is known as the control-to-output-current transfer function G_{co}.

$$\hat{i}_{\mathrm{od}} = G^{\mathrm{Y}}_{\mathrm{io\text{-}d}}\hat{u}_{\mathrm{in}} - Y^{\mathrm{Y}}_{\mathrm{o\text{-}d}}\hat{u}_{\mathrm{od}} + G^{\mathrm{Y}}_{\mathrm{cr\text{-}qd}}\hat{u}_{\mathrm{oq}} + G^{\mathrm{Y}}_{\mathrm{co\text{-}d}}\hat{d}_{\mathrm{d}} + G^{\mathrm{Y}}_{\mathrm{co\text{-}qd}}\hat{d}_{\mathrm{q}} \tag{2.46}$$

$$\hat{i}_{\mathrm{oq}} = G^{\mathrm{Y}}_{\mathrm{io\text{-}q}}\hat{u}_{\mathrm{in}} + G^{\mathrm{Y}}_{\mathrm{cr\text{-}dq}}\hat{u}_{\mathrm{od}} - Y^{\mathrm{Y}}_{\mathrm{o\text{-}q}}\hat{u}_{\mathrm{oq}} + G^{\mathrm{Y}}_{\mathrm{co\text{-}dq}}\hat{d}_{\mathrm{d}} + G^{\mathrm{Y}}_{\mathrm{co\text{-}q}}\hat{d}_{\mathrm{q}} \tag{2.47}$$

A linear model can be constructed based on the converter dynamics represented by (2.44) as shown inside the dashed box in Fig. 2.2.

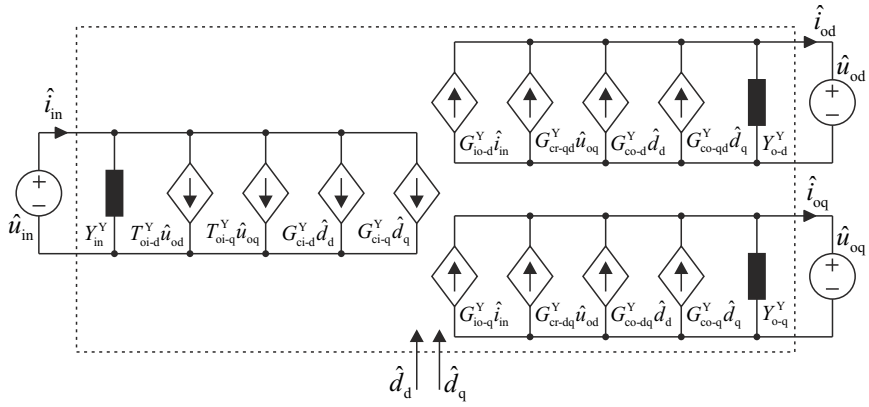

Fig. 2.2: Linear model of a grid-connected three-phase voltage-fed inverter.

The transfer functions in (2.44) and Fig. 2.2 for the VF-VSI without the parasitic elements can be given as presented in (2.48)–(2.63)[1]. The input admittance can be given by

$$Y^{\mathrm{Y}}_{\mathrm{in}} = \frac{\hat{i}_{\mathrm{in}}}{\hat{u}_{\mathrm{in}}} = \frac{3}{2}\frac{D_{\mathrm{d}}^2 + D_{\mathrm{q}}^2}{L}\frac{s}{\Delta_{\mathrm{Y}}}. \tag{2.48}$$

[1]A detailed Matlab m-file that can be used to obtain (2.48)–(2.63) can be found in Appendix A.

The output-to-input transfer functions can be given by

$$T_{\text{oi-d}}^{\text{Y}} = \frac{\hat{i}_{\text{in}}}{\hat{u}_{\text{od}}} = -\frac{3}{2}\frac{D_{\text{d}}}{L}\left(s - \frac{D_{\text{q}}\omega_{\text{s}}}{D_{\text{d}}}\right)\frac{1}{\Delta_{\text{Y}}}, \tag{2.49}$$

$$T_{\text{oi-q}}^{\text{Y}} = \frac{\hat{i}_{\text{in}}}{\hat{u}_{\text{oq}}} = -\frac{3}{2}\frac{D_{\text{q}}}{L}\left(s + \frac{D_{\text{d}}\omega_{\text{s}}}{D_{\text{q}}}\right)\frac{1}{\Delta_{\text{Y}}}. \tag{2.50}$$

The transfer functions between the control variable and input current can be given by

$$G_{\text{ci-d}}^{\text{Y}} = \frac{\hat{i}_{\text{in}}}{\hat{d}_{\text{d}}} = \frac{I_{\text{in}}}{D_{\text{d}}}\left(s + \frac{3}{2}\frac{D_{\text{d}}^2 U_{\text{in}}}{L I_{\text{in}}}\right)\frac{s}{\Delta_{\text{Y}}}, \tag{2.51}$$

$$G_{\text{ci-q}}^{\text{Y}} = \frac{\hat{i}_{\text{in}}}{\hat{d}_{\text{q}}} = \frac{3}{2}\frac{D_{\text{q}}U_{\text{in}}}{L}\left(s + \frac{D_{\text{q}}\omega_{\text{s}}}{D_{\text{d}}}\right)\frac{1}{\Delta_{\text{Y}}}. \tag{2.52}$$

The input-to-output transfer functions can be given by

$$G_{\text{io-d}}^{\text{Y}} = \frac{\hat{i}_{\text{od}}}{\hat{u}_{\text{in}}} = \frac{D_{\text{d}}}{L}\left(s + \frac{D_{\text{q}}\omega_{\text{s}}}{D_{\text{d}}}\right)\frac{1}{\Delta_{\text{Y}}}, \tag{2.53}$$

$$G_{\text{io-q}}^{\text{Y}} = \frac{\hat{i}_{\text{oq}}}{\hat{u}_{\text{in}}} = \frac{D_{\text{q}}}{L}\left(s - \frac{D_{\text{d}}\omega_{\text{s}}}{D_{\text{q}}}\right)\frac{1}{\Delta_{\text{Y}}}. \tag{2.54}$$

The output admittances and the cross-coupling transfer functions can be given by

$$Y_{\text{o-d}}^{\text{Y}} = -\frac{\hat{i}_{\text{od}}}{\hat{u}_{\text{od}}} = \frac{s}{L}\frac{1}{\Delta_{\text{Y}}}, \tag{2.55}$$

$$Y_{\text{o-q}}^{\text{Y}} = -\frac{\hat{i}_{\text{oq}}}{\hat{u}_{\text{oq}}} = \frac{s}{L}\frac{1}{\Delta_{\text{Y}}}, \tag{2.56}$$

$$G_{\text{cr-qd}}^{\text{Y}} = \frac{\hat{i}_{\text{od}}}{\hat{u}_{\text{oq}}} = -\frac{\omega_{\text{s}}}{L}\frac{1}{\Delta_{\text{Y}}}, \tag{2.57}$$

$$G_{\text{cr-dq}}^{\text{Y}} = \frac{\hat{i}_{\text{oq}}}{\hat{u}_{\text{od}}} = \frac{\omega_{\text{s}}}{L}\frac{1}{\Delta_{\text{Y}}}. \tag{2.58}$$

The transfer functions between the control variables and output currents can be given by

$$G_{\text{co-d}}^{\text{Y}} = \frac{\hat{i}_{\text{od}}}{\hat{d}_{\text{d}}} = \frac{U_{\text{in}}s}{L}\frac{1}{\Delta_{\text{Y}}}, \tag{2.59}$$

$$G_{\text{co-q}}^{\text{Y}} = \frac{\hat{i}_{\text{oq}}}{\hat{d}_{\text{q}}} = \frac{U_{\text{in}}s}{L}\frac{1}{\Delta_{\text{Y}}}, \tag{2.60}$$

$$G_{\text{co-qd}}^{\text{Y}} = \frac{\hat{i}_{\text{od}}}{\hat{d}_{\text{q}}} = \frac{U_{\text{in}}\omega_{\text{s}}}{L}\frac{1}{\Delta_{\text{Y}}}, \tag{2.61}$$

$$G_{\text{co-dq}}^{\text{Y}} = \frac{\hat{i}_{\text{oq}}}{\hat{d}_{\text{d}}} = -\frac{U_{\text{in}}\omega_{\text{s}}}{L}\frac{1}{\Delta_{\text{Y}}}. \tag{2.62}$$

The determinant Δ_{Y} of the transfer functions can be given by

$$\Delta_{\text{Y}} = s^2 + \omega_{\text{s}}^2. \tag{2.63}$$

2.2 Grid-Connected Current-Fed VSI

Fig. 2.3 presents a grid-connected CF-VSI. The topology is similar to the one presented in Fig. 2.1, but an additional input capacitor has been connected between the source and the VSI switch matrix. The input capacitor is necessary for the converter operation and is, therefore, part of the power stage along with the switch matrix and the output inductors. As with the VF-VSI, the input voltage has to be greater in magnitude than the output voltages for proper converter operation as discussed in Section 2.1. Accordingly, the input current has to be smaller in magnitude than the phase currents. This implies that the CF-VSI has boost-type characteristics (since the current level steps up between the source and load terminals) as will be analyzed in Section 2.6.

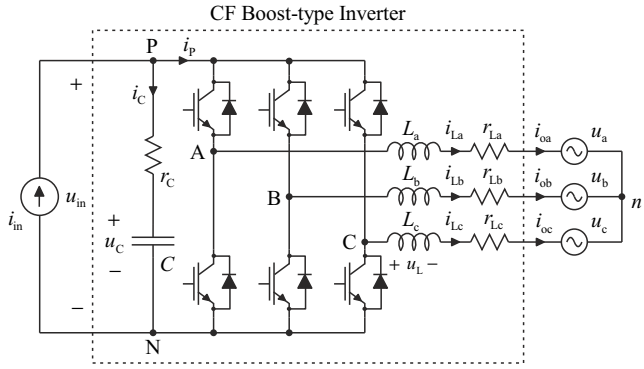

Fig. 2.3: Grid-connected three-phase current-fed VSI-type inverter.

In case of the CF-VSI in Fig. 2.3, the system inputs are the input current i_{in} and the grid phase voltages $u_{(\mathrm{a,b,c})\mathrm{n}}$. Thus, the outputs are the input voltage u_{in} and the grid phase currents $i_{\mathrm{o(a,b,c)}}$. Therefore, an input-voltage-controlled grid-connected converter, as the renewable-energy-related grid-connected VSI usually is, has to be analyzed as follows.

2.2.1 Average Model

This section will present the average-valued model for the CF-VSI in a similar manner as for the VF-VSI in Section 2.1. The average-valued model of a CF-VSI can be given using the notations of Fig. 2.3 as presented in (2.64)–(2.71). It is worth noting that the input voltage u_{in} is a system output and should not be present in (2.64)–(2.66), but is left there to simplify the notations at this point of the analyses. Upon constructing the small-signal state matrices an expression for input voltage as functions of the state and

input variables has to be substituted in the aforementioned equations.

$$\langle u_{\mathrm{La}}\rangle = d_{\mathrm{A}}\langle u_{\mathrm{in}}\rangle - r_{\mathrm{eq}}\langle i_{\mathrm{La}}\rangle - \langle u_{\mathrm{an}}\rangle - \langle u_{\mathrm{nN}}\rangle \tag{2.64}$$

$$\langle u_{\mathrm{Lb}}\rangle = d_{\mathrm{B}}\langle u_{\mathrm{in}}\rangle - r_{\mathrm{eq}}\langle i_{\mathrm{Lb}}\rangle - \langle u_{\mathrm{bn}}\rangle - \langle u_{\mathrm{nN}}\rangle \tag{2.65}$$

$$\langle u_{\mathrm{Lc}}\rangle = d_{\mathrm{C}}\langle u_{\mathrm{in}}\rangle - r_{\mathrm{eq}}\langle i_{\mathrm{Lc}}\rangle - \langle u_{\mathrm{cn}}\rangle - \langle u_{\mathrm{nN}}\rangle \tag{2.66}$$

$$\langle i_{\mathrm{C}}\rangle = -d_{\mathrm{A}}\langle i_{\mathrm{La}}\rangle - d_{\mathrm{B}}\langle i_{\mathrm{Lb}}\rangle - d_{\mathrm{C}}\langle i_{\mathrm{Lc}}\rangle + \langle i_{\mathrm{in}}\rangle \tag{2.67}$$

$$\langle u_{\mathrm{in}}\rangle = \langle u_{\mathrm{C}}\rangle + r_{\mathrm{C}}\langle i_{\mathrm{C}}\rangle \tag{2.68}$$

$$\langle i_{\mathrm{oa}}\rangle = \langle i_{\mathrm{La}}\rangle \tag{2.69}$$

$$\langle i_{\mathrm{ob}}\rangle = \langle i_{\mathrm{Lb}}\rangle \tag{2.70}$$

$$\langle i_{\mathrm{oc}}\rangle = \langle i_{\mathrm{Lc}}\rangle \tag{2.71}$$

Eqs. (2.64)–(2.66) can be expressed in the stationary reference frame using the space-vector theory similarly as presented in Section 2.1 in (2.13). The time derivative of the inductor current can be computed similarly as presented in (2.14)–(2.18). The capacitor current i_{C} in (2.67), in turn, can be expressed with the space-vector theory by

$$\langle i_{\mathrm{C}}\rangle = -\frac{3}{2}\Big[d_{\mathrm{d}}\langle i_{\mathrm{Ld}}\rangle + d_{\mathrm{q}}\langle i_{\mathrm{Lq}}\rangle\Big] + \langle i_{\mathrm{in}}\rangle. \tag{2.72}$$

The time derivative of the capacitor voltage (state variable) in the synchronous reference frame can be given using (2.72) and the capacitor voltage-current equation by

$$\frac{\mathrm{d}\langle u_{\mathrm{C}}\rangle}{\mathrm{d}t} = \frac{1}{C}\Big[-\frac{3}{2}\Big(d_{\mathrm{d}}\langle i_{\mathrm{Ld}}\rangle + d_{\mathrm{q}}\langle i_{\mathrm{Lq}}\rangle\Big) + \langle i_{\mathrm{in}}\rangle\Big]. \tag{2.73}$$

The input voltage in (2.68) can be expressed with (2.72) by

$$\langle u_{\mathrm{in}}\rangle = -\frac{3}{2}r_{\mathrm{C}}d_{\mathrm{d}}\langle i_{\mathrm{Ld}}\rangle - \frac{3}{2}r_{\mathrm{C}}d_{\mathrm{q}}\langle i_{\mathrm{Lq}}\rangle + \langle u_{\mathrm{C}}\rangle + r_{\mathrm{C}}\langle i_{\mathrm{in}}\rangle, \tag{2.74}$$

or with the capacitor voltage derivative by

$$\langle u_{\mathrm{in}}\rangle = r_{\mathrm{C}}C\frac{\mathrm{d}\langle u_{\mathrm{C}}\rangle}{\mathrm{d}t} + \langle u_{\mathrm{C}}\rangle. \tag{2.75}$$

Finally the average-valued equations in the synchronous reference frame can be given by substituting (2.74) into (2.17) and (2.18), and using (2.73), (2.75) and (2.20)–(2.21)

by

$$\frac{\mathrm{d}\langle i_{\mathrm{Ld}}\rangle}{\mathrm{d}t} = -\left(\frac{r_{\mathrm{eq}}}{L} + \frac{3}{2}\frac{r_{\mathrm{C}}d_{\mathrm{d}}^2}{L}\right)\langle i_{\mathrm{Ld}}\rangle - \left(-\omega_{\mathrm{s}} + \frac{3}{2}\frac{r_{\mathrm{C}}d_{\mathrm{d}}d_{\mathrm{q}}}{L}\right)\langle i_{\mathrm{Lq}}\rangle + \frac{d_{\mathrm{d}}}{L}\langle u_{\mathrm{C}}\rangle + \frac{r_{\mathrm{C}}d_{\mathrm{d}}}{L}\langle i_{\mathrm{in}}\rangle - \frac{1}{L}\langle u_{\mathrm{od}}\rangle, \tag{2.76}$$

$$\frac{\mathrm{d}\langle i_{\mathrm{Lq}}\rangle}{\mathrm{d}t} = -\left(\omega_{\mathrm{s}} + \frac{3}{2}\frac{r_{\mathrm{C}}d_{\mathrm{d}}d_{\mathrm{q}}}{L}\right)\langle i_{\mathrm{Ld}}\rangle - \left(\frac{r_{\mathrm{eq}}}{L} + \frac{3}{2}\frac{r_{\mathrm{C}}d_{\mathrm{q}}^2}{L}\right)\langle i_{\mathrm{Lq}}\rangle + \frac{d_{\mathrm{q}}}{L}\langle u_{\mathrm{C}}\rangle + \frac{r_{\mathrm{C}}d_{\mathrm{q}}}{L}\langle i_{\mathrm{in}}\rangle - \frac{1}{L}\langle u_{\mathrm{oq}}\rangle, \tag{2.77}$$

$$\frac{\mathrm{d}\langle u_{\mathrm{C}}\rangle}{\mathrm{d}t} = -\frac{3}{2}\frac{d_{\mathrm{d}}}{C}\langle i_{\mathrm{Ld}}\rangle - \frac{3}{2}\frac{d_{\mathrm{q}}}{C}\langle i_{\mathrm{Lq}}\rangle + \frac{1}{C}\langle i_{\mathrm{in}}\rangle, \tag{2.78}$$

$$\langle u_{\mathrm{in}}\rangle = \left(1 + r_{\mathrm{C}}C\frac{\mathrm{d}}{\mathrm{d}t}\right)\langle u_{\mathrm{C}}\rangle, \tag{2.79}$$

$$\langle i_{\mathrm{od}}\rangle = \langle i_{\mathrm{Ld}}\rangle, \tag{2.80}$$

$$\langle i_{\mathrm{oq}}\rangle = \langle i_{\mathrm{Lq}}\rangle. \tag{2.81}$$

Eqs. (2.76)–(2.81) are known as the synchronous-reference-frame average-valued or large-signal model for a CF-VSI.

2.2.2 Operating Point

The steady-state operating point can be obtained from the average-valued equations in (2.76)–(2.81) by letting the time derivatives be zero and replacing the lower case average values with their corresponding upper case steady-state values as

$$-\left(\frac{r_{\mathrm{eq}}}{L} + \frac{3}{2}\frac{r_{\mathrm{C}}D_{\mathrm{d}}^2}{L}\right)I_{\mathrm{Ld}} - \left(-\omega_{\mathrm{s}} + \frac{3}{2}\frac{r_{\mathrm{C}}D_{\mathrm{d}}D_{\mathrm{q}}}{L}\right)I_{\mathrm{Lq}} + \frac{D_{\mathrm{d}}}{L}U_{\mathrm{C}} + \frac{r_{\mathrm{C}}D_{\mathrm{d}}}{L}I_{\mathrm{in}} - \frac{1}{L}U_{\mathrm{od}} = 0, \tag{2.82}$$

$$-\left(\omega_{\mathrm{s}} + \frac{3}{2}\frac{r_{\mathrm{C}}D_{\mathrm{d}}D_{\mathrm{q}}}{L}\right)I_{\mathrm{Ld}} - \left(\frac{r_{\mathrm{eq}}}{L} + \frac{3}{2}\frac{r_{\mathrm{C}}D_{\mathrm{q}}^2}{L}\right)I_{\mathrm{Lq}} + \frac{D_{\mathrm{q}}}{L}U_{\mathrm{C}} + \frac{r_{\mathrm{C}}D_{\mathrm{q}}}{L}I_{\mathrm{in}} - \frac{1}{L}U_{\mathrm{oq}} = 0, \tag{2.83}$$

$$-\frac{3}{2}\frac{D_{\mathrm{d}}}{C}I_{\mathrm{Ld}} - \frac{3}{2}\frac{D_{\mathrm{q}}}{C}I_{\mathrm{Lq}} + \frac{1}{C}I_{\mathrm{in}} = 0, \tag{2.84}$$

$$U_{\mathrm{in}} = U_{\mathrm{C}}, \tag{2.85}$$

$$I_{\mathrm{od}} = I_{\mathrm{Ld}}, \tag{2.86}$$

$$I_{\mathrm{oq}} = I_{\mathrm{Ld}}, \tag{2.87}$$

The steady-state operating point for a case when only real power is transferred as defined by (2.27) and (2.28), can be calculated as follows: the steady-state value for the d-channel inductor current I_{Ld} can be obtained from (2.84) by substituting (2.27) yielding (2.29).

Substituting (2.27) and (2.29) in (2.82) yields a second order polynomial for the d-channel steady-state duty ratio D_{d} as given by (2.30), which can be solved as (2.31).

The q-channel duty ratio D_{q} can be solved by substituting (2.27), (2.28) and (2.29) in (2.83) yielding (2.33).

Equations (2.27), (2.28), (2.31)–(2.33) and $U_{\mathrm{in}}, I_{\mathrm{in}}, U_{\mathrm{od}}$ define the operating point of a CF-VSI, which is exactly the same as for a VF-VSI.

2.2.3 Linearized Model

The average-valued model is non-linear and has to be linearized at the predefined operating point as discussed in Chapter 1. Linearization can be performed by developing partial derivatives for the state (i_{Ld}, i_{Lq} and u_{C}), input (i_{in}, u_{od}, u_{oq}, d_{d} and d_{q}) and output variables (u_{in}, i_{od} and i_{oq}) in (2.76)–(2.81) as

$$\frac{\mathrm{d}\hat{i}_{\mathrm{Ld}}}{\mathrm{d}t} = -\left(\frac{r_{\mathrm{L}}}{L} + \frac{3}{2}\frac{r_{\mathrm{C}}D_{\mathrm{d}}^2}{L}\right)\hat{i}_{\mathrm{Ld}} - \left(-\omega_{\mathrm{s}} + \frac{3}{2}\frac{r_{\mathrm{C}}D_{\mathrm{d}}D_{\mathrm{q}}}{L}\right)\hat{i}_{\mathrm{Lq}} + \frac{D_{\mathrm{d}}}{L}\hat{u}_{\mathrm{C}} + \frac{r_{\mathrm{C}}D_{\mathrm{d}}}{L}\hat{i}_{\mathrm{in}} - \frac{1}{L}\hat{u}_{\mathrm{od}} + \frac{1}{L}\left(U_{\mathrm{in}} + r_{\mathrm{C}}I_{\mathrm{in}} - 3r_{\mathrm{C}}D_{\mathrm{d}}I_{\mathrm{Ld}} - \frac{3}{2}r_{\mathrm{C}}D_{\mathrm{q}}I_{\mathrm{Lq}}\right)\hat{d}_{\mathrm{d}} - \frac{3}{2}\frac{r_{\mathrm{C}}D_{\mathrm{d}}I_{\mathrm{Lq}}}{L}\hat{d}_{\mathrm{q}}, \quad (2.88)$$

$$\frac{\mathrm{d}\hat{i}_{\mathrm{Lq}}}{\mathrm{d}t} = -\left(\omega_{\mathrm{s}} + \frac{3}{2}\frac{r_{\mathrm{C}}D_{\mathrm{d}}D_{\mathrm{q}}}{L}\right)\hat{i}_{\mathrm{Ld}} - \left(\frac{r_{\mathrm{L}}}{L} + \frac{3}{2}\frac{r_{\mathrm{C}}D_{\mathrm{q}}^2}{L}\right)\hat{i}_{\mathrm{Lq}} + \frac{D_{\mathrm{q}}}{L}\hat{u}_{\mathrm{C}} + \frac{r_{\mathrm{C}}D_{\mathrm{q}}}{L}\hat{i}_{\mathrm{in}} - \frac{1}{L}\hat{u}_{\mathrm{oq}} - \frac{3}{2}\frac{r_{\mathrm{C}}D_{\mathrm{q}}I_{\mathrm{Ld}}}{L}\hat{d}_{\mathrm{d}} + \frac{1}{L}\left(U_{\mathrm{in}} + r_{\mathrm{C}}I_{\mathrm{in}} - \frac{3}{2}r_{\mathrm{C}}D_{\mathrm{d}}I_{\mathrm{Ld}} - 3r_{\mathrm{C}}D_{\mathrm{q}}I_{\mathrm{Lq}}\right)\hat{d}_{\mathrm{q}}, \quad (2.89)$$

$$\frac{\mathrm{d}\hat{u}_{\mathrm{C}}}{\mathrm{d}t} = -\frac{3}{2}\frac{D_{\mathrm{d}}}{C}\hat{i}_{\mathrm{Ld}} - \frac{3}{2}\frac{D_{\mathrm{q}}}{C}\hat{i}_{\mathrm{Lq}} + \frac{1}{C}\hat{i}_{\mathrm{in}} - \frac{3}{2}\frac{I_{\mathrm{Ld}}}{C}\hat{d}_{\mathrm{d}} - \frac{3}{2}\frac{I_{\mathrm{Lq}}}{C}\hat{d}_{\mathrm{q}}, \quad (2.90)$$

$$\hat{u}_{\mathrm{in}} = \left(1 + r_{\mathrm{C}}C\frac{\mathrm{d}}{\mathrm{d}t}\right)\hat{u}_{\mathrm{C}}, \quad (2.91)$$

$$\hat{i}_{\mathrm{od}} = \hat{i}_{\mathrm{Ld}}, \quad (2.92)$$

$$\hat{i}_{\mathrm{oq}} = \hat{i}_{\mathrm{Lq}}, \quad (2.93)$$

Eqs. (2.88)–(2.90) can be simplified using (2.27)–(2.29)

$$\frac{\mathrm{d}\hat{i}_{\mathrm{Ld}}}{\mathrm{d}t} = -\left(\frac{r_{\mathrm{L}}}{L} + \frac{3}{2}\frac{r_{\mathrm{C}}D_{\mathrm{d}}^2}{L}\right)\hat{i}_{\mathrm{Ld}} + \omega_{\mathrm{s}}\left(1 - \frac{r_{\mathrm{C}}I_{\mathrm{in}}}{U_{\mathrm{in}}}\right)\hat{i}_{\mathrm{Lq}} + \frac{D_{\mathrm{d}}}{L}\hat{u}_{\mathrm{C}} + \frac{r_{\mathrm{C}}D_{\mathrm{d}}}{L}\hat{i}_{\mathrm{in}} - \frac{1}{L}\hat{u}_{\mathrm{od}} + \frac{U_{\mathrm{in}} - r_{\mathrm{C}}I_{\mathrm{in}}}{L}\hat{d}_{\mathrm{d}}, \quad (2.94)$$

$$\frac{\mathrm{d}\hat{i}_{\mathrm{Lq}}}{\mathrm{d}t} = -\omega_{\mathrm{s}}\left(1+\frac{r_{\mathrm{C}}I_{\mathrm{in}}}{U_{\mathrm{in}}}\right)\hat{i}_{\mathrm{Ld}} - \left(\frac{r_{\mathrm{L}}}{L}+\frac{3}{2}\frac{r_{\mathrm{C}}D_{\mathrm{q}}^2}{L}\right)\hat{i}_{\mathrm{Lq}} + \frac{D_{\mathrm{q}}}{L}\hat{u}_{\mathrm{C}} + \frac{r_{\mathrm{C}}D_{\mathrm{q}}}{L}\hat{i}_{\mathrm{in}} - \frac{1}{L}\hat{u}_{\mathrm{oq}} - \frac{2}{3}\frac{r_{\mathrm{C}}\omega_{\mathrm{s}}I_{\mathrm{in}}^2}{U_{\mathrm{in}}D_{\mathrm{d}}^2}\hat{d}_{\mathrm{d}} + \frac{U_{\mathrm{in}}}{L}\hat{d}_{\mathrm{q}}, \tag{2.95}$$

$$\frac{\mathrm{d}\hat{u}_{\mathrm{C}}}{\mathrm{d}t} = -\frac{3}{2}\frac{D_{\mathrm{d}}}{C}\hat{i}_{\mathrm{Ld}} - \frac{3}{2}\frac{D_{\mathrm{q}}}{C}\hat{i}_{\mathrm{Lq}} + \frac{1}{C}\hat{i}_{\mathrm{in}} - \frac{I_{\mathrm{in}}}{D_{\mathrm{d}}C}\hat{d}_{\mathrm{d}}. \tag{2.96}$$

Eqs. (2.91)–(2.96) can be expressed in matrix form according to (1.4) as

$$\begin{aligned}\frac{\mathrm{d}\hat{\boldsymbol{x}}(t)}{\mathrm{d}t} &= \mathbf{A}\hat{\boldsymbol{x}}(t) + \mathbf{B}\hat{\boldsymbol{u}}(t),\\ \hat{\boldsymbol{y}}(t) &= \mathbf{C}\hat{\boldsymbol{x}}(t) + \mathbf{D}\hat{\boldsymbol{u}}(t),\end{aligned} \tag{2.97}$$

where the state, input and output-variable vectors are defined as

$$\hat{\boldsymbol{x}} = \begin{bmatrix}\hat{i}_{\mathrm{Ld}} & \hat{i}_{\mathrm{Lq}} & \hat{u}_{\mathrm{C}}\end{bmatrix}^{\mathrm{T}},\ \hat{\boldsymbol{u}} = \begin{bmatrix}\hat{i}_{\mathrm{in}} & \hat{u}_{\mathrm{od}} & \hat{u}_{\mathrm{oq}} & \hat{d}_{\mathrm{d}} & \hat{d}_{\mathrm{q}}\end{bmatrix}^{\mathrm{T}},\ \hat{\boldsymbol{y}} = \begin{bmatrix}\hat{u}_{\mathrm{in}} & \hat{i}_{\mathrm{od}} & \hat{i}_{\mathrm{oq}}\end{bmatrix}^{\mathrm{T}}, \tag{2.98}$$

and the state matrices $\mathbf{A}$, $\mathbf{B}$, $\mathbf{C}$ and $\mathbf{D}$ are defined as

$$\begin{aligned}\mathbf{A} &= \begin{bmatrix} -\left(\frac{r_{\mathrm{eq}}}{L}+\frac{3}{2}\frac{r_{\mathrm{C}}D_{\mathrm{d}}^2}{L}\right) & \omega_{\mathrm{s}}\left(1-\frac{r_{\mathrm{C}}I_{\mathrm{in}}}{U_{\mathrm{in}}}\right) & \frac{D_{\mathrm{d}}}{L} \\ -\omega_{\mathrm{s}}\left(1+\frac{r_{\mathrm{C}}I_{\mathrm{in}}}{U_{\mathrm{in}}}\right) & -\left(\frac{r_{\mathrm{eq}}}{L}+\frac{3}{2}\frac{r_{\mathrm{C}}D_{\mathrm{q}}^2}{L}\right) & \frac{D_{\mathrm{q}}}{L} \\ -\frac{3}{2}\frac{D_{\mathrm{d}}}{C} & -\frac{3}{2}\frac{D_{\mathrm{q}}}{C} & 0 \end{bmatrix},\\ \mathbf{B} &= \begin{bmatrix} \frac{r_{\mathrm{C}}D_{\mathrm{d}}}{L} & -\frac{1}{L} & 0 & \frac{U_{\mathrm{in}}-r_{\mathrm{C}}I_{\mathrm{in}}}{L} & 0 \\ \frac{r_{\mathrm{C}}D_{\mathrm{q}}}{L} & 0 & -\frac{1}{L} & -\frac{2}{3}\frac{r_{\mathrm{C}}\omega_{\mathrm{s}}I_{\mathrm{in}}^2}{U_{\mathrm{in}}D_{\mathrm{d}}^2} & \frac{U_{\mathrm{in}}}{L} \\ \frac{1}{C} & 0 & 0 & -\frac{I_{\mathrm{in}}}{D_{\mathrm{d}}C} & 0 \end{bmatrix},\\ \mathbf{C} &= \begin{bmatrix} 0 & 0 & 1+r_{\mathrm{C}}C\frac{\mathrm{d}}{\mathrm{d}t} \\ 1 & 0 & 0 \\ 0 & 1 & 0 \end{bmatrix},\quad \mathbf{D} = \mathbf{0},\end{aligned} \tag{2.99}$$

According to (1.7), Eqs. (2.97)–(2.99) can be used to solve the transfer functions between the input and output variables as

$$\boldsymbol{Y}(s) = \left[\mathbf{C}\left(s\mathbf{I}-\mathbf{A}\right)^{-1}\mathbf{B}+\mathbf{D}\right]\boldsymbol{U}(s) = \mathbf{G}_{\mathrm{H}}\boldsymbol{U}(s), \tag{2.100}$$

where the transfer function matrix $\mathbf{G}_{\mathrm{H}}$ is known as the modified H-parameter representation of a CF-VSI and is presented in (2.101). The top row describes the input dynamics and the two bottom rows the d-channel and q-channel output dynamics of the inverter. The term 'modified' is used since the output current flows out of the converter and has to be taken into account in the transfer function matrix by multiplying the output

admittances $Y_{\text{o-d}}$ and $Y_{\text{o-q}}$ by '-1'.

$$\begin{bmatrix} \hat{u}_{\text{in}} \\ \hat{i}_{\text{od}} \\ \hat{i}_{\text{oq}} \end{bmatrix} = \begin{bmatrix} Z_{\text{in}}^{\text{H}} & T_{\text{oi-d}}^{\text{H}} & T_{\text{oi-q}}^{\text{H}} & G_{\text{ci-d}}^{\text{H}} & G_{\text{ci-q}}^{\text{H}} \\ G_{\text{io-d}}^{\text{H}} & -Y_{\text{o-d}}^{\text{H}} & G_{\text{cr-qd}}^{\text{H}} & G_{\text{co-d}}^{\text{H}} & G_{\text{co-qd}}^{\text{H}} \\ G_{\text{io-q}}^{\text{H}} & G_{\text{cr-dq}}^{\text{H}} & -Y_{\text{o-q}}^{\text{H}} & G_{\text{co-dq}}^{\text{H}} & G_{\text{co-q}}^{\text{H}} \end{bmatrix} \begin{bmatrix} \hat{i}_{\text{in}} \\ \hat{u}_{\text{od}} \\ \hat{u}_{\text{oq}} \\ \hat{d}_{\text{d}} \\ \hat{d}_{\text{q}} \end{bmatrix} \tag{2.101}$$

The input dynamics as presented in (2.102) can be described as follows: the transfer function between the input current and the input voltage is known as the input impedance Z_{in}. The transfer function between the output voltages and the input voltage is known as the reverse or output-to-input transfer function or transmittance T_{oi}. The transfer function between the control variable and the input voltage is known as the control-to-input-voltage transfer function G_{ci}.

$$\hat{u}_{\text{in}} = Z_{\text{in}}^{\text{H}}\hat{i}_{\text{in}} + T_{\text{oi-d}}^{\text{H}}\hat{u}_{\text{od}} + T_{\text{oi-q}}^{\text{H}}\hat{u}_{\text{oq}} + G_{\text{ci-d}}^{\text{H}}\hat{d}_{\text{d}} + G_{\text{ci-q}}^{\text{H}}\hat{d}_{\text{q}} \tag{2.102}$$

The output dynamics as presented in (2.103) and (2.104) can be described as follows: the transfer function between the input current and the output current is known as the forward current gain or input-to-output transfer function or audio susceptibility G_{io}. The transfer function between the channel voltage and the same channel current is known as the output admittance Y_{o}. The transfer function between the channel voltage and the other channel current is known as the cross-coupling transfer function G_{cr}. The transfer function between the control variable and the output current is known as the control-to-output-current transfer function G_{co}.

$$\hat{i}_{\text{od}} = G_{\text{io-d}}^{\text{H}}\hat{i}_{\text{in}} - Y_{\text{o-d}}^{\text{H}}\hat{u}_{\text{od}} + G_{\text{cr-qd}}^{\text{H}}\hat{u}_{\text{oq}} + G_{\text{co-d}}^{\text{H}}\hat{d}_{\text{d}} + G_{\text{co-qd}}^{\text{H}}\hat{d}_{\text{q}} \tag{2.103}$$

$$\hat{i}_{\text{oq}} = G_{\text{io-q}}^{\text{H}}\hat{i}_{\text{in}} + G_{\text{cr-dq}}^{\text{H}}\hat{u}_{\text{od}} - Y_{\text{o-q}}^{\text{H}}\hat{u}_{\text{oq}} + G_{\text{co-dq}}^{\text{H}}\hat{d}_{\text{d}} + G_{\text{co-q}}^{\text{H}}\hat{d}_{\text{q}} \tag{2.104}$$

A linear model can be constructed based on the converter dynamics represented by (2.101) as shown inside the dashed box in Fig. 2.4.

The transfer functions in (2.101) and Fig. 2.4 for the CF-VSI without the parasitic elements can be given as presented in (2.105)–(2.120)[2]. The input impedance can be given by

$$Z_{\text{in}}^{\text{H}} = \frac{\hat{u}_{\text{in}}}{\hat{i}_{\text{in}}} = \frac{1}{C}\left(s^2 + \omega_{\text{s}}^2\right)\frac{1}{\Delta_{\text{H}}}. \tag{2.105}$$

[2]A detailed Matlab m-file that can be used to obtain (2.105)–(2.120) can be found in Appendix B.

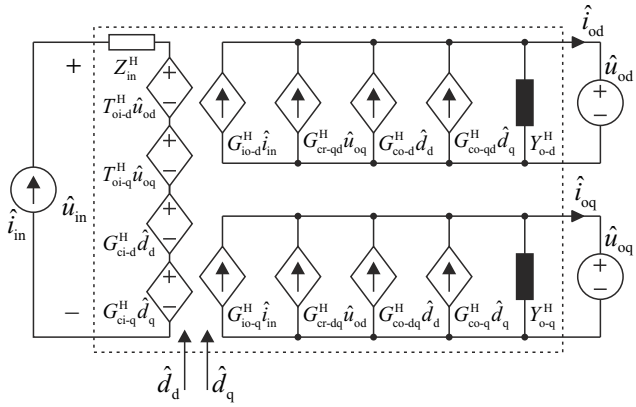

Fig. 2.4: Linear model of a grid-connected three-phase current-fed inverter.

The output-to-input transfer functions can be given by

$$T^{\mathrm{H}}_{\mathrm{oi\text{-}d}} = \frac{\hat{u}_{\mathrm{in}}}{\hat{u}_{\mathrm{od}}} = -\frac{3}{2}\frac{D_{\mathrm{d}}}{LC}\left(s - \frac{D_{\mathrm{q}}\omega_{\mathrm{s}}}{D_{\mathrm{d}}}\right)\frac{1}{\Delta_{\mathrm{H}}}, \tag{2.106}$$

$$T^{\mathrm{H}}_{\mathrm{oi\text{-}q}} = \frac{\hat{u}_{\mathrm{in}}}{\hat{u}_{\mathrm{oq}}} = -\frac{3}{2}\frac{D_{\mathrm{q}}}{LC}\left(s + \frac{D_{\mathrm{d}}\omega_{\mathrm{s}}}{D_{\mathrm{q}}}\right)\frac{1}{\Delta_{\mathrm{H}}}. \tag{2.107}$$

The transfer functions between the control variable and input current can be given by

$$G^{\mathrm{H}}_{\mathrm{ci\text{-}d}} = \frac{\hat{u}_{\mathrm{in}}}{\hat{d}_{\mathrm{d}}} = -\frac{I_{\mathrm{in}}}{D_{\mathrm{d}}C}\left(s + \frac{3}{2}\frac{D_{\mathrm{d}}^2 U_{\mathrm{in}}}{LI_{\mathrm{in}}}\right)\frac{s}{\Delta_{\mathrm{H}}}, \tag{2.108}$$

$$G^{\mathrm{H}}_{\mathrm{ci\text{-}q}} = \frac{\hat{u}_{\mathrm{in}}}{\hat{d}_{\mathrm{q}}} = -\frac{\omega_{\mathrm{s}} I_{\mathrm{in}}}{D_{\mathrm{d}}C}\left(s + \frac{3}{2}\frac{D_{\mathrm{d}}^2 U_{\mathrm{in}}}{LI_{\mathrm{in}}}\right)\frac{1}{\Delta_{\mathrm{H}}}. \tag{2.109}$$

The input-to-output transfer functions can be given by

$$G^{\mathrm{H}}_{\mathrm{io\text{-}d}} = \frac{\hat{i}_{\mathrm{od}}}{\hat{i}_{\mathrm{in}}} = \frac{D_{\mathrm{d}}}{LC}\left(s + \frac{D_{\mathrm{q}}\omega_{\mathrm{s}}}{D_{\mathrm{d}}}\right)\frac{1}{\Delta_{\mathrm{H}}}, \tag{2.110}$$

$$G^{\mathrm{H}}_{\mathrm{io\text{-}q}} = \frac{\hat{i}_{\mathrm{oq}}}{\hat{i}_{\mathrm{in}}} = \frac{D_{\mathrm{q}}}{LC}\left(s - \frac{D_{\mathrm{d}}\omega_{\mathrm{s}}}{D_{\mathrm{q}}}\right)\frac{1}{\Delta_{\mathrm{H}}}. \tag{2.111}$$

The output admittances and the cross-coupling transfer functions can be given by

$$Y^{\mathrm{H}}_{\mathrm{o\text{-}d}} = -\frac{\hat{i}_{\mathrm{od}}}{\hat{u}_{\mathrm{od}}} = \frac{1}{L}\left(s^2 + \frac{3}{2}\frac{D_{\mathrm{q}}^2}{LC}\right)\frac{1}{\Delta_{\mathrm{H}}}, \tag{2.112}$$

$$Y^{\mathrm{H}}_{\mathrm{o\text{-}q}} = -\frac{\hat{i}_{\mathrm{oq}}}{\hat{u}_{\mathrm{oq}}} = \frac{1}{L}\left(s^2 + \frac{3}{2}\frac{D_{\mathrm{q}}^2}{LC}\right)\frac{1}{\Delta_{\mathrm{H}}}, \tag{2.113}$$

$$G^{\mathrm{H}}_{\text{cr-qd}} = \frac{\hat{i}_{\mathrm{od}}}{\hat{u}_{\mathrm{oq}}} = -\frac{\omega_{\mathrm{s}}}{L}\left(s - \frac{I_{\mathrm{in}}}{U_{\mathrm{in}}C}\right)\frac{1}{\Delta_{\mathrm{H}}}, \tag{2.114}$$

$$G^{\mathrm{H}}_{\text{cr-dq}} = \frac{\hat{i}_{\mathrm{oq}}}{\hat{u}_{\mathrm{od}}} = \frac{\omega_{\mathrm{s}}}{L}\left(s + \frac{I_{\mathrm{in}}}{U_{\mathrm{in}}C}\right)\frac{1}{\Delta_{\mathrm{H}}}. \tag{2.115}$$

The transfer functions between the control variables and output currents can be given by

$$G^{\mathrm{H}}_{\text{co-d}} = \frac{\hat{i}_{\mathrm{od}}}{\hat{d}_{\mathrm{d}}} = \frac{U_{\mathrm{in}}s}{L}\left(s - \frac{I_{\mathrm{in}}}{U_{\mathrm{in}}C}\right)\frac{1}{\Delta_{\mathrm{H}}}, \tag{2.116}$$

$$G^{\mathrm{H}}_{\text{co-q}} = \frac{\hat{i}_{\mathrm{oq}}}{\hat{d}_{\mathrm{q}}} = \frac{U_{\mathrm{in}}s}{L}\left(s^2 + \frac{3}{2}\frac{D_{\mathrm{d}}^2}{LC}\right)\frac{1}{\Delta_{\mathrm{H}}}, \tag{2.117}$$

$$G^{\mathrm{H}}_{\text{co-qd}} = \frac{\hat{i}_{\mathrm{od}}}{\hat{d}_{\mathrm{q}}} = \frac{U_{\mathrm{in}}\omega_{\mathrm{s}}}{L}\left(s - \frac{I_{\mathrm{in}}}{U_{\mathrm{in}}C}\right)\frac{1}{\Delta_{\mathrm{H}}}, \tag{2.118}$$

$$G^{\mathrm{H}}_{\text{co-dq}} = \frac{\hat{i}_{\mathrm{oq}}}{\hat{d}_{\mathrm{d}}} = -\left(\frac{U_{\mathrm{in}}\omega_{\mathrm{s}}}{L} + \frac{2}{3}\frac{\omega_{\mathrm{s}}I_{\mathrm{in}}^2}{D_{\mathrm{d}}^2CU_{\mathrm{in}}}\right)\frac{1}{\Delta_{\mathrm{H}}}. \tag{2.119}$$

The determinant Δ_{H} of the transfer functions can be given by

$$\Delta_{\mathrm{H}} = s\left(s^2 + \frac{3}{2}\frac{D_{\mathrm{d}}^2 + D_{\mathrm{q}}^2}{LC} + \omega_{\mathrm{s}}^2\right). \tag{2.120}$$

2.3 Source Effect in Grid-Connected VF and CF Inverters

The dynamic representations obtained in the preceding sections describe the internal or un-terminated dynamics of the VF and CF-VSIs and are, therefore, computed using ideal source and load subsystems. However, all real sources and loads contain non-ideal internal impedances, which may change the inverter dynamics significantly. Therefore, it is crucial to be able to include such effects in the dynamic model in order to predict the dynamic behavior of the inverter correctly.

This section presents an explicit method to compute the effect of source non-idealities in the dynamics of grid-connected three-phase VF and CF inverters. The presented method is general and is applicable to all grid-connected VF and CF inverters regardless of the topology. The source-effect can include either the source impedance or an input filter connected between the source and the power stage or both.

2.3.1 Source-Affected Y-Parameter Model

Fig. 2.5 presents a source-affected model for a grid-connected VF inverter. Since the source might include parallel and series impedances, the input voltages $\hat{u}_{\mathrm{inS}}$, $\hat{u}_{\mathrm{in}}$ and input currents $\hat{i}_{\mathrm{inS}}$, $\hat{i}_{\mathrm{in}}$ may not be equal. Therefore, the source is modeled with a G-parameter representation (voltage-to-voltage) so that duality will exist in the source-side interface.

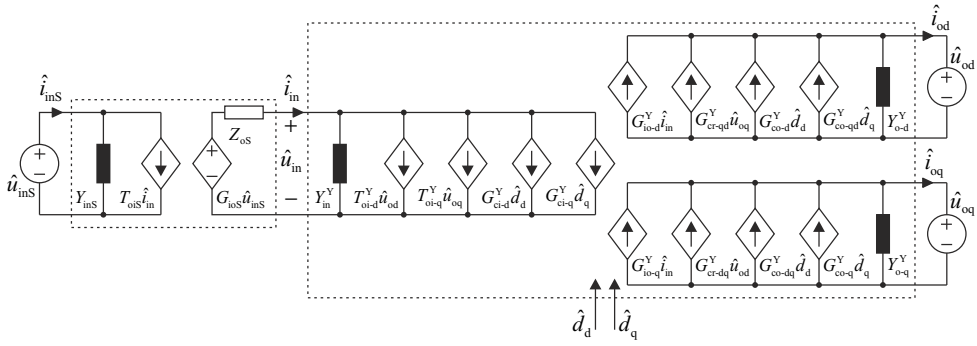

Fig. 2.5: Linear model of a grid-connected three-phase voltage-fed inverter with a non-ideal source.

The small-signal input voltage $\hat{u}_{\mathrm{in}}$ can be given according to Fig. 2.5 as

$$\hat{u}_{\mathrm{in}} = G_{\mathrm{ioS}}\hat{u}_{\mathrm{inS}} - Z_{\mathrm{oS}}\hat{i}_{\mathrm{in}}. \tag{2.121}$$

Substituting $\hat{i}_{\mathrm{in}}$ from (2.45) into (2.121) and solving for $\hat{u}_{\mathrm{in}}$ yields

$$\hat{u}_{\mathrm{in}} = \frac{G_{\mathrm{ioS}}}{1+Z_{\mathrm{oS}}Y_{\mathrm{in}}^{\mathrm{Y}}}\hat{u}_{\mathrm{inS}} - \frac{Z_{\mathrm{oS}}T_{\mathrm{oi\text{-}d}}^{\mathrm{Y}}}{1+Z_{\mathrm{oS}}Y_{\mathrm{in}}^{\mathrm{Y}}}\hat{u}_{\mathrm{od}} - \frac{Z_{\mathrm{oS}}T_{\mathrm{oi\text{-}q}}^{\mathrm{Y}}}{1+Z_{\mathrm{oS}}Y_{\mathrm{in}}^{\mathrm{Y}}}\hat{u}_{\mathrm{oq}} - \frac{Z_{\mathrm{oS}}C_{\mathrm{ci\text{-}d}}^{\mathrm{Y}}}{1+Z_{\mathrm{oS}}Y_{\mathrm{in}}^{\mathrm{Y}}}\hat{d}_{\mathrm{d}} - \frac{Z_{\mathrm{oS}}G_{\mathrm{ci\text{-}q}}^{\mathrm{Y}}}{1+Z_{\mathrm{oS}}Y_{\mathrm{in}}^{\mathrm{Y}}}\hat{d}_{\mathrm{q}}, \quad (2.122)$$

which can be substituted in the nominal dynamics represented by (2.44) yielding the source affected model as presented in (2.123)–(2.125), where the superscript extension 'S' denotes the source effect.

$$\hat{i}_{\mathrm{in}} = Y_{\mathrm{in}}^{\mathrm{YS}}\hat{u}_{\mathrm{inS}} + T_{\mathrm{oi\text{-}d}}^{\mathrm{YS}}\hat{u}_{\mathrm{od}} + T_{\mathrm{oi\text{-}q}}^{\mathrm{YS}}\hat{u}_{\mathrm{oq}} + G_{\mathrm{ci\text{-}d}}^{\mathrm{YS}}\hat{d}_{\mathrm{d}} + G_{\mathrm{ci\text{-}q}}^{\mathrm{YS}}\hat{d}_{\mathrm{q}} \quad (2.123)$$

$$\hat{i}_{\mathrm{od}} = G_{\mathrm{io\text{-}d}}^{\mathrm{YS}}\hat{u}_{\mathrm{inS}} - Y_{\mathrm{o\text{-}d}}^{\mathrm{YS}}\hat{u}_{\mathrm{od}} + G_{\mathrm{cr\text{-}qd}}^{\mathrm{YS}}\hat{u}_{\mathrm{oq}} + G_{\mathrm{co\text{-}d}}^{\mathrm{YS}}\hat{d}_{\mathrm{d}} + G_{\mathrm{co\text{-}qd}}^{\mathrm{YS}}\hat{d}_{\mathrm{q}} \quad (2.124)$$

$$\hat{i}_{\mathrm{oq}} = G_{\mathrm{io\text{-}q}}^{\mathrm{YS}}\hat{u}_{\mathrm{inS}} + G_{\mathrm{cr\text{-}dq}}^{\mathrm{YS}}\hat{u}_{\mathrm{od}} - Y_{\mathrm{o\text{-}q}}^{\mathrm{YS}}\hat{u}_{\mathrm{oq}} + G_{\mathrm{co\text{-}dq}}^{\mathrm{YS}}\hat{d}_{\mathrm{d}} + G_{\mathrm{co\text{-}q}}^{\mathrm{YS}}\hat{d}_{\mathrm{q}} \quad (2.125)$$

where

$$Y_{\mathrm{in}}^{\mathrm{YS}} = \frac{\hat{i}_{\mathrm{in}}}{\hat{u}_{\mathrm{inS}}} = \frac{G_{\mathrm{ioS}}}{1+Z_{\mathrm{oS}}Y_{\mathrm{in}}^{\mathrm{Y}}}Y_{\mathrm{in}}^{\mathrm{Y}}, \quad (2.126)$$

$$T_{\mathrm{oi\text{-}d}}^{\mathrm{YS}} = \frac{\hat{i}_{\mathrm{in}}}{\hat{u}_{\mathrm{od}}} = \frac{1}{1+Z_{\mathrm{oS}}Y_{\mathrm{in}}^{\mathrm{Y}}}T_{\mathrm{oi\text{-}d}}^{\mathrm{Y}}, \quad (2.127)$$

$$T_{\mathrm{oi\text{-}q}}^{\mathrm{YS}} = \frac{\hat{i}_{\mathrm{in}}}{\hat{u}_{\mathrm{oq}}} = \frac{1}{1+Z_{\mathrm{oS}}Y_{\mathrm{in}}^{\mathrm{Y}}}T_{\mathrm{oi\text{-}q}}^{\mathrm{Y}}, \quad (2.128)$$

$$G_{\mathrm{ci\text{-}d}}^{\mathrm{YS}} = \frac{\hat{i}_{\mathrm{in}}}{\hat{d}_{\mathrm{d}}} = \frac{1}{1+Z_{\mathrm{oS}}Y_{\mathrm{in}}^{\mathrm{Y}}}G_{\mathrm{ci\text{-}d}}^{\mathrm{Y}}, \quad (2.129)$$

$$G_{\mathrm{ci\text{-}q}}^{\mathrm{YS}} = \frac{\hat{i}_{\mathrm{in}}}{\hat{d}_{\mathrm{q}}} = \frac{1}{1+Z_{\mathrm{oS}}Y_{\mathrm{in}}^{\mathrm{Y}}}G_{\mathrm{ci\text{-}q}}^{\mathrm{Y}}, \quad (2.130)$$

$$G_{\mathrm{io\text{-}d}}^{\mathrm{YS}} = \frac{\hat{i}_{\mathrm{od}}}{\hat{u}_{\mathrm{inS}}} = \frac{G_{\mathrm{ioS}}}{1+Z_{\mathrm{oS}}Y_{\mathrm{in}}^{\mathrm{Y}}}G_{\mathrm{io\text{-}d}}^{\mathrm{Y}}, \quad (2.131)$$

$$Y_{\mathrm{o\text{-}d}}^{\mathrm{YS}} = -\frac{\hat{i}_{\mathrm{od}}}{\hat{u}_{\mathrm{od}}} = \frac{1+Z_{\mathrm{oS}}Y_{\mathrm{in\text{-}d\text{-}oc}}^{\mathrm{Y}}}{1+Z_{\mathrm{oS}}Y_{\mathrm{in}}^{\mathrm{Y}}}Y_{\mathrm{o\text{-}d}}^{\mathrm{Y}}, \quad (2.132)$$

$$G_{\mathrm{cr\text{-}qd}}^{\mathrm{YS}} = \frac{\hat{i}_{\mathrm{od}}}{\hat{u}_{\mathrm{oq}}} = \frac{1+Z_{\mathrm{oS}}Y_{\mathrm{in\text{-}qd\text{-}oc}}^{\mathrm{Y}}}{1+Z_{\mathrm{oS}}Y_{\mathrm{in}}^{\mathrm{Y}}}G_{\mathrm{cr\text{-}qd}}^{\mathrm{Y}}, \quad (2.133)$$

$$G_{\mathrm{co\text{-}d}}^{\mathrm{YS}} = \frac{\hat{i}_{\mathrm{od}}}{\hat{d}_{\mathrm{d}}} = \frac{1+Z_{\mathrm{oS}}Y_{\mathrm{in\text{-}d\text{-}\infty}}^{\mathrm{Y}}}{1+Z_{\mathrm{oS}}Y_{\mathrm{in}}^{\mathrm{Y}}}G_{\mathrm{co\text{-}d}}^{\mathrm{Y}}, \quad (2.134)$$

$$G^{\mathrm{YS}}_{\text{co-qd}} = \frac{\hat{i}_{\mathrm{od}}}{\hat{d}_{\mathrm{q}}} = \frac{1 + Z_{\mathrm{oS}} Y^{\mathrm{Y}}_{\text{in-qd-}\infty}}{1 + Z_{\mathrm{oS}} Y^{\mathrm{Y}}_{\mathrm{in}}} G^{\mathrm{Y}}_{\text{co-qd}}, \tag{2.135}$$

$$G^{\mathrm{YS}}_{\text{io-q}} = \frac{\hat{i}_{\mathrm{oq}}}{\hat{u}_{\mathrm{inS}}} = \frac{G_{\mathrm{ioS}}}{1 + Z_{\mathrm{oS}} Y^{\mathrm{Y}}_{\mathrm{in}}} G^{\mathrm{Y}}_{\text{io-q}}, \tag{2.136}$$

$$G^{\mathrm{YS}}_{\text{cr-dq}} = \frac{\hat{i}_{\mathrm{oq}}}{\hat{u}_{\mathrm{od}}} = \frac{1 + Z_{\mathrm{oS}} Y^{\mathrm{Y}}_{\text{in-dq-oc}}}{1 + Z_{\mathrm{oS}} Y^{\mathrm{Y}}_{\mathrm{in}}} G^{\mathrm{Y}}_{\text{cr-dq}}, \tag{2.137}$$

$$Y^{\mathrm{YS}}_{\text{o-q}} = -\frac{\hat{i}_{\mathrm{oq}}}{\hat{u}_{\mathrm{oq}}} = \frac{1 + Z_{\mathrm{oS}} Y^{\mathrm{Y}}_{\text{in-q-oc}}}{1 + Z_{\mathrm{oS}} Y^{\mathrm{Y}}_{\mathrm{in}}} Y^{\mathrm{Y}}_{\text{o-q}}, \tag{2.138}$$

$$G^{\mathrm{YS}}_{\text{co-dq}} = \frac{\hat{i}_{\mathrm{oq}}}{\hat{d}_{\mathrm{d}}} = \frac{1 + Z_{\mathrm{oS}} Y^{\mathrm{Y}}_{\text{in-dq-}\infty}}{1 + Z_{\mathrm{oS}} Y^{\mathrm{Y}}_{\mathrm{in}}} G^{\mathrm{Y}}_{\text{co-dq}}, \tag{2.139}$$

$$G^{\mathrm{YS}}_{\text{co-q}} = \frac{\hat{i}_{\mathrm{oq}}}{\hat{d}_{\mathrm{q}}} = \frac{1 + Z_{\mathrm{oS}} Y^{\mathrm{Y}}_{\text{in-q-}\infty}}{1 + Z_{\mathrm{oS}} Y^{\mathrm{Y}}_{\mathrm{in}}} G^{\mathrm{Y}}_{\text{co-q}}, \tag{2.140}$$

and

$$\begin{aligned} Y^{\mathrm{Y}}_{\text{in-d-oc}} &= Y^{\mathrm{Y}}_{\mathrm{in}} + \frac{T^{\mathrm{Y}}_{\text{oi-d}} G^{\mathrm{Y}}_{\text{io-d}}}{Y^{\mathrm{Y}}_{\text{o-d}}}, \quad Y^{\mathrm{Y}}_{\text{in-qd-oc}} = Y^{\mathrm{Y}}_{\mathrm{in}} - \frac{T^{\mathrm{Y}}_{\text{oi-q}} G^{\mathrm{Y}}_{\text{io-d}}}{G^{\mathrm{Y}}_{\text{cr-qd}}}, \\ Y^{\mathrm{Y}}_{\text{in-dq-oc}} &= Y^{\mathrm{Y}}_{\mathrm{in}} - \frac{T^{\mathrm{Y}}_{\text{oi-d}} G^{\mathrm{Y}}_{\text{io-q}}}{G^{\mathrm{Y}}_{\text{cr-dq}}}, \quad Y^{\mathrm{Y}}_{\text{in-q-oc}} = Y^{\mathrm{Y}}_{\mathrm{in}} + \frac{T^{\mathrm{Y}}_{\text{oi-q}} G^{\mathrm{Y}}_{\text{io-q}}}{Y^{\mathrm{Y}}_{\text{o-q}}}, \end{aligned} \tag{2.141}$$

$$\begin{aligned} Y^{\mathrm{Y}}_{\text{in-d-}\infty} &= Y^{\mathrm{Y}}_{\mathrm{in}} - \frac{G^{\mathrm{Y}}_{\text{ci-d}} G^{\mathrm{Y}}_{\text{io-d}}}{G^{\mathrm{Y}}_{\text{co-d}}}, \quad Y^{\mathrm{Y}}_{\text{in-qd-}\infty} = Y^{\mathrm{Y}}_{\mathrm{in}} - \frac{G^{\mathrm{Y}}_{\text{ci-q}} G^{\mathrm{Y}}_{\text{io-d}}}{G^{\mathrm{Y}}_{\text{co-qd}}}, \\ Y^{\mathrm{Y}}_{\text{in-dq-}\infty} &= Y^{\mathrm{Y}}_{\mathrm{in}} - \frac{G^{\mathrm{Y}}_{\text{ci-d}} G^{\mathrm{Y}}_{\text{io-q}}}{G^{\mathrm{Y}}_{\text{co-dq}}}, \quad Y^{\mathrm{Y}}_{\text{in-q-}\infty} = Y^{\mathrm{Y}}_{\mathrm{in}} - \frac{G^{\mathrm{Y}}_{\text{ci-q}} G^{\mathrm{Y}}_{\text{io-q}}}{G^{\mathrm{Y}}_{\text{co-q}}}. \end{aligned} \tag{2.142}$$

Since there might be parallel components in the source impedance, the source input current $\hat{i}_{\mathrm{inS}}$ and the converter input current $\hat{i}_{\mathrm{in}}$ may not be equal. The input current $\hat{i}_{\mathrm{inS}}$ can be given according to Fig. 2.5 by

$$\hat{i}_{\mathrm{inS}} = Y_{\mathrm{inS}} \hat{u}_{\mathrm{inS}} + T_{\mathrm{oiS}} \hat{i}_{\mathrm{in}}. \tag{2.143}$$

The dynamics between the system input variables ($\hat{u}_{\mathrm{inS}}$, $\hat{u}_{\mathrm{od}}$, $\hat{u}_{\mathrm{oq}}$, $\hat{d}_{\mathrm{d}}$ and $\hat{d}_{\mathrm{q}}$) and the source current $\hat{i}_{\mathrm{inS}}$ can be given by substituting (2.123) into (2.143) yielding

$$\hat{i}_{\mathrm{inS}} = Y^{\mathrm{YS}}_{\mathrm{inS}} \hat{u}_{\mathrm{inS}} + T^{\mathrm{YS}}_{\text{oi-dS}} \hat{u}_{\mathrm{od}} + T^{\mathrm{YS}}_{\text{oi-qS}} \hat{u}_{\mathrm{oq}} + G^{\mathrm{YS}}_{\text{ci-dS}} \hat{d}_{\mathrm{d}} + G^{\mathrm{YS}}_{\text{ci-qS}} \hat{d}_{\mathrm{q}}, \tag{2.144}$$

where

$$Y_{\text{inS}}^{\text{YS}} = \frac{\hat{i}_{\text{inS}}}{\hat{u}_{\text{inS}}} = \frac{1 + Y_{\text{in}}^{\text{Y}} Z_{\text{oS-}\infty}^{\text{Y}}}{1 + Z_{\text{oS}} Y_{\text{in}}^{\text{Y}}} Y_{\text{inS}}, \tag{2.145}$$

$$T_{\text{oi-dS}}^{\text{YS}} = \frac{\hat{i}_{\text{inS}}}{\hat{u}_{\text{od}}} = \frac{T_{\text{oiS}}}{1 + Z_{\text{oS}} Y_{\text{in}}^{\text{Y}}} T_{\text{oi-d}}^{\text{Y}}, \tag{2.146}$$

$$T_{\text{oi-qS}}^{\text{YS}} = \frac{\hat{i}_{\text{inS}}}{\hat{u}_{\text{oq}}} = \frac{T_{\text{oiS}}}{1 + Z_{\text{oS}} Y_{\text{in}}^{\text{Y}}} T_{\text{oi-q}}^{\text{Y}}, \tag{2.147}$$

$$G_{\text{ci-dS}}^{\text{YS}} = \frac{\hat{i}_{\text{inS}}}{\hat{d}_{\text{d}}} = \frac{T_{\text{oiS}}}{1 + Z_{\text{oS}} Y_{\text{in}}^{\text{Y}}} G_{\text{ci-d}}^{\text{Y}}, \tag{2.148}$$

$$G_{\text{ci-qS}}^{\text{YS}} = \frac{\hat{i}_{\text{inS}}}{\hat{d}_{\text{q}}} = \frac{T_{\text{oiS}}}{1 + Z_{\text{oS}} Y_{\text{in}}^{\text{Y}}} G_{\text{ci-q}}^{\text{Y}}, \tag{2.149}$$

and

$$Z_{\text{oS-}\infty} = Z_{\text{oS}} + \frac{T_{\text{oiS}} G_{\text{ioS}}}{Y_{\text{inS}}}. \tag{2.150}$$

The source-affected Y-parameter model can also be used to investigate the stability of the source/inverter interface by applying the Nyquist stability criterion to the impedance ratio $Z_{\text{oS}} Y_{\text{in}}^{\text{Y}} = Z_{\text{oS}} / Z_{\text{in}}^{\text{Y}}$, which is known as the minor loop gain and is found in (2.126)–(2.149).

2.3.2 Source-Affected H-Parameter Model

Fig. 2.6 presents a source-affected model for a grid-connected CF inverter. Since the source might include parallel and series impedances, the input voltages $\hat{u}_{\mathrm{inS}}$, $\hat{u}_{\mathrm{in}}$ and input currents $\hat{i}_{\mathrm{inS}}$, $\hat{i}_{\mathrm{in}}$ may not be the same. Therefore, the source is modeled with an H-parameter (current-to-current) representation so that duality will exist in the source-side interface.

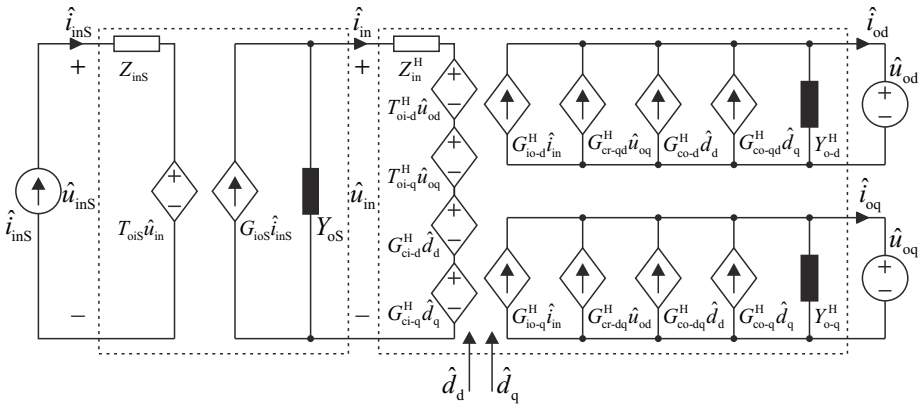

Fig. 2.6: Linear model of a grid-connected three-phase current-fed inverter with a non-ideal source.

The small-signal input current $\hat{i}_{\mathrm{in}}$ can be given according to Fig. 2.6 as

$$\hat{i}_{\mathrm{in}} = G_{\mathrm{ioS}}\hat{i}_{\mathrm{inS}} - Y_{\mathrm{oS}}\hat{u}_{\mathrm{in}}. \tag{2.151}$$

Substituting $\hat{u}_{\mathrm{in}}$ in (2.102) into (2.151) and solving for $\hat{i}_{\mathrm{in}}$ yields

$$\begin{aligned}\hat{i}_{\mathrm{in}} = \frac{G_{\mathrm{ioS}}}{1+Y_{\mathrm{oS}}Z^{\mathrm{H}}_{\mathrm{in}}}\hat{i}_{\mathrm{inS}} - \frac{Y_{\mathrm{oS}}T^{\mathrm{H}}_{\mathrm{oi\text{-}d}}}{1+Y_{\mathrm{oS}}Z^{\mathrm{H}}_{\mathrm{in}}}\hat{u}_{\mathrm{od}} - \frac{Y_{\mathrm{oS}}T^{\mathrm{H}}_{\mathrm{oi\text{-}q}}}{1+Y_{\mathrm{oS}}Z^{\mathrm{H}}_{\mathrm{in}}}\hat{u}_{\mathrm{oq}} \\ - \frac{Y_{\mathrm{oS}}G^{\mathrm{H}}_{\mathrm{ci\text{-}d}}}{1+Y_{\mathrm{oS}}Z^{\mathrm{H}}_{\mathrm{in}}}\hat{d}_{\mathrm{d}} - \frac{Y_{\mathrm{oS}}G^{\mathrm{H}}_{\mathrm{ci\text{-}q}}}{1+Y_{\mathrm{oS}}Z^{\mathrm{H}}_{\mathrm{in}}}\hat{d}_{\mathrm{q}},\end{aligned} \tag{2.152}$$

which can be substituted in the nominal dynamics represented by (2.101) yielding the source affected model as presented in (2.153)–(2.155), where the superscript extension 'S' denotes the source-effect.

$$\hat{u}_{\mathrm{in}} = Z^{\mathrm{HS}}_{\mathrm{in}}\hat{i}_{\mathrm{inS}} + T^{\mathrm{HS}}_{\mathrm{oi\text{-}d}}\hat{u}_{\mathrm{od}} + T^{\mathrm{HS}}_{\mathrm{oi\text{-}q}}\hat{u}_{\mathrm{oq}} + G^{\mathrm{HS}}_{\mathrm{ci\text{-}d}}\hat{d}_{\mathrm{d}} + G^{\mathrm{HS}}_{\mathrm{ci\text{-}q}}\hat{d}_{\mathrm{q}} \tag{2.153}$$

$$\hat{i}_{\mathrm{od}} = G^{\mathrm{HS}}_{\mathrm{io\text{-}d}}\hat{i}_{\mathrm{inS}} - Y^{\mathrm{HS}}_{\mathrm{o\text{-}d}}\hat{u}_{\mathrm{od}} + G^{\mathrm{HS}}_{\mathrm{cr\text{-}qd}}\hat{u}_{\mathrm{oq}} + G^{\mathrm{HS}}_{\mathrm{co\text{-}d}}\hat{d}_{\mathrm{d}} + G^{\mathrm{HS}}_{\mathrm{co\text{-}qd}}\hat{d}_{\mathrm{q}} \tag{2.154}$$

$$\hat{i}_{\mathrm{oq}} = G^{\mathrm{HS}}_{\mathrm{io\text{-}q}}\hat{i}_{\mathrm{inS}} + G^{\mathrm{HS}}_{\mathrm{cr\text{-}dq}}\hat{u}_{\mathrm{od}} - Y^{\mathrm{HS}}_{\mathrm{o\text{-}q}}\hat{u}_{\mathrm{oq}} + G^{\mathrm{HS}}_{\mathrm{co\text{-}dq}}\hat{d}_{\mathrm{d}} + G^{\mathrm{HS}}_{\mathrm{co\text{-}q}}\hat{d}_{\mathrm{q}} \tag{2.155}$$

where

$$Z_{\text{in}}^{\text{HS}} = \frac{\hat{u}_{\text{in}}}{\hat{i}_{\text{inS}}} = \frac{G_{\text{ioS}}}{1 + Y_{\text{oS}} Z_{\text{in}}^{\text{H}}} Z_{\text{in}}^{\text{H}}, \tag{2.156}$$

$$T_{\text{oi-d}}^{\text{HS}} = \frac{\hat{u}_{\text{in}}}{\hat{u}_{\text{od}}} = \frac{1}{1 + Y_{\text{oS}} Z_{\text{in}}^{\text{H}}} T_{\text{oi-d}}^{\text{H}}, \tag{2.157}$$

$$T_{\text{oi-q}}^{\text{HS}} = \frac{\hat{u}_{\text{in}}}{\hat{u}_{\text{oq}}} = \frac{1}{1 + Y_{\text{oS}} Z_{\text{in}}^{\text{H}}} T_{\text{oi-q}}^{\text{H}}, \tag{2.158}$$

$$G_{\text{ci-d}}^{\text{HS}} = \frac{\hat{u}_{\text{in}}}{\hat{d}_{\text{d}}} = \frac{1}{1 + Y_{\text{oS}} Z_{\text{in}}^{\text{H}}} G_{\text{ci-d}}^{\text{H}}, \tag{2.159}$$

$$G_{\text{ci-q}}^{\text{HS}} = \frac{\hat{u}_{\text{in}}}{\hat{d}_{\text{q}}} = \frac{1}{1 + Y_{\text{oS}} Z_{\text{in}}^{\text{H}}} G_{\text{ci-q}}^{\text{H}}, \tag{2.160}$$

$$G_{\text{io-d}}^{\text{HS}} = \frac{\hat{i}_{\text{od}}}{\hat{i}_{\text{inS}}} = \frac{G_{\text{ioS}}}{1 + Y_{\text{oS}} Z_{\text{in}}^{\text{H}}} G_{\text{io-d}}^{\text{H}}, \tag{2.161}$$

$$Y_{\text{o-d}}^{\text{HS}} = -\frac{\hat{i}_{\text{od}}}{\hat{u}_{\text{od}}} = \frac{1 + Y_{\text{oS}} Z_{\text{in-d-oc}}^{\text{H}}}{1 + Y_{\text{oS}} Z_{\text{in}}^{\text{H}}} Y_{\text{o-d}}^{\text{H}}, \tag{2.162}$$

$$G_{\text{cr-qd}}^{\text{HS}} = \frac{\hat{i}_{\text{od}}}{\hat{u}_{\text{oq}}} = \frac{1 + Y_{\text{oS}} Z_{\text{in-qd-oc}}^{\text{H}}}{1 + Y_{\text{oS}} Z_{\text{in}}^{\text{H}}} G_{\text{cr-qd}}^{\text{H}}, \tag{2.163}$$

$$G_{\text{co-d}}^{\text{HS}} = \frac{\hat{i}_{\text{od}}}{\hat{d}_{\text{d}}} = \frac{1 + Y_{\text{oS}} Z_{\text{in-d-}\infty}^{\text{H}}}{1 + Y_{\text{oS}} Z_{\text{in}}^{\text{H}}} G_{\text{co-d}}^{\text{H}}, \tag{2.164}$$

$$G_{\text{co-qd}}^{\text{HS}} = \frac{\hat{i}_{\text{od}}}{\hat{d}_{\text{q}}} = \frac{1 + Y_{\text{oS}} Z_{\text{in-qd-}\infty}^{\text{H}}}{1 + Y_{\text{oS}} Z_{\text{in}}^{\text{H}}} G_{\text{co-qd}}^{\text{H}}, \tag{2.165}$$

$$G_{\text{io-q}}^{\text{HS}} = \frac{\hat{i}_{\text{oq}}}{\hat{i}_{\text{inS}}} = \frac{G_{\text{ioS}}}{1 + Y_{\text{oS}} Z_{\text{in}}^{\text{H}}} G_{\text{io-q}}^{\text{H}}, \tag{2.166}$$

$$G_{\text{cr-dq}}^{\text{HS}} = \frac{\hat{i}_{\text{oq}}}{\hat{u}_{\text{od}}} = \frac{1 + Y_{\text{oS}} Z_{\text{in-dq-oc}}^{\text{H}}}{1 + Y_{\text{oS}} Z_{\text{in}}^{\text{H}}} G_{\text{cr-dq}}^{\text{H}}, \tag{2.167}$$

$$Y_{\text{o-q}}^{\text{HS}} = -\frac{\hat{i}_{\text{oq}}}{\hat{u}_{\text{oq}}} = \frac{1 + Y_{\text{oS}} Z_{\text{in-q-oc}}^{\text{H}}}{1 + Y_{\text{oS}} Z_{\text{in}}^{\text{H}}} Y_{\text{o-q}}^{\text{H}}, \tag{2.168}$$

$$G_{\text{co-dq}}^{\text{HS}} = \frac{\hat{i}_{\text{oq}}}{\hat{d}_{\text{d}}} = \frac{1 + Y_{\text{oS}} Z_{\text{in-dq-}\infty}^{\text{H}}}{1 + Y_{\text{oS}} Z_{\text{in}}^{\text{H}}} G_{\text{co-dq}}^{\text{H}}, \tag{2.169}$$

$$G_{\text{co-q}}^{\text{HS}} = \frac{\hat{i}_{\text{oq}}}{\hat{d}_{\text{q}}} = \frac{1 + Y_{\text{oS}} Z_{\text{in-q-}\infty}^{\text{H}}}{1 + Y_{\text{oS}} Z_{\text{in}}^{\text{H}}} G_{\text{co-q}}^{\text{H}}, \tag{2.170}$$

and

$$\begin{aligned} Z^{\mathrm{H}}_{\text{in-d-oc}} &= Z^{\mathrm{H}}_{\text{in}} + \frac{T^{\mathrm{H}}_{\text{oi-d}} G^{\mathrm{H}}_{\text{io-d}}}{Y^{\mathrm{H}}_{\text{o-d}}}, \quad Z^{\mathrm{H}}_{\text{in-qd-oc}} = Z^{\mathrm{H}}_{\text{in}} - \frac{T^{\mathrm{H}}_{\text{oi-q}} G^{\mathrm{H}}_{\text{io-d}}}{G^{\mathrm{H}}_{\text{cr-qd}}}, \\ Z^{\mathrm{H}}_{\text{in-dq-oc}} &= Z^{\mathrm{H}}_{\text{in}} - \frac{T^{\mathrm{H}}_{\text{oi-d}} G^{\mathrm{H}}_{\text{io-q}}}{G^{\mathrm{H}}_{\text{cr-dq}}}, \quad Z^{\mathrm{H}}_{\text{in-q-oc}} = Z^{\mathrm{H}}_{\text{in}} + \frac{T^{\mathrm{H}}_{\text{oi-q}} G^{\mathrm{H}}_{\text{io-q}}}{Y^{\mathrm{H}}_{\text{o-q}}}, \end{aligned} \tag{2.171}$$

$$\begin{aligned} Z^{\mathrm{H}}_{\text{in-d-}\infty} &= Z^{\mathrm{H}}_{\text{in}} - \frac{G^{\mathrm{H}}_{\text{ci-d}} G^{\mathrm{H}}_{\text{io-d}}}{G^{\mathrm{H}}_{\text{co-d}}}, \quad Z^{\mathrm{H}}_{\text{in-qd-}\infty} = Z^{\mathrm{H}}_{\text{in}} - \frac{G^{\mathrm{H}}_{\text{ci-q}} G^{\mathrm{H}}_{\text{io-d}}}{G^{\mathrm{H}}_{\text{co-qd}}}, \\ Z^{\mathrm{H}}_{\text{in-dq-}\infty} &= Z^{\mathrm{H}}_{\text{in}} - \frac{G^{\mathrm{H}}_{\text{ci-d}} G^{\mathrm{H}}_{\text{io-q}}}{G^{\mathrm{H}}_{\text{co-dq}}}, \quad Z^{\mathrm{H}}_{\text{in-q-}\infty} = Z^{\mathrm{H}}_{\text{in}} - \frac{G^{\mathrm{H}}_{\text{ci-q}} G^{\mathrm{H}}_{\text{io-q}}}{G^{\mathrm{H}}_{\text{co-q}}}. \end{aligned} \tag{2.172}$$

Since there might be series components in the source impedance (i.e. Z_{inS} in Fig. 2.5 may not be not zero), the source input voltage $\hat{u}_{\text{inS}}$ and the converter input voltage $\hat{u}_{\text{in}}$ may not be equal. The input voltage $\hat{u}_{\text{inS}}$ can be given according to Fig. 2.6 by

$$\hat{u}_{\text{inS}} = Z_{\text{inS}} \hat{\hat{i}}_{\text{inS}} + T_{\text{oiS}} \hat{u}_{\text{in}}. \tag{2.173}$$

The dynamics between the system input variables ($\hat{\hat{i}}_{\text{inS}}$, $\hat{u}_{\text{od}}$, $\hat{u}_{\text{oq}}$, $\hat{d}_{\text{d}}$ and $\hat{d}_{\text{q}}$) and the source current $\hat{\hat{i}}_{\text{inS}}$ can be given by substituting (2.153) into (2.173) yielding

$$\hat{u}_{\text{inS}} = Z^{\text{HS}}_{\text{inS}} \hat{\hat{i}}_{\text{inS}} + T^{\text{HS}}_{\text{oi-dS}} \hat{u}_{\text{od}} + T^{\text{HS}}_{\text{oi-qS}} \hat{u}_{\text{oq}} + G^{\text{HS}}_{\text{ci-dS}} \hat{d}_{\text{d}} + G^{\text{HS}}_{\text{ci-qS}} \hat{d}_{\text{q}} \tag{2.174}$$

where

$$Z^{\text{HS}}_{\text{inS}} = \frac{\hat{u}_{\text{inS}}}{\hat{\hat{i}}_{\text{inS}}} = \frac{1 + Z^{\mathrm{H}}_{\text{in}} Y_{\text{oS-}\infty}}{1 + Y_{\text{oS}} Z^{\mathrm{H}}_{\text{in}}} Z^{\mathrm{H}}_{\text{in}}, \tag{2.175}$$

$$T^{\text{HS}}_{\text{oi-dS}} = \frac{\hat{u}_{\text{inS}}}{\hat{u}_{\text{od}}} = \frac{T_{\text{oiS}}}{1 + Y_{\text{oS}} Z^{\mathrm{H}}_{\text{in}}} T^{\mathrm{H}}_{\text{oi-d}}, \tag{2.176}$$

$$T^{\text{HS}}_{\text{oi-qS}} = \frac{\hat{u}_{\text{inS}}}{\hat{u}_{\text{oq}}} = \frac{T_{\text{oiS}}}{1 + Y_{\text{oS}} Z^{\mathrm{H}}_{\text{in}}} T^{\mathrm{H}}_{\text{oi-q}}, \tag{2.177}$$

$$G^{\text{HS}}_{\text{ci-dS}} = \frac{\hat{u}_{\text{inS}}}{\hat{d}_{\text{d}}} = \frac{T_{\text{oiS}}}{1 + Y_{\text{oS}} Z^{\mathrm{H}}_{\text{in}}} G^{\mathrm{H}}_{\text{ci-d}}, \tag{2.178}$$

$$G^{\text{HS}}_{\text{ci-qS}} = \frac{\hat{u}_{\text{inS}}}{\hat{d}_{\text{q}}} = \frac{T_{\text{oiS}}}{1 + Y_{\text{oS}} Z^{\mathrm{H}}_{\text{in}}} G^{\mathrm{H}}_{\text{ci-q}}, \tag{2.179}$$

$$Y_{\text{oS-}\infty} = Y_{\text{oS}} + \frac{T_{\text{oiS}} G_{\text{ioS}}}{Z_{\text{inS}}}. \tag{2.180}$$

The source-affected H-parameter model can also be used to investigate the stability of the source/inverter interface by applying the Nyquist stability criterion to the impedance

ratio $Y_{\mathrm{oS}}Z_{\mathrm{in}}^{\mathrm{H}} = Z_{\mathrm{in}}^{\mathrm{H}}/Z_{\mathrm{oS}}$, which is known as the inverse minor loop gain and is found in (2.156)–(2.179).

2.4 Load Effect in Grid-Connected VF and CF Inverters

This section presents an explicit method to compute the effect of non-ideal load on the dynamics of grid-connected three-phase VF and CF inverters. The presented method is general and is applicable to all grid-connected VF and CF inverters regardless of the topology. The load-effect can include either the load impedance or an output filter connected between the load and the power stage or both.

2.4.1 Load-Affected Y-parameter Model

Fig. 2.7 presents a linear model for the grid-connected VF inverter with a non-ideal load. The high number of transfer functions caused by the cross-coupling terms (subscripts 'dq' and 'qd' in G_{cr}, G_{co}, Z_{inL}, T_{oiL}, G_{ioL} and Y_{oL}) makes the load-effect difficult to solve using the aforementioned figure. Fortunately, Fig. 2.7 can be simplified using the notations in (2.181)–(2.184) and Figs. 2.8 and 2.9 as presented in Fig. 2.10. After the simplification, the computation of the load-effect becomes simple matrix algebra as will be presented in the following.

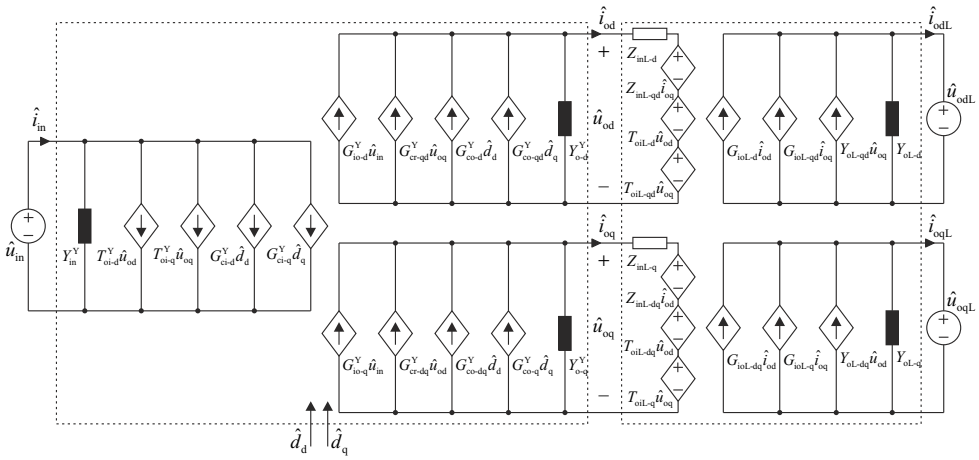

Fig. 2.7: Linear model of a grid-connected three-phase voltage-fed inverter with a non-ideal load.

$$\hat{\boldsymbol{i}}_{\mathrm{o}}^{\mathrm{s}} = \begin{bmatrix} \hat{i}_{\mathrm{od}} & \hat{i}_{\mathrm{oq}} \end{bmatrix}^{\mathrm{T}}, \quad \hat{\boldsymbol{u}}_{\mathrm{o}}^{\mathrm{s}} = \begin{bmatrix} \hat{u}_{\mathrm{od}} & \hat{u}_{\mathrm{oq}} \end{bmatrix}^{\mathrm{T}}, \quad \hat{\boldsymbol{d}}^{\mathrm{s}} = \begin{bmatrix} \hat{d}_{\mathrm{d}} & \hat{d}_{\mathrm{q}} \end{bmatrix}^{\mathrm{T}} \tag{2.181}$$

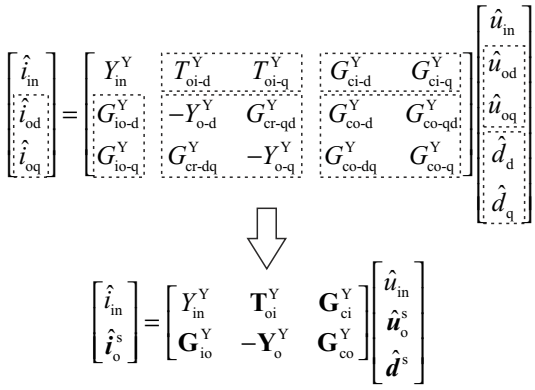

Fig. 2.8: The transfer function matrix of a three-phase grid-connected VF inverter in two different notations.

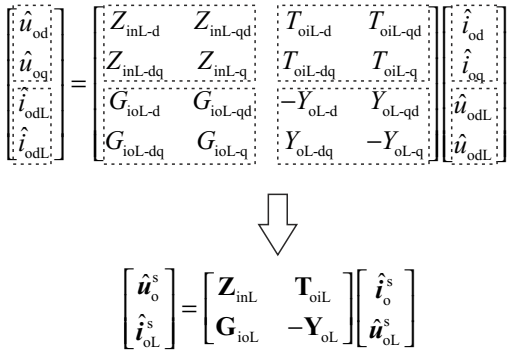

Fig. 2.9: The transfer function matrix of a passive three-phase circuit in two different notations.

$$\hat{\boldsymbol{i}}^{\mathrm{s}}_{\mathrm{oL}} = \begin{bmatrix} \hat{i}_{\mathrm{odL}} & \hat{i}_{\mathrm{oqL}} \end{bmatrix}^{\mathrm{T}}, \quad \hat{\boldsymbol{u}}^{\mathrm{s}}_{\mathrm{oL}} = \begin{bmatrix} \hat{u}_{\mathrm{odL}} & \hat{u}_{\mathrm{oqL}} \end{bmatrix}^{\mathrm{T}} \tag{2.182}$$

$$\begin{aligned} &\mathbf{T}^{\mathrm{Y}}_{\mathrm{oi}} = \begin{bmatrix} T^{\mathrm{Y}}_{\mathrm{oi\text{-}d}} & T^{\mathrm{Y}}_{\mathrm{oi\text{-}q}} \end{bmatrix}, \quad \mathbf{G}^{\mathrm{Y}}_{\mathrm{ci}} = \begin{bmatrix} G^{\mathrm{Y}}_{\mathrm{ci\text{-}d}} & G^{\mathrm{Y}}_{\mathrm{ci\text{-}q}} \end{bmatrix}, \quad \mathbf{G}^{\mathrm{Y}}_{\mathrm{io}} = \begin{bmatrix} G^{\mathrm{Y}}_{\mathrm{io\text{-}d}} & G^{\mathrm{Y}}_{\mathrm{io\text{-}q}} \end{bmatrix}^{\mathrm{T}} \\ &\mathbf{G}^{\mathrm{Y}}_{\mathrm{co}} = \begin{bmatrix} G^{\mathrm{Y}}_{\mathrm{co\text{-}d}} & G^{\mathrm{Y}}_{\mathrm{co\text{-}qd}} \\ G^{\mathrm{Y}}_{\mathrm{co\text{-}dq}} & G^{\mathrm{Y}}_{\mathrm{co\text{-}q}} \end{bmatrix}, \quad \mathbf{Y}^{\mathrm{Y}}_{\mathrm{o}} = \begin{bmatrix} Y^{\mathrm{Y}}_{\mathrm{o\text{-}d}} & -G^{\mathrm{Y}}_{\mathrm{cr\text{-}qd}} \\ -G^{\mathrm{Y}}_{\mathrm{cr\text{-}dq}} & Y^{\mathrm{Y}}_{\mathrm{o\text{-}q}} \end{bmatrix} \end{aligned} \tag{2.183}$$

$$\begin{aligned} &\mathbf{Z}_{\mathrm{inL}} = \begin{bmatrix} Z_{\mathrm{inL\text{-}d}} & Z_{\mathrm{inL\text{-}qd}} \\ Z_{\mathrm{inL\text{-}dq}} & Z_{\mathrm{inL\text{-}q}} \end{bmatrix}, \quad \mathbf{T}_{\mathrm{oiL}} = \begin{bmatrix} T_{\mathrm{oiL\text{-}d}} & T_{\mathrm{oiL\text{-}qd}} \\ T_{\mathrm{oiL\text{-}dq}} & T_{\mathrm{oiL\text{-}q}} \end{bmatrix} \\ &\mathbf{G}_{\mathrm{ioL}} = \begin{bmatrix} G_{\mathrm{ioL\text{-}d}} & G_{\mathrm{ioL\text{-}qd}} \\ G_{\mathrm{ioL\text{-}dq}} & G_{\mathrm{ioL\text{-}q}} \end{bmatrix}, \quad \mathbf{Y}_{\mathrm{oL}} = \begin{bmatrix} Y_{\mathrm{oL\text{-}d}} & -Y_{\mathrm{oL\text{-}qd}} \\ -Y_{\mathrm{oL\text{-}dq}} & Y_{\mathrm{oL\text{-}q}} \end{bmatrix} \end{aligned} \tag{2.184}$$

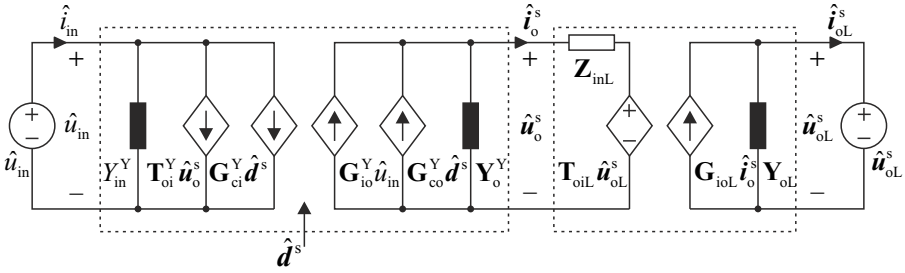

Fig. 2.10: Linear model of a grid-connected three-phase voltage-fed inverter with a non-ideal load.

The load effect can be computed by calculating the converter output voltage $\hat{\boldsymbol{u}}^{\mathrm{s}}_{\mathrm{o}}$ under the non-ideal case and substituting the result in the internal dynamics, which can be given for the VF-VSI according to Fig. 2.10

$$\hat{i}_{\mathrm{in}} = Y^{\mathrm{Y}}_{\mathrm{in}}\hat{u}_{\mathrm{in}} + \mathbf{T}^{\mathrm{Y}}_{\mathrm{oi}}\hat{\boldsymbol{u}}^{\mathrm{s}}_{\mathrm{o}} + \mathbf{G}^{\mathrm{Y}}_{\mathrm{ci}}\hat{\boldsymbol{d}}^{\mathrm{s}}, \tag{2.185}$$

$$\hat{\boldsymbol{i}}^{\mathrm{s}}_{\mathrm{o}} = \mathbf{G}^{\mathrm{Y}}_{\mathrm{io}}\hat{u}_{\mathrm{in}} - \mathbf{Y}^{\mathrm{Y}}_{\mathrm{o}}\hat{\boldsymbol{u}}^{\mathrm{s}}_{\mathrm{o}} + \mathbf{G}^{\mathrm{Y}}_{\mathrm{co}}\hat{\boldsymbol{d}}^{\mathrm{s}}. \tag{2.186}$$

According to Fig. 2.10 the inverter output terminal voltage $\hat{\boldsymbol{u}}^{\mathrm{s}}_{\mathrm{o}}$ can be given by

$$\hat{\boldsymbol{u}}^{\mathrm{s}}_{\mathrm{o}} = \mathbf{Z}_{\mathrm{inL}}\hat{\boldsymbol{i}}^{\mathrm{s}}_{\mathrm{o}} + \mathbf{T}_{\mathrm{oiL}}\hat{\boldsymbol{u}}^{\mathrm{s}}_{\mathrm{oL}}. \tag{2.187}$$

Substituting (2.186) in (2.187) and solving for the voltage $\hat{\boldsymbol{u}}_{\mathrm{o}}^{\mathrm{s}}$ yields

$$\hat{\boldsymbol{u}}_{\mathrm{o}}^{\mathrm{s}} = \left(\mathbf{I} + \mathbf{Z}_{\mathrm{inL}}\mathbf{Y}_{\mathrm{o}}^{\mathrm{Y}}\right)^{-1}\mathbf{Z}_{\mathrm{inL}}\mathbf{G}_{\mathrm{io}}^{\mathrm{Y}}\hat{u}_{\mathrm{in}} + \left(\mathbf{I} + \mathbf{Z}_{\mathrm{inL}}\mathbf{Y}_{\mathrm{o}}^{\mathrm{Y}}\right)^{-1}\mathbf{T}_{\mathrm{oiL}}\hat{\boldsymbol{u}}_{\mathrm{oL}}^{\mathrm{s}} + \left(\mathbf{I} + \mathbf{Z}_{\mathrm{inL}}\mathbf{Y}_{\mathrm{o}}^{\mathrm{Y}}\right)^{-1}\mathbf{Z}_{\mathrm{inL}}\mathbf{G}_{\mathrm{co}}^{\mathrm{Y}}\hat{\boldsymbol{d}}^{\mathrm{s}}, \quad (2.188)$$

which can be substituted in the nominal dynamics represented by (2.185) and (2.186) yielding the load-affected model as presented in (2.189) and (2.190), where the superscript extension 'L' denotes the load-effect.

$$\hat{i}_{\mathrm{in}} = Y_{\mathrm{in}}^{\mathrm{YL}}\hat{u}_{\mathrm{in}} + \mathbf{T}_{\mathrm{oi}}^{\mathrm{YL}}\hat{\boldsymbol{u}}_{\mathrm{oL}}^{\mathrm{s}} + \mathbf{G}_{\mathrm{ci}}^{\mathrm{YL}}\hat{\boldsymbol{d}}^{\mathrm{s}} \quad (2.189)$$

$$\hat{\boldsymbol{i}}_{\mathrm{o}}^{\mathrm{s}} = \mathbf{G}_{\mathrm{io}}^{\mathrm{YL}}\hat{u}_{\mathrm{in}} - \mathbf{Y}_{\mathrm{o}}^{\mathrm{YL}}\hat{\boldsymbol{u}}_{\mathrm{oL}}^{\mathrm{s}} + \mathbf{G}_{\mathrm{co}}^{\mathrm{YL}}\hat{\boldsymbol{d}}^{\mathrm{s}} \quad (2.190)$$

where

$$Y_{\mathrm{in}}^{\mathrm{YL}} = \frac{\hat{i}_{\mathrm{in}}}{\hat{u}_{\mathrm{in}}} = Y_{\mathrm{in}}^{\mathrm{Y}} + \mathbf{T}_{\mathrm{oi}}^{\mathrm{Y}}\left(\mathbf{I} + \mathbf{Z}_{\mathrm{inL}}\mathbf{Y}_{\mathrm{o}}^{\mathrm{Y}}\right)^{-1}\mathbf{Z}_{\mathrm{inL}}\mathbf{G}_{\mathrm{io}}^{\mathrm{Y}}, \quad (2.191)$$

$$\mathbf{T}_{\mathrm{oi}}^{\mathrm{YL}} = \frac{\hat{i}_{\mathrm{in}}}{\hat{\boldsymbol{u}}_{\mathrm{oL}}^{\mathrm{s}}} = \mathbf{T}_{\mathrm{oi}}^{\mathrm{Y}}\left(\mathbf{I} + \mathbf{Z}_{\mathrm{inL}}\mathbf{Y}_{\mathrm{o}}^{\mathrm{Y}}\right)^{-1}\mathbf{T}_{\mathrm{oiL}}, \quad (2.192)$$

$$\mathbf{G}_{\mathrm{ci}}^{\mathrm{YL}} = \frac{\hat{i}_{\mathrm{in}}}{\hat{\boldsymbol{d}}^{\mathrm{s}}} = \mathbf{G}_{\mathrm{ci}}^{\mathrm{Y}} + \mathbf{T}_{\mathrm{oi}}^{\mathrm{Y}}\left(\mathbf{I} + \mathbf{Z}_{\mathrm{inL}}\mathbf{Y}_{\mathrm{o}}^{\mathrm{Y}}\right)^{-1}\mathbf{Z}_{\mathrm{inL}}\mathbf{G}_{\mathrm{co}}^{\mathrm{Y}}, \quad (2.193)$$

$$\mathbf{G}_{\mathrm{io}}^{\mathrm{YL}} = \frac{\hat{\boldsymbol{i}}_{\mathrm{o}}^{\mathrm{s}}}{\hat{u}_{\mathrm{in}}} = \left[\mathbf{I} - \mathbf{Y}_{\mathrm{o}}^{\mathrm{Y}}\left(\mathbf{I} + \mathbf{Z}_{\mathrm{inL}}\mathbf{Y}_{\mathrm{o}}^{\mathrm{Y}}\right)^{-1}\mathbf{Z}_{\mathrm{inL}}\right]\mathbf{G}_{\mathrm{io}}^{\mathrm{Y}}, \quad (2.194)$$

$$\mathbf{Y}_{\mathrm{o}}^{\mathrm{YL}} = -\frac{\hat{\boldsymbol{i}}_{\mathrm{o}}^{\mathrm{s}}}{\hat{\boldsymbol{u}}_{\mathrm{oL}}^{\mathrm{s}}} = \mathbf{Y}_{\mathrm{o}}^{\mathrm{Y}}\left(\mathbf{I} + \mathbf{Z}_{\mathrm{inL}}\mathbf{Y}_{\mathrm{o}}^{\mathrm{Y}}\right)^{-1}\mathbf{T}_{\mathrm{oiL}}, \quad (2.195)$$

$$\mathbf{G}_{\mathrm{co}}^{\mathrm{YL}} = \frac{\hat{\boldsymbol{i}}_{\mathrm{o}}^{\mathrm{s}}}{\hat{\boldsymbol{d}}^{\mathrm{s}}} = \left[\mathbf{I} - \mathbf{Y}_{\mathrm{o}}^{\mathrm{Y}}\left(\mathbf{I} + \mathbf{Z}_{\mathrm{inL}}\mathbf{Y}_{\mathrm{o}}^{\mathrm{Y}}\right)^{-1}\mathbf{Z}_{\mathrm{inL}}\right]\mathbf{G}_{\mathrm{co}}^{\mathrm{Y}}, \quad (2.196)$$

Since there might be parallel components in the load impedance, the load current $\hat{\boldsymbol{i}}_{\mathrm{oL}}^{\mathrm{s}}$ and the converter output current $\hat{\boldsymbol{i}}_{\mathrm{o}}^{\mathrm{s}}$ may not be equal. The load current $\hat{\boldsymbol{i}}_{\mathrm{oL}}^{\mathrm{s}}$ can be given according to Fig. 2.10 by

$$\hat{\boldsymbol{i}}_{\mathrm{oL}}^{\mathrm{s}} = \mathbf{G}_{\mathrm{ioL}}\hat{\boldsymbol{i}}_{\mathrm{o}}^{\mathrm{s}} - \mathbf{Y}_{\mathrm{oL}}\hat{\boldsymbol{u}}_{\mathrm{oL}}^{\mathrm{s}}. \quad (2.197)$$

The dynamics between the system input variables ($\hat{u}_{\mathrm{in}}$, $\hat{\boldsymbol{u}}_{\mathrm{oL}}^{\mathrm{s}}$ and $\hat{\boldsymbol{d}}^{\mathrm{s}}$) and the load current $\hat{\boldsymbol{i}}_{\mathrm{oL}}^{\mathrm{s}}$ can be given by substituting (2.190) into (2.197) yielding

$$\hat{\boldsymbol{i}}_{\mathrm{o}}^{\mathrm{s}} = \mathbf{G}_{\mathrm{ioL}}^{\mathrm{YL}}\hat{u}_{\mathrm{in}} - \mathbf{Y}_{\mathrm{oL}}^{\mathrm{YL}}\hat{\boldsymbol{u}}_{\mathrm{oL}}^{\mathrm{s}} + \mathbf{G}_{\mathrm{coL}}^{\mathrm{YL}}\hat{\boldsymbol{d}}^{\mathrm{s}}, \quad (2.198)$$

where

$$\mathbf{G}_{\mathrm{ioL}}^{\mathrm{YL}} = \frac{\hat{\boldsymbol{i}}_{\mathrm{o}}^{\mathrm{s}}}{\hat{u}_{\mathrm{in}}} = \mathbf{G}_{\mathrm{ioL}} \left[\mathbf{I} - \mathbf{Y}_{\mathrm{o}}^{\mathrm{Y}} \left(\mathbf{I} + \mathbf{Z}_{\mathrm{inL}} \mathbf{Y}_{\mathrm{o}}^{\mathrm{Y}} \right)^{-1} \mathbf{Z}_{\mathrm{inL}} \right] \mathbf{G}_{\mathrm{io}}^{\mathrm{Y}}, \tag{2.199}$$

$$\mathbf{Y}_{\mathrm{oL}}^{\mathrm{YL}} = -\frac{\hat{\boldsymbol{i}}_{\mathrm{o}}^{\mathrm{s}}}{\hat{\boldsymbol{u}}_{\mathrm{oL}}^{\mathrm{s}}} = \mathbf{Y}_{\mathrm{oL}} + \mathbf{G}_{\mathrm{ioL}} \mathbf{Y}_{\mathrm{o}}^{\mathrm{Y}} \left(\mathbf{I} + \mathbf{Z}_{\mathrm{inL}} \mathbf{Y}_{\mathrm{o}}^{\mathrm{Y}} \right)^{-1} \mathbf{T}_{\mathrm{oiL}}, \tag{2.200}$$

$$\mathbf{G}_{\mathrm{coL}}^{\mathrm{YL}} = \frac{\hat{\boldsymbol{i}}_{\mathrm{o}}^{\mathrm{s}}}{\hat{\boldsymbol{d}}^{\mathrm{s}}} = \mathbf{G}_{\mathrm{ioL}} \left[\mathbf{I} - \mathbf{Y}_{\mathrm{o}}^{\mathrm{Y}} \left(\mathbf{I} + \mathbf{Z}_{\mathrm{inL}} \mathbf{Y}_{\mathrm{o}}^{\mathrm{Y}} \right)^{-1} \mathbf{Z}_{\mathrm{inL}} \right] \mathbf{G}_{\mathrm{co}}^{\mathrm{Y}}. \tag{2.201}$$

The load-affected Y-parameter model can also be used to investigate the stability of the inverter/load interface by applying the Nyquist stability criterion to the impedance ratio matrix $\mathbf{Z}_{\mathrm{inL}} \mathbf{Y}_{\mathrm{o}}^{\mathrm{Y}}$ in Eq. (2.202), which is known as the inverse minor loop gain and can be found from (2.191)–(2.201). Eq. (2.202) will be simplified into a more usable form upon computing the load-affected transfer functions for the H-parameter model at the end of the next section.

$$\begin{aligned} \mathbf{Z}_{\mathrm{inL}} \mathbf{Y}_{\mathrm{o}}^{\mathrm{Y}} &= \begin{bmatrix} Z_{\mathrm{inL\text{-}d}} & Z_{\mathrm{inL\text{-}qd}} \\ Z_{\mathrm{inL\text{-}dq}} & Z_{\mathrm{inL\text{-}q}} \end{bmatrix} \begin{bmatrix} Y_{\mathrm{o\text{-}d}}^{\mathrm{Y}} & -G_{\mathrm{cr\text{-}qd}}^{\mathrm{Y}} \\ -G_{\mathrm{cr\text{-}dq}}^{\mathrm{Y}} & Y_{\mathrm{o\text{-}q}}^{\mathrm{Y}} \end{bmatrix} \\ &= \begin{bmatrix} Z_{\mathrm{inL\text{-}d}} Y_{\mathrm{o\text{-}d}}^{\mathrm{Y}} - Z_{\mathrm{inL\text{-}qd}} G_{\mathrm{cr\text{-}dq}}^{\mathrm{Y}} & Z_{\mathrm{inL\text{-}qd}} Y_{\mathrm{o\text{-}q}}^{\mathrm{Y}} - Z_{\mathrm{inL\text{-}d}} G_{\mathrm{cr\text{-}qd}}^{\mathrm{Y}} \\ Z_{\mathrm{inL\text{-}dq}} Y_{\mathrm{o\text{-}d}}^{\mathrm{Y}} - Z_{\mathrm{inL\text{-}q}} G_{\mathrm{cr\text{-}dq}}^{\mathrm{Y}} & Z_{\mathrm{inL\text{-}q}} Y_{\mathrm{o\text{-}q}}^{\mathrm{Y}} - Z_{\mathrm{inL\text{-}dq}} G_{\mathrm{cr\text{-}qd}}^{\mathrm{Y}} \end{bmatrix} \end{aligned} \tag{2.202}$$

2.4.2 Load-Affected H-parameter Model

Fig. 2.11 presents a linear model for the grid-connected VF inverter with a non-ideal load, which can be simplified using similar procedures as in Section 2.4.1 as presented in Fig. 2.12. After the simplification, the computation of the load-effect becomes simple matrix algebra as will be presented in the following.

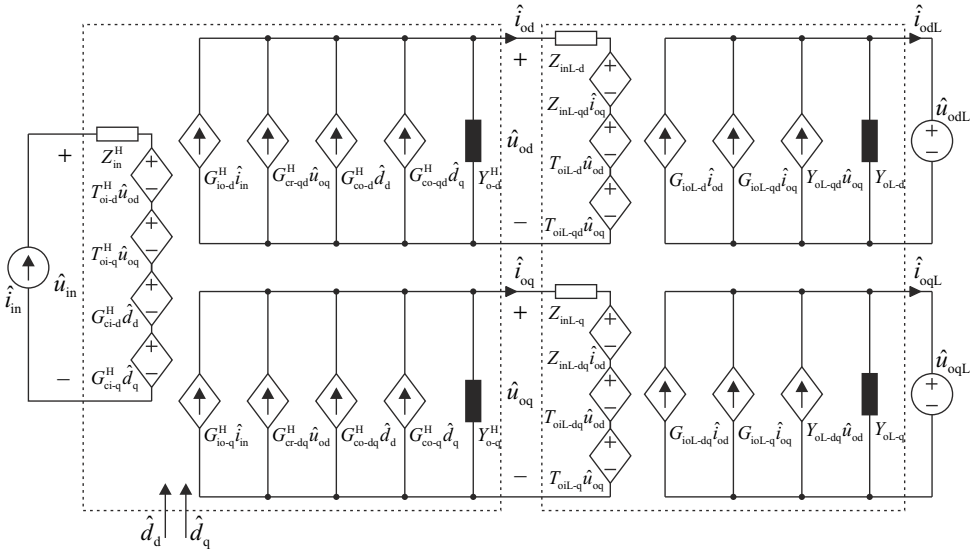

Fig. 2.11: Linear model of a grid-connected three-phase current-fed inverter with a non-ideal load.

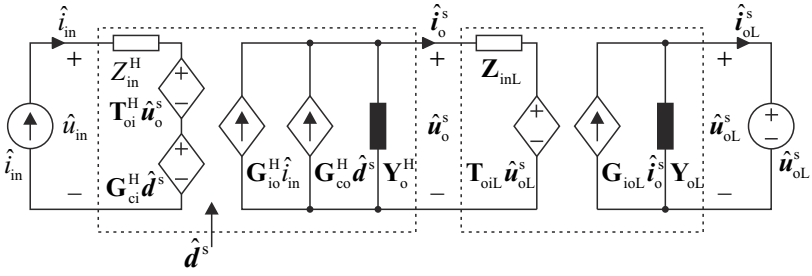

Fig. 2.12: Linear model of a grid-connected three-phase current-fed inverter with a non-ideal load.

The load-effect can be computed by calculating the converter output voltage $\hat{\boldsymbol{u}}^{s}_{o}$ under the non-ideal case and substituting the result in the internal dynamics, which can be given for the CF-VSI according to Fig. 2.12 by

$$\hat{u}_{in} = Z^{H}_{in}\hat{i}_{in} + \mathbf{T}^{H}_{oi}\hat{\boldsymbol{u}}^{s}_{o} + \mathbf{G}^{H}_{ci}\hat{\boldsymbol{d}}^{s}, \tag{2.203}$$

$$\hat{\boldsymbol{i}}_{\mathrm{o}}^{\mathrm{s}} = \mathbf{G}_{\mathrm{io}}^{\mathrm{H}}\hat{i}_{\mathrm{in}} - \mathbf{Y}_{\mathrm{o}}^{\mathrm{H}}\hat{\boldsymbol{u}}_{\mathrm{o}}^{\mathrm{s}} + \mathbf{G}_{\mathrm{co}}^{\mathrm{H}}\hat{\boldsymbol{d}}^{\mathrm{s}}. \tag{2.204}$$

According to Fig. 2.12 the inverter output terminal voltage $\hat{\boldsymbol{u}}_{\mathrm{o}}^{\mathrm{s}}$ can be given by

$$\hat{\boldsymbol{u}}_{\mathrm{o}}^{\mathrm{s}} = \mathbf{Z}_{\mathrm{inL}}\hat{\boldsymbol{i}}_{\mathrm{o}}^{\mathrm{s}} + \mathbf{T}_{\mathrm{oiL}}\hat{\boldsymbol{u}}_{\mathrm{oL}}^{\mathrm{s}}. \tag{2.205}$$

Substituting (2.204) in (2.205) and solving for the voltage $\hat{\boldsymbol{u}}_{\mathrm{o}}^{\mathrm{s}}$ yields

$$\begin{aligned}\hat{\boldsymbol{u}}_{\mathrm{o}}^{\mathrm{s}} = \left(\mathbf{I} + \mathbf{Z}_{\mathrm{inL}}\mathbf{Y}_{\mathrm{o}}^{\mathrm{H}}\right)^{-1}\mathbf{Z}_{\mathrm{inL}}\mathbf{G}_{\mathrm{io}}^{\mathrm{H}}\hat{i}_{\mathrm{in}} + \left(\mathbf{I} + \mathbf{Z}_{\mathrm{inL}}\mathbf{Y}_{\mathrm{o}}^{\mathrm{H}}\right)^{-1}\mathbf{T}_{\mathrm{oiL}}\hat{\boldsymbol{u}}_{\mathrm{oL}}^{\mathrm{s}} \\ + \left(\mathbf{I} + \mathbf{Z}_{\mathrm{inL}}\mathbf{Y}_{\mathrm{o}}^{\mathrm{H}}\right)^{-1}\mathbf{Z}_{\mathrm{inL}}\mathbf{G}_{\mathrm{co}}^{\mathrm{H}}\hat{\boldsymbol{d}}^{\mathrm{s}},\end{aligned} \tag{2.206}$$

which can be substituted in the nominal dynamics represented by (2.203) and (2.204) yielding the load-affected model as presented in (2.207) and (2.208), where the superscript extension 'L' denotes the load-effect.

$$\hat{u}_{\mathrm{in}} = Z_{\mathrm{in}}^{\mathrm{HL}}\hat{i}_{\mathrm{in}} + \mathbf{T}_{\mathrm{oi}}^{\mathrm{HL}}\hat{\boldsymbol{u}}_{\mathrm{oL}}^{\mathrm{s}} + \mathbf{G}_{\mathrm{ci}}^{\mathrm{HL}}\hat{\boldsymbol{d}}^{\mathrm{s}} \tag{2.207}$$

$$\hat{\boldsymbol{i}}_{\mathrm{o}}^{\mathrm{s}} = \mathbf{G}_{\mathrm{io}}^{\mathrm{HL}}\hat{i}_{\mathrm{in}} - \mathbf{Y}_{\mathrm{o}}^{\mathrm{HL}}\hat{\boldsymbol{u}}_{\mathrm{oL}}^{\mathrm{s}} + \mathbf{G}_{\mathrm{co}}^{\mathrm{HL}}\hat{\boldsymbol{d}}^{\mathrm{s}} \tag{2.208}$$

where

$$Z_{\mathrm{in}}^{\mathrm{HL}} = \frac{\hat{u}_{\mathrm{in}}}{\hat{i}_{\mathrm{in}}} = Z_{\mathrm{in}}^{\mathrm{H}} + \mathbf{T}_{\mathrm{oi}}^{\mathrm{H}}\left(\mathbf{I} + \mathbf{Z}_{\mathrm{inL}}\mathbf{Y}_{\mathrm{o}}^{\mathrm{H}}\right)^{-1}\mathbf{Z}_{\mathrm{inL}}\mathbf{G}_{\mathrm{io}}^{\mathrm{H}}, \tag{2.209}$$

$$\mathbf{T}_{\mathrm{oi}}^{\mathrm{HL}} = \frac{\hat{u}_{\mathrm{in}}}{\hat{\boldsymbol{u}}_{\mathrm{oL}}^{\mathrm{s}}} = \mathbf{T}_{\mathrm{oi}}^{\mathrm{H}}\left(\mathbf{I} + \mathbf{Z}_{\mathrm{inL}}\mathbf{Y}_{\mathrm{o}}^{\mathrm{H}}\right)^{-1}\mathbf{T}_{\mathrm{oiL}}, \tag{2.210}$$

$$\mathbf{G}_{\mathrm{ci}}^{\mathrm{HL}} = \frac{\hat{u}_{\mathrm{in}}}{\hat{\boldsymbol{d}}^{\mathrm{s}}} = \mathbf{G}_{\mathrm{ci}}^{\mathrm{H}} + \mathbf{T}_{\mathrm{oi}}^{\mathrm{H}}\left(\mathbf{I} + \mathbf{Z}_{\mathrm{inL}}\mathbf{Y}_{\mathrm{o}}^{\mathrm{H}}\right)^{-1}\mathbf{Z}_{\mathrm{inL}}\mathbf{G}_{\mathrm{co}}^{\mathrm{H}}, \tag{2.211}$$

$$\mathbf{G}_{\mathrm{io}}^{\mathrm{HL}} = \frac{\hat{\boldsymbol{i}}_{\mathrm{o}}^{\mathrm{s}}}{\hat{i}_{\mathrm{in}}} = \left[\mathbf{I} - \mathbf{Y}_{\mathrm{o}}^{\mathrm{H}}\left(\mathbf{I} + \mathbf{Z}_{\mathrm{inL}}\mathbf{Y}_{\mathrm{o}}^{\mathrm{H}}\right)^{-1}\mathbf{Z}_{\mathrm{inL}}\right]\mathbf{G}_{\mathrm{io}}^{\mathrm{H}}, \tag{2.212}$$

$$\mathbf{Y}_{\mathrm{o}}^{\mathrm{HL}} = -\frac{\hat{\boldsymbol{i}}_{\mathrm{o}}^{\mathrm{s}}}{\hat{\boldsymbol{u}}_{\mathrm{oL}}^{\mathrm{s}}} = \mathbf{Y}_{\mathrm{o}}^{\mathrm{H}}\left(\mathbf{I} + \mathbf{Z}_{\mathrm{inL}}\mathbf{Y}_{\mathrm{o}}^{\mathrm{H}}\right)^{-1}\mathbf{T}_{\mathrm{oiL}}, \tag{2.213}$$

$$\mathbf{G}_{\mathrm{co}}^{\mathrm{HL}} = \frac{\hat{\boldsymbol{i}}_{\mathrm{o}}^{\mathrm{s}}}{\hat{\boldsymbol{d}}^{\mathrm{s}}} = \left[\mathbf{I} - \mathbf{Y}_{\mathrm{o}}^{\mathrm{H}}\left(\mathbf{I} + \mathbf{Z}_{\mathrm{inL}}\mathbf{Y}_{\mathrm{o}}^{\mathrm{H}}\right)^{-1}\mathbf{Z}_{\mathrm{inL}}\right]\mathbf{G}_{\mathrm{co}}^{\mathrm{H}}, \tag{2.214}$$

Since there might be parallel components in the load impedance, the load current $\hat{\boldsymbol{i}}_{\mathrm{oL}}^{\mathrm{s}}$ and the converter output current $\hat{\boldsymbol{i}}_{\mathrm{o}}^{\mathrm{s}}$ may not be equal. The load current $\hat{\boldsymbol{i}}_{\mathrm{oL}}^{\mathrm{s}}$ can be given according to Fig. 2.12 by

$$\hat{\boldsymbol{i}}_{\mathrm{oL}}^{\mathrm{s}} = \mathbf{G}_{\mathrm{ioL}}\hat{\boldsymbol{i}}_{\mathrm{o}}^{\mathrm{s}} - \mathbf{Y}_{\mathrm{oL}}\hat{\boldsymbol{u}}_{\mathrm{oL}}^{\mathrm{s}}. \tag{2.215}$$

The dynamics between the system input variables ($\hat{i}_{\mathrm{in}}$, $\hat{\boldsymbol{u}}^{\mathrm{s}}_{\mathrm{oL}}$ and $\hat{\boldsymbol{d}}^{\mathrm{s}}$) and the load current $\hat{\boldsymbol{i}}^{\mathrm{s}}_{\mathrm{oL}}$ can be given by substituting (2.208) into (2.215) yielding

$$\hat{\boldsymbol{i}}^{\mathrm{s}}_{\mathrm{o}} = \mathbf{G}^{\mathrm{HL}}_{\mathrm{ioL}}\hat{i}_{\mathrm{in}} - \mathbf{Y}^{\mathrm{HL}}_{\mathrm{oL}}\hat{\boldsymbol{u}}^{\mathrm{s}}_{\mathrm{oL}} + \mathbf{G}^{\mathrm{HL}}_{\mathrm{coL}}\hat{\boldsymbol{d}}^{\mathrm{s}} \tag{2.216}$$

where

$$\mathbf{G}^{\mathrm{HL}}_{\mathrm{ioL}} = \frac{\hat{\boldsymbol{i}}^{\mathrm{s}}_{\mathrm{o}}}{\hat{i}_{\mathrm{in}}} = \mathbf{G}_{\mathrm{ioL}}\left[\mathbf{I} - \mathbf{Y}^{\mathrm{H}}_{\mathrm{o}}\left(\mathbf{I} + \mathbf{Z}_{\mathrm{inL}}\mathbf{Y}^{\mathrm{H}}_{\mathrm{o}}\right)^{-1}\mathbf{Z}_{\mathrm{inL}}\right]\mathbf{G}^{\mathrm{H}}_{\mathrm{io}}, \tag{2.217}$$

$$\mathbf{Y}^{\mathrm{HL}}_{\mathrm{oL}} = -\frac{\hat{\boldsymbol{i}}^{\mathrm{s}}_{\mathrm{o}}}{\hat{\boldsymbol{u}}^{\mathrm{s}}_{\mathrm{oL}}} = \mathbf{Y}_{\mathrm{oL}} + \mathbf{G}_{\mathrm{ioL}}\mathbf{Y}^{\mathrm{H}}_{\mathrm{o}}\left(\mathbf{I} + \mathbf{Z}_{\mathrm{inL}}\mathbf{Y}^{\mathrm{H}}_{\mathrm{o}}\right)^{-1}\mathbf{T}_{\mathrm{oiL}}, \tag{2.218}$$

$$\mathbf{G}^{\mathrm{HL}}_{\mathrm{coL}} = \frac{\hat{\boldsymbol{i}}^{\mathrm{s}}_{\mathrm{o}}}{\hat{\boldsymbol{d}}^{\mathrm{s}}} = \mathbf{G}_{\mathrm{ioL}}\left[\mathbf{I} - \mathbf{Y}^{\mathrm{H}}_{\mathrm{o}}\left(\mathbf{I} + \mathbf{Z}_{\mathrm{inL}}\mathbf{Y}^{\mathrm{H}}_{\mathrm{o}}\right)^{-1}\mathbf{Z}_{\mathrm{inL}}\right]\mathbf{G}^{\mathrm{H}}_{\mathrm{co}}. \tag{2.219}$$

Eqs. (2.209)–(2.214) and (2.217)–(2.219) can be simplified into usable notation by neglecting the cross coupling terms in $\mathbf{G}^{\mathrm{H}}_{\mathrm{co}}$, $\mathbf{Y}^{\mathrm{H}}_{\mathrm{o}}$, $\mathbf{Z}_{\mathrm{inL}}$, $\mathbf{T}_{\mathrm{oiL}}$, $\mathbf{G}_{\mathrm{ioL}}$ and $\mathbf{Y}_{\mathrm{oL}}$ in (2.183) and (2.184), i.e. by using

$$\mathbf{G}^{\mathrm{H}}_{\mathrm{co}} = \begin{bmatrix} G^{\mathrm{H}}_{\mathrm{co\text{-}d}} & 0 \\ 0 & G^{\mathrm{H}}_{\mathrm{co\text{-}q}} \end{bmatrix}, \quad \mathbf{Y}^{\mathrm{H}}_{\mathrm{o}} = \begin{bmatrix} Y^{\mathrm{H}}_{\mathrm{o\text{-}d}} & 0 \\ 0 & Y^{\mathrm{H}}_{\mathrm{o\text{-}q}} \end{bmatrix}, \tag{2.220}$$

and

$$\begin{aligned} \mathbf{Z}_{\mathrm{inL}} &= \begin{bmatrix} Z_{\mathrm{inL\text{-}d}} & 0 \\ 0 & Z_{\mathrm{inL\text{-}q}} \end{bmatrix}, \quad \mathbf{T}_{\mathrm{oiL}} = \begin{bmatrix} T_{\mathrm{oiL\text{-}d}} & 0 \\ 0 & T_{\mathrm{oiL\text{-}q}} \end{bmatrix}, \\ \mathbf{G}_{\mathrm{ioL}} &= \begin{bmatrix} G_{\mathrm{ioL\text{-}d}} & 0 \\ 0 & G_{\mathrm{ioL\text{-}q}} \end{bmatrix}, \quad \mathbf{Y}_{\mathrm{oL}} = \begin{bmatrix} Y_{\mathrm{oL\text{-}d}} & 0 \\ 0 & Y_{\mathrm{oL\text{-}q}} \end{bmatrix}, \end{aligned} \tag{2.221}$$

as given by[3]

$$Z_{\text{in}}^{\text{HL-r}} = \frac{\hat{u}_{\text{in}}}{\hat{i}_{\text{in}}} = \frac{1 + Z_{\text{inL-d}} Y_{\text{o-d-sc}}^{\text{H}}}{1 + Y_{\text{o-d}}^{\text{H}} Z_{\text{inL-d}}} Z_{\text{in}}^{\text{H}} + \frac{G_{\text{io-q}}^{\text{H}} T_{\text{oi-q}}^{\text{H}} Z_{\text{inL-q}}}{1 + Y_{\text{o-q}}^{\text{H}} Z_{\text{inL-q}}}, \tag{2.222}$$

$$T_{\text{oi-d}}^{\text{HL-r}} = \frac{\hat{u}_{\text{in}}}{\hat{u}_{\text{odL}}} = \frac{T_{\text{oiL-d}}}{1 + Y_{\text{o-d}}^{\text{H}} Z_{\text{inL-d}}} T_{\text{oi-d}}^{\text{H}}, \tag{2.223}$$

$$T_{\text{oi-q}}^{\text{HL-r}} = \frac{\hat{u}_{\text{in}}}{\hat{u}_{\text{oqL}}} = \frac{T_{\text{oiL-q}}}{1 + Y_{\text{o-q}}^{\text{H}} Z_{\text{inL-q}}} T_{\text{oi-q}}^{\text{H}}, \tag{2.224}$$

$$G_{\text{ci-d}}^{\text{HL-r}} = \frac{\hat{u}_{\text{in}}}{\hat{d}_{\text{d}}} = \frac{1 + Z_{\text{inL-d}} Y_{\text{o-d-}\infty}^{\text{H}}}{1 + Y_{\text{o-d}}^{\text{H}} Z_{\text{inL-d}}} G_{\text{ci-d}}^{\text{H}}, \tag{2.225}$$

$$G_{\text{ci-q}}^{\text{HL-r}} = \frac{\hat{u}_{\text{in}}}{\hat{d}_{\text{q}}} = \frac{1 + Z_{\text{inL-q}} Y_{\text{o-q-}\infty}^{\text{H}}}{1 + Y_{\text{o-q}}^{\text{H}} Z_{\text{inL-q}}} G_{\text{ci-q}}^{\text{H}}, \tag{2.226}$$

$$G_{\text{io-d}}^{\text{HL-r}} = \frac{\hat{i}_{\text{od}}}{\hat{i}_{\text{in}}} = \frac{1}{1 + Y_{\text{o-d}}^{\text{H}} Z_{\text{inL-d}}} G_{\text{io-d}}^{\text{H}}, \tag{2.227}$$

$$Y_{\text{o-d}}^{\text{HL-r}} = -\frac{\hat{i}_{\text{od}}}{\hat{u}_{\text{odL}}} = \frac{T_{\text{oiL-d}}}{1 + Y_{\text{o-d}}^{\text{H}} Z_{\text{inL-d}}} Y_{\text{o-d}}^{\text{H}}, \tag{2.228}$$

$$G_{\text{co-d}}^{\text{HL-r}} = \frac{\hat{i}_{\text{od}}}{\hat{d}_{\text{d}}} = \frac{1}{1 + Y_{\text{o-d}}^{\text{H}} Z_{\text{inL-d}}} G_{\text{co-d}}^{\text{H}}, \tag{2.229}$$

$$G_{\text{io-q}}^{\text{HL-r}} = \frac{\hat{i}_{\text{oq}}}{\hat{i}_{\text{in}}} = \frac{1}{1 + Y_{\text{o-q}}^{\text{H}} Z_{\text{inL-q}}} G_{\text{io-q}}^{\text{H}}, \tag{2.230}$$

$$Y_{\text{o-q}}^{\text{HL-r}} = -\frac{\hat{i}_{\text{oq}}}{\hat{u}_{\text{oqL}}} = \frac{T_{\text{oiL-q}}}{1 + Y_{\text{o-q}}^{\text{H}} Z_{\text{inL-q}}} Y_{\text{o-q}}^{\text{H}}, \tag{2.231}$$

$$G_{\text{co-q}}^{\text{HL-r}} = \frac{\hat{i}_{\text{oq}}}{\hat{d}_{\text{q}}} = \frac{1}{1 + Y_{\text{o-q}}^{\text{H}} Z_{\text{inL-q}}} G_{\text{co-q}}^{\text{H}}, \tag{2.232}$$

$$G_{\text{ioL-d}}^{\text{HL-r}} = \frac{\hat{i}_{\text{odL}}}{\hat{i}_{\text{in}}} = \frac{G_{\text{ioL-d}}}{1 + Y_{\text{o-d}}^{\text{H}} Z_{\text{inL-d}}} G_{\text{io-d}}^{\text{H}}, \tag{2.233}$$

$$Y_{\text{oL-d}}^{\text{HL-r}} = -\frac{\hat{i}_{\text{odL}}}{\hat{u}_{\text{odL}}} = \frac{1 + Y_{\text{o-d}}^{\text{H}} Z_{\text{inL-d-oc}}}{1 + Y_{\text{o-d}}^{\text{H}} Z_{\text{inL-d}}} Y_{\text{oL-d}}, \tag{2.234}$$

$$G_{\text{coL-d}}^{\text{HL-r}} = \frac{\hat{i}_{\text{odL}}}{\hat{d}_{\text{d}}} = \frac{G_{\text{ioL-d}}}{1 + Y_{\text{o-d}}^{\text{H}} Z_{\text{inL-d}}} G_{\text{co-d}}^{\text{H}}, \tag{2.235}$$

[3] A detailed Matlab m-file that can be used to obtain (2.222)–(2.238) can be found in Appendix C.

$$G^{\text{HL-r}}_{\text{ioL-q}} = \frac{\hat{i}_{\text{oqL}}}{\hat{i}_{\text{in}}} = \frac{G_{\text{ioL-q}}}{1 + Y^{\text{H}}_{\text{o-q}} Z_{\text{inL-q}}} G^{\text{H}}_{\text{io-q}}, \tag{2.236}$$

$$Y^{\text{HL-r}}_{\text{oL-q}} = -\frac{\hat{i}_{\text{oqL}}}{\hat{u}_{\text{oqL}}} = \frac{1 + Y^{\text{H}}_{\text{o-q}} Z_{\text{inL-q-oc}}}{1 + Y^{\text{H}}_{\text{o-q}} Z_{\text{inL-q}}} Y_{\text{oL-q}}, \tag{2.237}$$

$$G^{\text{HL-r}}_{\text{coL-q}} = \frac{\hat{i}_{\text{oqL}}}{\hat{d}_{\text{q}}} = \frac{G_{\text{ioL-q}}}{1 + Y^{\text{H}}_{\text{o-q}} Z_{\text{inL-q}}} G^{\text{H}}_{\text{co-q}}, \tag{2.238}$$

and

$$Y^{\text{H}}_{\text{o-d-sc}} = Y^{\text{H}}_{\text{o-d}} + \frac{T^{\text{H}}_{\text{oi-d}} G^{\text{H}}_{\text{io-d}}}{Z^{\text{H}}_{\text{in}}}, \tag{2.239}$$

$$Y^{\text{H}}_{\text{o-d-}\infty} = Y^{\text{H}}_{\text{o-d}} + \frac{T^{\text{H}}_{\text{oi-d}} G^{\text{H}}_{\text{co-d}}}{G^{\text{H}}_{\text{ci-d}}}, \tag{2.240}$$

$$Y^{\text{H}}_{\text{o-q-}\infty} = Y^{\text{H}}_{\text{o-q}} + \frac{T^{\text{H}}_{\text{oi-q}} G^{\text{H}}_{\text{co-q}}}{G^{\text{H}}_{\text{ci-q}}}, \tag{2.241}$$

$$Z_{\text{inL-d-oc}} = Z_{\text{inL-d}} + \frac{G_{\text{ioL-d}} T_{\text{oiL-d}}}{Y_{\text{oL-d}}}, \tag{2.242}$$

$$Z_{\text{inL-q-oc}} = Z_{\text{inL-q}} + \frac{G_{\text{ioL-q}} T_{\text{oiL-q}}}{Y_{\text{oL-q}}}, \tag{2.243}$$

where the superscript 'HL-r' denotes a load-affected reduced-order H-parameter transfer function.

The reduced-order load-affected model for a CF-VSI as presented in (2.222)–(2.238) contains also the load-affected transfer functions in the q-channel output dynamics as opposed to Puukko, Messo, Nousiainen, Huusari and Suntio (2011); Puukko and Suntio (2012b), which was computed only for the d-channel dynamics.

The justification of using the presented reduced-order model is presented in Appendix D, where frequency responses from a VSI switching model in Matlab Simulink (i.e. frequency responses that include the cross-coupling effects) are shown to correlate with the predictions obtained by the reduced-order load-affected model.

The load-affected H-parameter model can also be used to investigate the stability of the inverter/load interface by applying the Nyquist stability criterion to the impedance ratio matrix $\mathbf{Z}_{\text{inL}} \mathbf{Y}^{\text{H}}_{\text{o}}$ in (2.244), which is known as the inverse minor loop gain and can be found from (2.209)–(2.219). The inverse minor loop gain can be simplified using the reduced-order model as presented in (2.245) and can be found from (2.222)–(2.238).

$$\begin{aligned}\mathbf{Z}_{\text{inL}}\mathbf{Y}_{\text{o}}^{\text{H}} &= \begin{bmatrix} Z_{\text{inL-d}} & Z_{\text{inL-qd}} \\ Z_{\text{inL-dq}} & Z_{\text{inL-q}} \end{bmatrix} \begin{bmatrix} Y_{\text{o-d}}^{\text{H}} & -G_{\text{cr-qd}}^{\text{H}} \\ -G_{\text{cr-dq}}^{\text{H}} & Y_{\text{o-q}}^{\text{H}} \end{bmatrix} \\ &= \begin{bmatrix} Z_{\text{inL-d}}Y_{\text{o-d}}^{\text{H}} - Z_{\text{inL-qd}}G_{\text{cr-dq}}^{\text{H}} & Z_{\text{inL-qd}}Y_{\text{o-q}}^{\text{H}} - Z_{\text{inL-d}}G_{\text{cr-qd}}^{\text{H}} \\ Z_{\text{inL-dq}}Y_{\text{o-d}}^{\text{H}} - Z_{\text{inL-q}}G_{\text{cr-dq}}^{\text{H}} & Z_{\text{inL-q}}Y_{\text{o-q}}^{\text{H}} - Z_{\text{inL-dq}}G_{\text{cr-qd}}^{\text{H}} \end{bmatrix}\end{aligned} \tag{2.244}$$

$$\begin{aligned}\mathbf{Z}_{\text{inL}}\mathbf{Y}_{\text{o}}^{\text{H}} &= \begin{bmatrix} Z_{\text{inL-d}} & 0 \\ 0 & Z_{\text{inL-q}} \end{bmatrix} \begin{bmatrix} Y_{\text{o-d}}^{\text{H}} & 0 \\ 0 & Y_{\text{o-q}}^{\text{H}} \end{bmatrix} \\ &= \begin{bmatrix} Z_{\text{inL-d}}Y_{\text{o-d}}^{\text{H}} & 0 \\ 0 & Z_{\text{inL-q}}Y_{\text{o-q}}^{\text{H}} \end{bmatrix}\end{aligned} \tag{2.245}$$

2.5 Closed-Loop Transfer Functions for a Grid-Connected CF Inverter

A grid-connected VSI that is used to feed the power generated by a dc source (i.e. a PVG, a wind generator with an ac-dc converter, etc.) into the utility grid incorporates a cascaded input-voltage-output-current control scheme as illustrated in Fig. 2.13. The input-voltage controller provides a reference for the d-channel output current so that all the power supplied by the source is fed to the utility grid. The q-channel current reference, in turn, is typically set to zero to obtain unity power factor. High-bandwidth current control loops resulting in high VSI output impedance, i.e. current source characteristics, are desired. High output impedance ensures that undistorted sinusoidal currents can be injected into the grid even under distorted grid-voltage conditions. The input-voltage controller is designed to have a lower bandwidth than the current loops, typically in the order of few tens of Hertz for three-phase applications. The input voltage reference is obtained from the MPPT algorithm in single-stage PV applications. In two-stage applications the input voltage reference for a VSI can be considered constant and is dependent on the peak value of the grid-voltages.

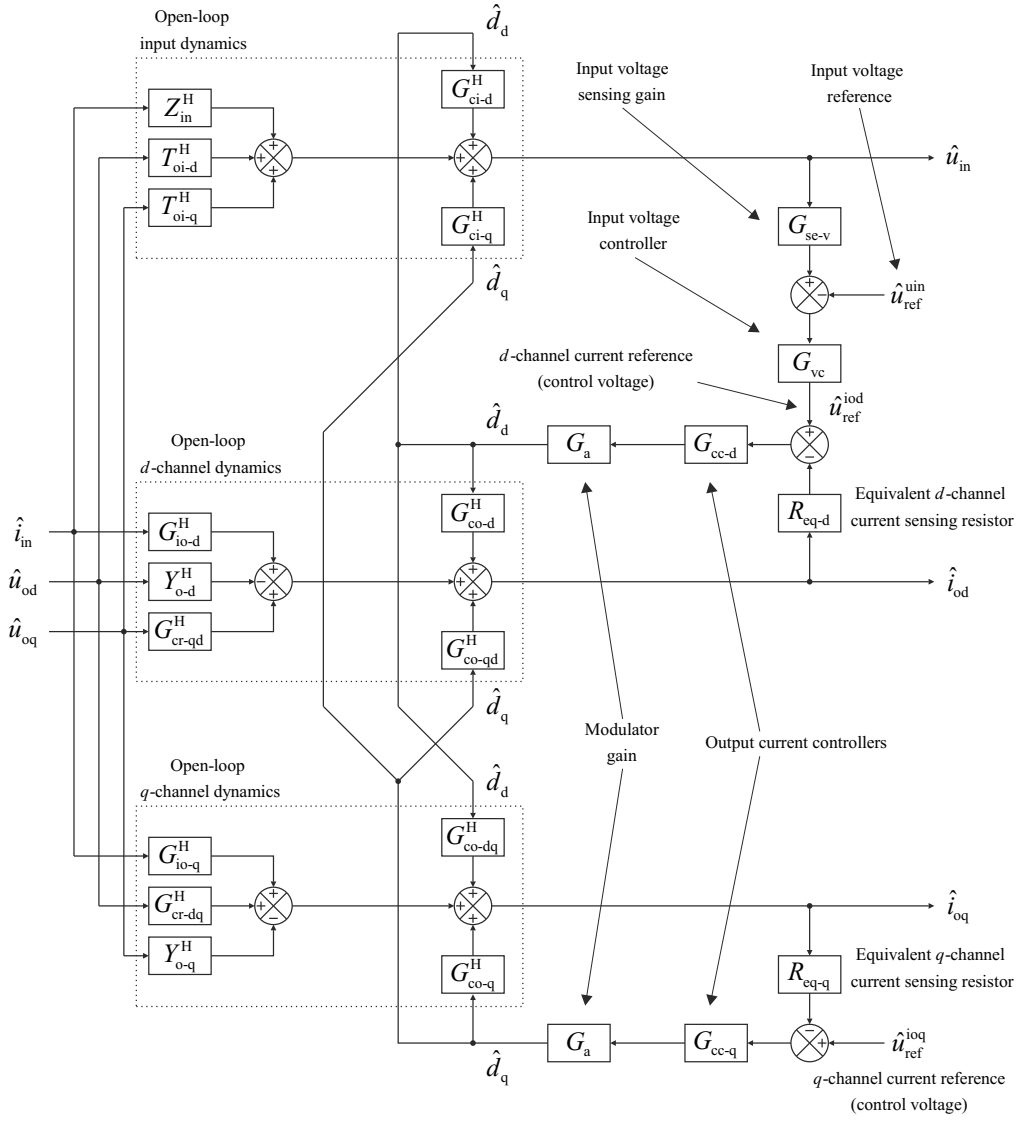

Fig. 2.13: Control-block diagram for a grid-connected CF inverter with a cascaded input-voltage-output-current control scheme.

2.5.1 Complete Model

Solving the closed-loop transfer functions for a cascaded control scheme, such as in Fig. 2.13, is recommended to be done step by step by first computing the closed-loop transfer functions when only the output-current control is active and then treating the obtained model as an "open-loop" system for the input voltage control. Solving the transfer functions directly from Fig. 2.13 would be too laborious.

Fig. 2.14 presents a control block diagram for an output-current controlled CF inverter. The model includes all the cross-coupling terms ($G^{\mathrm{H}}_{\text{cr-qd}}$, $G^{\mathrm{H}}_{\text{cr-dq}}$, $G^{\mathrm{H}}_{\text{co-qd}}$ and $G^{\mathrm{H}}_{\text{co-dq}}$). According to Fig 2.14, the d and q-channel duty ratios can be given by

$$\hat{d}_{\mathrm{d}} = -\frac{1}{G^{\mathrm{H}}_{\text{co-d}}} L_{\text{out-d}} \hat{i}_{\mathrm{od}} + \frac{1}{R_{\text{eq-d}} G^{\mathrm{H}}_{\text{co-d}}} L_{\text{out-d}} \hat{u}^{\mathrm{iod}}_{\mathrm{ref}}, \tag{2.246}$$

$$\hat{d}_{\mathrm{q}} = -\frac{1}{G^{\mathrm{H}}_{\text{co-q}}} L_{\text{out-q}} \hat{i}_{\mathrm{oq}} + \frac{1}{R_{\text{eq-q}} G^{\mathrm{H}}_{\text{co-q}}} L_{\text{out-q}} \hat{u}^{\mathrm{ioq}}_{\mathrm{ref}}, \tag{2.247}$$

where

$$L_{\text{out-d}} = R_{\text{eq-d}} G_{\text{cc-d}} G_{\mathrm{a}} G^{\mathrm{H}}_{\text{co-d}}, \tag{2.248}$$

$$L_{\text{out-q}} = R_{\text{eq-q}} G_{\text{cc-q}} G_{\mathrm{a}} G^{\mathrm{H}}_{\text{co-q}}, \tag{2.249}$$

are the current control loop gains, $R_{\text{eq-(d,q)}}$ are the equivalent current sensing resistors, $G_{\text{cc-(d,q)}}$ current controller transfer functions, G_{a} modulator gain, and $G^{\mathrm{H}}_{\text{co-(d,q)}}$ the control-to-output-current transfer functions.

Substituting (2.246) and (2.247) in the nominal open-loop dynamics represented by (2.102)–(2.104) and solving for $\hat{u}_{\mathrm{in}}$, $\hat{i}_{\mathrm{od}}$ and $\hat{i}_{\mathrm{oq}}$ yields

$$\hat{u}_{\mathrm{in}} = Z^{\mathrm{out}}_{\mathrm{in}} \hat{i}_{\mathrm{in}} + T^{\mathrm{out}}_{\text{oi-d}} \hat{u}_{\mathrm{od}} + T^{\mathrm{out}}_{\text{oi-q}} \hat{u}_{\mathrm{oq}} + G^{\mathrm{out}}_{\text{ci-d}} \hat{u}^{\mathrm{iod}}_{\mathrm{ref}} + G^{\mathrm{out}}_{\text{ci-q}} \hat{u}^{\mathrm{ioq}}_{\mathrm{ref}}, \tag{2.250}$$

$$\hat{i}_{\mathrm{od}} = G^{\mathrm{out}}_{\text{io-d}} \hat{i}_{\mathrm{in}} - Y^{\mathrm{out}}_{\text{o-d}} \hat{u}_{\mathrm{od}} + G^{\mathrm{out}}_{\text{cr-qd}} \hat{u}_{\mathrm{oq}} + G^{\mathrm{out}}_{\text{co-d}} \hat{u}^{\mathrm{iod}}_{\mathrm{ref}} + G^{\mathrm{out}}_{\text{co-qd}} \hat{u}^{\mathrm{ioq}}_{\mathrm{ref}}, \tag{2.251}$$

$$\hat{i}_{\mathrm{oq}} = G^{\mathrm{out}}_{\text{io-q}} \hat{i}_{\mathrm{in}} + G^{\mathrm{out}}_{\text{cr-dq}} \hat{u}_{\mathrm{od}} - Y^{\mathrm{out}}_{\text{o-q}} \hat{u}_{\mathrm{oq}} + G^{\mathrm{out}}_{\text{co-dq}} \hat{u}^{\mathrm{iod}}_{\mathrm{ref}} + G^{\mathrm{out}}_{\text{co-q}} \hat{u}^{\mathrm{ioq}}_{\mathrm{ref}}, \tag{2.252}$$

where the superscript 'out' indicates that the output current control loops are closed, and the above closed-loop transfer functions can be given by

$$Z^{\mathrm{out}}_{\mathrm{in}} = \frac{\hat{u}_{\mathrm{in}}}{\hat{i}_{\mathrm{in}}} = Z^{\mathrm{H}}_{\mathrm{in}} - \frac{L_{\text{out-d}}}{1 + L_{\text{out-d}}} \frac{G^{\mathrm{H}}_{\text{io-d}} G^{\mathrm{H}}_{\text{ci-d}}}{G^{\mathrm{H}}_{\text{co-d}}} - \frac{L_{\text{out-q}}}{1 + L_{\text{out-q}}} \frac{G^{\mathrm{H}}_{\text{io-q}} G^{\mathrm{H}}_{\text{ci-q}}}{G^{\mathrm{H}}_{\text{co-q}}}, \tag{2.253}$$

$$T^{\mathrm{out}}_{\text{oi-d}} = \frac{\hat{u}_{\mathrm{in}}}{\hat{u}_{\mathrm{od}}} = T^{\mathrm{H}}_{\text{oi-d}} + Y^{\mathrm{out}}_{\text{o-d}} \frac{G^{\mathrm{H}}_{\text{ci-d}}}{G^{\mathrm{H}}_{\text{co-d}}} L_{\text{out-d}} - G^{\mathrm{out}}_{\text{cr-dq}} \frac{G^{\mathrm{H}}_{\text{ci-q}}}{G^{\mathrm{H}}_{\text{co-q}}} L_{\text{out-q}}, \tag{2.254}$$

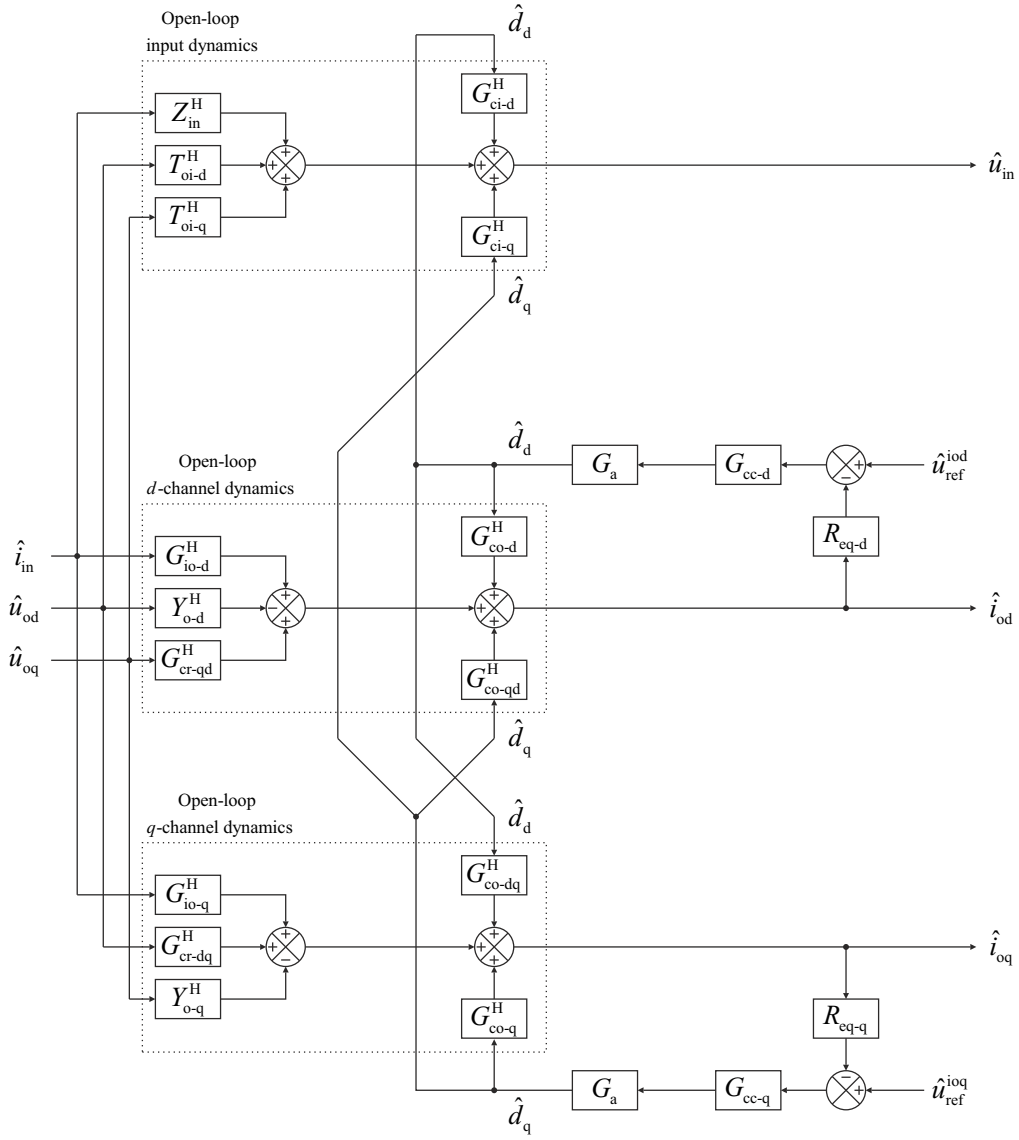

Fig. 2.14: Control-block diagram for an output-current-controlled grid-connected CF inverter.

$$T_{\text{oi-q}}^{\text{out}} = \frac{\hat{u}_{\text{in}}}{\hat{u}_{\text{oq}}} = T_{\text{oi-q}}^{\text{H}} - G_{\text{cr-qd}}^{\text{out}} \frac{G_{\text{ci-d}}^{\text{H}}}{G_{\text{co-d}}^{\text{H}}} L_{\text{out-d}} + Y_{\text{o-q}}^{\text{out}} \frac{G_{\text{ci-q}}^{\text{H}}}{G_{\text{co-q}}^{\text{H}}} L_{\text{out-q}}, \tag{2.255}$$

$$G_{\text{ci-d}}^{\text{out}} = \frac{\hat{u}_{\text{in}}}{\hat{u}_{\text{ref}}^{\text{iod}}} = \frac{G_{\text{ci-d}}^{\text{H}}}{R_{\text{eq-d}}^{\text{H}} G_{\text{co-d}}^{\text{H}}} L_{\text{out-d}} - G_{\text{co-d}}^{\text{out}} \frac{G_{\text{ci-d}}^{\text{H}}}{G_{\text{co-d}}^{\text{H}}} L_{\text{out-d}} - G_{\text{co-qd}}^{\text{out}} \frac{G_{\text{ci-q}}^{\text{H}}}{G_{\text{co-q}}^{\text{H}}} L_{\text{out-q}}, \tag{2.256}$$

$$G_{\text{ci-q}}^{\text{out}} = \frac{\hat{u}_{\text{in}}}{\hat{u}_{\text{ref}}^{\text{ioq}}} = \frac{G_{\text{ci-q}}^{\text{H}}}{R_{\text{eq-q}}^{\text{H}} G_{\text{co-q}}^{\text{H}}} L_{\text{out-q}} - G_{\text{co-qd}}^{\text{out}} \frac{G_{\text{ci-d}}^{\text{H}}}{G_{\text{co-d}}^{\text{H}}} L_{\text{out-d}} - G_{\text{co-q}}^{\text{out}} \frac{G_{\text{ci-q}}^{\text{H}}}{G_{\text{co-q}}^{\text{H}}} L_{\text{out-q}}. \tag{2.257}$$

$$G_{\text{io-d}}^{\text{out}} = \frac{\hat{i}_{\text{od}}}{\hat{i}_{\text{in}}} = \frac{G_{\text{io-d}}^{\text{H}} - G_{\text{io-q}}^{\text{H}} \frac{G_{\text{co-qd}}^{\text{H}}}{G_{\text{co-q}}^{\text{H}}} \frac{L_{\text{out-q}}}{1+L_{\text{out-q}}}}{1 + L_{\text{out-d}} \left(1 - \frac{G_{\text{co-qd}}^{\text{H}} G_{\text{co-dq}}^{\text{H}}}{G_{\text{co-d}}^{\text{H}} G_{\text{co-q}}^{\text{H}}} \frac{L_{\text{out-q}}}{1+L_{\text{out-q}}}\right)}, \tag{2.258}$$

$$Y_{\text{o-d}}^{\text{out}} = -\frac{\hat{i}_{\text{od}}}{\hat{u}_{\text{od}}} = \frac{Y_{\text{o-d}}^{\text{H}} + G_{\text{cr-dq}}^{\text{H}} \frac{G_{\text{co-qd}}^{\text{H}}}{G_{\text{co-q}}^{\text{H}}} \frac{L_{\text{out-q}}}{1+L_{\text{out-q}}}}{1 + L_{\text{out-d}} \left(1 - \frac{G_{\text{co-qd}}^{\text{H}} G_{\text{co-dq}}^{\text{H}}}{G_{\text{co-d}}^{\text{H}} G_{\text{co-q}}^{\text{H}}} \frac{L_{\text{out-q}}}{1+L_{\text{out-q}}}\right)}, \tag{2.259}$$

$$G_{\text{cr-qd}}^{\text{out}} = \frac{\hat{i}_{\text{od}}}{\hat{u}_{\text{oq}}} = \frac{G_{\text{cr-qd}}^{\text{H}} + Y_{\text{o-q}}^{\text{H}} \frac{G_{\text{co-qd}}^{\text{H}}}{G_{\text{co-q}}^{\text{H}}} \frac{L_{\text{out-q}}}{1+L_{\text{out-q}}}}{1 + L_{\text{out-d}} \left(1 - \frac{G_{\text{co-qd}}^{\text{H}} G_{\text{co-dq}}^{\text{H}}}{G_{\text{co-d}}^{\text{H}} G_{\text{co-q}}^{\text{H}}} \frac{L_{\text{out-q}}}{1+L_{\text{out-q}}}\right)}, \tag{2.260}$$

$$G_{\text{co-d}}^{\text{out}} = \frac{\hat{i}_{\text{od}}}{\hat{u}_{\text{ref}}^{\text{iod}}} = \frac{L_{\text{out-d}}}{R_{\text{eq-d}}} \frac{1 - \frac{G_{\text{co-qd}}^{\text{H}} G_{\text{co-dq}}^{\text{H}}}{G_{\text{co-d}}^{\text{H}} G_{\text{co-q}}^{\text{H}}} \frac{L_{\text{out-q}}}{1+L_{\text{out-q}}}}{1 + L_{\text{out-d}} \left(1 - \frac{G_{\text{co-qd}}^{\text{H}} G_{\text{co-dq}}^{\text{H}}}{G_{\text{co-d}}^{\text{H}} G_{\text{co-q}}^{\text{H}}} \frac{L_{\text{out-q}}}{1+L_{\text{out-q}}}\right)}, \tag{2.261}$$

$$G_{\text{co-qd}}^{\text{out}} = \frac{\hat{i}_{\text{od}}}{\hat{u}_{\text{ref}}^{\text{ioq}}} = \frac{G_{\text{co-qd}}^{\text{H}}}{G_{\text{co-q}}^{\text{H}}} \frac{L_{\text{out-q}}}{R_{\text{eq-q}}} \frac{1 - \frac{L_{\text{out-q}}}{1+L_{\text{out-q}}}}{1 + L_{\text{out-d}} \left(1 - \frac{G_{\text{co-qd}}^{\text{H}} G_{\text{co-dq}}^{\text{H}}}{G_{\text{co-d}}^{\text{H}} G_{\text{co-q}}^{\text{H}}} \frac{L_{\text{out-q}}}{1+L_{\text{out-q}}}\right)}, \tag{2.262}$$

$$G_{\text{io-q}}^{\text{out}} = \frac{\hat{i}_{\text{oq}}}{\hat{i}_{\text{in}}} = \frac{G_{\text{io-q}}^{\text{H}} - G_{\text{io-d}}^{\text{H}} \frac{G_{\text{co-dq}}^{\text{H}}}{G_{\text{co-d}}^{\text{H}}} \frac{L_{\text{out-d}}}{1+L_{\text{out-d}}}}{1 + L_{\text{out-q}} \left(1 - \frac{G_{\text{co-qd}}^{\text{H}} G_{\text{co-dq}}^{\text{H}}}{G_{\text{co-d}}^{\text{H}} G_{\text{co-q}}^{\text{H}}} \frac{L_{\text{out-d}}}{1+L_{\text{out-d}}}\right)}, \tag{2.263}$$

$$G_{\text{cr-dq}}^{\text{out}} = \frac{\hat{i}_{\text{oq}}}{\hat{u}_{\text{od}}} = \frac{G_{\text{cr-dq}}^{\text{H}} + Y_{\text{o-d}}^{\text{H}} \frac{G_{\text{co-dq}}^{\text{H}}}{G_{\text{co-d}}^{\text{H}}} \frac{L_{\text{out-d}}}{1+L_{\text{out-d}}}}{1 + L_{\text{out-q}} \left(1 - \frac{G_{\text{co-qd}}^{\text{H}} G_{\text{co-dq}}^{\text{H}}}{G_{\text{co-d}}^{\text{H}} G_{\text{co-q}}^{\text{H}}} \frac{L_{\text{out-d}}}{1+L_{\text{out-d}}}\right)}, \tag{2.264}$$

$$Y_{\text{o-q}}^{\text{out}} = -\frac{\hat{i}_{\text{oq}}}{\hat{u}_{\text{oq}}} = \frac{Y_{\text{o-q}}^{\text{H}} + G_{\text{cr-qd}}^{\text{H}} \frac{G_{\text{co-dq}}^{\text{H}}}{G_{\text{co-d}}^{\text{H}}} \frac{L_{\text{out-d}}}{1+L_{\text{out-d}}}}{1 + L_{\text{out-q}} \left(1 - \frac{G_{\text{co-qd}}^{\text{H}} G_{\text{co-dq}}^{\text{H}}}{G_{\text{co-d}}^{\text{H}} G_{\text{co-q}}^{\text{H}}} \frac{L_{\text{out-d}}}{1+L_{\text{out-d}}}\right)}, \tag{2.265}$$

$$G_{\text{co-dq}}^{\text{out}} = \frac{\hat{i}_{\text{oq}}}{\hat{u}_{\text{ref}}^{\text{iod}}} = \frac{G_{\text{co-dq}}^{\text{H}}}{G_{\text{co-d}}^{\text{H}}} \frac{L_{\text{out-d}}}{R_{\text{eq-d}}} \frac{1 - \frac{L_{\text{out-d}}}{1+L_{\text{out-d}}}}{1 + L_{\text{out-q}} \left(1 - \frac{G_{\text{co-qd}}^{\text{H}} G_{\text{co-dq}}^{\text{H}}}{G_{\text{co-d}}^{\text{H}} G_{\text{co-q}}^{\text{H}}} \frac{L_{\text{out-d}}}{1+L_{\text{out-d}}}\right)}, \tag{2.266}$$

$$G_{\text{co-q}}^{\text{out}} = \frac{\hat{i}_{\text{oq}}}{\hat{u}_{\text{ref}}^{\text{ioq}}} = \frac{L_{\text{out-q}}}{R_{\text{eq-q}}} \frac{1 - \frac{G_{\text{co-qd}}^{\text{H}} G_{\text{co-dq}}^{\text{H}}}{G_{\text{co-d}}^{\text{H}} G_{\text{co-q}}^{\text{H}}} \frac{L_{\text{out-d}}}{1+L_{\text{out-d}}}}{1 + L_{\text{out-q}} \left(1 - \frac{G_{\text{co-qd}}^{\text{H}} G_{\text{co-dq}}^{\text{H}}}{G_{\text{co-d}}^{\text{H}} G_{\text{co-q}}^{\text{H}}} \frac{L_{\text{out-d}}}{1+L_{\text{out-d}}}\right)}, \tag{2.267}$$

It is worth noting that $L_{\text{out-d}}$ in (2.248) and $L_{\text{out-q}}$ in (2.249) are not the "complete" d and q-channel current control loop gains because of the cross-coupling terms. According to (2.258)–(2.267), the d and q-channel current control loop gains can be given by

$$L_{\text{OUT-D}} = L_{\text{out-d}} \left(1 - \frac{G_{\text{co-qd}}^{\text{H}} G_{\text{co-dq}}^{\text{H}}}{G_{\text{co-d}}^{\text{H}} G_{\text{co-q}}^{\text{H}}} \frac{L_{\text{out-q}}}{1 + L_{\text{out-q}}}\right), \tag{2.268}$$

$$L_{\text{OUT-Q}} = L_{\text{out-q}} \left(1 - \frac{G_{\text{co-qd}}^{\text{H}} G_{\text{co-dq}}^{\text{H}}}{G_{\text{co-d}}^{\text{H}} G_{\text{co-q}}^{\text{H}}} \frac{L_{\text{out-d}}}{1 + L_{\text{out-d}}}\right), \tag{2.269}$$

according to which the output current control loops can be designed.

Next the effect of input voltage control can be computed based on Fig. 2.15 and (2.250)–(2.252). According to Fig. 2.15, the d-channel current reference (control voltage $\hat{u}_{\text{ref}}^{\text{iod}}$) can be given by

$$\hat{u}_{\text{ref}}^{\text{iod}} = G_{\text{se-v}} G_{\text{vc}} \hat{u}_{\text{in}} - G_{\text{vc}} \hat{u}_{\text{ref}}^{\text{uin}}, \tag{2.270}$$

where $G_{\text{se-v}}$ is the input voltage sensing gain and G_{vc} is the input voltage controller.

Substituting (2.270) to (2.250) and solving for the $\hat{u}_{\text{in}}$ yields

$$\hat{u}_{\text{in}} = Z_{\text{in}}^{\text{out-in}} \hat{i}_{\text{in}} + T_{\text{oi-d}}^{\text{out-in}} \hat{u}_{\text{od}} + T_{\text{oi-q}}^{\text{out-in}} \hat{u}_{\text{oq}} + G_{\text{ci-d}}^{\text{out-in}} \hat{u}_{\text{ref}}^{\text{uin}} + G_{\text{ci-q}}^{\text{out-in}} \hat{u}_{\text{ref}}^{\text{ioq}} \tag{2.271}$$

where the superscript 'out-in' refers to the cascaded control scheme, i.e. that both the input-voltage and output-current loops are closed, and

$$Z_{\text{in}}^{\text{out-in}} = \frac{\hat{u}_{\text{in}}}{\hat{i}_{\text{in}}} = \frac{Z_{\text{in}}^{\text{out}}}{1 - L_{\text{in}}}, \tag{2.272}$$

$$T_{\text{oi-d}}^{\text{out-in}} = \frac{\hat{u}_{\text{in}}}{\hat{u}_{\text{od}}} = \frac{T_{\text{oi-d}}^{\text{out}}}{1 - L_{\text{in}}}, \tag{2.273}$$

$$T_{\text{oi-q}}^{\text{out-in}} = \frac{\hat{u}_{\text{in}}}{\hat{u}_{\text{oq}}} = \frac{T_{\text{oi-q}}^{\text{out}}}{1 - L_{\text{in}}}, \tag{2.274}$$

$$G_{\text{ci-d}}^{\text{out-in}} = \frac{\hat{u}_{\text{in}}}{\hat{u}_{\text{ref}}^{\text{uin}}} = -\frac{1}{G_{\text{se-v}}} \frac{L_{\text{in}}}{1 - L_{\text{in}}}, \tag{2.275}$$

$$G_{\text{ci-q}}^{\text{out-in}} = \frac{\hat{u}_{\text{in}}}{\hat{u}_{\text{ref}}^{\text{ioq}}} = \frac{G_{\text{ci-q}}^{\text{out}}}{1 - L_{\text{in}}}. \tag{2.276}$$

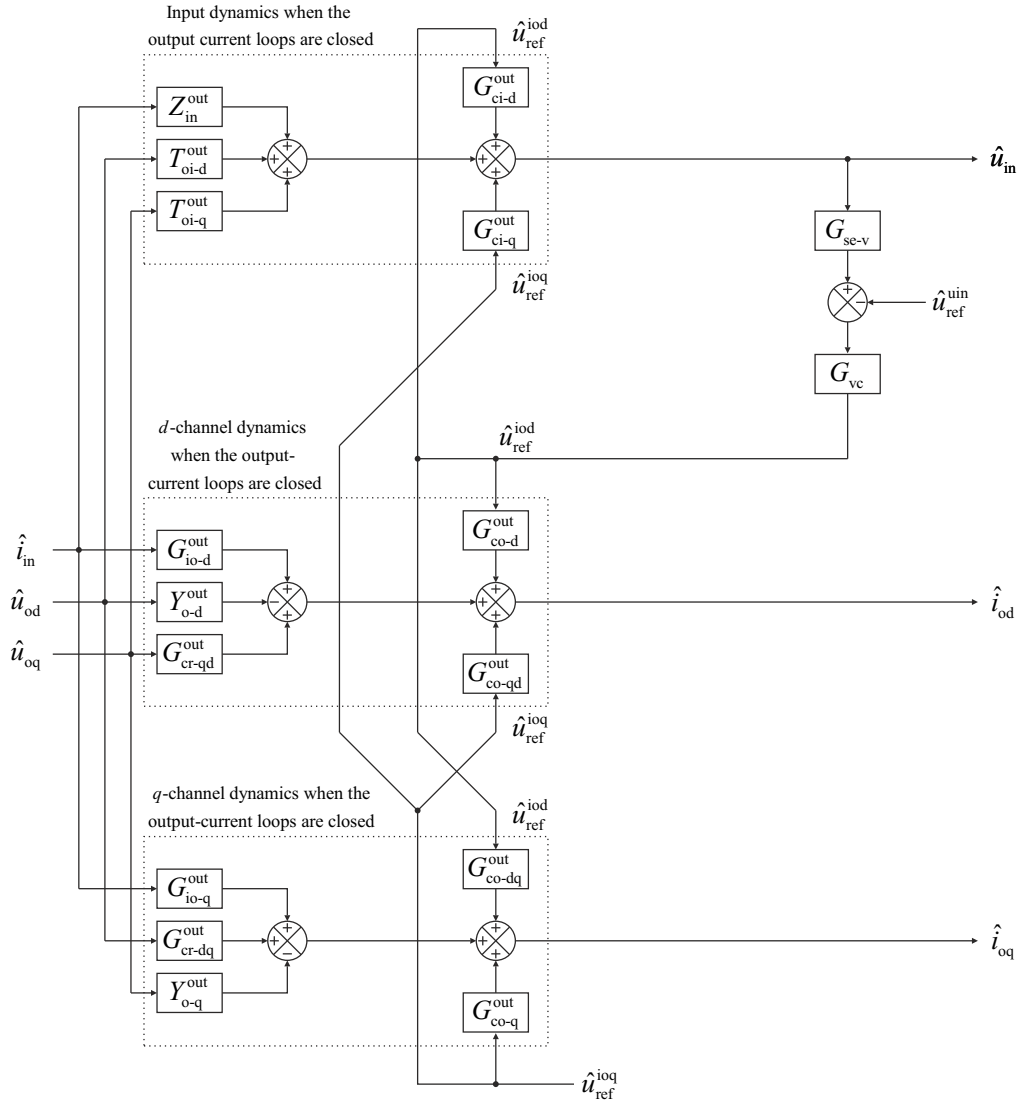

Fig. 2.15: Control-block diagram for a grid-connected CF inverter with a cascaded input-voltage-output-current control scheme.

The input voltage control loop gain can be given by

$$L_{\text{in}} = G_{\text{se-v}} G_{\text{vc}} G_{\text{ci-d}}^{\text{out}}, \tag{2.277}$$

where $G_{\text{se-v}}$ is the input voltage sensing gain, G_{vc} is the transfer function for the input voltage controller and $G_{\text{ci-d}}^{\text{out}}$ is the transfer function between the input voltage and the d-channel current reference. The minus sign in front of L_{in} in (2.272)–(2.276) is caused by the fact that the control error signal between the measured input voltage $G_{\text{se-v}}\hat{u}_{\text{in}}$ and the reference $\hat{u}_{\text{ref}}^{\text{uin}}$ has to be inverted for proper inverter operation (Figs. 2.13 and 2.15).

The output dynamics under the cascaded control scheme can be computed by substituting (2.270) and (2.271) in (2.251) and (2.252) yielding

$$\hat{i}_{\text{od}} = G_{\text{io-d}}^{\text{out-in}}\hat{i}_{\text{in}} - Y_{\text{o-d}}^{\text{out-in}}\hat{u}_{\text{od}} + G_{\text{cr-qd}}^{\text{out-in}}\hat{u}_{\text{oq}} + G_{\text{co-d}}^{\text{out-in}}\hat{u}_{\text{ref}}^{\text{uin}} + G_{\text{co-qd}}^{\text{out-in}}\hat{u}_{\text{ref}}^{\text{ioq}}, \tag{2.278}$$

$$\hat{i}_{\text{oq}} = G_{\text{io-q}}^{\text{out-in}}\hat{i}_{\text{in}} + G_{\text{cr-dq}}^{\text{out-in}}\hat{u}_{\text{od}} - Y_{\text{o-q}}^{\text{out-in}}\hat{u}_{\text{oq}} + G_{\text{co-dq}}^{\text{out-in}}\hat{u}_{\text{ref}}^{\text{uin}} + G_{\text{co-q}}^{\text{out-in}}\hat{u}_{\text{ref}}^{\text{ioq}}, \tag{2.279}$$

where

$$G_{\text{io-d}}^{\text{out-in}} = \frac{\hat{i}_{\text{od}}}{\hat{i}_{\text{in}}} = \frac{G_{\text{io-d}}^{\text{out}}}{1 - L_{\text{in}}} - \frac{L_{\text{in}}}{1 - L_{\text{in}}} G_{\text{io-d-}\infty}^{\text{out}} \tag{2.280}$$

$$Y_{\text{o-d}}^{\text{out-in}} = -\frac{\hat{i}_{\text{od}}}{\hat{u}_{\text{od}}} = \frac{Y_{\text{o-d}}^{\text{out}}}{1 - L_{\text{in}}} - \frac{L_{\text{in}}}{1 - L_{\text{in}}} Y_{\text{o-d-}\infty}^{\text{out}} \tag{2.281}$$

$$G_{\text{cr-qd}}^{\text{out-in}} = \frac{\hat{i}_{\text{od}}}{\hat{u}_{\text{oq}}} = \frac{G_{\text{cr-qd}}^{\text{out}}}{1 - L_{\text{in}}} - \frac{L_{\text{in}}}{1 - L_{\text{in}}} G_{\text{cr-qd-}\infty}^{\text{out}} \tag{2.282}$$

$$G_{\text{co-d}}^{\text{out-in}} = \frac{\hat{i}_{\text{od}}}{\hat{u}_{\text{ref}}^{\text{uin}}} = -\frac{L_{\text{in}}}{1 - L_{\text{in}}} \frac{G_{\text{co-d}}^{\text{out}}}{G_{\text{se-v}} G_{\text{ci-d}}^{\text{out}}} \tag{2.283}$$

$$G_{\text{co-qd}}^{\text{out-in}} = \frac{\hat{i}_{\text{od}}}{\hat{u}_{\text{ref}}^{\text{ioq}}} = \frac{G_{\text{co-qd}}^{\text{out}}}{1 - L_{\text{in}}} - \frac{L_{\text{in}}}{1 - L_{\text{in}}} G_{\text{co-qd-}\infty}^{\text{out}} \tag{2.284}$$

$$G_{\text{io-d-}\infty}^{\text{out}} = G_{\text{io-d}}^{\text{out}} - \frac{Z_{\text{in}}^{\text{out}} G_{\text{co-d}}^{\text{out}}}{G_{\text{ci-d}}^{\text{out}}} \tag{2.285}$$

$$Y_{\text{o-d-}\infty}^{\text{out}} = Y_{\text{o-d}}^{\text{out}} + \frac{T_{\text{oi-d}}^{\text{out}} G_{\text{co-d}}^{\text{out}}}{G_{\text{ci-d}}^{\text{out}}} \tag{2.286}$$

$$G_{\text{cr-qd-}\infty}^{\text{out}} = G_{\text{cr-qd}}^{\text{out}} - \frac{T_{\text{oi-q}}^{\text{out}} G_{\text{co-d}}^{\text{out}}}{G_{\text{ci-d}}^{\text{out}}} \tag{2.287}$$

$$G_{\text{co-qd-}\infty}^{\text{out}} = G_{\text{co-qd}}^{\text{out}} - \frac{G_{\text{ci-q}}^{\text{out}} G_{\text{co-d}}^{\text{out}}}{G_{\text{ci-d}}^{\text{out}}} \tag{2.288}$$

$$G_{\text{io-q}}^{\text{out-in}} = \frac{\hat{i}_{\text{oq}}}{\hat{i}_{\text{in}}} = \frac{G_{\text{io-q}}^{\text{out}}}{1 - L_{\text{in}}} - \frac{L_{\text{in}}}{1 - L_{\text{in}}} G_{\text{io-q-}\infty}^{\text{out}} \tag{2.289}$$

$$G_{\text{cr-dq}}^{\text{out-in}} = \frac{\hat{i}_{\text{oq}}}{\hat{u}_{\text{od}}} = \frac{G_{\text{cr-dq}}^{\text{out}}}{1 - L_{\text{in}}} - \frac{L_{\text{in}}}{1 - L_{\text{in}}} G_{\text{cr-dq-}\infty}^{\text{out}} \tag{2.290}$$

$$Y_{\text{o-q}}^{\text{out-in}} = -\frac{\hat{i}_{\text{oq}}}{\hat{u}_{\text{oq}}} = \frac{Y_{\text{o-q}}^{\text{out}}}{1 - L_{\text{in}}} - \frac{L_{\text{in}}}{1 - L_{\text{in}}} Y_{\text{o-q-}\infty}^{\text{out}} \tag{2.291}$$

$$G_{\text{co-dq}}^{\text{out-in}} = \frac{\hat{i}_{\text{oq}}}{\hat{u}_{\text{ref}}^{\text{uin}}} = -\frac{L_{\text{in}}}{1 - L_{\text{in}}} \frac{G_{\text{co-dq}}^{\text{out}}}{G_{\text{se-v}} G_{\text{ci-d}}^{\text{out}}} \tag{2.292}$$

$$G_{\text{co-q}}^{\text{out-in}} = \frac{\hat{i}_{\text{oq}}}{\hat{u}_{\text{ref}}^{\text{ioq}}} = \frac{G_{\text{co-q}}^{\text{out}}}{1 - L_{\text{in}}} - \frac{L_{\text{in}}}{1 - L_{\text{in}}} G_{\text{co-q-}\infty}^{\text{out}} \tag{2.293}$$

$$G_{\text{io-q-}\infty}^{\text{out}} = G_{\text{io-q}}^{\text{out}} - \frac{Z_{\text{in}}^{\text{out}} G_{\text{co-dq}}^{\text{out}}}{G_{\text{ci-d}}^{\text{out}}} \tag{2.294}$$

$$G_{\text{cr-dq-}\infty}^{\text{out}} = G_{\text{cr-dq}}^{\text{out}} - \frac{T_{\text{oi-d}}^{\text{out}} G_{\text{co-dq}}^{\text{out}}}{G_{\text{ci-d}}^{\text{out}}} \tag{2.295}$$

$$Y_{\text{o-q-}\infty}^{\text{out}} = Y_{\text{o-q}}^{\text{out}} + \frac{T_{\text{oi-q}}^{\text{out}} G_{\text{co-dq}}^{\text{out}}}{G_{\text{ci-d}}^{\text{out}}} \tag{2.296}$$

$$G_{\text{co-q-}\infty}^{\text{out}} = G_{\text{co-q}}^{\text{out}} - \frac{G_{\text{ci-q}}^{\text{out}} G_{\text{co-dq}}^{\text{out}}}{G_{\text{ci-d}}^{\text{out}}} \tag{2.297}$$

Eqs. (2.271)–(2.297) represent the closed-loop dynamics of a grid-connected input-voltage-output-current controlled CF inverter. However, solving the aforementioned transfer functions with the parasitic elements included, e.g. in Matlab even by using transfer function reduction tools such as *'minreal'* or *'balred'*, can become too complex. Furthermore, there is no point in solving the closed-loop dynamics without the parasitic elements because the phase and gain margins from this kind of a model would not represent the true margins from the actual prototype. The major cause for the complexity of the transfer functions in a three-phase inverter origins from the cross-coupling transfer functions $G_{\text{cr-qd}}^{\text{H}}$, $G_{\text{cr-dq}}^{\text{H}}$, $G_{\text{co-qd}}^{\text{H}}$ and $G_{\text{co-dq}}^{\text{H}}$. A reduced-order model was used in Section 2.4.2 to simplify the load-affected three-phase inverter model. Similar methods will be used in the following subsection to simplify the presented closed-loop model.

2.5.2 Reduced-Order Model

The reduced-order model for a grid-connected inverter can be obtained by neglecting the cross-coupling transfer functions as depicted in Fig. 2.16. The reduced-order transfer functions when the output current control is active (Fig. 2.17) can be obtained from

(2.253)–(2.267) by substituting $G^{\mathrm{H}}_{\text{cr-qd}} = G^{\mathrm{H}}_{\text{cr-dq}} = G^{\mathrm{H}}_{\text{co-qd}} = G^{\mathrm{H}}_{\text{co-dq}} = 0$ as given by (2.298)–(2.315), where the superscript extension '-r' denotes a reduced-order transfer function.

The input dynamics under the output current control can be given by

$$Z^{\text{out-r}}_{\text{in}} = \frac{\hat{u}_{\text{in}}}{\hat{i}_{\text{in}}} = \frac{Z^{\mathrm{H}}_{\text{in}}}{1 + L_{\text{out-d}}} + \frac{L_{\text{out-d}}}{1 + L_{\text{out-d}}} Z^{\text{H-r}}_{\text{in-}\infty} - \frac{L_{\text{out-q}}}{1 + L_{\text{out-q}}} \frac{G^{\mathrm{H}}_{\text{io-q}} G^{\mathrm{H}}_{\text{ci-q}}}{G^{\mathrm{H}}_{\text{co-q}}}, \tag{2.298}$$

$$T^{\text{out-r}}_{\text{oi-d}} = \frac{\hat{u}_{\text{in}}}{\hat{u}_{\text{od}}} = \frac{T^{\mathrm{H}}_{\text{oi-d}}}{1 + L_{\text{out-d}}} + \frac{L_{\text{out-d}}}{1 + L_{\text{out-d}}} T^{\text{H-r}}_{\text{oi-d-}\infty}, \tag{2.299}$$

$$T^{\text{out-r}}_{\text{oi-q}} = \frac{\hat{u}_{\text{in}}}{\hat{u}_{\text{oq}}} = \frac{T^{\mathrm{H}}_{\text{oi-q}}}{1 + L_{\text{out-q}}} + \frac{L_{\text{out-q}}}{1 + L_{\text{out-q}}} T^{\text{H-r}}_{\text{oi-q-}\infty}, \tag{2.300}$$

$$G^{\text{out-r}}_{\text{ci-d}} = \frac{\hat{u}_{\text{in}}}{\hat{u}^{\text{iod}}_{\text{ref}}} = \frac{L_{\text{out-d}}}{1 + L_{\text{out-d}}} \frac{G^{\mathrm{H}}_{\text{ci-d}}}{R_{\text{eq-d}} G^{\mathrm{H}}_{\text{co-d}}}, \tag{2.301}$$

$$G^{\text{out-r}}_{\text{ci-q}} = \frac{\hat{u}_{\text{in}}}{\hat{u}^{\text{ioq}}_{\text{ref}}} = \frac{L_{\text{out-q}}}{1 + L_{\text{out-q}}} \frac{G^{\mathrm{H}}_{\text{ci-q}}}{R_{\text{eq-q}} G^{\mathrm{H}}_{\text{co-q}}}. \tag{2.302}$$

where

$$Z^{\text{H-r}}_{\text{in-}\infty} = Z^{\mathrm{H}}_{\text{in}} - \frac{G^{\mathrm{H}}_{\text{io-d}} G^{\mathrm{H}}_{\text{ci-d}}}{G^{\mathrm{H}}_{\text{co-d}}} \tag{2.303}$$

$$T^{\text{H-r}}_{\text{oi-d-}\infty} = T^{\mathrm{H}}_{\text{oi-d}} + \frac{Y^{\mathrm{H}}_{\text{o-d}} G^{\mathrm{H}}_{\text{ci-d}}}{G^{\mathrm{H}}_{\text{co-d}}} \tag{2.304}$$

$$T^{\text{H-r}}_{\text{oi-q-}\infty} = T^{\mathrm{H}}_{\text{oi-q}} + \frac{Y^{\mathrm{H}}_{\text{o-q}} G^{\mathrm{H}}_{\text{ci-q}}}{G^{\mathrm{H}}_{\text{co-q}}} \tag{2.305}$$

The d and q-channel output dynamics under the output current control, in turn, can be given by

$$G^{\text{out-r}}_{\text{io-d}} = \frac{\hat{i}_{\text{od}}}{\hat{i}_{\text{in}}} = \frac{G^{\mathrm{H}}_{\text{io-d}}}{1 + L_{\text{out-d}}}, \tag{2.306}$$

$$Y^{\text{out-r}}_{\text{o-d}} = -\frac{\hat{i}_{\text{od}}}{\hat{u}_{\text{od}}} = \frac{Y^{\mathrm{H}}_{\text{o-d}}}{1 + L_{\text{out-d}}}, \tag{2.307}$$

$$G^{\text{out-r}}_{\text{cr-qd}} = \frac{\hat{i}_{\text{od}}}{\hat{u}_{\text{oq}}} = 0, \tag{2.308}$$

$$G^{\text{out-r}}_{\text{co-d}} = \frac{\hat{i}_{\text{od}}}{\hat{u}^{\text{iod}}_{\text{ref}}} = \frac{1}{R_{\text{eq-d}}} \frac{L_{\text{out-d}}}{1 + L_{\text{out-d}}}, \tag{2.309}$$

$$G^{\text{out-r}}_{\text{co-qd}} = \frac{\hat{i}_{\text{od}}}{\hat{u}^{\text{ioq}}_{\text{ref}}} = 0, \tag{2.310}$$

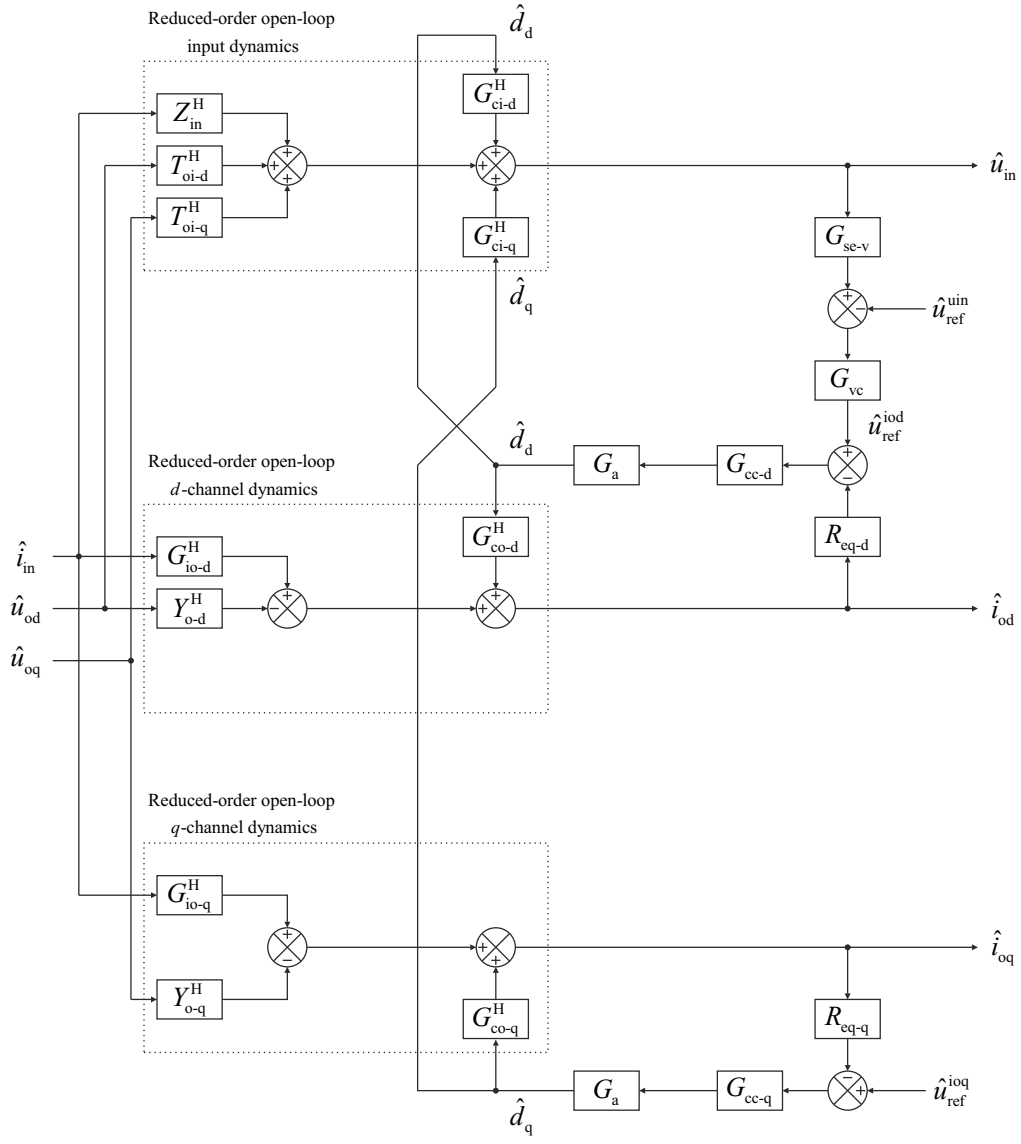

Fig. 2.16: Reduced-order control-block diagram for a grid-connected CF inverter with a cascaded input-voltage-output-current control scheme.

$$G_{\text{io-q}}^{\text{out-r}} = \frac{\hat{i}_{\text{oq}}}{\hat{i}_{\text{in}}} = \frac{G_{\text{io-q}}^{\text{H}}}{1 + L_{\text{out-q}}}, \tag{2.311}$$

$$G_{\text{cr-dq}}^{\text{out-r}} = \frac{\hat{i}_{\text{oq}}}{\hat{u}_{\text{od}}} = 0, \tag{2.312}$$

$$Y_{\text{o-q}}^{\text{out-r}} = -\frac{\hat{i}_{\text{oq}}}{\hat{u}_{\text{oq}}} = \frac{Y_{\text{o-q}}^{\text{H}}}{1 + L_{\text{out-q}}}, \tag{2.313}$$

$$G_{\text{co-dq}}^{\text{out-r}} = \frac{\hat{i}_{\text{oq}}}{\hat{u}_{\text{ref}}^{\text{iod}}} = 0, \tag{2.314}$$

$$G_{\text{co-q}}^{\text{out-r}} = \frac{\hat{i}_{\text{oq}}}{\hat{u}_{\text{ref}}^{\text{ioq}}} = \frac{1}{R_{\text{eq-q}}} \frac{L_{\text{out-q}}}{1 + L_{\text{out-q}}}, \tag{2.315}$$

The reduced-order transfer functions with a cascaded control scheme can be obtained from (2.271)–(2.297). The input dynamics with a cascaded control scheme can be given by

$$\begin{aligned} Z_{\text{in}}^{\text{out-in-r}} = \frac{\hat{u}_{\text{in}}}{\hat{i}_{\text{in}}} = {} & \frac{Z_{\text{in}}^{\text{H}}}{(1 + L_{\text{out-d}})(1 - L_{\text{in}})} + \frac{L_{\text{out-d}}}{(1 + L_{\text{out-d}})(1 - L_{\text{in}})} Z_{\text{in-}\infty}^{\text{H-r}} \\ & - \frac{L_{\text{out-q}}}{(1 + L_{\text{out-q}})(1 - L_{\text{in}})} \frac{G_{\text{io-q}}^{\text{H}} G_{\text{ci-q}}^{\text{H}}}{G_{\text{co-q}}^{\text{H}}}, \end{aligned} \tag{2.316}$$

$$T_{\text{oi-d}}^{\text{out-in-r}} = \frac{\hat{u}_{\text{in}}}{\hat{u}_{\text{od}}} = \frac{T_{\text{oi-d}}^{\text{H}}}{(1 + L_{\text{out-d}})(1 - L_{\text{in}})} + \frac{L_{\text{out-d}}}{(1 + L_{\text{out-d}})(1 - L_{\text{in}})} T_{\text{oi-d-}\infty}^{\text{H-r}}, \tag{2.317}$$

$$T_{\text{oi-q}}^{\text{out-in-r}} = \frac{\hat{u}_{\text{in}}}{\hat{u}_{\text{oq}}} = \frac{T_{\text{oi-q}}^{\text{H}}}{(1 + L_{\text{out-q}})(1 - L_{\text{in}})} + \frac{L_{\text{out-q}}}{(1 + L_{\text{out-q}})(1 - L_{\text{in}})} T_{\text{oi-q-}\infty}^{\text{H-r}}, \tag{2.318}$$

$$G_{\text{ci-d}}^{\text{out-in-r}} = \frac{\hat{u}_{\text{in}}}{\hat{u}_{\text{ref}}^{\text{uin}}} = -\frac{1}{G_{\text{se-v}}} \frac{L_{\text{in}}}{1 - L_{\text{in}}}, \tag{2.319}$$

$$G_{\text{ci-q}}^{\text{out-in-r}} = \frac{\hat{u}_{\text{in}}}{\hat{u}_{\text{ref}}^{\text{ioq}}} = \frac{L_{\text{out-q}}}{(1 + L_{\text{out-q}})(1 - L_{\text{in}})} \frac{G_{\text{ci-q}}^{\text{H}}}{R_{\text{eq-q}} G_{\text{co-q}}^{\text{H}}}. \tag{2.320}$$

The d and q-channel output dynamics with a cascaded control scheme can be given by

$$G_{\text{io-d}}^{\text{out-in-r}} = \frac{\hat{i}_{\text{od}}}{\hat{i}_{\text{in}}} = \frac{G_{\text{io-d}}^{\text{H}}}{(1 + L_{\text{out-d}})(1 - L_{\text{in}})} - \frac{L_{\text{in}}}{1 - L_{\text{in}}} G_{\text{io-d-}\infty}^{\text{H-r}} \tag{2.321}$$

$$Y_{\text{o-d}}^{\text{out-in-r}} = -\frac{\hat{i}_{\text{od}}}{\hat{u}_{\text{od}}} = \frac{Y_{\text{o-d}}^{\text{H}}}{(1 + L_{\text{out-d}})(1 - L_{\text{in}})} - \frac{L_{\text{in}}}{1 - L_{\text{in}}} Y_{\text{o-d-}\infty}^{\text{H-r}} \tag{2.322}$$

$$G_{\text{cr-qd}}^{\text{out-in-r}} = \frac{\hat{i}_{\text{od}}}{\hat{u}_{\text{oq}}} = -\frac{L_{\text{in}}}{1 - L_{\text{in}}} G_{\text{cr-qd-}\infty}^{\text{H-r}} \tag{2.323}$$

$$G_{\text{co-d}}^{\text{out-in-r}} = \frac{\hat{i}_{\text{od}}}{\hat{u}_{\text{ref}}^{\text{uin}}} = -\frac{L_{\text{in}}}{1 - L_{\text{in}}} \frac{G_{\text{co-d}}^{\text{H}}}{G_{\text{se-v}} G_{\text{ci-d}}^{\text{H}}} \tag{2.324}$$

$$G_{\text{co-qd}}^{\text{out-in-r}} = \frac{\hat{i}_{\text{od}}}{\hat{u}_{\text{ref}}^{\text{ioq}}} = -\frac{L_{\text{in}}}{1 - L_{\text{in}}} G_{\text{co-qd-}\infty}^{\text{H-r}} \tag{2.325}$$

where

$$G_{\text{io-d-}\infty}^{\text{H-r}} = G_{\text{io-d}}^{\text{H}} - \frac{Z_{\text{in}}^{\text{H}} G_{\text{co-d}}^{\text{H}}}{G_{\text{ci-d}}^{\text{H}}} \tag{2.326}$$

$$Y_{\text{o-d-}\infty}^{\text{H-r}} = Y_{\text{o-d}}^{\text{H}} + \frac{T_{\text{oi-d}}^{\text{H}} G_{\text{co-d}}^{\text{H}}}{G_{\text{ci-d}}^{\text{H}}} \tag{2.327}$$

$$G_{\text{cr-qd-}\infty}^{\text{H-r}} = -\frac{T_{\text{oi-q}}^{\text{H}} G_{\text{co-d}}^{\text{H}}}{G_{\text{ci-d}}^{\text{H}}} \tag{2.328}$$

$$G_{\text{co-qd-}\infty}^{\text{H-r}} = -\frac{G_{\text{ci-q}}^{\text{H}} G_{\text{co-d}}^{\text{H}}}{G_{\text{ci-d}}^{\text{H}}} \tag{2.329}$$

and

$$G_{\text{io-q}}^{\text{out-in-r}} = \frac{\hat{i}_{\text{oq}}}{\hat{i}_{\text{in}}} = \frac{G_{\text{io-q}}^{\text{H}}}{1 + L_{\text{out-q}}}, \tag{2.330}$$

$$G_{\text{cr-dq}}^{\text{out-in-r}} = \frac{\hat{i}_{\text{oq}}}{\hat{u}_{\text{od}}} = 0, \tag{2.331}$$

$$Y_{\text{o-q}}^{\text{out-in-r}} = -\frac{\hat{i}_{\text{oq}}}{\hat{u}_{\text{oq}}} = \frac{Y_{\text{o-q}}^{\text{H}}}{1 + L_{\text{out-q}}}, \tag{2.332}$$

$$G_{\text{co-dq}}^{\text{out-in-r}} = \frac{\hat{i}_{\text{oq}}}{\hat{u}_{\text{ref}}^{\text{uin}}} = 0, \tag{2.333}$$

$$G_{\text{co-q}}^{\text{out-in-r}} = \frac{\hat{i}_{\text{oq}}}{\hat{u}_{\text{ref}}^{\text{ioq}}} = \frac{1}{R_{\text{eq-q}}} \frac{L_{\text{out-q}}}{1 + L_{\text{out-q}}}, \tag{2.334}$$

It is worth noting that the cascaded control scheme does not affect the q-channel dynamics (as can be noticed by comparing (2.311)–(2.315) and (2.330)–(2.334)) because the input voltage controller produces a reference for the d-channel current, and the d and q-channels are decoupled in the reduced-order model.

The justification of using the presented reduced-order model is presented in Appendix E, where frequency responses from a VSI switching model in Matlab Simulink (i.e. frequency responses that include the cross-coupling effects) are shown to correlate with the predictions obtained by the reduced-order closed-loop model.

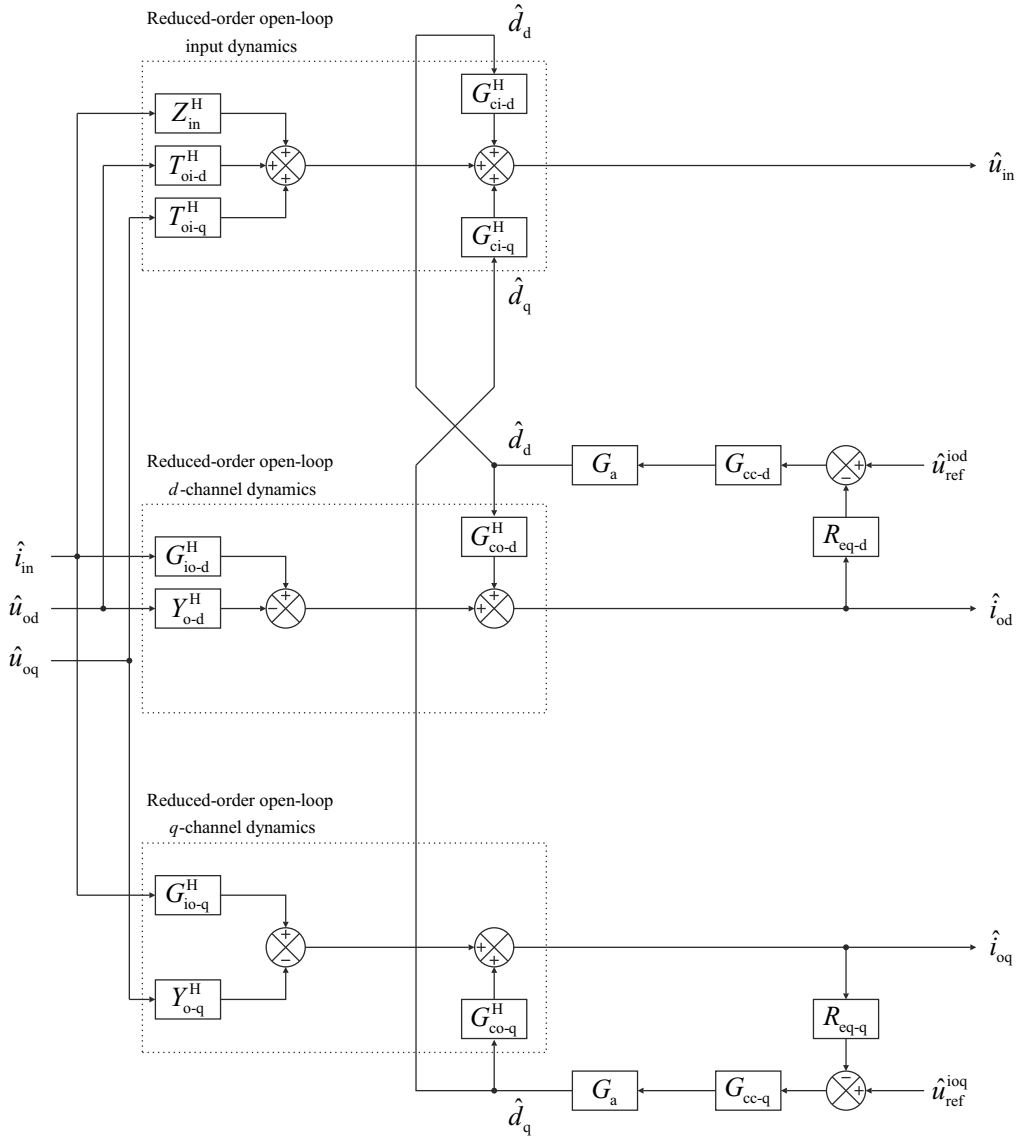

Fig. 2.17: Reduced-order control-block diagram for an output-current-controlled grid-connected CF inverter.

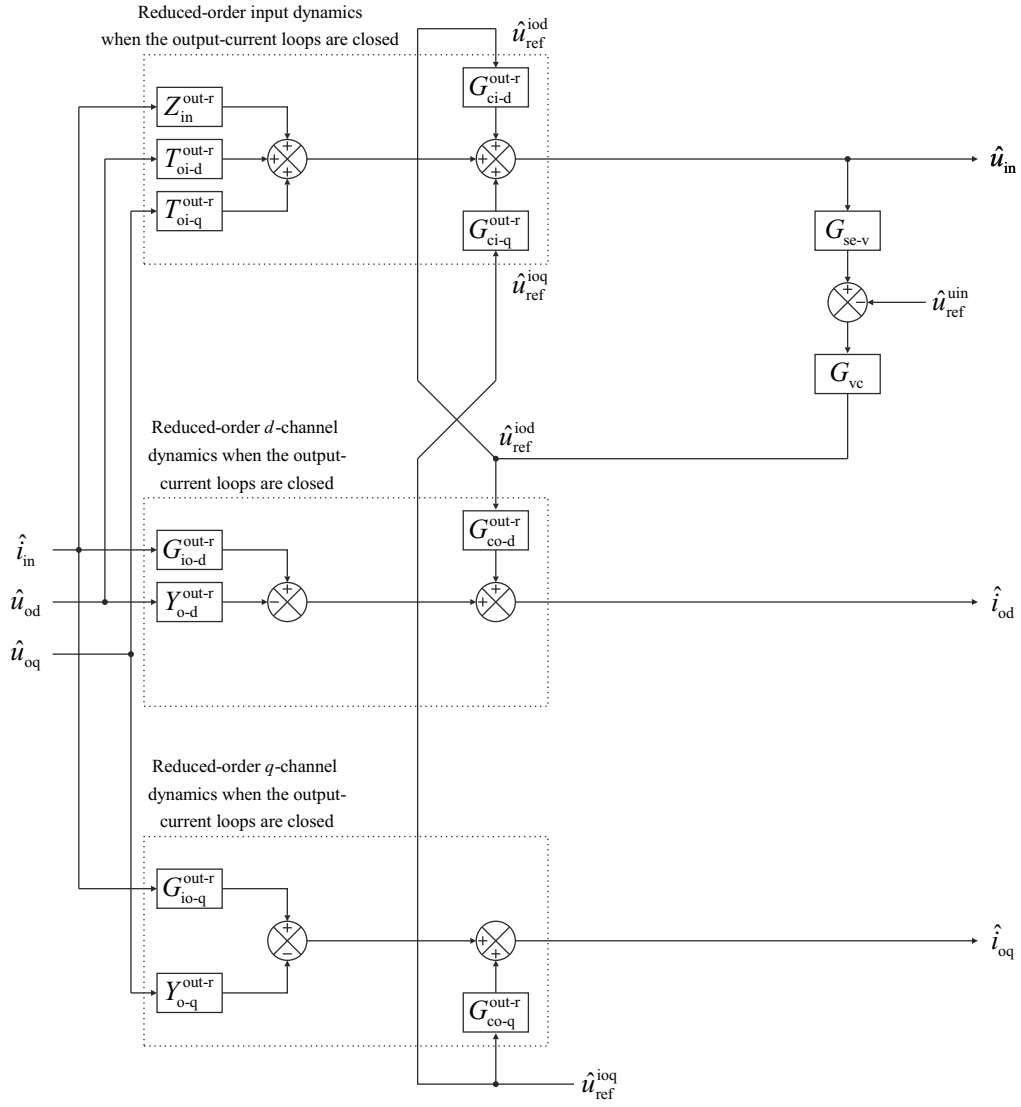

Fig. 2.18: Reduced-order control-block diagram for a grid-connected CF inverter with a cascaded input-voltage-output-current control scheme.

2.6 Comparison Between the Dynamic Properties of VF and CF-VSIs

In order to compare the dynamic properties between the analyzed VF and CF-VSIs in Figs. 2.1 and 2.3, an input capacitor needs to be added to the VF-VSI. This can be done by using the procedures described in Section 2.3. The input capacitor is not necessary for the converter operation and can, therefore, be considered as an input filter as presented in Fig. 2.19.

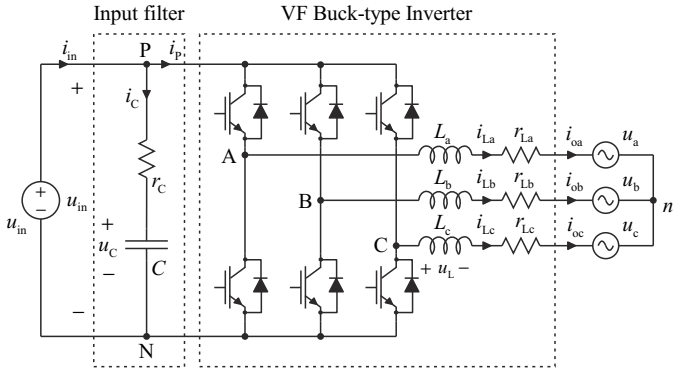

Fig. 2.19: Grid-connected three-phase voltage-fed VSI-type inverter with an input capacitor.

Let's first compute the necessary transfer functions (Y_{inS}, T_{oiS}, G_{ioS} and Z_{oS} in Fig. 2.5) for the input filter. Fig. 2.19 can be drawn as presented in Fig. 2.20 if only the input filter is considered. According to Fig. 2.20, the following expressions can be written:

$$\begin{aligned} i_{\mathrm{in}} &= \frac{1}{r_{\mathrm{C}} + \frac{1}{sC}} u_{\mathrm{in}} + i_{\mathrm{o}}, \\ u_{\mathrm{o}} &= u_{\mathrm{in}}. \end{aligned} \tag{2.335}$$

The G-parameter representation in Fig. 1.7 can be redrawn as presented in Fig. 2.21, since the input filter is a passive component. According to Fig. 2.21, the following expressions can be written:

$$\begin{aligned} \hat{i}_{\mathrm{in}} &= Y_{\mathrm{in}} \hat{u}_{\mathrm{in}} + T_{\mathrm{oi}} \hat{i}_{\mathrm{o}}, \\ \hat{u}_{\mathrm{o}} &= G_{\mathrm{io}} \hat{u}_{\mathrm{in}} - Z_{\mathrm{o}} \hat{i}_{\mathrm{o}}. \end{aligned} \tag{2.336}$$

Taking into account that the model in (2.335) is linear, comparing (2.335) and (2.336), denoting the transfer functions according to the notations of Fig. 2.5, and neglecting the

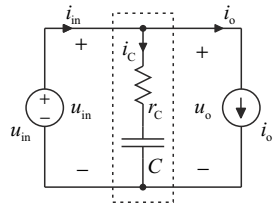

Fig. 2.20: Input filter for the converter in Fig. 2.19.

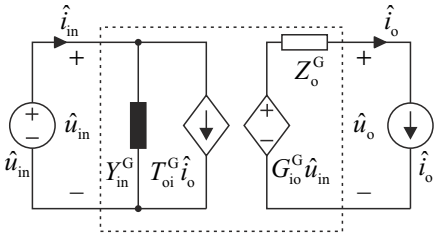

Fig. 2.21: Linear model for the filter in Fig. 2.20.

parasitic elements yields

$$\begin{aligned} Y_{\mathrm{inS}} &= sC, \quad T_{\mathrm{oiS}} = 1, \\ G_{\mathrm{ioS}} &= 1, \quad Z_{\mathrm{oS}} = 0, \end{aligned} \tag{2.337}$$

which can be used to compute the dynamic effect of the input capacitor for the dynamics of the VF-VSI. By considering (2.337) and Fig. 2.5, it is obvious that the input capacitor is an admittance Y_{inS} in parallel with the VF-VSI input admittance $Y_{\mathrm{in}}^{\mathrm{Y}}$. Accordingly, the input capacitor changes only the input admittance of the VF-VSI according to $Y_{\mathrm{in}}^{\mathrm{YS}} = Y_{\mathrm{in}}^{\mathrm{Y}} + Y_{\mathrm{inS}}$ as can be verified by comparing (2.338)–(2.343) and (2.344)–(2.349).

Using the symbolic transfer functions presented in (2.48)–(2.63) for the VF-VSI, Eq. (2.337), and the source-affected Y-parameter model for a VF inverter in (2.123)–(2.124) and Eq. (2.144) yields the following transfer functions:

$$Y_{\mathrm{in}}^{\mathrm{YS}} = \frac{\hat{i}_{\mathrm{inS}}}{\hat{u}_{\mathrm{inS}}} = sC\left(s^2 + \frac{3}{2}\frac{D_{\mathrm{d}}^2 + D_{\mathrm{q}}^2}{LC} + \omega_{\mathrm{s}}^2\right)\frac{1}{\Delta_{\mathrm{YS}}}, \tag{2.338}$$

$$Y_{\text{o-d}}^{\mathrm{YS}} = -\frac{\hat{i}_{\mathrm{od}}}{\hat{u}_{\mathrm{od}}} = \frac{s}{L}\frac{1}{\Delta_{\mathrm{YS}}}, \tag{2.339}$$

$$G_{\text{co-d}}^{\mathrm{YS}} = \frac{\hat{i}_{\mathrm{od}}}{\hat{d}_{\mathrm{d}}} = \frac{U_{\mathrm{in}}s}{L}\frac{1}{\Delta_{\mathrm{YS}}}, \tag{2.340}$$

$$G_{\text{co-q}}^{\text{YS}} = \frac{\hat{i}_{\text{oq}}}{\hat{d}_{\text{q}}} = \frac{U_{\text{in}} s}{L} \frac{1}{\Delta_{\text{YS}}}, \tag{2.341}$$

$$G_{\text{ci-d}}^{\text{YS}} = \frac{\hat{i}_{\text{in}}}{\hat{d}_{\text{d}}} = G_{\text{ci-dS}}^{\text{YS}} = \frac{\hat{i}_{\text{inS}}}{\hat{d}_{\text{d}}} = \frac{I_{\text{in}}}{D_{\text{d}}} s \left(s + \frac{2U_{\text{in}} D_{\text{d}}^2}{2I_{\text{in}}} \right) \frac{1}{\Delta_{\text{YS}}}, \tag{2.342}$$

$$\Delta_{\text{YS}} = s^2 + \omega_{\text{s}}^2. \tag{2.343}$$

The corresponding transfer functions for the VF-VSI without the input capacitor have been rewritten here to ease the comparison:

$$Y_{\text{in}}^{\text{Y}} = \frac{\hat{i}_{\text{in}}}{\hat{u}_{\text{in}}} = \frac{3}{2} \frac{D_{\text{d}}^2 + D_{\text{q}}^2}{L} \frac{s}{\Delta_{\text{Y}}}, \tag{2.344}$$

$$Y_{\text{o-d}}^{\text{Y}} = -\frac{\hat{i}_{\text{od}}}{\hat{u}_{\text{od}}} = \frac{s}{L} \frac{1}{\Delta_{\text{Y}}}, \tag{2.345}$$

$$G_{\text{co-d}}^{\text{Y}} = \frac{\hat{i}_{\text{od}}}{\hat{d}_{\text{d}}} = \frac{U_{\text{in}} s}{L} \frac{1}{\Delta_{\text{Y}}}, \tag{2.346}$$

$$G_{\text{co-q}}^{\text{Y}} = \frac{\hat{i}_{\text{oq}}}{\hat{d}_{\text{q}}} = \frac{U_{\text{in}} s}{L} \frac{1}{\Delta_{\text{Y}}}, \tag{2.347}$$

$$G_{\text{ci-d}}^{\text{Y}} = \frac{\hat{i}_{\text{in}}}{\hat{d}_{\text{d}}} = \frac{I_{\text{in}}}{D_{\text{d}}} \left(s + \frac{3}{2} \frac{D_{\text{d}}^2 U_{\text{in}}}{L I_{\text{in}}} \right) \frac{s}{\Delta_{\text{Y}}}, \tag{2.348}$$

$$\Delta_{\text{Y}} = s^2 + \omega_{\text{s}}^2. \tag{2.349}$$

The corresponding transfer functions for the CF-VSI have been rewritten here to ease the comparison:

$$Z_{\text{in}}^{\text{H}} = \frac{\hat{u}_{\text{in}}}{\hat{i}_{\text{in}}} = \frac{1}{C} \left(s^2 + \omega_{\text{s}}^2 \right) \frac{1}{\Delta_{\text{H}}}, \tag{2.350}$$

$$Y_{\text{o-d}}^{\text{H}} = -\frac{\hat{i}_{\text{od}}}{\hat{u}_{\text{od}}} = \frac{1}{L} \left(s^2 + \frac{3}{2} \frac{D_{\text{q}}^2}{LC} \right) \frac{1}{\Delta_{\text{H}}}, \tag{2.351}$$

$$G_{\text{co-d}}^{\text{H}} = \frac{\hat{i}_{\text{od}}}{\hat{d}_{\text{d}}} = \frac{U_{\text{in}} s}{L} \left(s - \frac{I_{\text{in}}}{U_{\text{in}} C} \right) \frac{1}{\Delta_{\text{H}}}, \tag{2.352}$$

$$G_{\text{co-q}}^{\text{H}} = \frac{\hat{i}_{\text{oq}}}{\hat{d}_{\text{q}}} = \frac{U_{\text{in}} s}{L} \left(s^2 + \frac{3}{2} \frac{D_{\text{d}}^2}{LC} \right) \frac{1}{\Delta_{\text{H}}}, \tag{2.353}$$

$$G_{\text{ci-d}}^{\text{H}} = \frac{\hat{u}_{\text{in}}}{\hat{d}_{\text{d}}} = -\frac{I_{\text{in}}}{D_{\text{d}} C} \left(s + \frac{3}{2} \frac{D_{\text{d}}^2 U_{\text{in}}}{L I_{\text{in}}} \right) \frac{s}{\Delta_{\text{H}}}, \tag{2.354}$$

$$\Delta_{\text{H}} = s \left(s^2 + \frac{3}{2} \frac{D_{\text{d}}^2 + D_{\text{q}}^2}{LC} + \omega_{\text{s}}^2 \right). \tag{2.355}$$

The following analysis is based on the inverter parameters presented in Appendix H.

The parameters $R_{\mathrm{load(a,b,c)}}$ and r_{pv} in Tables H.1 and H.2 are irrelevant at this point of the analyses, but are necessary parameters for the analysis presented in Chapter 4. Operating-point values are defined by the line denoted 'MPP' in Table H.2. According to the CF-VSI transfer functions in (2.350)–(2.355) (denoted in the following figures as 'CF'), VF-VSI transfer functions in (2.344)–(2.349) (denoted in the following figures as 'VF') and source-affected VF-VSI transfer functions in (2.338)–(2.343) (denoted in the following figures as 'VF+Cin') a few interesting conclusions can be drawn: the input impedances of the VF converter with the input capacitor and the CF converter are equal as given by

$$Z_{\mathrm{in}}^{\mathrm{H}} = \frac{1}{Y_{\mathrm{in}}^{\mathrm{YS}}}, \tag{2.356}$$

and illustrated in Fig. 2.22. The output admittances of the two converters, on the contrary, are different as can be seen in (2.351) and (2.339), and Fig. 2.23. This can be understood by considering how impedance is defined: voltage source is considered as a short circuit and current source as an open-circuit. Accordingly, the input capacitor in a VF-VSI does not have an influence on the output impedance (or admittance) as it does in CF-VSI.

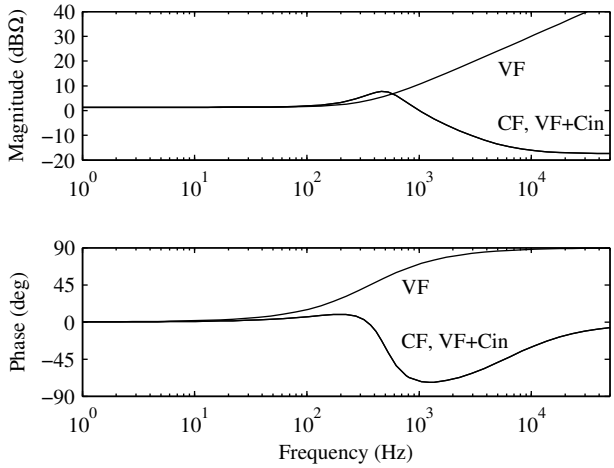

Fig. 2.22: Input impedance Z_{in}.

The d-channel grid current control of a VF-VSI can be designed based on a transfer function that is dictated mostly by the admittance of the output inductor as can be noticed from (2.340) and Fig. 2.24. However, an input-voltage-controlled VSI or a CF-VSI is a higher-order dynamic system compared to the VF-VSI because there is a duty ratio dependent resonance in the determinant (2.355). In addition, a right-half-plane

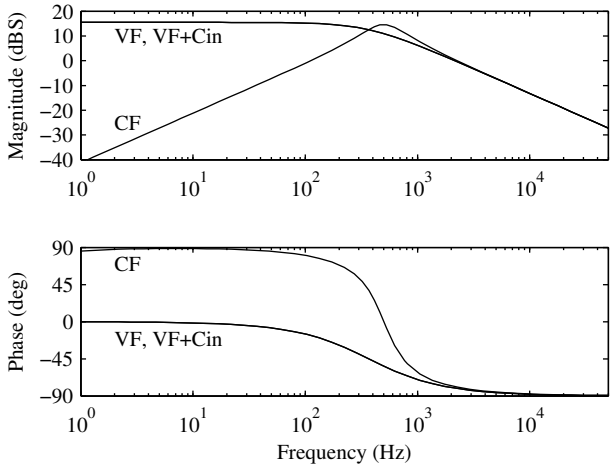

Fig. 2.23: Output admittance $Y_{\text{o-d}}$

(RHP) zero can be found on the d-channel control-to-output-current transfer function in (2.352) and Fig. 2.24 at an angular frequency of

$$\omega_{\text{RHP}} = \frac{I_{\text{in}}}{U_{\text{in}} C}. \tag{2.357}$$

This means that an input-voltage-controlled VSI (i.e. a CF-VSI) has a non-minimum-phase-output-control dynamics compared to the minimum-phase dynamics of a VF-VSI. Also the sign of the control related transfer functions are changed.

The q-channel grid current control resembles buck-type characteristics in both cases, i.e. the transfer function does not incorporate a RHP-zero or resonant behavior, as can be seen in (2.341), (2.352) and Fig. 2.25.

Based on the presented transfer functions, it can be concluded that the inverter dynamics change profoundly when the input source is changed from current to voltage source and vice versa. Therefore, it is crucial to determine the system inputs and outputs correctly for each specific application in order to capture the true system dynamics.

Furthermore, a RHP-zero and duty-ratio-dependent resonance in the determinant are typical properties of boost-type converters which justifies naming the CF-VSI as a CF boost-type inverter as discussed in Section 2.2. The VF-VSI, in turn, does not show similar characteristics and is commonly referred to as a buck-type topology in the literature.

Detailed Matlab m-files that can be used to obtain the transfer functions and Bode diagrams shown in this section can be found in Appendix F.

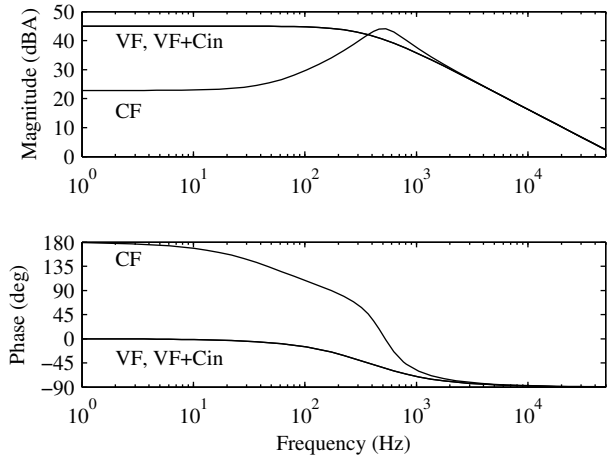

Fig. 2.24: d-channel control-to-output-current transfer function $G_{\text{co-d}}$.

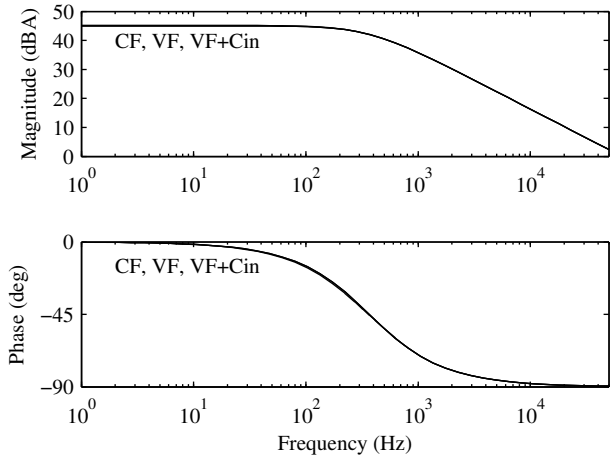

Fig. 2.25: q-channel control-to-output-current transfer function $G_{\text{co-q}}$.

3 THREE-PHASE INVERTER FREQUENCY-DOMAIN MODEL VERIFICATION

A small-signal model can be validated by comparing the predictions obtained by the model and the measurements from a prototype. Measuring transfer functions from dc-dc converters is a simple and trivial task, which can nowadays be done in a matter of a few seconds using broadband excitation signals (Roinila et al., 2009, 2010). However, similar measurements from a three-phase converter are more complex since the injection of the small-signal excitation and frequency response measurements include processing of virtual quantities, i.e. the dq-components of duty ratios, grid currents and voltages.

This chapter discusses the issues in measuring three-phase converter transfer functions and proposes a measurement setup utilizing digital signal processing (DSP) for the verification of the proposed small-signal model. Also the significance of using an active load for validating grid-connected inverter operation instead of passive resistive or resistive-inductive load is analyzed.

3.1 Measuring Three-Phase Inverter Transfer Functions

The three-phase inverter under test was supplied with an Agilent Technologies E4360A solar array simulator emulating a real PV generator. An Elgar SW 5250A programmable power supply was used to emulate a three-phase grid loading the inverter. Star-connected resistors were added in parallel with the Elgar to absorb the power generated by the inverter (and Elgar), since Elgar can only operate as a power supply. The grid had to be constructed as presented since an adequate programmable grid simulator was not available for the measurements. It is also worth noting that the inverter cannot be loaded with pure resistors since it would result in heavily damped frequency responses, which do not correspond with real grid-connected applications as will be shown Chapter 3.2. In order to properly measure the frequency responses, the three-phase voltages have to be generated by an external source to the point of connection.

Three-phase voltages and currents were transformed into the synchronous reference frame using a Spectrum Digital eZdspF28335 DSP board utilizing a Texas Instruments TMS320F28335 digital signal processor. The d and q-components of the inverter output currents and grid voltages were further converted into analogue signals using the PWM

outputs of the DSP board so that they could be fed to the Venable Instruments Model 3120 frequency response analyzer.

Park's transformation requires that the angle of the grid voltage space vector is known. The angle could be obtained with some kind of a grid synchronization method such as phase locked loop (PLL). However, the purpose of this measurement setup was to verify the model presented in Section 2, so the effect of grid synchronization had to be excluded from the converter dynamics. Therefore, the three-phase voltage reference angle θ_{ref} was generated inside the DSP and used in Park's transformation blocks (denoted as 'abc/dq' in the following figures) as well as fed to Elgar as an external trigger signal thus enabling ideal grid synchronization. The voltage reference angle θ_{ref} inside the DSP is a saw-tooth waveform with a frequency of 50 Hz. The trigger signal for Elgar, in turn, is a rectangular wave which has a positive value for the positive half cycle of phase-a voltage u_{a} and equals zero during the negative cycle as depicted in Fig. 3.1. Detailed schematic drawings about the measurement setups are presented in Figs. 3.2–3.4.

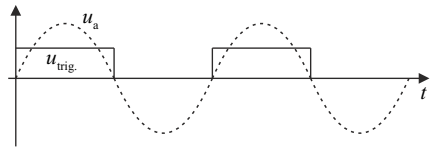

Fig. 3.1: External synchronization signal for Elgar.

Other noteworthy matters regarding three-phase converter transfer function measurements include:

1. Some analogue-to-digital (AD) converters require only positive voltages as inputs. This naturally affects the inverter hardware design since the measurement circuits have to be designed to measure ac quantities over a dc offset.

2. The AD and digital-to-analogue (DA) conversions introduce different gains to the converted signals.

3. The DSP implementation introduces delays to the measurements due to the sampling effect.

4. The main components affecting the measurement precision are the resolution of AD and DA conversions, since the Venable frequency response analyzer has an input accuracy of ± 0.05 dB according to its data sheet.

3.1.1 Small-Signal Injection to Input Current

A general procedure to measure a transfer function set, e.g. in (2.44) and (2.101), is to perturb i.e. to add a small-signal excitation to an input variable one at a time and

measure the gain and phase behavior between the corresponding input variable and one of the output variables. Excitation injection to the input current i_{in} (input variable for a PV inverter) enables measurement of the three transfer functions in the first column of (2.101) and can be made with the measurement setup as presented in Fig. 3.2. The injection circuit composes of a series connected injection transformer and a capacitor. The voltage injection from Venable creates a current injection according to

$$i_{\text{inj}} = C_{\text{inj}} \frac{\mathrm{d}u_{\text{inj}}}{\mathrm{d}t}. \tag{3.1}$$

The input current i_{in} is fed to one channel of Venable and either u_{in} (to measure Z_{in}), i_{od} (to measure $G_{\text{io-d}}$) or i_{oq} (to measure $G_{\text{io-q}}$) to the other channel.

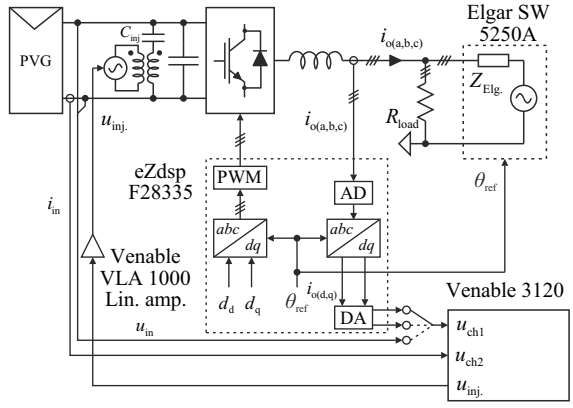

Fig. 3.2: Measurement setup for input current related transfer functions.

3.1.2 Small-Signal Injection to Output Voltages

Excitation injection to the output voltages can be made with the amplitude modulation function of Elgar (Fig. 3.3). The injection is fed to the external modulation input of Elgar and each of the three phase voltages is amplitude modulated with the same modulating signal.

The presented procedure results in summing a small-signal excitation to the d-channel voltage since the synchronous reference frame is tied to the phase voltages, which is why the d-channel voltage represents the peak value of the phase voltages and the q-channel voltage is zero. This enables the measurement of transfer functions in the second column of (2.101).

The major drawback with the proposed measurement setup is that the amplitude modulation cannot induce a large enough injection to the q-channel voltage u_{oq} so that the transfer functions in the third column of (2.101) could be measured reliably. The

q-channel voltage related transfer functions can be measured with different measurement techniques e.g. by using capacitive load connection or disconnection and identification procedures as done by Valdivia et al. (2012). However, the procedure described by Valdivia et al. (2012) cannot verify the control or input current related transfer functions, since the injection can only be made to the output voltages.

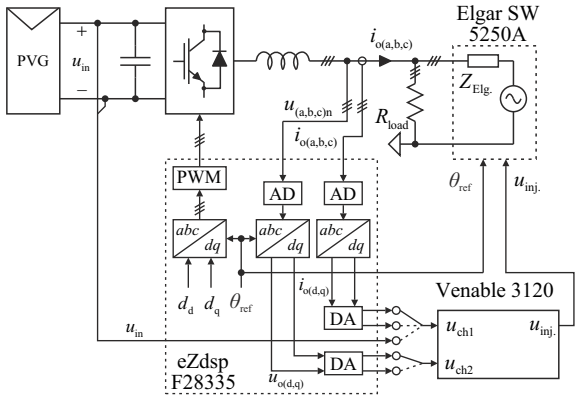

Fig. 3.3: Measurement setup for output voltage related transfer functions.

3.1.3 Small-Signal Injection to Control Variables

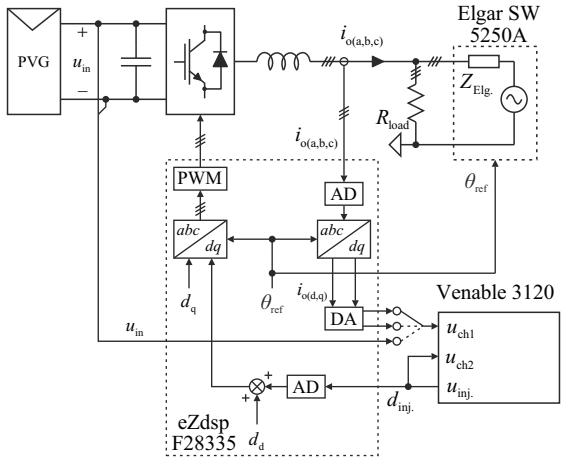

Fig. 3.4: Measurement setup for d-channel control related transfer functions.

Small-signal injection to the control variables can be made by feeding the duty-ratio excitation signal (d_{inj}) to the AD converter and summing the injection inside the DSP to the duty ratios. Fig. 3.4 presents the small-signal injection to the d-channel duty ratio

d_{d}. The d and q-channel output currents i_{od} and i_{oq} are calculated inside the DSP and converted to analogue signals using the PWM outputs of the DSP board and fed to the other input terminal of Venable to measure control-to-output-current transfer functions. In case the control-to-input-voltage transfer function is measured, the input voltage u_{in} is fed into Venable instead of the output current. The injection to the q-channel duty ratio can be made as above. The small-signal excitation of the duty ratios d_{d} and d_{q} enable the measurement of the fourth and fifth columns in (2.101).

3.2 Dynamic effect of resistive vs. active load

The best way to test a grid-connected inverter would be to use the actual utility grid as a load where the generated power could be fed resulting in an authentic testing environment. However, in many cases it would be necessary to test the inverter e.g. under predefined grid conditions (strong/weak grid) or during different kinds of faults (such as over/under voltages/frequencies, voltage sags, one/three-phase short-circuits, etc.) which would not be possible to do in a controlled manner using the utility grid. A programmable grid emulator would provide these kinds of functionalities, but they can be too expensive for small power electronics companies or research groups in universities. Therefore it could be an attractive option to test an inverter only by using a cheap resistive load.

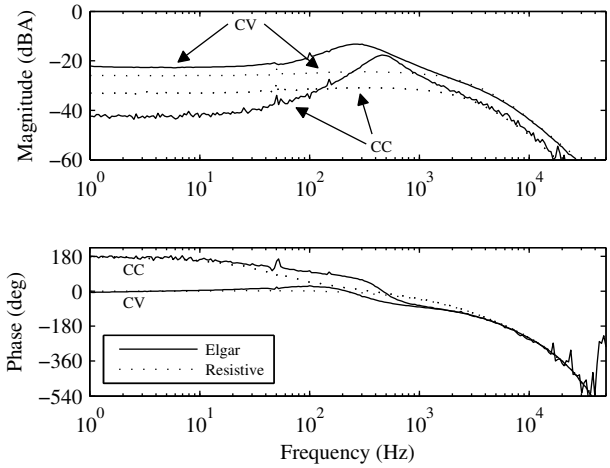

Fig. 3.5: Measured d-channel control-to-output-current transfer function $G_{\text{co-d}}$. Solid line is obtained using the parallel connection of Elgar and the load resistances, dotted line using only resistive load.

Fig. 3.5 shows measured d-channel control-to-output-current transfer functions $G_{\text{co-d}}$ when either resistive or active load (Elgar with the resistors) was used. It can be seen that the responses using resistive load, which is denoted in the figure as 'Resistive', are

heavily damped and the low-frequency gain of the transfer function is changed compared to the active load, which is denoted in the figure as 'Elgar'. Accordingly, the dynamic behavior of a grid-connected inverter cannot be verified with resistive load neither in frequency nor time-domain.

4 DYNAMIC EFFECT OF PHOTOVOLTAIC GENERATOR

The first section of this chapter presents the dynamic properties of a PVG and defines the most significant parameters that will have an effect on the dynamics of a converter connected to a PVG.

The last section of this chapter analyzes the effects of a PVG on the dynamic behavior of a grid-connected VSI-type three-phase inverter. Theoretical analyses are verified with experimental measurements in both cases.

4.1 Dynamic Characteristics of a Photovoltaic Generator

The one-diode model of a PV cell introduced in Chapter 1 has been redrawn in Fig. 4.1. Although the model has been formulated for a single PV cell, it can also be used to model the operation of a PV module (i.e. a series connection of PV cells) or a PV generator (i.e. a series and/or parallel connection of PV modules) by scaling model parameters as presented by Villalva et al. (2009a).

The measured static and dynamic characteristics of a Raloss SR30-36 PV module are shown in Fig. 4.2. The measurement setup is composed of the PV module illuminated by a fluorescent lamp unit capable of producing uniform illumination with a radiation intensity of 500 W/m^2. The fluorescent lamps were driven by an electronic ballast consisting of resonant inverters. More details about the measurement setup and the PV module have been reported earlier in detail by Mäki et al. (2010); Nousiainen et al. (2012); Puukko, Nousiainen, Mäki, Messo, Huusari and Suntio (2012).

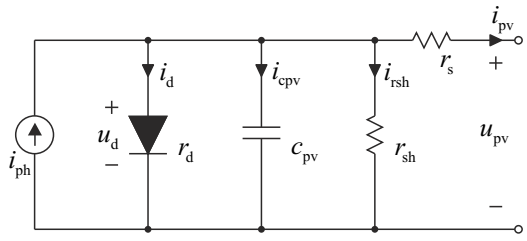

Fig. 4.1: Simplified electrical equivalent circuit of a photovoltaic cell.

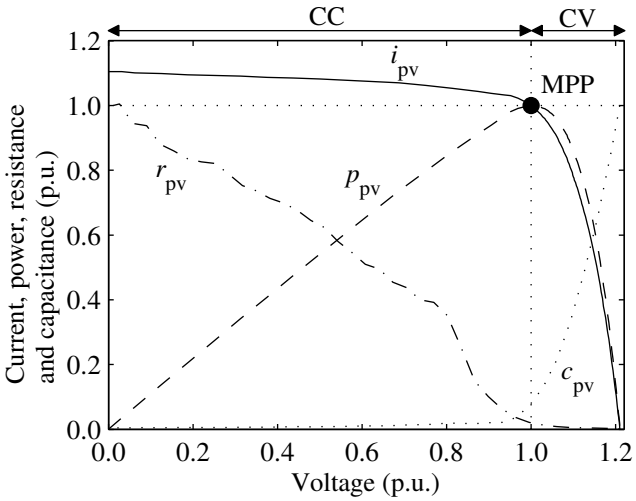

Fig. 4.2: Measured electrical characteristics of a Raloss SR30-36 PV module.

The measured electrical characteristics of the Raloss PV module are shown in Fig. 4.2 in terms of its dynamic resistance $r_{\mathrm{pv}} = r_{\mathrm{s}} + r_{\mathrm{d}} || r_{\mathrm{sh}}$ and capacitance c_{pv}, which are clearly non-linear and operating-point-dependent variables. Fig. 4.2 has been scaled so that the MPP current and voltage, maximum power, short-circuit value of the r_{pv} and open-circuit value of the c_{pv} are 1 p.u. each. Fig. 4.2 has been obtained by measuring the PV module impedances starting from the open circuit (OC) and ending to the short circuit (SC). Measurement data is presented in Table G.1 in Appendix G.

The dynamic resistance represents the low-frequency value of the measured impedances that are shown in Fig. 4.3 at three different operating points for illustrative purposes. According to Fig. 4.3, the PV module behaves like an RC-circuit up to typical PE converter switching frequencies. Therefore, the use of the one-diode model in Fig. 4.1 is justified and c_{pv} can be approximated from the measured PVG impedances by

$$c_{\mathrm{pv}} \approx \frac{1}{2\pi r_{\mathrm{pv,\text{-}3dB}} f_{\text{-}3\mathrm{dB}}}, \tag{4.1}$$

where $f_{\text{-}3\mathrm{dB}}$ is the cut-off frequency of the impedance magnitude curve and $r_{\mathrm{pv,\text{-}3dB}}$ is the magnitude of r_{pv} at the frequency $f_{\text{-}3\mathrm{dB}}$. Eq. (4.1) gives a good estimate for c_{pv} in the constant current region (CCR, i.e. at voltages below the MPP voltage), since $r_{\mathrm{d}} || r_{\mathrm{sh}} >> r_{\mathrm{s}}$. In the constant voltage region (CVR, i.e. at voltages above the MPP voltage), (4.1) slightly underestimates c_{pv} since $r_{\mathrm{d}} || r_{\mathrm{sh}}$ and r_{s} are in the same order of magnitude, but is still sufficiently accurate.

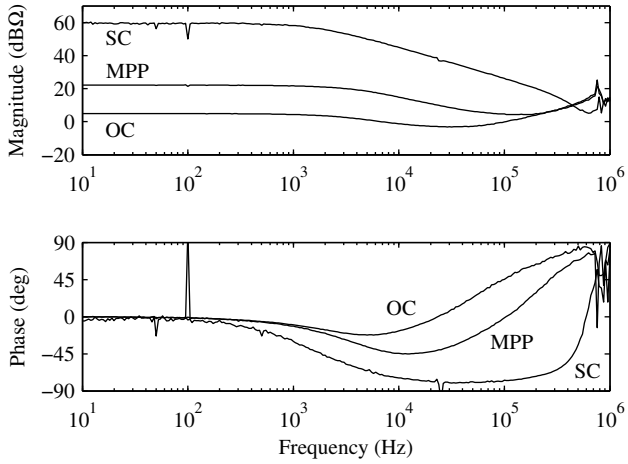

Fig. 4.3: Measured PVG impedances at short circuit (SC), maximum power point (MPP) and open circuit (OC).

The dynamic and static resistances of a PVG coincide at the MPP in which

$$\frac{\mathrm{d}p_{\mathrm{pv}}}{\mathrm{d}u_{\mathrm{pv}}} = \frac{\mathrm{d}(u_{\mathrm{pv}} i_{\mathrm{pv}})}{\mathrm{d}u_{\mathrm{pv}}} = I_{\mathrm{pv}} + U_{\mathrm{pv}} \frac{\mathrm{d}i_{\mathrm{pv}}}{\mathrm{d}u_{\mathrm{pv}}} = 0, \tag{4.2}$$

where I_{pv} and U_{pv} are the operating point current and voltage. Considering (4.2) and Fig. 4.2, it is obvious that $r_{\mathrm{pv}} = -\mathrm{d}u_{\mathrm{pv}}/\mathrm{d}i_{\mathrm{pv}}$ is greater in magnitude than $R_{\mathrm{pv}} = U_{\mathrm{pv}}/I_{\mathrm{pv}}$ at voltages less than the MPP voltage, i.e. at the CCR, and lower in magnitude at voltages higher than the MPP voltage, i.e. at the CVR, since the r_{pv}-curve is monotonic. Accordingly, a PVG incorporates current-source-like behavior at the CCR (since the internal impedance is high) and voltage-source-like behavior at the CVR (since the internal impedance is low) although the PVG is internally a non-linear current source as discussed.

4.2 Effect of PV Generator on Three-Phase VSI-Type Inverter Dynamics

The frequency response measurements presented in this section are based on the measurement setup introduced in Chapter 3 and prototype power-stage and operating point parameters in Appendix H. Detailed Matlab m-files that can be used to obtain the transfer functions and bode diagrams presented in this section can be found in Appendix I.

The effect of a non-ideal source in three-phase CF inverter dynamics can be taken into account by using the procedures presented in Section 2.3.2. In case of PVGs, the

source output impedance Z_{oS} can be given according to Fig. 4.1 by

$$Z_{\mathrm{oS}} = r_{\mathrm{s}} + r_{\mathrm{d}} || r_{\mathrm{sh}} || \frac{1}{s c_{\mathrm{pv}}}, \tag{4.3}$$

which can be approximated at low frequencies by

$$Z_{\mathrm{oS}} \approx r_{\mathrm{s}} + r_{\mathrm{d}} || r_{\mathrm{sh}} = r_{\mathrm{pv}}. \tag{4.4}$$

Only by using (4.4), the three-phase inverter small-signal model can be simplified enough so that the dynamic behavior of the converter can be examined with analytic expressions. Considering the source-affected small-signal model presented in Fig. 2.6 and (2.153)–(2.155) and using the following notations

$$\begin{aligned} &Z_{\mathrm{inS}} = 0, \quad T_{\mathrm{oiS}} = 1, \\ &G_{\mathrm{ioS}} = 1, \quad Y_{\mathrm{oS}} = 1/Z_{\mathrm{oS}} = 1/r_{\mathrm{pv}}, \end{aligned} \tag{4.5}$$

yields source-affected d-channel control-to-output-current ($G^{\mathrm{HS}}_{\mathrm{co\text{-}d}}$) and control-to-input-voltage ($G^{\mathrm{HS}}_{\mathrm{ci\text{-}d}}$), and q-channel control-to-output-current ($G^{\mathrm{HS}}_{\mathrm{co\text{-}q}}$) transfer function as given by

$$G^{\mathrm{HS}}_{\mathrm{co\text{-}d}} = \frac{\hat{i}_{\mathrm{od}}}{\hat{d}_{\mathrm{d}}} = \frac{U_{\mathrm{in}}}{L} s \left[s - \frac{1}{C} \left(\frac{I_{\mathrm{in}}}{U_{\mathrm{in}}} - \frac{1}{r_{\mathrm{pv}}} \right) \right] \frac{1}{\Delta_{\mathrm{HS}}}, \tag{4.6}$$

$$G^{\mathrm{HS}}_{\mathrm{co\text{-}q}} = \frac{\hat{i}_{\mathrm{oq}}}{\hat{d}_{\mathrm{q}}} = \frac{U_{\mathrm{in}}}{L} \left(s^2 + \frac{1}{r_{\mathrm{pv}} C} s + \frac{3}{2} \frac{D_{\mathrm{d}}^2}{LC} \right) \frac{1}{\Delta_{\mathrm{HS}}}, \tag{4.7}$$

$$G^{\mathrm{HS}}_{\mathrm{ci\text{-}d}} = \frac{\hat{u}_{\mathrm{in}}}{\hat{d}_{\mathrm{d}}} = -\frac{I_{\mathrm{in}}}{D_{\mathrm{d}} C} s \left(s + \frac{3}{2} \frac{D_{\mathrm{d}}^2 U_{\mathrm{in}}}{L I_{\mathrm{in}}} \right) \frac{1}{\Delta_{\mathrm{HS}}}, \tag{4.8}$$

$$\Delta_{\mathrm{HS}} = s \left(s^2 + \frac{1}{r_{\mathrm{pv}} C} s + \frac{3}{2} \frac{D_{\mathrm{d}}^2 + D_{\mathrm{q}}^2}{LC} + \omega_{\mathrm{s}}^2 \right) + \frac{\omega_{\mathrm{s}}^2}{r_{\mathrm{pv}} C}. \tag{4.9}$$

The determinant of the source-affected transfer functions Δ_{HS} in (4.9) reveals that its roots are resonant if r_{pv} is large (i.e. at the CCR) and that it has real-valued roots if r_{pv} is small (i.e. at the CVR), which means that the r_{pv} has a general effect on all transfer functions by changing the damping of the system according to the PVG operating point. It can be concluded that a VSI-type converter has resonant behavior when supplied by a PVG at the CCR and highly damped dynamics when supplied by a PVG at the CVR.

4.2.1 Output Current Control

According to (4.6), r_{pv} modifies the magnitude of $G_{\mathrm{co\text{-}d}}^{\mathrm{HS}}$ and the location of its zero in the complex plane. The frequency for the $G_{\mathrm{co\text{-}d}}^{\mathrm{HS}}$ zero can be given by

$$\omega_{\mathrm{z}} = \frac{1}{C}\left(\frac{I_{\mathrm{in}}}{U_{\mathrm{in}}} - \frac{1}{r_{\mathrm{pv}}}\right) = \frac{1}{C}\left(\frac{1}{R_{\mathrm{pv}}} - \frac{1}{r_{\mathrm{pv}}}\right). \tag{4.10}$$

Taking into account that the dynamic resistance r_{pv} coincides with the static resistance $R_{\mathrm{pv}} = U_{\mathrm{pv}}/I_{\mathrm{pv}} = U_{\mathrm{in}}/I_{\mathrm{in}}$ at the MPP, is larger in magnitude than the R_{pv} at the CCR and lower in magnitude at the CVR as discussed, the location of (4.10) in the complex plane can be given by

$$\begin{aligned}
&\text{CVR:} \quad r_{\mathrm{pv}} < R_{\mathrm{pv}} \Rightarrow \omega_{\mathrm{z}} < 0 \quad \text{LHP,} \\
&\text{MPP:} \quad r_{\mathrm{pv}} = R_{\mathrm{pv}} \Rightarrow \omega_{\mathrm{z}} = 0 \quad \text{Origin,} \\
&\text{CCR:} \quad r_{\mathrm{pv}} > R_{\mathrm{pv}} \Rightarrow \omega_{\mathrm{z}} > 0 \quad \text{RHP.}
\end{aligned} \tag{4.11}$$

The measured d-channel control-to-output-current transfer function in Fig. 4.4[1] verifies that that a RHP zero appears and the transfer function sign changes when the operating point of the PVG moves from the CVR to the CCR. Comparing Figs. 2.24 and 4.4 reveals that the output-current-control-dynamics of a VSI-type PV inverter resemble CF-VSI-type dynamics in the CCR, and VF-VSI-type dynamics in the CVR.

Naturally PV inverters should be designed to be stable at all possible PVG operating points. For a VSI-type inverter this means that stability has to be guaranteed at operating points between the minimum input voltage $U_{\mathrm{in,min}}$ required by the VSI power-stage (that depends on the modulation method and the grid voltage amplitudes) and the PVG open-circuit voltage. According to control engineering principles, the control bandwidth has to be limited to frequencies below the RHP zero for stable operation with reasonable control performance (Skogestad and Postlethwaite, 1998). The highest possible frequency for the RHP zero (typically in the order of few Hertz of few tens of Hertz) can be given according to (4.10) by

$$\omega_{\mathrm{RHP,max}} = \frac{I_{\mathrm{in,max}}}{U_{\mathrm{in,min}}C}, \tag{4.12}$$

which applies for a situation deep in the CCR where $r_{\mathrm{pv}} >> R_{\mathrm{pv}}$. However, even $\omega_{\mathrm{RHP,max}}$ would result in too low control bandwidth that cannot guarantee high enough power quality for a grid-connected inverter. Furthermore, the lowest possible frequency for the RHP zero is actually close to zero as can be understood by considering (4.11)

[1] Curves have been redrawn separately in Appendix I Figs. I.1–I.3 to ease distinguishing different curves from each other.

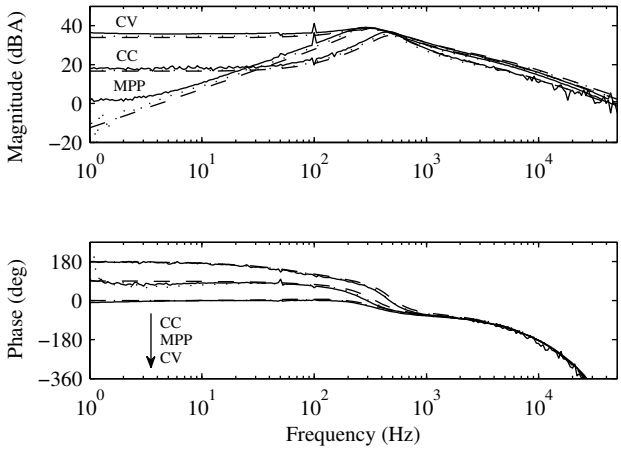

Fig. 4.4: d-channel control-to-output-current transfer function $G_{\text{co-d}}^{\text{HS}}$. Measurements with solid lines, predictions using measured source impedance with dotted lines and predictions using (4.4) with dashed lines.

at a point just below the MPP voltage, i.e. marginally at the CCR. As a consequence, it is impossible to obtain a stable d-channel current control loop that would have high enough bandwidth in the CCR.

Moreover, a stable control system in the CCR would actually try to maximize the control error signal if it was used in the CVR (and *vice versa*) because the transfer function changes its sign between the CCR and the CVR. As a conclusion, it is impossible to design a d-channel current controller that would

1. be stable both in CCR and CVR of a PVG, and

2. have high enough bandwidth in the CCR even in the best-case scenario, i.e. under $\omega_{\text{RHP,max}}$.

This implies that a grid-connected PV inverter that has only output-side control could only operate in CVR, because a high-bandwidth output-current-control is a must in grid-connected applications. Fortunately, a high-bandwidth current loop can be stabilized at the CCR by using a cascaded input-voltage-output-current control structure, where an input-voltage-control loop generates a reference for the d-channel current as will be shown in Section 4.2.2.

According to Fig. 4.4, the high-frequency behavior of $G_{\text{co-d}}^{\text{HS}}$ is quite similar in all operating regions. Therefore, the d-channel current controller can be designed based on either one of the transfer functions if the low-frequency behavior is neglected.

According to Fig. 4.5[2], the q-channel grid-current control $G_{\text{co-q}}^{\text{HS}}$ resembles buck-type characteristics (i.e. it is similar to the d and q-channel control-to-output-current transfer functions for a VF-VSI) regardless of the PVG operating point. The transfer function does not incorporate a RHP zero although the determinant has an operating-point-dependent resonant term, but has actually only minor effects on the transfer function as can be seen in Fig. 4.5. The only aspect limiting the bandwidth of the q-channel current control is the delay caused by the DSP control.

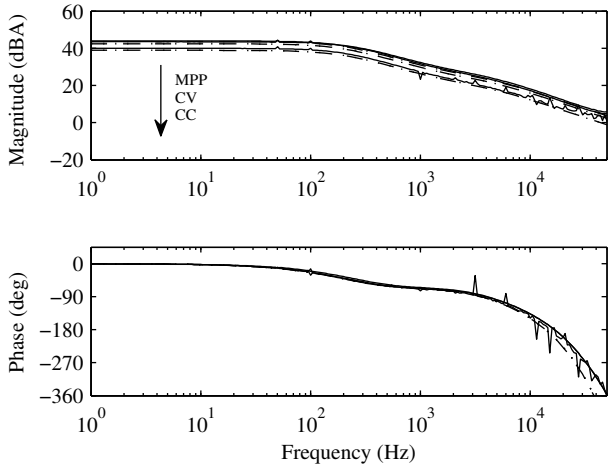

Fig. 4.5: q-channel control-to-output-current transfer function $G_{\text{co-q}}^{\text{HS}}$. Measurements with solid lines, predictions using measured source impedance with dotted lines and predictions using (4.4) with dashed lines.

The output-current-control performance can be evaluated according to the transfer function between the current reference and the current as given by

$$G_{\text{co-d}}^{\text{out-rS}} = \frac{\hat{i}_{\text{od}}}{\hat{u}_{\text{ref}}^{\text{iod}}} = \frac{1}{R_{\text{eq-d}}} \frac{L_{\text{out-d}}^{\text{rS}}}{1 + L_{\text{out-d}}^{\text{rS}}}, \tag{4.13}$$

$$G_{\text{co-q}}^{\text{out-rS}} = \frac{\hat{i}_{\text{oq}}}{\hat{u}_{\text{ref}}^{\text{ioq}}} = \frac{1}{R_{\text{eq-q}}} \frac{L_{\text{out-q}}^{\text{rS}}}{1 + L_{\text{out-q}}^{\text{rS}}}, \tag{4.14}$$

where

$$L_{\text{out-d}}^{\text{rS}} = R_{\text{eq-d}} G_{\text{cc-d}} G_{\text{a}} G_{\text{co-d}}^{\text{HS}}, \tag{4.15}$$

$$L_{\text{out-q}}^{\text{rS}} = R_{\text{eq-q}} G_{\text{cc-q}} G_{\text{a}} G_{\text{co-q}}^{\text{HS}}, \tag{4.16}$$

[2]Curves have been redrawn separately in Appendix I Figs. I.4–I.6 to ease distinguishing different curves from each other.

are the reduced-order source-affected d and q-channel-current-control loop gains.

4.2.2 Input Voltage Control

When the output current controllers have been designed, the input voltage controller can be designed based on the transfer function between the d-channel current reference and the input voltage $G_{\text{ci-d}}^{\text{out-rS}}$ in (2.301). The output current loop crossover frequency is typically up to a few decades higher than input voltage loop crossover frequency, so $G_{\text{ci-d}}^{\text{out-rS}}$ can be simplified by assuming infinite d-channel output current loop gain as given by

$$G_{\text{ci-d}}^{\text{out-rS}} = \frac{\hat{u}_{\text{in}}}{\hat{u}_{\text{ref}}^{\text{iod}}} = \frac{L_{\text{out-d}}}{1 + L_{\text{out-d}}} \frac{G_{\text{ci-d}}^{\text{HS}}}{R_{\text{eq-d}} G_{\text{co-d}}^{\text{HS}}} \overset{L_{\text{out-d}} \to \infty}{\approx} \frac{G_{\text{ci-d}}^{\text{HS}}}{R_{\text{eq-d}} G_{\text{co-d}}^{\text{HS}}}, \tag{4.17}$$

where the superscript extension '-rS' indicates that a reduced-order and source-affected transfer function is considered. The input voltage control dynamics in its frequency range can, thus, be analyzed without taking into account the current controller transfer function.

According to (4.17), the d-channel control-to-input-voltage transfer function $G_{\text{ci-d}}^{\text{HS}}$ in (4.8) can be found at the numerator of $G_{\text{ci-d}}^{\text{out-rS}}$. Fortunately, a PVG does not introduce any operation point dependent zeros, only a duty ratio dependent resonance to $G_{\text{ci-d}}^{\text{HS}}$ as can be verified from Fig. 4.6[3].

The d-channel control-to-output-current transfer function $G_{\text{co-d}}^{\text{HS}}$, in turn, can be found at the denominator of $G_{\text{ci-d}}^{\text{out-rS}}$ as shown in (4.17), which means that the input-voltage-control loop

$$L_{\text{in}}^{\text{rS}} = G_{\text{se-v}} G_{\text{vc}} G_{\text{ci-d}}^{\text{out-rS}} \tag{4.18}$$

in (2.277) incorporates a RHP pole when the operating point of the PVG is in the CCR, because $G_{\text{co-d}}^{\text{HS}}$ contains a RHP zero as previously analyzed. The RHP pole in the input-voltage-control loop origins from the cascaded input-voltage-output-current control scheme and naturally causes design constraints in the input voltage loop. The RHP pole is also used in Section 4.2.3 to formulate a design rule between the input capacitance and the input-voltage-control loop stability. It can also be concluded that the cascaded control structure is not needed only for MPPT purposes but is actually essential for being able to operate at all PVG operating points.

Fig. 4.7 presents the transfer function according to which the input-voltage-control loop shall be designed. The effect of the RHP pole in the CCR is clearly visible. Fur-

[3]Curves have been redrawn separately in Appendix I Figs. I.7–I.9 to ease distinguishing different curves from each other.

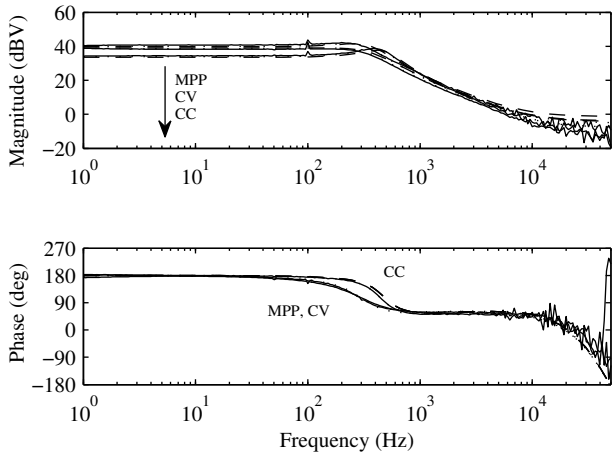

Fig. 4.6: d-channel control-to-input-voltage transfer function $G_{\text{ci-d}}^{\text{HS}}$. Measurements with solid lines, predictions using measured source impedance with dotted lines and predictions using (4.4) with dashed lines.

thermore, $G_{\text{ci-d}}^{\text{out-rS}}$ shows similar phase flip at low frequencies as the $G_{\text{co-d}}^{\text{HS}}$, which actually means that the input-voltage-control loop generates a current reference for the current controller that has a correct sign irrespective of the operating region.

The stabilizing effect of the input-voltage-control loop can be analyzed as follows. The transfer functions under the output current control only contain the output current control loop gain $L_{\text{out-d}}^{\text{rS}}$ at the denominator, which in turn contains a RHP zero. Designing a control loop that would have a bandwidth over the RHP zero would result in instability because the RHP zero causes phase lag which, in turn, would cause the $L_{\text{out-d}}^{\text{rS}} = -1$ at some frequency below the RHP. However, in PV applications the current loop crossover frequency has to be designed higher than the RHP zero frequency. Fortunately, the input-voltage-loop stabilizes the unstable current loop because the closed loop transfer functions under the cascaded control scheme contain a term $(1 + L_{\text{out-d}}^{\text{rS}})(1 - L_{\text{in}}^{\text{rS}})$ at the denominator, which can be given according to (4.15), (4.17), and (4.18) as presented in (4.19), if the input-voltage-control loop is designed to have a bandwidth over the RHP frequency.

$$(1 + L_{\text{out-d}}^{\text{rS}})(1 - L_{\text{in}}^{\text{rS}}) \approx -L_{\text{out-d}}^{\text{rS}} L_{\text{in}}^{\text{rS}} \approx G_{\text{cc-d}} G_{\text{a}} G_{\text{se-v}} G_{\text{vc}} G_{\text{ci-d}}^{\text{HS}} \tag{4.19}$$

Clearly the denominator of the closed-loop transfer functions under a cascaded control scheme does not incorporate a RHP term because the transfer function $G_{\text{co-d}}^{\text{HS}}$ is not present.

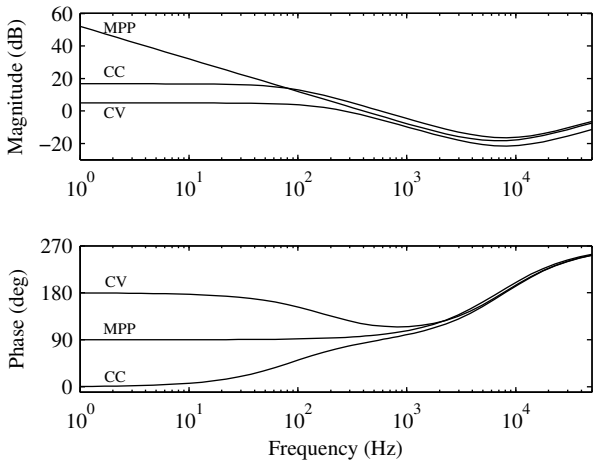

Fig. 4.7: Transfer function from the d-channel current reference to the input voltage $G_{\text{ci-d}}^{\text{out-rS}}$.

4.2.3 Input Capacitor Design Rule

In case of a RHP pole in the control loop, the loop crossover frequency has to be greater than the RHP pole frequency in order to achieve stable operation with reasonable control performance (Skogestad and Postlethwaite, 1998). Sometimes a factor of two is included between the necessary crossover frequency and the RHP pole frequency for additional margin (Kolar et al., 2011). On the other hand, the input voltage of a three-phase inverter can contain ripple components also well below the switching frequency. In such a case, the input-voltage control loop has to be designed to have sufficient attenuation at the frequency where ripple or disturbance is found in order to prevent it from polluting the grid current reference and causing harmonics in the grid current. The lowest frequency where input-voltage ripple can be expected would be at twice the grid frequency (ω_{grid}) if imbalance exists in the grid. This implies that the voltage-loop crossover frequency may need to be less than $2\omega_{\text{grid}}$ and is typically in the range of few tens of Hertz for three-phase inverters.

A VSI-type inverter requires a minimum dc-link voltage $U_{\text{in,min}}$ that can be given according to the peak value of the grid voltage: twice or $\sqrt{3}$ times the peak for three-phase inverter depending on the modulating method. This minimum-voltage operating point most probably lies in the CCR of a PVG, since the MPP voltage cannot be specified as the minimum input voltage due to uncertainties in the PVG parameters and environmental conditions.

The worst case in terms of the input-voltage control occurs when the RHP pole frequency is the highest, which can be given as presented in (4.12). An inequality for the

voltage-loop crossover frequency ω_{loop} can be given according to the RHP pole frequency and the ω_{grid} by

$$k_{\text{grid}}\omega_{\text{grid}} = \omega_{\text{loop}} \geq k_{\text{RHP}}\omega_{\text{RHP,max}}. \tag{4.20}$$

A safety factor $k_{\text{RHP}} = 2$ in (4.20) can be found e.g. in Kolar et al. (2011). Because the worst-case operating point is assumed to exist in the CCR, the maximum input current $I_{\text{in,max}}$ in (4.12) could be assumed to be the short-circuit current of the PVG I_{sc} in the standard test conditions (1000 W/m^2), because in the CCR $i_{\text{pv}} \approx I_{\text{sc}}$. According to Luoma et al. (2012), the short-term irradiance might exceed the standard test conditions due to cloud enhancement, which could compromise the inverter stability based on (4.12) and (4.20). A maximum input current can thus be presented as $I_{\text{in,max}} = k_{\text{i}}I_{\text{sc}}$, where a safety margin $k_{\text{i}} = 1.5$ is selected based on observed maximum momentarily irradiances of 1500 W/m^2 Luoma et al. (2012). Combining the rules in (4.12) and (4.20), a minimum input capacitance C_{min} guaranteeing stable operation of a single-stage three-phase VSI-type PV inverter in all possible operating points along the PVG IU-curve can be given by

$$C_{\text{min}} = \frac{k_{\text{RHP}}k_{\text{i}}}{k_{\text{grid}}} \frac{I_{\text{sc}}}{U_{\text{in-min}}\omega_{\text{grid}}}. \tag{4.21}$$

Fig. 4.8 illustrates the proposed constraints between the minimum input capacitance normalized by the PVG short-circuit current ($C_{\text{min}}/I_{\text{sc}}$) and the input-voltage-loop crossover frequency ($k_{\text{grid}}\omega_{\text{grid}}$) for single-stage three-phase VSI-type PV inverter based on (4.21). The border between stable and unstable regions is obtained using $k_{\text{i}} = 1$ and $k_{\text{RHP}} = 1$, i.e. without safety margins. However, the figure also presents minimum capacitances when the safety margins discussed earlier are included ($k_{\text{i}} = 1.5$ and $k_{\text{RHP}} = 2$). The minimum input voltages are given with and without the third-harmonic-injection modulation method for a 230 V$_{\text{rms}}$/50 Hz utility grid.

According to Fig. 4.8, the control-system-based design criterion becomes significant with low input-voltage-loop-bandwidth requirements. A reasonable trade-off between the minimum input capacitance and the voltage-loop crossover frequency is between 50–100 Hz for the three-phase inverter, which results in capacitances between 5–7 μF/A.

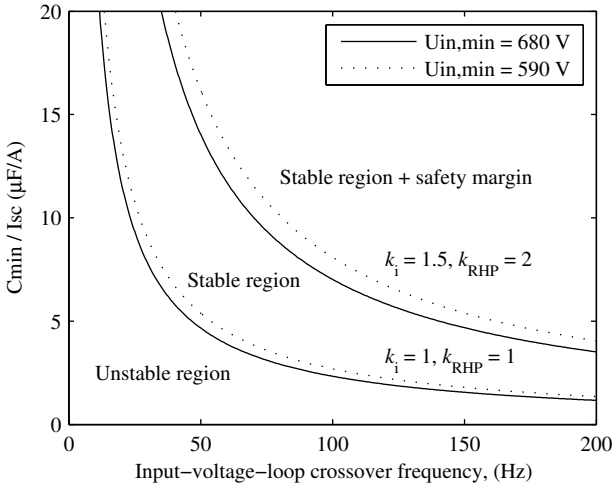

Fig. 4.8: $C_{\min}/I_{\mathrm{sc}}$ as a function of voltage-loop crossover frequency f_{loop}.

5 CONCLUSIONS

5.1 Final Conclusions

This thesis provided a comprehensive study of the dynamic properties of grid-connected three-phase VSI-type inverters in PV applications. The study concentrated on proper dynamic modeling of the VSI power stage and the dynamic effect of the PVG.

The background of grid-connected renewable power generation was reviewed in Chapter 1 and it was pointed out that the energy portfolio in the future will be a mixture of existing technologies with an increasing portion of different renewables. Different PV power system grid-integration schemes were introduced and the importance of a cascaded input-voltage output-current control scheme in PV inverters was emphasized. The input-voltage control in grid-connected inverters necessitates that the inverter is considered as a CF topology, which is not properly recognized in the literature and is one of the main contributions of this thesis. The dynamic properties of PVGs were introduced and several unambiguities in analyzing three-phase PV power systems were pointed out.

The dynamic properties of grid-connected three-phase VSI-type inverters were analyzed in Chapter 2. One of the main contributions of this chapter was to explicitly formulate a method to include the effects of source/load non-idealities in the small-signal models of grid-connected three-phase inverters. The method is general and can be applied to all VF and CF inverters regardless of the topology. Furthermore, it was shown that the dynamic properties of grid-connected VSI-type inverters are determined not only by the power stage but also by the application where it is to be used. It was shown that VF and CF-VSIs have completely different dynamic properties although their power stages resemble each other. All grid-connected inverters that are used in renewable power production applications are actually CF-VSIs although the majority of articles consider them to be VF-VSIs.

A measurement setup for performing three-phase inverter frequency response measurements was proposed in Chapter 3. The problematics in measuring transfer functions from a three-phase converter were also discussed. The major issue is the processing of virtual quantities, i.e. current and voltages in the synchronous reference frame, that do not exist in real life. Also, the significance of using an active load instead of passive (resistive or resistive-inductive) was emphasized.

The dynamic properties of a PVG were presented in Chapter 4. The most significant parameters that will have an effect on the dynamics of a converter connected to a PVG were also discussed. The last section of the chapter analyzed the effects of a PVG on the dynamic behavior of a grid-connected VSI-type three-phase inverter. Theoretical analyses were verified with experimental measurements in both cases. A new control-design-based sizing constraint for the input capacitance of VSI-type inverters in PV applications was proposed.

The sizing constraint originates from an operating-point-dependent pole in the input-voltage-control loop of grid-connected input-voltage-controlled inverters in PV applications. The location of the pole on the complex plane can be given explicitly according to the input capacitance, operating point voltage and current, and the dynamic resistance of the PVG. The pole shifts between the left and right halves of the complex plane according to the operating point along the PVG IU-curve. Naturally, the pole causes control-system-design constraints when it is located on the right half of the complex plane. Furthermore, the RHP pole frequency is inversely proportional to the input capacitance, which implies that minimizing the input capacitance can lead to an unstable input voltage loop, because the control loop has to be designed so that the loop crossover frequency is higher than the RHP pole frequency.

Therefore, a design rule between the input-capacitor sizing and input-voltage-control design was proposed in Chapter 4. Typically, the input capacitor design is based on energy-based design criteria, e.g. input-voltage ripple or transient behavior. The energy-based criteria are important, although subjective, and do not necessarily guarantee inverter stability. Therefore, in addition to the energy-based criteria, the rule proposed in this thesis should always be considered, because it guarantees the stability of the inverter, which results in a more reliable and robust PV inverter design.

5.2 Future Research Topics

This thesis analyzed the dynamic properties of a basic three-phase VSI-type inverter with "an L-type grid interface" in PV applications. Interesting future research topics could include:

1. The dynamic effect of an "LCL-type grid interface" for a VSI-type inverter can be formulated either by using the model presented in this thesis and computing a source-effect for a "CL-type" output filter as introduced or by constructing a small-signal model for a VSI by considering the "LCL-type grid interface" as a part of the power stage. It would be interesting to study how a control system for such an inverter should be designed and what is the dynamic effect if the grid-side inductor current would be controlled instead of the inverter-side inductor.

2. How does the grid synchronization shape the output impedance and can it include negative-resistor-like behavior? If so, can the negative output impedance -behavior be prevented with proper grid synchronization and/or control system design?

3. Does the MPP-tracking algorithm create feedback *and feedforward* loops, because both system input (i_{pv}) and system output variables (u_{pv}) are processed in the control system? How does this change the converter dynamics?

4. The dynamic effect of space-vector modulation and the "input-voltage feedforward". The input-voltage feedforward in grid-connected inverters is actually a feedback because the input voltage is a system output. It is known that feedforward does not affect stability but feedback can. What is the dynamic effect of space-vector modulation in grid-connected VSIs?

5. This thesis analyzed single-stage inverters. In Messo et al. (2012) ([P11] in Section 1.6.1), the dynamic effect of a MPP-tracking dc-dc converter connected in between the PVG and a VSI was investigated. More thorough understanding about the possible interactions between the individual power stages and the dynamic properties of the overall system would be valuable.

REFERENCES

Abbott, D. (2010). Keeping the energy debate clean: How do we supply the world's energy needs?, *Proc. IEEE* **98**(1): 42–66. DOI: 10.1109/JPROC.2009.2035162.

Alepuz, S., Bordonau, J. and Peracaula, J. (1999). Dynamic analysis of three-level voltage-source inverters applied to power regulation, *IEEE Power Electron. Specialists Conf., PESC*, pp. 721–726. DOI: 10.1109/PESC.1999.785589.

Alepuz, S., Busquets-Monge, S., Bordonau, J., Gago, J., González, D. and Balcells, J. (2006). Interfacing renewable energy sources to the utility grid using a three-level inverter, *IEEE Trans. Ind. Electron.* **53**(5): 1504–1511. DOI: 10.1109/TIE.2006.882021.

Alepuz, S., Salaet, J., Busquets, S. and Bordonau, J. (2005). Load voltage and output current control of three-level voltage source inverters, *IEEE Annu. Conf. Ind. Electron. Soc., IECON*, pp. 739–744. DOI: 10.1109/IECON.2005.1568996.

Alepuz, S., Salaet, J., Gilabert, A., Bordonau, J. and Peracaula, J. (2003). Optimal regulator with integral action and gain-scheduling for the comprehensive control of three-level NPC VSI, *IEEE Power Electron. Specialists Conf., PESC*, pp. 1420–1425. DOI: 10.1109/PESC.2003.1216795.

Araújo, S. V., Zacharias, P. and Mallwitz, R. (2010). Highly efficient single-phase transformerless inverters for grid-connected photovoltaic systems, *IEEE Trans. Ind. Electron.* **57**(9): 3118–3128. DOI: 10.1109/TIE.2009.2037654.

Bae, H., Lee, J., Park, S. and Cho, B. H. (2008). Large-signal stability analysis of solar array power system, *IEEE Trans. Aerosp. Electron. Syst.* **44**(2): 534–547. DOI: 10.1109/TAES.2008.4560205.

Barroso, L. A., Rudnick, H., Sensfuss, F. and Linares, P. (2010). The green effect: Economic and market impacts of renewable energy development in spain, germany, and latin america, *IEEE Power & Energy Mag.* **8**(5): 22–35. DOI: 10.1109/MPE.2010.937595.

Bordonau, J., Cosan, M., Borojevic, D., Mao, H. and Lee, F. C. (1997). A state-space model for the comprehensive dynamic analysis of three-level voltage-source inverters, *IEEE Power Electron. Specialists Conf., PESC*, pp. 942–948. DOI: 10.1109/PESC.1997.616837.

Bose, B. K. (2010). Global warming: Energy, environmental pollution, and the impact of power electronics, *IEEE Ind. Electron. Mag.* **4**(1): 6–17. DOI: 10.1109/MIE.2010.935860.

Bull, S. R. (2001). Renewable energy today and tomorrow, *Proc. IEEE* **89**(8): 1216–1226. DOI: 10.1109/5.940290.

Cao, D., Jiang, S., Yu, X. and Peng, F. Z. (2011). Low-cost semi-Z-source inverter for single-phase photovoltaic systems, *IEEE Trans. Power Electron.* **26**(12): 3514–3523. DOI: 10.1109/TPEL.2011.2148728.

Carrasco, J. M., Franquelo, L. G., Bialasiewicz, J. T., Galván, E., Guisado, R. C. P., Prats, M. A. M., León, J. I. and Moreno-Alfonso, N. (2006). Power-electronic systems for the grid integration of renewable energy sources: a survey, *IEEE Trans. Ind. Electron.* **53**(4): 1002–1016. DOI: 10.1109/TIE.2006.878356.

Castilla, M., Miret, J., Matas, J., de Vicuna, L. G. and Guerrero, J. M. (2008). Linear current control scheme with series resonant harmonic compensator for single-phase grid-connected photovoltaic inverters, *IEEE Trans. Ind. Electron.* **55**(7): 2724–2733. DOI: 10.1109/TIE.2008.920585.

Céspedes, M. and Sun, J. (2009). Renewable energy systems instability involving grid-parallel inverters, *IEEE Appl. Power Electron. Conf. Expo., APEC*, pp. 1971–1977. DOI: 10.1109/APEC.2009.4802943.

Chen, X. and Sun, J. (2011). A study of renewable energy system harmonic resonance based on a DG test-bed, *IEEE Appl. Power Electron. Conf. Expo., APEC*, pp. 995–1002. DOI: 10.1109/APEC.2011.5744716.

Chen, Y. and Smedley, K. (2008). Three-phase boost-type grid-connected inverter, *IEEE Trans. Power Electron.* **23**(5): 2301–2309. DOI: 10.1109/TPEL.2008.2003025.

Chenvidhya, D., Kirtikara, K. and Jivacate, C. (2005). PV module dynamic impedance and its voltage and frequency dependencies, *Sol. Energ. Mat. Sol. C.* **86**(2): 243–251. DOI: 10.1016/j.solmat.2004.07.005.

Enslin, J. H. R. (2005). Opportunities in hybrid energy networks using power electronic interfaces, *Int. Conf. Future Power Systems, FPS*, pp. 1–7. DOI: 10.1109/FPS.2005.204212.

Enslin, J. H. R. and Heskes, P. J. M. (2004). Harmonic interaction between a large number of distributed power inverters and the distribution network, *IEEE Trans. Power Electron.* **19**(6): 1586–1593. DOI: 10.1109/TPEL.2004.836615.

Esram, T. and Chapman, P. L. (2007). Comparison of photovoltaic array maximum power point tracking techniques, *IEEE Trans. Energy Convers.* **22**(2): 439–449. DOI: 10.1109/TEC.2006.874230.

Femia, N., Lisi, G., Petrone, G., Spagnuolo, G. and Vitelli, M. (2008). Distributed maximum power point tracking of photovoltaic arrays: novel approach and system analysis, *IEEE Trans. Ind. Electron.* **55**(7): 2610–2621. DOI: 10.1109/TIE.2008.924035.

Figueres, E., Garcerá, G., Sandia, J., González-Espín, F. J., Calvo, J. and Vales, M. (2007). Dynamic analysis of three-phase photovoltaic inverters with a high order grid filter, *IEEE Int. Symp. Ind. Electron., ISIE*, pp. 691–696. DOI: 10.1109/ISIE.2007.4374680.

Figueres, E., Garcerá, G., Sandia, J., González-Espín, F. and Rubio, J. C. (2009). Sensitivity study of the dynamics of three-phase photovoltaic inverters with an LCL grid filter, *IEEE Trans. Ind. Electron.* **56**(3): 706–717. DOI: 10.1109/TIE.2008.2010175.

Fratta, A., Griffero, G., Guglielmi, P., Nieddu, S. and Villata, F. (2002). Minimum capacitor size in DC/DC/AC converters by means of novel PWM technique and DC-link structure, *IEEE Int. Symp. Ind. Electron., ISIE*, Vol. 3, pp. 789–794. DOI: 10.1109/ISIE.2002.1025833.

Goh, H. S., Armstrong, M. and Zahawi, B. (2009). The effect of grid operating conditions on the current controller performance of grid connected photovoltaic inverters, *European Conf. Power Electron. Applicat., EPE*, pp. 1–8.

Guerrero, J. M., Blaabjerg, F., Zhelev, T., Hemmes, K., Monmasson, E., Jemei, S., Comech, M. P., Granadiano, R. and Frau, J. I. (2010). Distributed generation: Toward a new energy paradigm, *IEEE Ind. Electron. Mag.* **4**(1): 52–64. DOI: 10.1109/MIE.2010.935862.

Hart, E. K., Stoutenburg, E. D. and Jacobson, M. Z. (2012). The potential of intermittent renewables to meet electric power demand: Current methods and emerging analytical techniques, *Proc. IEEE* **100**(2): 322–334. DOI: 10.1109/JPROC.2011.2144951.

Heskes, P. J. M., Myrzik, J. M. A. and Kling, W. L. (2010). Harmonic distortion and oscillatory voltages and the role of negative impedance, *IEEE Power Energy Soc. General Meeting*, pp. 1–7. DOI: 10.1109/PES.2010.5588137.

Hiti, S., Boroyevich, D. and Cuadros, C. (1994). Small-signal modeling and control of three-phase PWM converters, *IEEE Ind. Applicat. Soc. Annu. Meeting, IAS*, pp. 1143–1150. DOI: 10.1109/IAS.1994.377572.

Jain, S. and Agarwal, V. (2007). Comparison of the performance of maximum power point tracking schemes applied to single-stage grid-connected photovoltaic systems, *IET Electr. Power Appl.* **1**(5): 753–762. DOI: 10.1049/iet-epa:20060475.

Kjaer, S. B., Pedersen, J. K. and Blaabjerg, F. (2005). A review of single-phase grid-connected inverters for photovoltaic modules, *IEEE Trans. Ind. Appl.* **41**(5): 1292–13061. DOI: 10.1109/TIA.2005.853371.

Kolar, J. W., Friedli, T., Krismer, F., Looser, A., Schweizer, M., Steimer, P. and Bevirt, J. (2011). Conceptualization and multi-objective optimization of the electric system of an airborne wind turbine, *IEEE Int. Symp. Ind. Electron., ISIE*, pp. 32–55. DOI: 10.1109/ISIE.2011.5984131.

Konstantopoulos, G. C. and Alexandridis, A. T. (2011). An innovated nonlinear voltage regulator for DC/DC converters: Theoretical and experimental results on PV applications, *IET Renew. Power Gener. Conf., RPG*, Edinburgh, U.K., pp. 1–6. DOI: 10.1049/cp.2011.0132.

Kotsopoulos, A., Duarte, J. L. and Hendrix, M. A. M. (2001). A predictive control scheme for DC voltage and AC current in grid-connected photovoltaic inverters with minimum DC link capacitance, *IEEE Annu. Conf. Ind. Electron. Soc., IECON*, pp. 1994–1999. DOI: 10.1109/IECON.2001.975597.

Krein, P. T. and Balog, R. S. (2009). Cost-effective hundred-year life for single-phase inverters and rectifiers in solar and LED lighting applications based on minimum capacitance requirements and a ripple power port, *IEEE Appl. Power Electron. Conf. Expo., APEC*, pp. 620–625. DOI: 10.1109/APEC.2009.4802723.

Kroposki, B., Margolis, R. and Ton, D. (2009). Harnessing the Sun: An overview of solar technologies, *IEEE Power & Energy Mag.* **7**(3): 22–33. DOI: 10.1109/MPE.2009.932305.

Kroposki, B., Pink, C., DeBlasio, R., Thomas, H., Simoes, M. and Sen, P. K. (2010). Benefits of power electronic interfaces for distributed energy systems, *IEEE Trans. Energy Convers.* **25**(3): 901–908. DOI: 10.1109/TEC.2010.2053975.

Kwon, J.-M., Nam, K.-H. and Kwon, B.-H. (2006). Photovoltaic power conditioning system with line connection, *IEEE Trans. Ind. Electron.* **53**(4): 1048–1054. DOI: 10.1109/TIE.2006.878329.

Lee, J. H., Bae, H. S. and Cho, B. H. (2008). Resistive control for a photovoltaic battery charging system using a microcontroller, *IEEE Trans. Ind. Electron.* **55**(7): 2767–2775. DOI: 10.1109/TIE.2008.922594.

Leppäaho, J., Nousiainen, L., Puukko, J., Huusari, J. and Suntio, T. (2010). Implementing current-fed converters by adding an input capacitor at the input of voltage-fed converter for interfacing solar generator, *Int. Power Electron. Motion*

Control Conf. Expo., EPE-PEMC, Ohrid, Macedonia, pp. T12–81–T12–88. DOI: 10.1109/EPEPEMC.2010.5606791.

Liserre, M., Sauter, T. and Hung, J. Y. (2010). Future energy systems: Integrating renewable energy sources into the smart power grid through industrial electronics, *IEEE Ind. Electron. Mag.* **4**(1): 18–37. DOI: 10.1109/MIE.2010.935861.

Liserre, M., Teodorescu, R. and Blaabjerg, F. (2004). Stability of grid-connected PV inverters with large grid impedance variation, *IEEE Power Electron. Specialists Conf., PESC*, pp. 4773–4779. DOI: 10.1109/PESC.2004.1354843.

Liu, B., Duan, S. and Cai, T. (2011). Photovoltaic DC-building-module-based BIPV system - concept and design considerations, *IEEE Trans. Power Electron.* **26**(5): 1418–1429. DOI: 10.1109/TPEL.2010.2085087.

Liu, S. and Dougal, R. A. (2002). Dynamic multiphysics model for solar array, *IEEE Trans. Energy Convers.* **17**(2): 285–294. DOI: 10.1109/TEC.2002.1009482.

Luoma, J., Kleissl, J. and Murray, K. (2012). Optimal inverter sizing considering cloud enhancement, *Solar Energy* **86**(1): 421–429. DOI: 10.1016/j.solener.2011.10.012.

Messo, T., Puukko, J. and Suntio, T. (2012). Effect of MPP-tracking DC/DC converter on VSI-based photovoltaic inverter dynamics, *IET Power Electron. Machines Drives Conf., PEMD*, Bristol, UK, pp. 1–6. DOI: 10.1049/cp.2012.0334.

Middlebrook, R. D. (1988). Small-signal modeling of pulse-width modulated swithced-mode power converters, *Proc. IEEE* **76**(4): 343–354. DOI: 10.1109/5.4421.

Middlebrook, R. D. and Ćuk, S. (1976). A general unified approach to modelling switching-converter power stages, *IEEE Power Electron. Specialists Conf., PESC*, pp. 18–34.

Middlebrook, R. D. and Ćuk, S. (1977). A general unified approach to modelling switching-converter power stages, *Int. J. Electronics* **42**(6): 521–550. DOI: 10.1080/00207217708900678.

Mirafzal, B., Saghaleini, M. and Kaviani, A. K. (2011). An SVPWM-based switching pattern for stand-alone and grid-connected three-phase single-stage boost inverter, *IEEE Trans. Power Electron.* **26**(4): 1102–1111. DOI: 10.1109/TPEL.2010.2089806.

Mäki, A. and Valkealahti, S. (2012). Power losses in long string and parallel-connected short strings of series-connected silicon-based photovoltaic modules due to partial shading conditions, *IEEE Trans. Energy Convers.* **27**(1): 173–183. DOI: 10.1109/TEC.2011.2175928.

Mäki, A., Valkealahti, S. and Suntio, T. (2010). Dynamic terminal characteristics of a photovoltaic generator, *Int. Power Electron. Motion Control Conf. Expo., EPE-PEMC*, Ohrid, Macedonia, pp. T12–76–T12–80. DOI: 10.1109/EPEPEMC.2010.5606786.

Ngo, K. D. T. (1986). Low frequency characterization of PWM converters, *IEEE Trans. Power Electron.* **PE-1**(4): 223–230. DOI: 10.1109/TPEL.1986.4766314.

Nousiainen, L., Puukko, J., Mäki, A., Messo, T., Huusari, J., Jokipii, J., Viinamaki, J., Lobera, D. T., Valkealahti, S. and Suntio, T. (2012). Photovoltaic generator as an input source for power electronic converters, *IEEE Trans. Power Electron.* **PP**(99): 1. DOI: 10.1109/TPEL.2012.2209899.

Nousiainen, L., Puukko, J. and Suntio, T. (2011a). Appearance of a RHP-zero in VSI-based photovoltaic converter control dynamics, *IEEE Int. Telecommun. Energy Conf., INTELEC*, Amsterdam, The Netherlands, pp. 1–8. DOI: 10.1109/INTLEC.2011.6099893.

Nousiainen, L., Puukko, J. and Suntio, T. (2011b). Simple VSI-based single-phase inverter: dynamical effect of photovoltaic generator and multiplier-based grid synchronization, *IET Renew. Power Gener. Conf., RPG*, Edinburgh, U.K., pp. 1–6. DOI: 10.1049/cp.2011.0118.

Omura, I. (2010). Future role of power electronics, *IEEE Int. Conf. Integrated Power Electron. Syst., CIPS*, pp. 1–9.

Park, R. H. (1929). Two-reaction theory of synchronous machines: Generalized method of analysis, part i, *Trans. American Institute of Electrical Engineers* **48**(3): 716–727. DOI: 10.1109/T-AIEE.1929.5055275.

Petrone, G., Spagnuolo, G., Teodorescu, R., Veerachary, M. and Vitelli, M. (2008). Reliability issues in photovoltaic power processing systems, *IEEE Trans. Ind. Electron.* **55**(7): 2569–2580. DOI: 10.1109/TIE.2008.924016.

Photong, C., Klumpner, C. and Wheeler, P. (2010). Evaluation of single-stage power converte topologies for grid-connected photovoltaic, *IEEE Int. Conf. Ind. Technology, ICIT*, pp. 1161–1168. DOI: 10.1109/ICIT.2010.5472595.

Prodanović, M. and Green, T. C. (2003). Control and filter design of three-phase inverters for high power quality grid connection, *IEEE Trans. Power Electron.* **18**(1): 373–380. DOI: 10.1109/TPEL.2002.807166.

Puukko, J., Messo, T., Nousiainen, L., Huusari, J. and Suntio, T. (2011). Negative output impedance in three-phase grid-connected renewable energy source inverters based on

reduced-order model, *IET Renew. Power Gener. Conf., RPG*, Edinburgh, U.K., pp. 1–6. DOI: 10.1049/cp.2011.0128.

Puukko, J., Messo, T. and Suntio, T. (2011). Effect of photovoltaic generator on a typical VSI-based three-phase grid-connected photovoltaic inverter dynamics, *IET Renew. Power Gener. Conf., RPG*, Edinburgh, U.K., pp. 1–6. DOI: 10.1049/cp.2011.0127.

Puukko, J., Nousiainen, L., Mäki, A., Messo, T., Huusari, J. and Suntio, T. (2012). Photovoltaic generator as an input source for power electronic converters, *Int. Power Electron. Motion Control Conf. Expo., EPE-PEMC*, Novi Sad, Serbia, pp. 1–9.

Puukko, J., Nousiainen, L. and Suntio, T. (2011). Effect of minimizing input capacitance in VSI-based renewable energy source converters, *IEEE Int. Telecommun. Energy Conf., INTELEC*, Amsterdam, The Netherlands, pp. 1–9. DOI: 10.1109/INTLEC.2011.6099891.

Puukko, J., Nousiainen, L. and Suntio, T. (2012). Three-phase photovoltaic inverter small-signal modelling and model verification, *IET Power Electron. Machines Drives Conf., PEMD*, Bristol, UK, pp. 1–6. DOI: 10.1049/cp.2012.0351.

Puukko, J. and Suntio, T. (2012a). Dynamic properties of a VSI-based three-phase inverter in photovoltaic application, *IET Renew. Power Gener.* **PP**: 1. Accepted for publication.

Puukko, J. and Suntio, T. (2012b). Modelling the effect of non-ideal load in three-phase converter dynamics, *IET Electron. Lett.* **48**(7): 402–404. DOI: 10.1049/el.2011.3663.

Rabkowski, J., Peftitsis, D. and Nee, H.-P. (2012). Design steps towards a 40-kVA SiC inverter with an efficiency exceeding 99.5 %, *IEEE Appl. Power Electron. Conf. Expo., APEC*, pp. 1536–1543. DOI: 10.1109/APEC.2012.6166024.

Rodriguez, C. and Amaratunga, G. A. J. (2008). Long-lifetime power inverter for photovoltaic AC modules, *IEEE Trans. Ind. Electron.* **55**(7): 2593–2601. DOI: 10.1109/TIE.2008.922401.

Roinila, T., Vilkko, M. and Suntio, T. (2009). Fast loop gain measurement of a switched-mode converter using a binary signal with a specified fourier amplitude spectrum, *IEEE Trans. Power Electron.* **24**(12): 2746–2755. DOI: 10.1109/TPEL.2009.2027706.

Roinila, T., Vilkko, M. and Suntio, T. (2010). Frequency-response measurement of switched-mode power supplies in the presence of nonlinear distortions, *IEEE Trans. Power Electron.* **25**(8): 2179–2189. DOI: 10.1109/TPEL.2010.2043688.

Sahan, B., Vergara, A. N., Henze, N., Engler, A. and Zacharias, P. (2008). A single-stage PV module integrated converter based on a low-power current-source inverter, *IEEE Trans. Ind. Electron.* **55**(7): 2602–2609. DOI: 10.1109/TIE.2008.924160.

Schonardie, M. F. and Martins, D. C. (2007). Solar grid-connected three-phase system with active and reactive power control and input voltage clamped, *IEEE Int. Conf. Electron. Circuits and Syst., ICECS*, pp. 463–466. DOI: 10.1109/ICECS.2007.4511030.

Schonardie, M. F. and Martins, D. C. (2008). Application of the dq0 transformation in the three-phase grid-connected PV systems with active and reactive power control, *IEEE Int. Conf. Sustainable Energy Technologies, ICSET*, pp. 18–23. DOI: 10.1109/ICSET.2008.4746965.

Skogestad, S. and Postlethwaite, I. (1998). *Multivariable feedback control*, John Wiley & Sons Ltd, England. 559 pp.

Sun, J. (2008). AC power electronic systems: Stability and power quality, *IEEE Workshop on Control and Modeling for Power Electron., COMPEL*, pp. 1–10. DOI: 10.1109/COMPEL.2008.4634697.

Sun, J. (2009). Small-signal methods for AC distributed power systems: A review, *IEEE Trans. Power Electron.* **24**(11): 2545–2554. DOI: 10.1109/TPEL.2009.2029859.

Sun, K., Zhang, L., Xing, Y. and Guerrero, J. M. (2011). A distributed control strategy based on DC bus signaling for modular photovoltaic generation systems with battery energy storage, *IEEE Trans. Power Electron.* **26**(10): 3032–3045. DOI: 10.1109/TPEL.2011.2127488.

Suntio, T. (2009). *Dynamic Profile of Switched-Mode Converter: Modeling, Analysis and Control*, Wiley-VCH, Germany. 357 pp.

Suntio, T., Puukko, J., Nousiainen, L., Huusari, J. and Messo, T. (2011). Change of paradigm in power electronic converters used in renewable energy applications, *IEEE Int. Telecommun. Energy Conf., INTELEC*, Amsterdam, The Netherlands, pp. 1–9. DOI: 10.1109/INTLEC.2011.6099800.

Taggart, S., James, G., Dong, Z. and Russell, C. (2012). The future of renewables linked by a transnational asian grid, *Proc. IEEE* **100**(2): 348–359. DOI: 10.1109/JPROC.2011.2159089.

Teodorescu, R. and Blaabjerg, F. (2004). Flexible control of small wind turbines with grid failure detection operating in stand-alone and grid-connected mode, *IEEE Trans. Power Electron.* **19**(5): 1323–1332. DOI: 10.1109/TPEL.2004.833452.

Thongpron, J., Kirtikara, K. and Jivacate, C. (2006). A method for the determination of dynamic resistance of photovoltaic modules under illumination, *Sol. Energ. Mat. Sol. C.* **90**(18-19): 3078–3084. DOI: 10.1016/j.solmat.2006.06.029.

Tirumala, R., Imbertson, P., Mohan, N., Henze, C. and Bonn, R. (2002). An efficient, low cost DC-AC inverter for photovoltaic systems with increased reliability, *IEEE Annu. Conf. Ind. Electron. Soc., IECON*, pp. 1095–1100. DOI: 10.1109/IECON.2002.1185425.

Trujillo, C., Velasco, D., Garcerá, G., Figueres, E. and Guacaneme, J. (2012). Reconfigurable control scheme for a PV microinverter working in both grid connected and island modes, *IEEE Trans. Ind. Electron.* **PP**(99): 1–11. DOI: 10.1109/TIE.2011.2177615.

Tse, C. K. (1998). *Linear Circuit Analysis*, Addison Wesley Longman, Inc., UK. 307 pp.

Tse, K. K., Ho, B. M. T., Chung, H. S.-H. and Hui, S. Y. R. (2004). A comparative study of maximum-power-point trackers for photovoltaic panels using switching-frequency modulation scheme, *IEEE Trans. Ind. Electron.* **51**(2): 410–418. DOI: 10.1109/TIE.2004.825226.

Valdivia, V., Lazaro, A., Barrado, A., Zumel, P., Fernandez, C. and Sanz, M. (2012). Black-box modeling of three-phase voltage source inverters for system-level analysis, *IEEE Trans. Ind. Electron.* **PP**(99): 1. DOI: 10.1109/TIE.2011.2167730.

Valkealahti, S. (2011). Forecasting the future of renewables, *in* J. Blanco and H. Kheradmand (eds), *Climate Change - Socioeconomic Effects*, InTech, chapter 22, pp. 425–440. ISBN 978-953-307-411-5.

Venturini, R. P., Scarpa, V. V. R., Spiazzi, G. and Buso, S. (2008). Analysis of limit cycle oscillations in maximum power point tracking algorithms, *IEEE Power Electron. Specialists Conf., PESC*, pp. 378–384. DOI: 10.1109/PESC.2008.4591959.

Vighetti, S., Ferrieux, J.-P. and Lembeye, Y. (2012). Optimization and design of a cascaded DC/DC converter devoted to grid-connected photovoltaic systems, *IEEE Trans. Power Electron.* **27**(4): 2018–2027. DOI: 10.1109/TPEL.2011.2167159.

Villalva, M. G., de Siqueira, T. G. and Ruppert, E. (2010). Voltage regulation of photovoltaic arrays: small-signal analysis and control design, *IET Power Electron.* **3**(6): 869–880. DOI: 10.1049/iet-pel.2008.0344.

Villalva, M. G., Gazoli, J. R. and Filho, E. R. (2009a). Comprehensive approach to modeling and simulation of photovoltaic arrays, *IEEE Trans. Power Electron.* **24**(5): 1198–1208. DOI: 10.1109/TPEL.2009.2013862.

Villalva, M. G., Gazoli, J. R. and Filho, E. R. (2009b). Modeling and control of a three-phase isolated grid-connected converter fed by a photovoltaic array, *Brazilian Power Electron. Conf., COBEP*, pp. 202–210. DOI: 10.1109/COBEP.2009.5347682.

Visscher, K. and Heskes, P. J. M. (2005). A method for operational grid and load impedance measurements, *Int. Conf. Future Power Systems, FPS*, pp. 1–4. DOI: 10.1109/FPS.2005.204324.

Wang, F., Duarte, J. L., Hendrix, M. A. M. and Ribeiro, P. F. (2011). Modeling and anlysis of grid harmonic distortion impact of aggregated DG inverters, *IEEE Trans. Power Electron.* **26**(3): 786–797. DOI: 10.1109/TPEL.2010.2091286.

Wiese, A., Kaltschmitt, M. and Lee, W. Y. (2009). Renewable power generation: a status report, *Renewable Energy Focus* **10**(4): 64–69. DOI: 10.1016/S1755-0084(09)70157-7.

Wiese, A., Kleineidam, P., Schallenberg, K., Ulrich, A. J. and Kaltschmitt, M. (2010). Renewable power generation: a status report, *Renewable Energy Focus* **11**(4): 34–39. DOI: 10.1016/S1755-0084(10)70090-9.

Wu, J.-F., Chang, C.-H., Lin, L.-C. and Kuo, C.-L. (2011). Power loss comparison of single- and two-stage grid connected photovoltaic systems, *IEEE Trans. Energy Convers.* **26**(2): 707–715. DOI: 10.1109/TEC.2011.2123897.

Xiao, W., Dunford, W. G., Palmer, P. R. and Capel, A. (2007). Regulation of photovoltaic voltage, *IEEE Trans. Ind. Electron.* **54**(3): 1365–1374. DOI: 10.1109/TIE.2007.893059.

Xiao, W., Elnosh, A., Khadkikar, V. and Zeineldin, H. (2011). Overview of maximum power point tracking technologies for photovoltaic power systems, *IEEE Annu. Conf. Ind. Electron. Soc., IECON*, pp. 3900–3905. DOI: 10.1109/IECON.2011.6119946.

Yazdani, A. and Dash, P. P. (2009). A control methodology and characterization of dynamics for a photovoltaic (pv) system interfaced with a distribution network, *IEEE Trans. Power Del.* **24**(3): 1538–1551. DOI: 10.1109/TPWRD.2009.2016632.

Yazdani, A., Fazio, A. R. D., Ghoddami, H., Russo, M., Kazerani, M., Jatskevich, J., Strunz, K., Leva, S. and Martinez, J. A. (2011). Modeling guidelines and a benchmark for power system simulation studies of three-phase single-stage photovoltaic systems, *IEEE Trans. Power Del.* **26**(2): 1247–1264. DOI: 10.1109/TPWRD.2010.2084599.

Zhao, Z., Xu, M., Chen, Q., Lai, J.-S. and Cho, Y. (2012). Derivation, analysis, and implementation of a boost-buck converter-based high-efficiency PV inverter, *IEEE Trans. Power Electron.* **27**(3): 1304–1313. DOI: 10.1109/TPEL.2011.2163805.

A VF-VSI TRANSFER FUNCTIONS IN SECTION 2.1

This appendix presents the code for a Matlab m-file that can be used to obtain the symbolic transfer functions for the VF-VSI found in (2.48)–(2.63) in Section 2.1 "Grid-Connected Voltage-Fed VSI".

```
################################################################################
#  M-file begins!                                                              #
################################################################################

% Joonas Puukko
% Tampere University of Technology
% Department of Electrical Energy Engineering
% 2012
% Filename: VFbuck_ss_symb_nopar.m

% State-space for a three-phase VF-VSI:
% Symbolic transfer functions w/o the parasitic elements

clear all
clc

% Symbolic variables
    syms iLd iLq uin iin uod uoq dd dq
    syms ILd ILq Uin Iin Uod Uoq Dd Dq
    syms ws L rL rsw req
    syms s

% Linearized state matrices
    Am = [  0, ws
          -ws,  0];

    Bm = [Dd/L, -1/L,    0, Uin/L,     0
          Dq/L,    0, -1/L,     0, Uin/L];
```

```
    Cm = [3*Dd/2, 3*Dq/2
               1,      0
               0,      1];

    Dm = [0, 0, 0, Iin/Dd, 0
          0, 0, 0,      0, 0
          0, 0, 0,      0, 0];

    Im = eye(2);

% Solving the transfer function matrix
    deter = simplify(det(s*Im - Am));
    Ypar  = simplify((Cm * inv(s*Im - Am) * Bm) + Dm);

    Yin  = simplify(Ypar(1,1));
    Toid = simplify(Ypar(1,2));
    Toiq = simplify(Ypar(1,3));
    Gcid = simplify(Ypar(1,4));
    Gciq = simplify(Ypar(1,5));

    Giod  = simplify(Ypar(2,1));
    Yod   = simplify(-Ypar(2,2));
    Gcrqd = simplify(-Ypar(2,3));
    Gcod  = simplify(Ypar(2,4));
    Gcoqd = simplify(Ypar(2,5));

    Gioq  = simplify(Ypar(3,1));
    Gcrdq = simplify(-Ypar(3,2));
    Yoq   = simplify(-Ypar(3,3));
    Gcodq = simplify(Ypar(3,4));
    Gcoq  = simplify(Ypar(3,5));

% Transfer functions w/o the determinant
    Yin_nodeter  = simplify(Ypar(1,1)*deter);
    Toid_nodeter = simplify(Ypar(1,2)*deter);
    Toiq_nodeter = simplify(Ypar(1,3)*deter);
    Gcid_nodeter = simplify(Ypar(1,4)*deter);
    Gciq_nodeter = simplify(Ypar(1,5)*deter);

    Giod_nodeter  = simplify(Ypar(2,1)*deter);
    Yod_nodeter   = simplify(-Ypar(2,2)*deter);
    Gcrqd_nodeter = simplify(-Ypar(2,3)*deter);
```

```
    Gcod_nodeter  = simplify(Ypar(2,4)*deter);
    Gcoqd_nodeter = simplify(Ypar(2,5)*deter);

    Gioq_nodeter  = simplify(Ypar(3,1)*deter);
    Gcrdq_nodeter = simplify(-Ypar(3,2)*deter);
    Yoq_nodeter   = simplify(-Ypar(3,3)*deter);
    Gcodq_nodeter = simplify(Ypar(3,4)*deter);
    Gcoq_nodeter  = simplify(Ypar(3,5)*deter);

##############################################################################
#  M-file ends!                                                              #
##############################################################################
```

B CF-VSI TRANSFER FUNCTIONS IN SECTION 2.2

This appendix presents the code for a Matlab m-file that can be used to obtain the symbolic transferfunctions for the CF-VSI found in (2.105)–(2.120) in Section 2.2 "Grid-Connected Current-Fed VSI".

```
################################################################################
#  M-file begins!                                                              #
################################################################################

% Joonas Puukko
% Tampere University of Technology
% Department of Electrical Energy Engineering
% 2012
% Filename: CFboost_ss_symb_nopar.m

% State-space for a three-phase CF-VSI:
% Symbolic transfer functions w/o the parasitic elements

clear all
clc

% Symbolic variables
    syms iLd iLq uC uin iin uod uoq dd dq
    syms ILd ILq UC Uin Iin Uod Uoq Dd Dq
    syms ws L rL C rC rsw req
    syms s

% Linearized state matrices
    Am = [            0,            ws, Dd/L
                    -ws,             0, Dq/L
          -(3*Dd)/(2*C), -(3*Dq)/(2*C),    0];

    Bm = [  0, -1/L,    0,       Uin/L,     0
            0,    0, -1/L,           0, Uin/L
          1/C,    0,    0, -Iin/(Dd*C),     0];
```

```
    Cm = [0, 0, 1
          1, 0, 0
          0, 1, 0];

    Dm = [0, 0, 0, 0, 0
          0, 0, 0, 0, 0
          0, 0, 0, 0, 0];

    Im = eye(3);

% Solving the transfer function matrix
    deter = simplify(det(s*Im - Am));
    Hpar  = simplify((Cm * inv(s*Im - Am) * Bm) + Dm);

    Zin_H  = simplify(Hpar(1,1));
    Toid_H = simplify(Hpar(1,2));
    Toiq_H = simplify(Hpar(1,3));
    Gcid_H = simplify(Hpar(1,4));
    Gciq_H = simplify(Hpar(1,5));

    Giod_H  = simplify(Hpar(2,1));
    Yod_H   = simplify(-Hpar(2,2));
    Gcrqd_H = simplify(Hpar(2,3));
    Gcod_H  = simplify(Hpar(2,4));
    Gcoqd_H = simplify(Hpar(2,5));

    Gioq_H  = simplify(Hpar(3,1));
    Gcrdq_H = simplify(Hpar(3,2));
    Yoq_H   = simplify(-Hpar(3,3));
    Gcodq_H = simplify(Hpar(3,4));
    Gcoq_H  = simplify(Hpar(3,5));

% Transfer functions w/o the determinant
    Zin_nodeter  = simplify(Hpar(1,1)*deter);
    Toid_nodeter = simplify(Hpar(1,2)*deter);
    Toiq_nodeter = simplify(Hpar(1,3)*deter);
    Gcid_nodeter = simplify(Hpar(1,4)*deter);
    Gciq_nodeter = simplify(Hpar(1,5)*deter);

    Giod_nodeter  = simplify(Hpar(2,1)*deter);
    Yod_nodeter   = simplify(-Hpar(2,2)*deter);
```

```
    Gcrqd_nodeter = simplify(-Hpar(2,3)*deter);
    Gcod_nodeter  = simplify(Hpar(2,4)*deter);
    Gcoqd_nodeter = simplify(Hpar(2,5)*deter);

    Gioq_nodeter  = simplify(Hpar(3,1)*deter);
    Gcrdq_nodeter = simplify(-Hpar(3,2)*deter);
    Yoq_nodeter   = simplify(-Hpar(3,3)*deter);
    Gcodq_nodeter = simplify(Hpar(3,4)*deter);
    Gcoq_nodeter  = simplify(Hpar(3,5)*deter);

##########################################################################################
#  M-file ends!                                                                          #
##########################################################################################
```

C LOAD-AFFECTED CF-VSI TRANSFER FUNCTIONS IN SECTION 2.4.2

This appendix presents the code for a Matlab m-file that can be used to obtain the load-affected transfer functions for the CF-VSI found in (2.222)–(2.238) in Section 2.4.2 "Load-Affected H-parameter Model".

```
################################################################################
#  M-file begins!                                                              #
################################################################################

% Joonas Puukko
% Tampere University of Technology
% Department of Electrical Energy Engineering
% 2012
% Filename: CFboost_ss_symb_load.m

% Load-affected transfer functions for the CF-VSI

clear all
clc

% Symbolic variables
    syms Zin_H Toid_H Toiq_H Gcid_H Gciq_H
    syms Giod_H Yod_H Gcod_H
    syms Gioq_H Yoq_H Gcoq_H
    syms ZinLd ZinLq ToiLd ToiLq GioLd GioLq YoLd YoLq

% Transfer function matrices w/o the cross-coupling terms
    Toi_H = [Toid_H, Toiq_H];
    Gci_H = [Gcid_H, Gciq_H];
    Gio_H = [Giod_H
             Gioq_H];
    Gco_H = [Gcod_H, 0
             0,      Gcoq_H];
```

```
    Yo_H  = [Yod_H, 0
             0,     Yoq_H];

    ZinL  = [ZinLd, 0
             0,     ZinLq];
    ToiL  = [ToiLd, 0
             0,     ToiLq];
    GioL  = [GioLd, 0
             0,     GioLq];
    YoL   = [YoLd, 0
             0,    YoLq];

    I = eye(2);

% Computation of the load-effect
    Zin_HL = simplify(Zin_H + Toi_H*inv(I+ZinL*Yo_H)*ZinL*Gio_H);
    Toi_HL = simplify(Toi_H*inv(I+ZinL*Yo_H)*ToiL);
    Gci_HL = simplify(Gci_H + Toi_H*inv(I+ZinL*Yo_H)*ZinL*Gco_H);

    Gio_HL = simplify((I - Yo_H*inv(I+ZinL*Yo_H)*ZinL)*Gio_H);
    Yo_HL  = simplify(Yo_H*inv(I+ZinL*Yo_H)*ToiL);
    Gco_HL = simplify((I - Yo_H*inv(I+ZinL*Yo_H)*ZinL)*Gco_H);

    GioL_HL = simplify(GioL*(I - Yo_H*inv(I+ZinL*Yo_H)*ZinL)*Gio_H);
    YoL_HL  = simplify(YoL + GioL*Yo_H*inv(I+ZinL*Yo_H)*ToiL);
    GcoL_HL = simplify(GioL*(I - Yo_H*inv(I+ZinL*Yo_H)*ZinL)*Gco_H);

################################################################################
#  M-file ends!                                                                #
################################################################################
```

D REDUCED-ORDER LOAD-AFFECTED TRANSFER FUNCTIONS IN SECTION 2.4.2

This appendix presents a comparison between the frequency responses from a VSI switching model in Matlab Simulink (i.e. frequency responses that include the cross-coupling effects) and predictions obtained by the reduced-order load-affected model presented in Section 2.4.2. The responses show high correlation, which justifies the use of the reduced-order model in computing the load-effect.

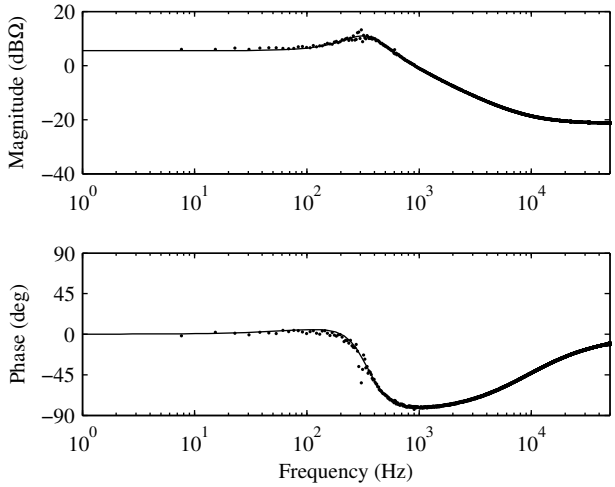

Fig. D.1: Load-affected input impedance. Prediction obtained by the reduced-order load-affected input impedance $Z_{\text{in}}^{\text{HL-r}} = \hat{u}_{\text{in}}/\hat{i}_{\text{in}}$ with solid line, frequency response from a Matlab Simulink model with dots.

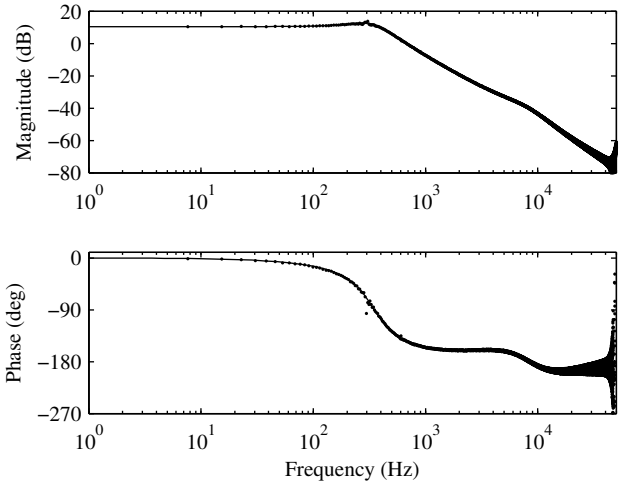

Fig. D.2: Load-affected d-channel transmittance. Prediction obtained by the reduced-order load-affected d-channel transmittance $T_{\text{oi-d}}^{\text{HL-r}} = \hat{u}_{\text{in}}/\hat{u}_{\text{odL}}$ with solid line, frequency response from a Matlab Simulink model with dots.

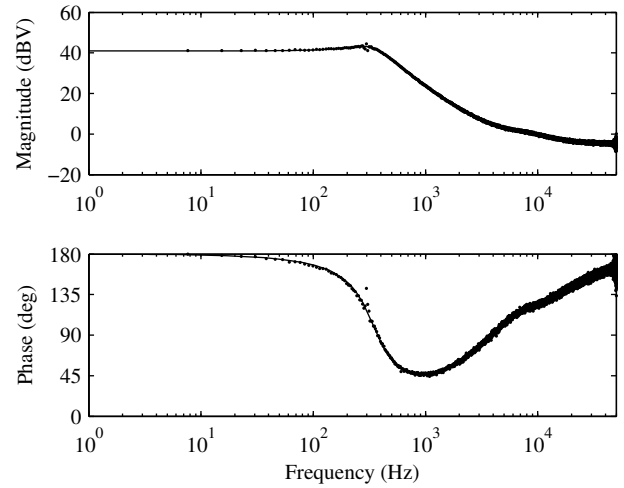

Fig. D.3: Load-affected d-channel control-to-input-voltage transfer function. Prediction obtained by the reduced-order load-affected d-channel control-to-input-voltage transfer function $G_{\text{ci-d}}^{\text{HL-r}} = \hat{u}_{\text{in}}/\hat{d}_{\text{d}}$ with solid line, frequency response from a Matlab Simulink model with dots.

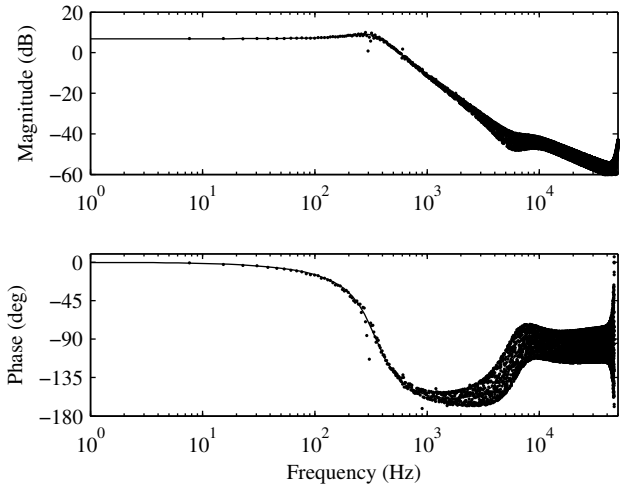

Fig. D.4: Load-affected d-channel forward transfer function. Prediction obtained by the reduced-order load-affected d-channel forward transfer function $G_{\text{io-d}}^{\text{HL-r}} = \hat{i}_{\text{od}}/\hat{i}_{\text{in}}$ with solid line, frequency response from a Matlab Simulink model with dots.

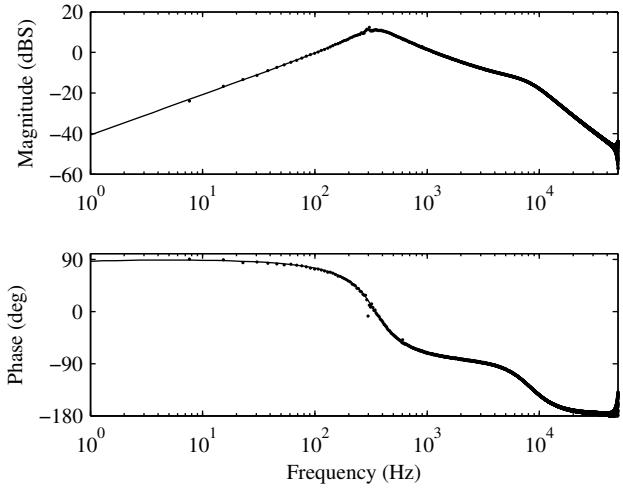

Fig. D.5: Load-affected d-channel output admittance. Prediction obtained by the reduced-order load-affected d-channel output admittance $Y_{\text{o-d}}^{\text{HL-r}} = \hat{i}_{\text{od}}/\hat{u}_{\text{odL}}$ with solid line, frequency response from a Matlab Simulink model with dots.

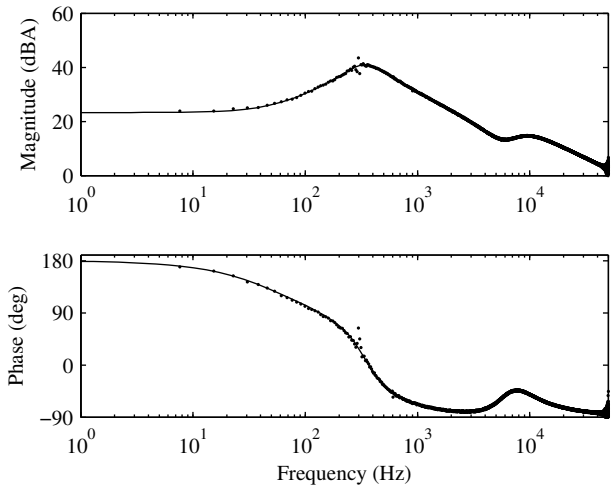

Fig. D.6: Load-affected d-channel control-to-outpu-current transfer function. Prediction obtained by the reduced-order load-affected d-channel control-to-output-current transfer function $G_{\text{co-d}}^{\text{HL-r}} = \hat{i}_{\text{od}}/\hat{d}_{\text{d}}$ with solid line, frequency response from a Matlab Simulink model with dots.

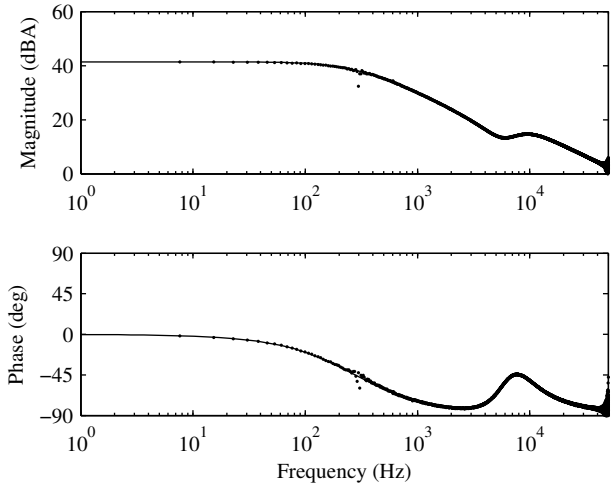

Fig. D.7: Load-affected q-channel control-to-outpu-current transfer function. Prediction obtained by the reduced-order load-affected q-channel control-to-output-current transfer function $G_{\text{co-q}}^{\text{HL-r}} = \hat{i}_{\text{oq}}/\hat{d}_{\text{q}}$ with solid line, frequency response from a Matlab Simulink model with dots.

Note! Running these m-files requires the m-files 'VFandCF_param.m' and 'CFboost_ss_tfs.m' presented in Appendix F.

```
################################################################################
#  M-file begins!                                                              #
################################################################################

% Joonas Puukko
% Tampere University of Technology
% Department of Electrical Energy Engineering
% 2012
% Filename: CLfilter_param.m

% Parameter values for the CL-type output filter

% #### Component values ####
    Lf = L;
    rLf = rL;
    Cf = 10e-6;
    rCf = 50e-3 + 2;

    ZLf = s*Lf + rLf;
    ZCf = 1/(s*Cf) + rCf;
    ZL1 = ZCf;
    ZL2 = ZLf;

################################################################################
#  M-file ends and different m-file begins!                                    #
################################################################################

% Joonas Puukko
% Tampere University of Technology
% Department of Electrical Energy Engineering
% 2012
% Filename: CFboost_ss_tfs_load.m

% Reduced-order load-affected transfer functions for a CF-VSI

ZinL = minreal(ZL1*ZL2 / (ZL1 + ZL2));  % (ZinL_d = ZinL_q = ZinL)
ToiL = minreal(ZL1 / (ZL1 + ZL2));      % (ToiL_d = ToiL_q = ToiL)
GioL = minreal(ToiL);                   % (GioL_d = GioL_q = GioL = ToiL)
YoL  = minreal(1 / (ZL1 + ZL2));        % (YoL_d = YoL_q = YoL)
```

```
Yod_H_sc   = minreal(Yod_H + Giod_H*Toid_H/Zin_H);
Yod_H_inf  = minreal(Yod_H + Toid_H*Gcod_H/Gcid_H);
Yoq_H_inf  = minreal(Yoq_H + Toiq_H*Gcoq_H/Gciq_H);
ZinL_oc = minreal(ZinL + ToiL*GioL/YoL);

Zin_HL   = minreal((1 + ZinL*Yod_H_sc) / (1 + ZinL*Yod_H) * Zin_H
               + Gioq_H*Toiq_H*ZinL/(1+ZinL*Yoq_H)); % uin/iin
Toid_HL = minreal(ToiL / (1 + ZinL*Yod_H) * Toid_H);  % uin/uodL
Toiq_HL = minreal(ToiL / (1 + ZinL*Yoq_H) * Toiq_H);  % uin/uoqL
Gcid_HL = minreal((1 + ZinL*Yod_H_inf) / (1 + ZinL*Yod_H) * Gcid_H); %uin/dd
Gciq_HL = minreal((1 + ZinL*Yoq_H_inf) / (1 + ZinL*Yoq_H) * Gciq_H); %uin/dq

Giod_HL = minreal(1 / (1 + ZinL*Yod_H) * Giod_H);     % iod/iin
Yod_HL  = minreal(ToiL / (1 + ZinL*Yod_H) * Yod_H);   % iod/uodL
Gcod_HL = minreal(1 / (1 + ZinL*Yod_H) * Gcod_H);     % iod/dd

Gioq_HL = minreal(1 / (1 + ZinL*Yoq_H) * Gioq_H);     % ioq/iin
Yoq_HL  = minreal(ToiL / (1 + ZinL*Yoq_H) * Yoq_H);   % ioq/uoqL
Gcoq_HL = minreal(1 / (1 + ZinL*Yoq_H) * Gcoq_H);     % ioq/dq

Giod_HL2 = minreal(GioL / (1 + ZinL*Yod_H) * Giod_H); % iodL/iin
Yod_HL2  = minreal((1 + Yod_H*ZinL_oc) / (1 + ZinL*Yod_H) * YoL); % iodL/uodL
Gcod_HL2 = minreal(GioL / (1 + ZinL*Yod_H) * Gcod_H); % iodL/dd

################################################################################
#  M-file ends!                                                                #
################################################################################
```

E REDUCED-ORDER CLOSED-LOOP TRANSFER FUNCTIONS IN SECTION 2.5.2

This appendix presents a comparison between the frequency responses from a VSI switching model in Matlab Simulink (i.e. frequency responses that include the cross-coupling effects) and predictions obtained by the reduced-order closed-loop model presented in Section 2.5.2. The responses show high correlation, which justifies the use of the reduced-order model in computing the closed-loop transfer functions.

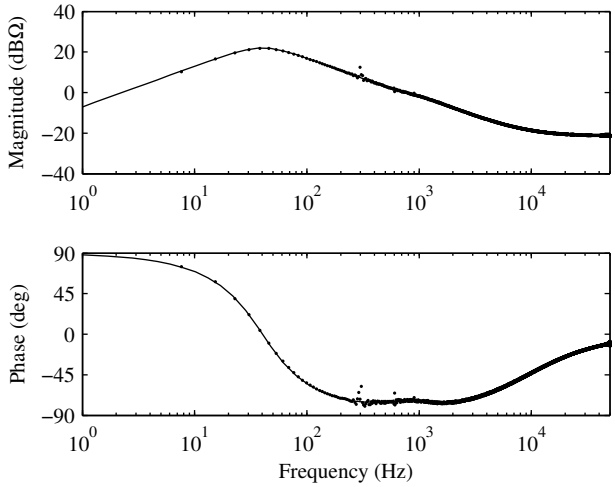

Fig. E.1: Closed-loop input impedance with a cascaded control scheme. Prediction obtained by the reduced-order closed-loop input impedance $Z_{\text{in}}^{\text{out-in-r}} = \hat{u}_{\text{in}}/\hat{i}_{\text{in}}$ with solid line, frequency response from a Matlab Simulink model with dots.

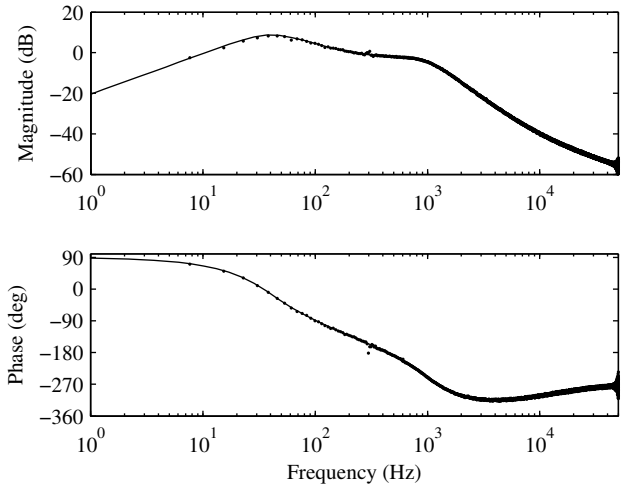

Fig. E.2: Closed-loop d-channel transmittance with a cascaded control scheme. Prediction obtained by the reduced-order closed-loop d-channel transmittance $T_{\text{oi-d}}^{\text{out-in-r}} = \hat{u}_{\text{in}}/\hat{u}_{\text{odL}}$ with solid line, frequency response from a Matlab Simulink model with dots.

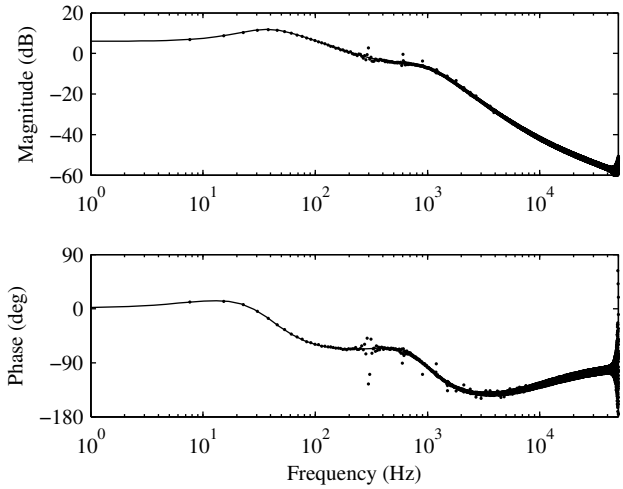

Fig. E.3: Closed-loop d-channel forward transfer function. Prediction obtained by the reduced-order closed-loop d-channel forward transfer function $G_{\text{io-d}}^{\text{out-in-r}} = \hat{i}_{\text{od}}/\hat{i}_{\text{in}}$ with solid line, frequency response from a Matlab Simulink model with dots.

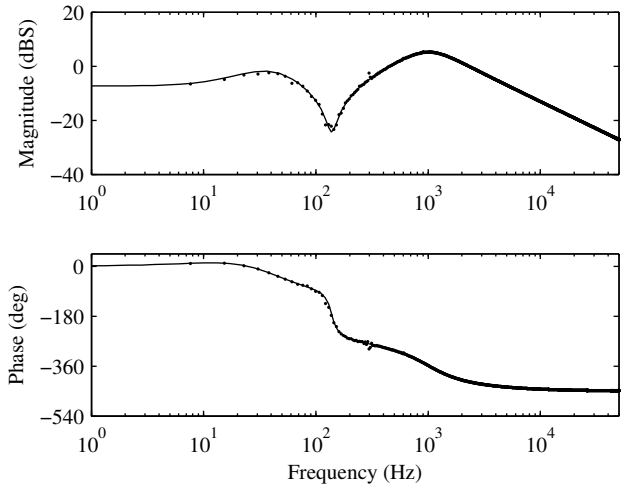

Fig. E.4: Closed-loop d-channel output admittance. Prediction obtained by the reduced-order closed-loop d-channel output admittance $Y_{\text{o-d}}^{\text{out-in-r}} = \hat{i}_{\text{od}}/\hat{u}_{\text{od}}$ with solid line, frequency response from a Matlab Simulink model with dots.

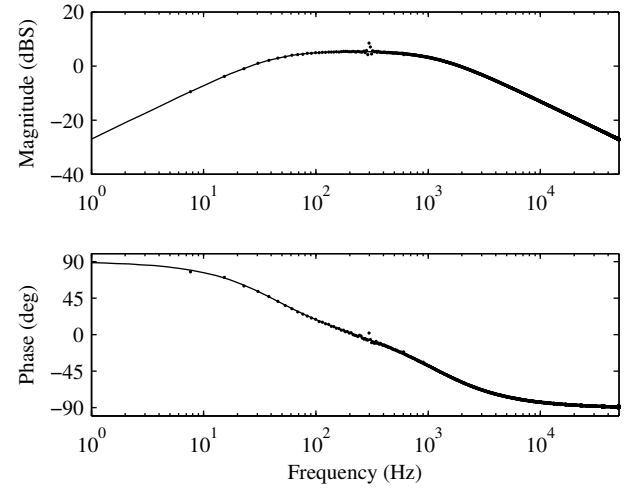

Fig. E.5: Closed-loop q-channel output admittance. Prediction obtained by the reduced-order closed-loop q-channel output admittance $Y_{\text{o-q}}^{\text{out-in-r}} = \hat{i}_{\text{oq}}/\hat{u}_{\text{oq}}$ with solid line, frequency response from a Matlab Simulink model with dots.

Note! Running these m-files requires the m-file 'CFboost_ss_tfs.m' presented in Appendix F.

```
##########################################################################################
#  M-file begins!                                                                        #
##########################################################################################

% Joonas Puukko
% Tampere University of Technology
% Department of Electrical Energy Engineering
% 2012
% Filename: VFandCF_param.m

clear all
clc
s = tf('s');

% #### Component values ####
    fs = 100e3; % Hz
    Ts = 1/fs;       % Switching cycle, sampling delay

    Iin = 2;            % A
    Uin = 30;           % V

    Uod = 8.6;          % V
    Uoq = 0; % V
    f_grid = 50; % Hz
    ws = 2*pi*f_grid; % rad/s

    L = 73e-6;          % H
    rL = 15e-3;         % ohm
    ron = 0.1;          % ohm
    C = 2*100e-6;       % F
    rC = 85e-3;         % ohm
    Rs = 50e-3;
    req = rL + ron + Rs;
    R1 = req;

% #### Steady state values ####

    Uc  = Uin;
    Ioq = 0;
```

```
    ILq = Ioq;

    % Uin*Dd^2 - Uod*Dd - (2*R1*Iin)/3 = 0
    a = Uin;
    b = -Uod;
    c = -(2*R1*Iin)/3;

    Dd = (-b + sqrt(b^2 - 4*a*c)) / (2*a);
    ILd = (2*Iin) / (3*Dd);
    Dq = (ws * L * ILd) / Uin;


% #### Modulator gain ####
    Vm = 1;
    Ga = 1/Vm;

% #### D-channel current ctrl ####
    Gse_d = 1;              % Sensing transfer function
    Kfd = 0.25;             %
    wzd = 2*pi*1e3;         % Hz
    wpd = 2*pi*50e3;        % Hz
    Gcc_d = Kfd * (s + wzd) / (s^2/(wpd) + s);   % Controller

% #### Q-channel current ctrl ####
    Gse_q = 1;              % Sensing transfer function
    Kfq = 0.25;             %
    wzq = 2*pi*60;          % Hz
    wpq = 2*pi*50e3;        % Hz
    Gcc_q = Kfq * (s + wzq) / (s^2/(wpq) + s);    % Controller

% #### Input voltage ctrl ####
    Gse_v = 1;              % Sensing transfer function
    Kfv = 0.015;            %
    wzv = 2*pi*15;          % Hz
    wpv = 2*pi*600;         % Hz
    Gcc_v = Kfv * (s + wzv) / (s^2/(wpv) + s);    % Controller


run CFboost_ss_tfs
run CFboost_closedloop
```

```
################################################################################
#  M-file ends and different m-file begins!                                    #
################################################################################

% Joonas Puukko
% Tampere University of Technology
% Department of Electrical Energy Engineering
% 2012
% Filename: CFboost_closedloop.m

% Current loop gains without the input voltage control:
    Lid = minreal(Rs*Gse_d*Gcc_d*Ga*Gcod_H);
    Liq = minreal(Rs*Gse_q*Gcc_q*Ga*Gcoq_H);
    LID = minreal(Lid * (1 - Gcoqd_H*Gcodq_H/(Gcod_H*Gcoq_H)*Liq/(1+Liq)));
    LIQ = minreal(Liq * (1 - Gcoqd_H*Gcodq_H/(Gcod_H*Gcoq_H)*Lid/(1+Lid)));

% Gcid_H_out, input voltage controller is designed according to this
    Gcid_H_out = minreal(Gcid_H * Ga*Gcc_d / (1 + Lid));

% Input voltage loop gain
    Lv = minreal(Gse_v*Gcc_v*Gcid_H_out);

    Zin_H_inf = minreal(Zin_H - Giod_H*Gcid_H/Gcod_H);
    Toid_H_inf = minreal(Toid_H + Yod_H*Gcid_H/Gcod_H);
    Toiq_H_inf = minreal(Toiq_H + Yoq_H*Gciq_H/Gcoq_H);

    Zin_H_out = minreal(Zin_H/(1+Lid) + Lid/(1+Lid)*Zin_H_inf
                        - Liq/(1+Liq)*Gioq_H*Gciq_H/Gcoq_H);
    Toid_H_out = minreal(Toid_H/(1+Lid) + Lid/(1+Lid)*Toid_H_inf);
    Toiq_H_out = minreal(Toiq_H/(1+Liq) + Liq/(1+Liq)*Toiq_H_inf);
    Gcid_H_out = minreal(Lid/(1+Lid)*Gcid_H/(Rs*Gse_d*Gcod_H));
    Gciq_H_out = minreal(Liq/(1+Liq)*Gciq_H/(Rs*Gse_q*Gcoq_H));

    Zin_H_out_in = minreal(Zin_H/((1+Lid)*(1-Lv))
                           + Lid/((1+Lid)*(1-Lv))*Zin_H_inf
                           - Liq/((1+Liq)*(1-Lv))*Gioq_H*Gciq_H/Gcoq_H);
    Toid_H_out_in = minreal(Toid_H/((1+Lid)*(1-Lv))
                            + Lid/((1+Lid)*(1-Lv))*Toid_H_inf);
    Toiq_H_out_in = minreal(Toiq_H/((1+Liq)*(1-Lv))
                            + Liq/((1+Liq)*(1-Lv))*Toiq_H_inf);
    Gcid_H_out_in = minreal(-1/Gse_v*Lv/(1-Lv));
    Gciq_H_out_in = minreal(Liq/((1+Liq)*(1-Lv))*Gciq_H/(Rs*Gse_q*Gcoq_H));
```

```
    Giod_H_inf  = minreal(Giod_H - Zin_H*Gcod_H/Gcid_H);
    Yod_H_inf   = minreal(Yod_H + Toid_H*Gcod_H/Gcid_H);
    Gcrqd_H_inf = minreal(-Toiq_H*Gcod_H/Gcid_H);
    Gcoqd_H_inf = minreal(-Gciq_H*Gcod_H/Gcid_H);

    Giod_H_out = minreal(Giod_H/(1+Lid));
    Yod_H_out  = minreal(Yod_H/(1+Lid));
    Gcod_H_out = minreal(1/(Rs*Gse_d)*Lid/(1+Lid));

    Giod_H_out_in = minreal(Giod_H/((1+Lid)*(1-Lv)) - Lv/(1-Lv)*Giod_H_inf);
    Yod_H_out_in  = minreal(Yod_H/((1+Lid)*(1-Lv)) - Lv/(1-Lv)*Yod_H_inf);
    Gcod_H_out_in = minreal(-1/Gse_v*Lv/(1-Lv)*Gcod_H/Gcid_H);

    Gioq_H_out = minreal(Gioq_H/(1+Liq));
    Yoq_H_out  = minreal(Yoq_H/(1+Liq));
    Gcoq_H_out = minreal(1/(Rs*Gse_q)*Liq/(1+Liq));

    Gioq_H_out_in = Gioq_H_out;
    Yoq_H_out_in  = Yoq_H_out;
    Gcoq_H_out_in = Gcoq_H_out;
##############################################################################
#  M-file ends!                                                              #
##############################################################################
```

F TRANSFER FUNCTIONS FOR THE VF/CF-VSI COMPARISON IN SECTION 2.6

This appendix presents the code for a Matlab m-file that can be used to obtain the transfer functions and bode diagrams presented in Section 2.6 “Comparison Between the Dynamic Properties of VF and CF-VSIs”.

```
################################################################################
#  M-file begins!                                                              #
################################################################################

% Joonas Puukko
% Tampere University of Technology
% Department of Electrical Energy Engineering
% 2012
% Filename: VFandCF_param.m

s = tf('s');

% Parameter values for the VF and CF-VSIs

% Component values
    fs = 100e3;         % Hz
    Ts = 1/fs;          % Switching cycle, sampling delay

    Iin = 2;            % A
    Uin = 30;           % V

    Uod = 8.6;          % V
    Uoq = 0;            % V
    f_grid = 50;        % Hz
    ws = 2*pi*f_grid;

    L = 73e-6;            % H
    rL = 15e-3;           % ohm
```

```
    ron = 0.1;            % ohm
    C = 2*100e-6;         % F
    rC = 135e-3;          % ohm
    Rs = 50e-3;           % ohm
    req = rL + ron + Rs;  % ohm

% Steady state values
    Uc  = Uin;
    Ioq = 0;
    ILq = Ioq;

    % Uin*Dd^2 - Uod*Dd - (2*req*Iin)/3 = 0
    a = Uin;
    b = -Uod;
    c = -(2*req*Iin)/3;

    Dd = (-b + sqrt(b^2 - 4*a*c)) / (2*a);
    ILd = (2*Iin) / (3*Dd);
    Dq = (ws * L * ILd) / Uin;

################################################################################
#  M-file ends and different m-file begins!                                    #
################################################################################

% Joonas Puukko
% Tampere University of Technology
% Department of Electrical Energy Engineering
% 2012
% Filename: VFbuck_ss_tfs.m

% State-space for a three-phase VF-VSI:
% Symbolic transfer functions

% Linearized state matrices
    Am = [-req/L,     ws
             -ws, -req/L];

    Bm = [Dd/L, -1/L,    0, Uin/L,     0
          Dq/L,    0, -1/L,     0, Uin/L];
```

```
    Cm = [(3*Dd)/2, (3*Dq)/2
                1,        0
                0,        1];

    Dm = [0, 0, 0, Iin/Dd, 0
          0, 0, 0,      0, 0
          0, 0, 0,      0, 0];

    Im = eye(2);


% Solving the transfer function matrix

    Ypar  = minreal((Cm * inv(s*Im - Am) * Bm) + Dm);

    Yin_Y  = minreal(Ypar(1,1));
    Toid_Y = minreal(Ypar(1,2));
    Toiq_Y = minreal(Ypar(1,3));
    Gcid_Y = minreal(Ypar(1,4));
    Gciq_Y = minreal(Ypar(1,5));

    Giod_Y  = minreal(Ypar(2,1));
    Yod_Y   = minreal(-Ypar(2,2));
    Gcrqd_Y = minreal(Ypar(2,3));
    Gcod_Y  = minreal(Ypar(2,4));
    Gcoqd_Y = minreal(Ypar(2,5));

    Gioq_Y  = minreal(Ypar(3,1));
    Gcrdq_Y = minreal(Ypar(3,2));
    Yoq_Y   = minreal(-Ypar(3,3));
    Gcodq_Y = minreal(Ypar(3,4));
    Gcoq_Y  = minreal(Ypar(3,5));

% Source-affected transfer functions
    % Source transfer functions
        GioS_Y = 1;
        YinS_Y = 1/(rC + 1/(s*C));
        ZoS_Y  = 0;
        ToiS_Y = 1;
```

```
    % Solving the source affected transfer functions
        ZoSinf_Y = minreal(ZoS_Y + (ToiS_Y*GioS_Y)/YinS_Y);
        Yin_YS = minreal((1+Yin_Y*ZoSinf_Y)/(1+Yin_Y*ZoS_Y)*YinS_Y);

        Yin_oc_d_Y = minreal(Yin_Y + (Toid_Y*Giod_Y)/Yod_Y);
        Yod_YS = minreal((1+ZoS_Y*Yin_oc_d_Y)/(1+ZoS_Y*Yin_Y)*Yod_Y);

        Yin_inf_d_Y = minreal(Yin_Y - (Gcid_Y*Giod_Y)/Gcod_Y);
        Gcod_YS = minreal((1+ZoS_Y*Yin_inf_d_Y)/(1+ZoS_Y*Yin_Y)*Gcod_Y);

        Yin_inf_q_Y = minreal(Yin_Y - (Gciq_Y*Gioq_Y)/Gcoq_Y);
        Gcoq_YS = minreal((1+ZoS_Y*Yin_inf_q_Y)/(1+ZoS_Y*Yin_Y)*Gcoq_Y);

        Gcid_YS = minreal(1/(1+ZoS_Y*Yin_Y)*Gcid_Y);

        GcidS_YS = minreal(ToiS_Y/(1+ZoS_Y*Yin_Y)*Gcid_Y);

################################################################################
#  M-file ends and different m-file begins!                                    #
################################################################################

% Joonas Puukko
% Tampere University of Technology
% Department of Electrical Energy Engineering
% 2012
% Filename: CFboost_ss_tfs.m

% State-space for a three-phase CF-VSI:
% Symbolic transfer functions

% Linearized state matrices
    Am = [-(req/L + (3*rC*Dd^2)/(2*L)),        ws*(1 - (rC*Iin)/Uin), Dd/L
                -ws*(1 + (rC*Iin)/Uin), -(req/L + (3*rC*Dq^2)/(2*L)), Dq/L
                        -(3*Dd)/(2*C),                -(3*Dq)/(2*C),   0];

    Bm = [rC*Dd/L, -1/L,    0,              (Uin - rC*Iin)/L,     0
          rC*Dq/L,    0, -1/L, -(2*rC*ws*Iin^2)/(3*Uin*Dd^2), Uin/L
              1/C,    0,    0,                   -Iin/(Dd*C),     0];

    Cm = [0, 0, (1 + s*rC*C)
          1, 0,            0
          0, 1,            0];
```

```
    Dm = [0, 0, 0, 0, 0
          0, 0, 0, 0, 0
          0, 0, 0, 0, 0];

    Im = eye(3);

% Solving the transfer function matrix

    Hpar  = minreal((Cm * inv(s*Im - Am) * Bm) + Dm);

    Zin_H  = minreal(Hpar(1,1));
    Toid_H = minreal(Hpar(1,2));
    Toiq_H = minreal(Hpar(1,3));
    Gcid_H = minreal(Hpar(1,4));
    Gciq_H = minreal(Hpar(1,5));

    Giod_H   = minreal(Hpar(2,1));
    Yod_H    = minreal(-Hpar(2,2));
    Gcrqd_H  = minreal(Hpar(2,3));
    Gcod_H   = minreal(Hpar(2,4));
    Gcoqd_H  = minreal(Hpar(2,5));

    Gioq_H   = minreal(Hpar(3,1));
    Gcrdq_H  = minreal(Hpar(3,2));
    Yoq_H    = minreal(-Hpar(3,3));
    Gcodq_H  = minreal(Hpar(3,4));
    Gcoq_H   = minreal(Hpar(3,5));

##########################################################################################
#  M-file ends!                                                                          #
##########################################################################################
```

G RALOSS MEASUREMENT DATA

Table G.1: Raloss SR30-36 PV module measurement data.

U_{pv} (V)	I_{pv} (A)	P_{pv} (W)	r_{pv} (dBΩ)	r_{pv} (Ω)	R_{pv} (dBΩ)	R_{pv} (Ω)	c_{pv} (μF)
18.712	0.000	0.000	4.933	1.76	N/A	N/A	23.08
18.394	0.227	4.175	6.708	2.16	38.17	81.03	19.77
17.896	0.461	8.250	9.347	2.93	31.78	38.82	15.12
17.404	0.630	10.965	12.187	4.07	28.83	27.63	11.22
16.902	0.752	12.710	15.146	5.72	27.03	22.48	7.69
16.393	0.833	13.655	18.570	8.48	25.88	19.68	4.90
15.896	0.885	14.068	22.179	12.85	25.09	17.96	2.98
15.395	0.925	14.240	26.166	20.34	24.42	16.64	1.67
14.910	0.942	14.045	30.815	34.73	23.99	15.83	0.84
14.401	0.948	13.652	35.632	60.48	23.63	15.19	0.50
13.894	0.953	13.241	39.841	98.19	23.27	14.58	0.46
13.408	0.965	12.939	43.209	144.69	22.86	13.89	0.40
12.898	0.957	12.343	47.808	245.69	22.59	13.48	0.42
12.392	0.959	11.884	50.654	340.97	22.23	12.92	0.44
11.903	0.962	11.451	51.602	380.27	21.85	12.37	0.35
11.398	0.975	11.113	51.777	388.01	21.36	11.69	0.33
10.909	0.969	10.571	52.550	424.12	21.03	11.26	0.30
10.401	0.974	10.131	52.879	440.50	20.57	10.68	0.27
9.909	0.963	9.542	53.618	479.60	20.25	10.29	0.25
9.402	0.970	9.120	53.874	493.96	19.73	9.69	0.23
8.912	0.967	8.618	54.481	529.70	19.29	9.22	0.22
8.406	0.977	8.213	54.996	562.06	18.69	8.60	0.20
7.894	0.966	7.626	55.631	604.70	18.25	8.17	0.19
7.407	0.972	7.200	55.928	625.73	17.64	7.62	0.18
6.900	0.983	6.783	56.337	655.89	16.93	7.02	0.19
6.392	0.988	6.315	56.633	678.64	16.22	6.47	0.17
5.908	0.979	5.784	56.805	692.21	15.61	6.03	0.15
5.396	0.974	5.256	57.083	714.71	14.87	5.54	0.14
4.905	0.970	4.758	57.269	730.21	14.08	5.06	0.14
4.397	0.976	4.291	57.667	764.43	13.07	4.51	0.13
3.908	0.980	3.830	58.019	796.05	12.01	3.99	0.13
3.398	0.973	3.306	58.076	801.34	10.86	3.49	0.12
2.908	0.975	2.835	58.167	809.73	9.49	2.98	0.12
2.400	0.974	2.338	58.422	833.86	7.83	2.46	0.12
1.891	0.974	1.842	58.627	853.76	5.76	1.94	0.11
1.403	0.982	1.378	59.172	909.09	3.10	1.43	0.12
0.893	0.972	0.868	59.236	915.79	-0.74	0.92	0.10
0.405	0.982	0.398	59.775	974.48	-7.69	0.41	0.11
0.166	0.976	0.162	59.735	969.95	-15.39	0.17	0.10

H THREE-PHASE PV INVERTER PROTOTYPE

This appendix presents the prototype power-stage and parameters used in this thesis.

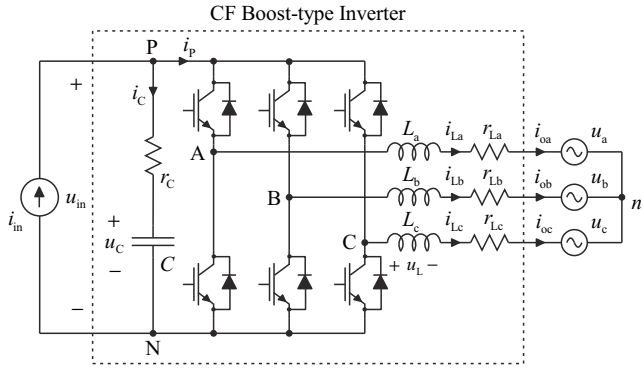

Fig. H.1: Three-phase PV inverter prototype.

The prototype power-stage component values are presented in Table H.1

Table H.1: Three-phase inverter prototype power-stage parameters.

$L_{a,b,c}$ (μH)	C (μF)	$R_{load(a,b,c)}$ (Ω)	f_{sw} (kHz)
73	200	1.2	100

The prototype operating point parameters are presented in Table H.2

Table H.2: Three-phase inverter prototype operating point parameters.

	I_{in} (A)	U_{in} (V)	U_{od} (V)	U_{oq} (V)	r_{pv} (Ω)
CCR	2.16	20.0	8.6	0.0	245.5
MPP	2.00	30.0	8.6	0.0	15.0
CVR	1.24	34.8	8.6	0.0	3.4

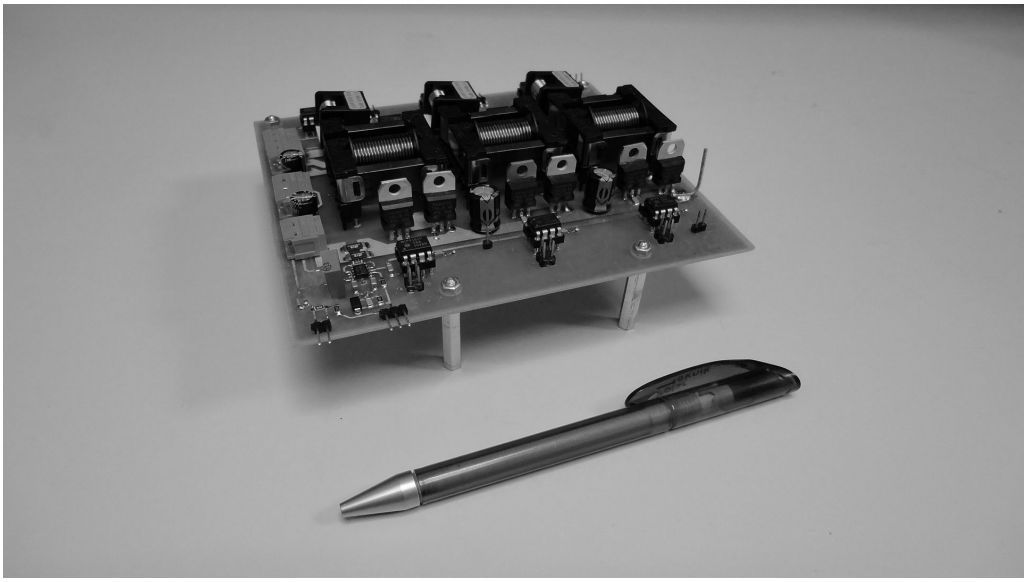

Fig. H.2: Three-phase PV inverter prototype.

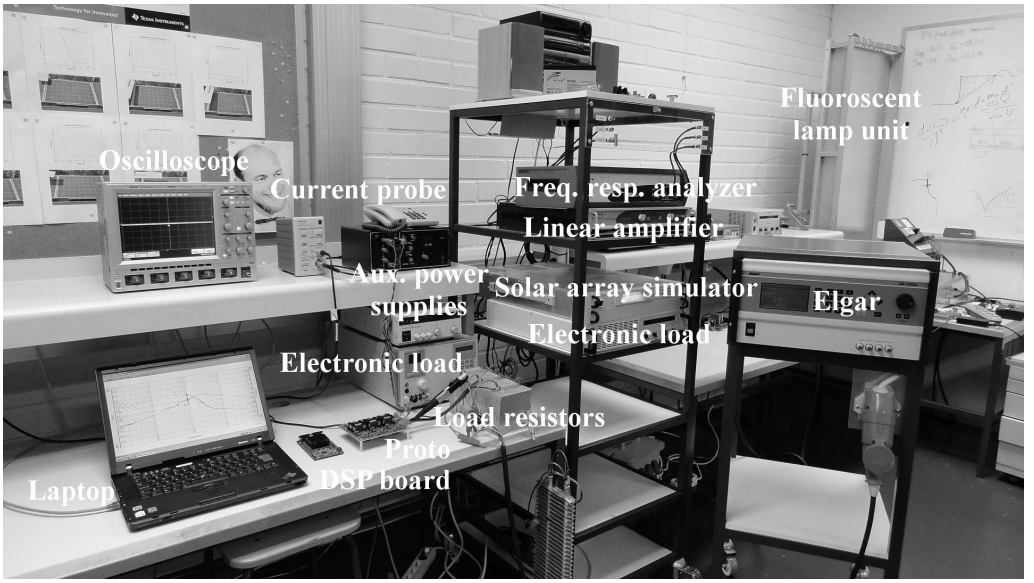

Fig. H.3: Laboratory measurement setup.

I TRANSFER FUNCTIONS FOR THE ANALYSIS IN SECTION 4.2

This appendix presents the code for a Matlab m-file that can be used to obtain the symbolic transfer functions presented in Section 4.2 “Effect of PV Generator on Three-Phase VSI-Type Inverter Dynamics”. The m-file ‘CFboost_ss_symb_nopar.m’ introduced in Appendix B is needed to run the m-file ‘CFboost_ss_symb_PVGsource.m’ presented in this appendix!

```
################################################################################
#  M-file begins!                                                              #
################################################################################

% Joonas Puukko
% Tampere University of Technology
% Department of Electrical Energy Engineering
% 2012
% Filename: CFboost_ss_symb_PVGsource.m

% State-space for a three-phase CF-VSI:
% Source-affected symbolic transfer functions

clear all
clc

% First let's run the m-file that contains the nominal transfer functions
    run CFboost_ss_symb_nopar

% Symbolic variables
    syms rpv

    GioS = 1;
    YoS  = 1/rpv;
```

```
% Special parameters
    Zin_oc_d_H  = simplify(Zin_H + Toid_H*Giod_H/Yod_H);
    Zin_oc_qd_H = simplify(Zin_H - Toiq_H*Giod_H/Gcrqd_H);
    Zin_oc_dq_H = simplify(Zin_H - Toid_H*Gioq_H/Gcrdq_H);
    Zin_oc_q_H  = simplify(Zin_H + Toiq_H*Gioq_H/Yoq_H);

    Zin_inf_d_H  = simplify(Zin_H - Gcid_H*Giod_H/Gcod_H);
    Zin_inf_qd_H = simplify(Zin_H - Gciq_H*Giod_H/Gcoqd_H);
    Zin_inf_dq_H = simplify(Zin_H - Gcid_H*Gioq_H/Gcodq_H);
    Zin_inf_q_H  = simplify(Zin_H - Gciq_H*Gioq_H/Gcoq_H);

% Source-affected transfer functions
    Zin_HS = simplify(GioS / (1 + YoS*Zin_H) * Zin_H);
    Toid_HS = simplify(1 / (1 + YoS*Zin_H) * Toid_H);
    Toiq_HS = simplify(1 / (1 + YoS*Zin_H) * Toiq_H);
    Gcid_HS = simplify(1 / (1 + YoS*Zin_H) * Gcid_H);
    Gciq_HS = simplify(1 / (1 + YoS*Zin_H) * Gciq_H);

    Giod_HS  = simplify(GioS / (1 + YoS*Zin_H) * Giod_H);
    Yod_HS   = simplify((1 + YoS*Zin_oc_d_H) / (1 + YoS*Zin_H) * Yod_H);
    Gcrqd_HS = simplify((1 + YoS*Zin_oc_qd_H) / (1 + YoS*Zin_H) * Gcrqd_H);
    Gcod_HS  = simplify((1 + YoS*Zin_inf_d_H) / (1 + YoS*Zin_H) * Gcod_H);
    Gcoqd_HS = simplify((1 + YoS*Zin_inf_qd_H) / (1 + YoS*Zin_H) * Gcoqd_H);

    Gioq_HS  = simplify(GioS / (1 + YoS*Zin_H) * Gioq_H);
    Gcrdq_HS = simplify((1 + YoS*Zin_oc_dq_H) / (1 + YoS*Zin_H) * Gcrdq_H);
    Yoq_HS   = simplify((1 + YoS*Zin_oc_q_H) / (1 + YoS*Zin_H) * Yoq_H);
    Gcodq_HS = simplify((1 + YoS*Zin_inf_dq_H) / (1 + YoS*Zin_H) * Gcodq_H);
    Gcoq_HS  = simplify((1 + YoS*Zin_inf_q_H) / (1 + YoS*Zin_H) * Gcoq_H);

    [Zin_HS_num, Zin_HS_den] = numden(Zin_HS);
    [Toid_HS_num, Toid_HS_den] = numden(Toid_HS);
    [Toiq_HS_o_num, Toiq_HS_den] = numden(Toiq_HS);
    [Gcid_HS_o_num, Gcid_HS_den] = numden(Gcid_HS);
    [Gciq_HS_o_num, Gciq_HS_den] = numden(Gciq_HS);

    [Giod_HS_num,  Giod_HS_den]  = numden(Giod_HS);
    [Yod_HS_num,   Yod_HS_den]   = numden(Yod_HS);
    [Gcrqd_HS_num, Gcrqd_HS_den] = numden(Gcrqd_HS);
    [Gcod_HS_num,  Gcod_HS_den]  = numden(Gcod_HS);
    [Gcoqd_HS_num, Gcoqd_HS_den] = numden(Gcoqd_HS);
```

```
    [Gioq_HS_num,  Gioq_HS_den]  = numden(Gioq_HS);
    [Gcrdq_HS_num, Gcrdq_HS_den] = numden(Gcrdq_HS);
    [Yoq_HS_num,   Yoq_HS_den]   = numden(Yoq_HS);
    [Gcodq_HS_num, Gcodq_HS_den] = numden(Gcodq_HS);
    [Gcoq_HS_num,  Gcoq_HS_den]  = numden(Gcoq_HS);

##############################################################################
#  M-file ends                                                               #
##############################################################################
```

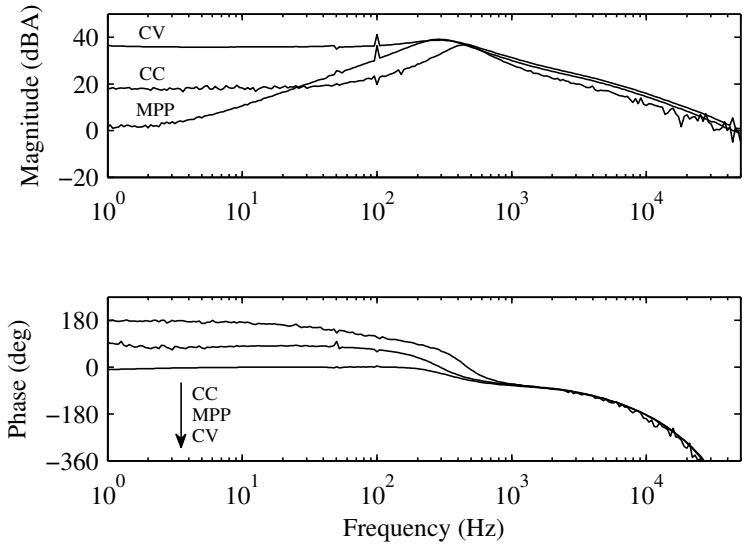

Fig. I.1: Measured d-channel control-to-output-current transfer function $G_{\text{co-d}}^{\text{HS}}$.

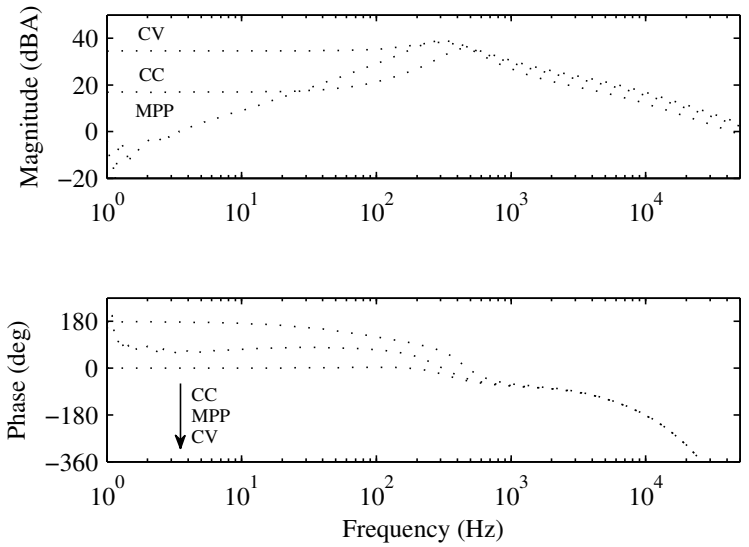

Fig. I.2: Predicted d-channel control-to-output-current transfer function $G_{\text{co-d}}^{\text{HS}}$ using measured source impedance.

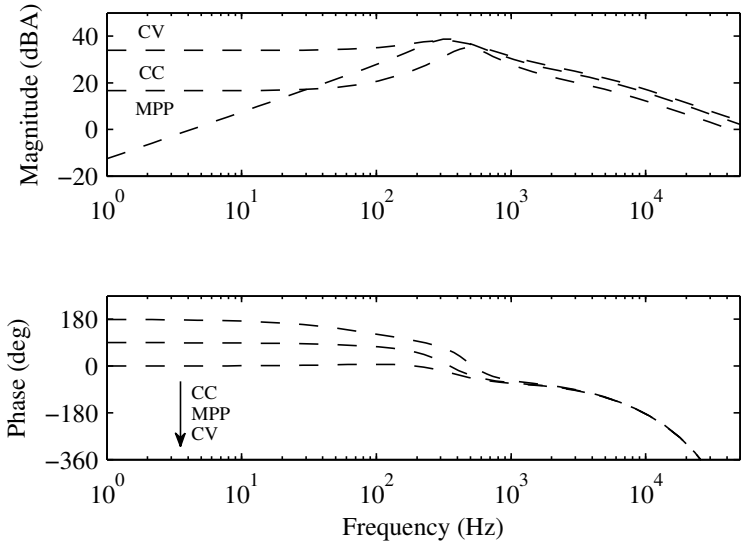

Fig. I.3: Predicted d-channel control-to-output-current transfer function $G_{\text{co-d}}^{\text{HS}}$ using (4.4) as source impedance.

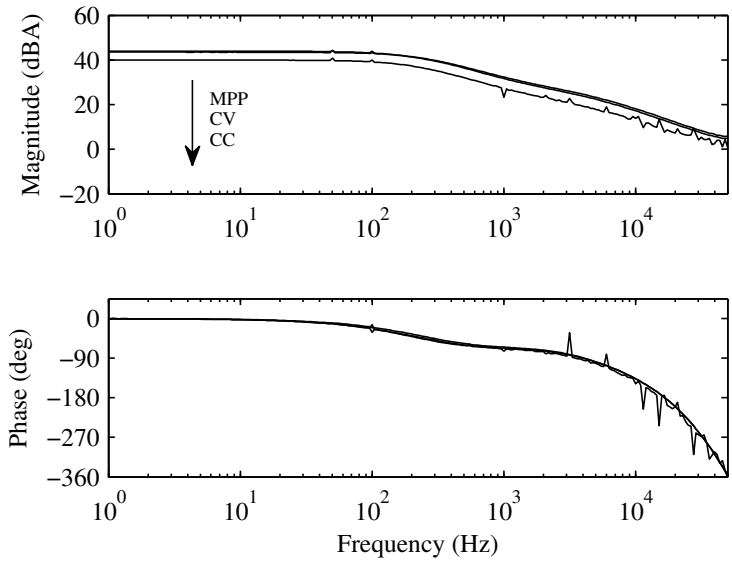

Fig. I.4: Measured q-channel control-to-output-current transfer function $G_{\text{co-d}}^{\text{HS}}$.

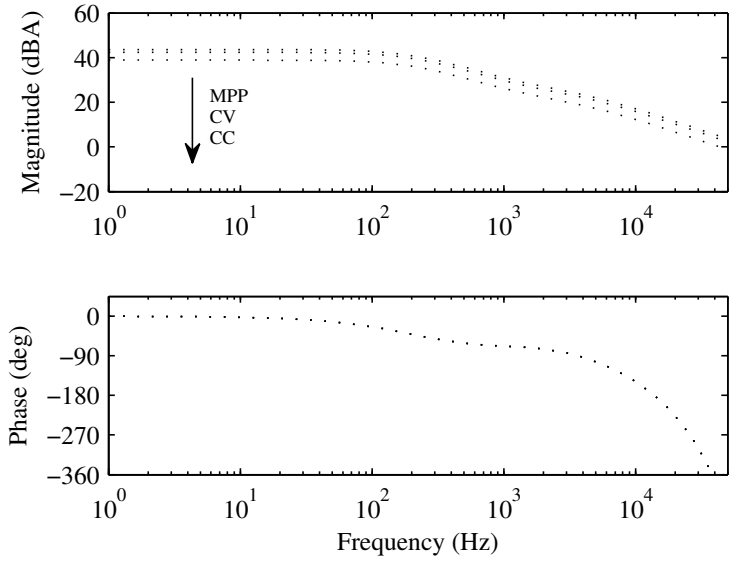

Fig. I.5: Predicted q-channel control-to-output-current transfer function $G_{\text{co-d}}^{\text{HS}}$ using measured source impedance.

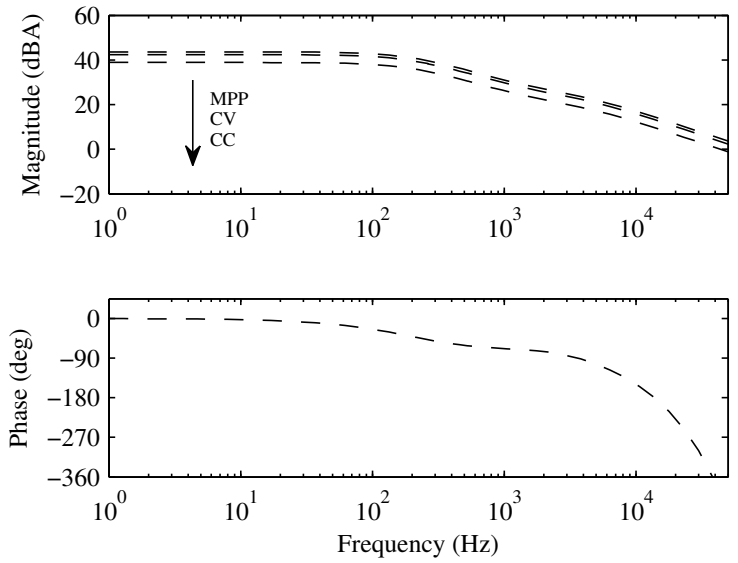

Fig. I.6: Predicted q-channel control-to-output-current transfer function $G_{\text{co-d}}^{\text{HS}}$ using (4.4) as source impedance.

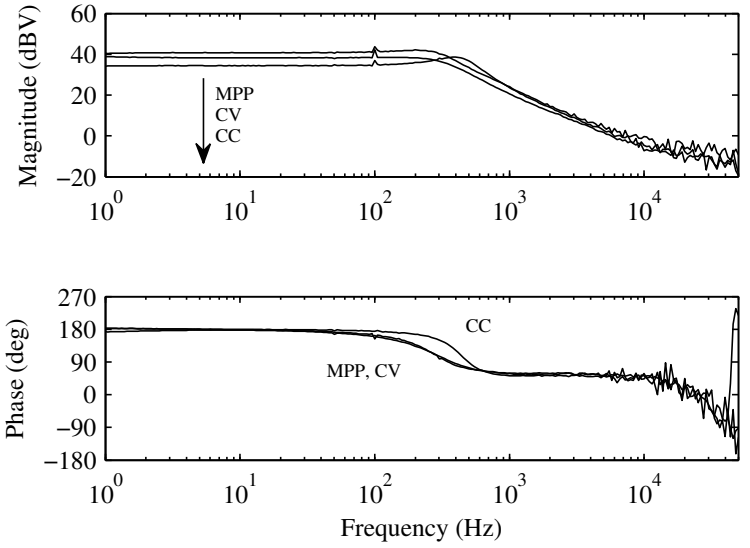

Fig. I.7: Measured d-channel control-to-input-voltage transfer function $G_{\text{ci-d}}^{\text{HS}}$.

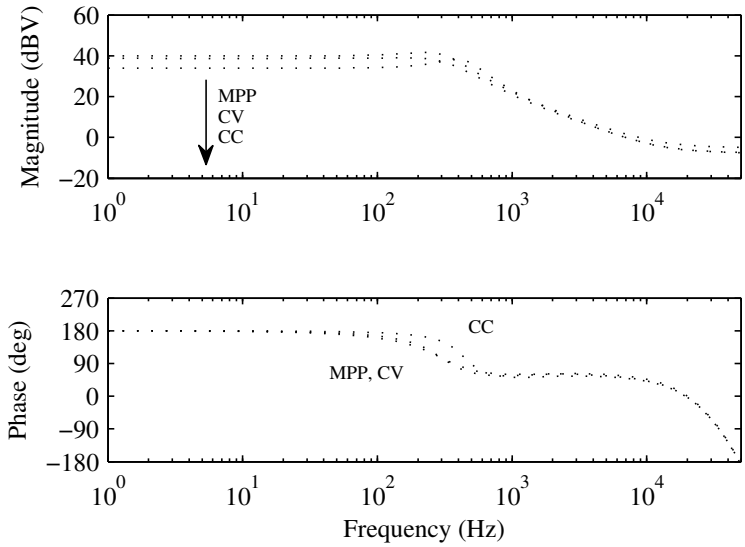

Fig. I.8: Predicted d-channel control-to-input-voltage transfer function $G_{\text{ci-d}}^{\text{HS}}$ using measured source impedance.

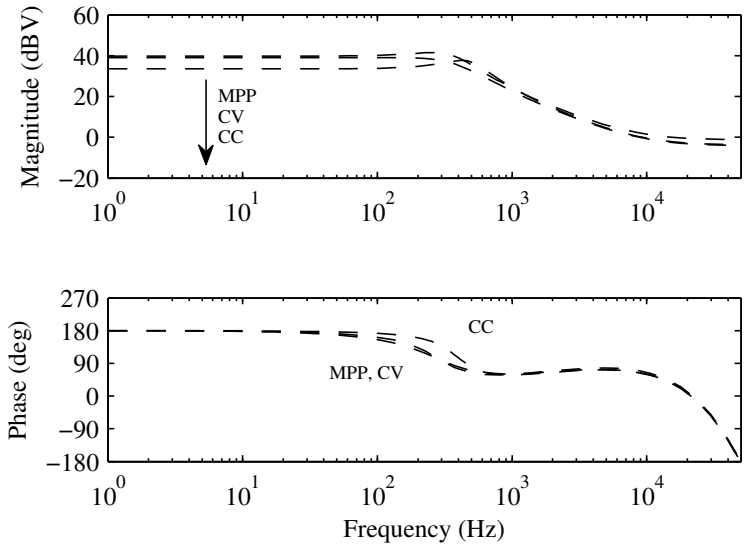

Fig. I.9: Predicted d-channel control-to-input-voltage transfer function $G_{\text{ci-d}}^{\text{HS}}$ using (4.4) as source impedance.

Tampereen teknillinen yliopisto
PL 527
33101 Tampere

Tampere University of Technology
P.O.B. 527
FI-33101 Tampere, Finland

ISBN 978-952-15-2930-6
ISSN 1459-2045